RESTRICTIONS IN THE DARK SECTOR OF THE UNIVERSE AND MODIFIED GRAVITY WITH LARGE SCALE STRUCTURE AND GRAVITATIONAL WAVES

By

DAVID FIGUERUELO HERNÁN

VNiVERSiDAD D SALAMANCA

A PhD dissertation submitted to the University of Salamanca in accordance with the requirements of the degree of DOCTOR OF FUNDAMENTAL PHYSICS AND MATHEMATICS in the Faculty of Science.

SALAMANCA, JUNE 2023

RESTRICTIONS IN THE DARK SECTOR OF THE UNIVERSE AND MODIFIED GRAVITY WITH LARGE SCALE STRUCTURE AND GRAVITATIONAL WAVES

AUTHOR

David Figueruelo Hernán

SUPERVISOR

Dr. Jose Beltrán Jiménez

DIRECTOR OF THE RESEARCH WORK

Dr. Prof. Fernando Atrio Barandela

SALAMANCA, JUNE 2023

DECLARACIÓN

Yo, Dr. Jose Beltrán Jiménez, Profesor Titular del área de Física Teórica en el Departamento de Física Fundamental de la Universidad de Salamanca
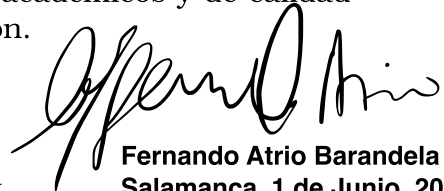
y

Yo, Dr. Fernando Atrio Barandela, Catedrático del área de Física Teórica en el Departamento de Física Fundamental de la Universidad de Salamanca,

CERTIFICAMOS:

Que el trabajo de investigación desarrollado en la presente tesis doctoral por el investigador David Figueruelo Hernán para optar al Título de Doctor por la Universidad de Salamanca con la Mención de Doctorado Internacional cumple con los requisitos formales, académicos y de calidad requeridos, autorizando por tanto su presentación.

Firmado por BELTRAN
JIMENEZ JOSE - ***5470**
el día 01/06/2023 con un

FIRMADO: .... Y ....

Fernando Atrio Barandela
Salamanca, 1 de Junio, 2023.

i

ABSTRACT

The current paradigm of Cosmology is founded on the Λ Cold Dark Matter (ΛCDM) prescription, thanks to the enormous amount of experiments in agreement with it. The building process of the ΛCDM paradigm has three pillars, namely: General Relativity, the Cosmological Principle and the presence of a puzzling Dark Sector. However, ΛCDM model is not able to answer all questions. For example, about the intrinsic nature of the Dark Sector, certain issues on the formation of structures in the Universe and current tensions between datasets. Consequently, the last word has yet to be spoken regarding the description of the Cosmos. Because of that, this PhD dissertation intends to be a step forward in the improvement of our cosmological knowledge.

After two chapters devoted to the current concordance model and its main problems respectively, as an introduction, the main topic of this PhD thesis is presented in the third chapter: the so-called pure momentum transfer models. They are an alternative description of the Cosmos which add to the concordance scenario the presence of a momentum exchange between certain components of the Universe involving the Dark Sector. That kind of interactions preserve the background cosmology while modifying the perturbation regime, where precisely certain tensions have emerged in recent times. Moreover, we can also understand them as the macroscopic description of a microscopic force acting in the Dark Sector due to a yet invisible charge. The main implication of this pure momentum exchange is the freezing of the density perturbations of the pressureless fluid, leading to a late-time mechanism eraser of structure. In this thesis, we first present three different momentum transfer models to subsequently thoroughly study, both analytically and numerically, their background cosmology and their linear perturbation regime. We then explore all the different effects on several observables to later use the most recent data to constrain the model parameters along with the cosmological parameters. After that, we devote a chapter to the analyses of how future planned surveys will be capable or not of disentangling the presence of the pure momentum transfer interactions. In the final chapter, we focus on the very small scales where the non-linear physics takes place, as the next natural step once the background and linear cosmology has been studied along with the performance of future surveys. We analyse how these models affect the formation of structures in our Cosmos, using the first one presented before as a proxy. Finally, we summarise the work done and we present our conclusions together with the possible future prospects and open questions.

RESUMEN

El paradigma actual de la Cosmología es el modelo de Constante Cosmológica con Materia Oscura Fría, llamado modelo ΛCDM, debido a la gran cantidad de experimentos que así lo confirman. Dicho paradigma cosmológico está basado en tres pilares: Relatividad General, el Principio Cosmológico y un enigmático Sector Oscuro. Sin embargo, el modelo ΛCDM no es capaz de resolver satisfactoriamente todas las cuestiones que se le plantean, como puede ser la naturaleza intrínseca de dicho Sector Oscuro, diferentes problemas en las formación de las estructuras del Universo o las recientes inconsistencias entre diferentes experimentos. De tal forma que aún queda camino por recorrer para poder hallar una descripción plenamente satisfactoria para nuestro Cosmos, siendo este el objetivo de esta tesis doctoral.

Comenzaremos dedicando dos capítulos a explicar el modelo de concordancia ΛCDM y sus principales problemas, sirviéndonos pues de introducción, para luego presentar el principal tema de esta tesis doctoral: los modelos de transferencia de momento. Se tratan de descripciones alternativas al ΛCDM para nuestro Universo que agregan a la descripción actual la posible presencia de un cierto intercambio de momento entre distintos componentes del Universo, especialmente de aquellos pertenecientes a su Sector Oscuro. Tienen la peculiaridad de preservar la cosmología de fondo y por tanto sólo actuar a nivel de las perturbaciones, donde precisamente han surgido discrepancias últimamente entre distintos experimentos. La anterior interacción puede ser entendida como el resultado macroscópico de una fuerza aún por descubrir actuando dentro del Sector Oscuro y causada por una carga oscura que nuestros detectores no han podido desentrañar debido a su propia naturaleza. A nivel de consecuencias, dichas interacciones se manifiestan como una reducción en el proceso de acreción de materia en las distintas estructuras del Universo que es eficiente en los estadios más tardíos del Universo. En esta tesis doctoral, primero presentamos tres modelos diferentes donde se da tal transferencia de momento para luego estudiarlos detalladamente tanto de forma analítica como de forma numérica. Se analizará su cosmología de fondo y el régimen lineal de perturbaciones para luego determinar sus posibles efectos en diferentes observables y, para finalizar, confrontarlos a los datos más recientes disponibles con el fin de constreñir sus parámetros. En el siguiente capítulo, analizaremos como los futuros experimentos serán capaces o no de detectar las interacciones estudiadas. Finalmente, en el último capítulo, estudiaremos como es el régimen no lineal de dichos modelos viendo como pueden cambiar el proceso de formación de estructuras en el Cosmos. Para acabar y así cerrar, presentaremos nuestras conclusiones sobre el trabajo aquí realizado y comentaremos sobre cuestiones futuras a continuar.

AGRADECIMIENTOS

Quiero comenzar, como no puede ser de otra forma, expresando mi más profunda gratitud a quien ha sido mi supervisor, a Jose, durante estos cuatro años que ha durado este viaje. Primero por la confianza que tuvo en mí para darme la oportunidad de empezar a trabajar en lo que luego ha acabado siendo esta tesis doctoral y, segundo, por la ayuda, guía y libertad que he tenido durante todo este tiempo para realizar las distintas investigaciones. También quiero agradecerle por la ética investigadora que me ha trasmitido, la cual me parece muy necesaria en este mundo. Aunque por encima de todo a quien quiero agradecer no es a mi supervisor, sino a la persona que había detrás. Gracias porque he sido muy feliz haciendo esta tesis doctoral y, siendo sincero, si tuviera que volver a 2019 tengo claro que volvería a empezar la tesis aquí.

Quiero también destacar aquí a mi director del trabajo de investigación, Fernando. Primero, porque creo que es honesto admitir que sin ese TFG allá por el 2018 no estaría aquí ni mucho menos y, segundo, por la dirección del trabajo de investigación que ha engendrado esta tesis doctoral, por las discusiones científicas y sobre docencia que hemos tenido y también por el buen trato que siempre ha tenido hacia mí.

En segundo lugar quiero agradecer a quien ha sido mi compañía en este viaje, a los doctorandos. En especial a quienes, como Paz y Carlos, ya no están aquí pero me ayudaron cuando casi era un bebé recién llegado que no tenía ni idea de donde se estaba metiendo, a quien ha recorrido el duro camino casi a la vez, Miguel, y a quienes la dichosa juventud les hace que les quede camino por recorrer, David, Riccardo y Gabri. Una de las mejores cosas que me llevo de estos años es vuestra amistad y creo que es precisamente eso lo que más destacaría. Hemos formado un grupo de amigos que venían cada día a pasárselo bien, trabajando también, y que siempre estábamos dispuestos a ayudar al otro, aunque alguna que otra broma haya caído por el camino.

Por otro lado, también quiero agradecer a Dario y a Florencia, con quienes más he trabajado estos años y que me han enseñado mucho desde otras perspectivas. Creo que los años que coincidimos estimularon mucho mi capacidad investigadora y además el ambiente de trabajo siempre fue muy bueno. Quiero agradecer a todo el grupo GRACUS por la ayuda, disposición y discusiones que me han hecho prosperar como investigador y también por todas las actividades externas que hemos acabando haciendo, desde deportes a congresos pasando por cervezas. Honestamente, ha sido un entorno tremendamente acogedor. En general, quiero agradecer a todo el Depar-

tamento de Física Fundamental por toda la ayuda y facilidades en estos años.

Por otro lado, estoy profundamente agradecido a la gente que me acogió en las estancias que he hecho, a Antonio, Raúl, David, Hans, y Jose María. Habéis sido indispensables para ampliar mis conocimientos en diferentes áreas de la Cosmología mucho más allá de lo que hubiera podido pensar. En especial quiero destacar mi paso por Oslo, donde a David y Hans les agradezco la oportunidad de estar allí tres meses, lo cual para mí fue una experiencia personal única. Le agradezco a toda la gente del Instituto de Astrofísica Teórica de Oslo por la acogida allí y el buen ambiente que hubo. También a Jose María, y a toda la gente del Insituto Niels Bohr, por la oportunidad de estar allí en Copenhague un mes. Finalmente, quiero agradecer a toda la gente con la que tenido el honor de trabajar desde la distancia en estos años, a Miguel, Shinji, Wilmar y Enea. Gracias porque he aprendido muchísimo de vosotros.

Quiero acabar agradeciendo a mi familia por haberme llevado hasta aquí. A mi padre Marce, a mi madre Merce y a mi hermano Álvaro. También a mis abuelos. A la Yaya, y a Paca y Tomás que, aunque no estén ya aquí con nosotros, sé que me estarán viendo desde algún lugar.

This PhD dissertation is based on the work of the last four years at the Department of Fundamental Physics of the University of Salamanca, which derived into a total of 7 publications in specialised journals, 5 of them related to the main topic of this thesis and 2 of them in other topics, and 1 pre-print related to the main topic under peer review by the time of the publication of this PhD dissertation. Moreover, the results were presented in 3 international conferences and a total of 4 research visits were done.

The list of publications related to this PhD dissertation with the exact contribution done is the following:

- **Title:** On cosmological signatures of Baryons-Dark Energy elastic couplings.
  Authors: Jose Beltrán Jiménez, Dario Bettoni, David Figueruelo and Florencia A. Teppa Pannia.
  DOI: 10.1088/1475-7516/2020/08/020
  Published in: Journal of Cosmology and Astroparticle Physics 08 (2020), 020.
  e-Print: 2004.14661 [astro-ph.CO]
  Contribution: developing of the analytical part, creation of the modified version of CLASS, obtaining the results and interpreting them. Collaboration in the writing of the paper.

- **Title:** Velocity-dependent interacting Dark Energy and Dark Matter with a Lagrangian description of perfect fluids.
  Authors: Jose Beltrán Jiménez, Dario Bettoni, David Figueruelo, Florencia A. Teppa Pannia and Shinji Tsujikawa.
  DOI: 10.1088/1475-7516/2021/03/085
  Published in: Journal of Cosmology and Astroparticle 03 (2021), 085.
  e-Print: 2012.12204 [astro-ph.CO]
  Contribution: developing and interpreting the model and its consequences. Collaboration in the writing of the paper.

- **Title:** J-PAS: Forecasts for Dark Matter - Dark Energy elastic couplings.
  Authors: David Figueruelo et al.
  DOI: 10.1088/1475-7516/2021/07/022
  Published in: Journal of Cosmology and Astroparticle 07 (2021), 022.
  e-Print: 2103.01571 [astro-ph.CO]
  Contribution: creation of the modified version of CLASS, obtaining the results and interpreting them. Providing the observables and functions required for the FARO code, obtaining and interpreting the results. FARO code credits should be

attributed to Miguel Aparicio Resco. Collaboration in the writing of the paper.
Comments: This is an official paper of the J-PAS collaboration.

- **Title:** Probing elastic interactions in the Dark Sector and the role of S_8.
  Authors: Jose Beltrán Jiménez, Dario Bettoni, David Figueruelo, Florencia A. Teppa Pannia and Shinji Tsujikawa.
  DOI: 10.1103/PhysRevD.104.103503
  Published in: Physical Review D 104 (2021) 10, 103503.
  e-Print: 2106.11222 [astro-ph.CO]
  Contribution: developing and interpreting the model and its consequences. A modified `CLASS` code was developed with success for the first model studied, a `CAMB` code was developed by Florencia Anabella Teppa Pannia for the second model. Collaboration in the writing of the paper.

- **Title:** Momentum transfer in the Dark Sector and lensing convergence in upcoming galaxy surveys.
  Authors: Wilmar Cardona and David Figueruelo.
  DOI: 10.1088/1475-7516/2022/12/010
  Published in: Journal of Cosmology and Astroparticle 12 (2022), 010.
  e-Print: 2209.12583 [astro-ph.CO]
  Contribution: developing the modified version of `CLASS` code, creation of a `MontePython` likelihood module to perform the forecast, obtaining and interpreting the results. Collaboration in the writing of the paper.

The list of pre-prints related to this PhD dissertation with the exact contribution done is the following:

- **Title:** A smoking gun from the power spectrum dipole for elastic interactions in the Dark Sector.
  Authors: Jose Beltrán Jiménez, Enea Di Dio and David Figueruelo.
  e-Print: 2212.08617 [astro-ph.CO]
  Sent to: Journal of Cosmology and Astroparticle.
  Contribution: developing of the modified version of `CLASS` code, creation of a `FORTRAN` code to perform the forecast, obtaining and interpreting the results. Collaboration in the writing of the paper.

The list of publications not related to the main topic of this PhD dissertation is the following:

- **Title:** The miniJPAS survey: A preview of the Universe in 56 colors.
  Authors: Silvia Bonoli at al.
  DOI: 10.1051/0004-6361/202038841
  Published in: Astronomy and Astrophysics 653 (2021) A31.
  e-Print: 2007.01910 [astro-ph.CO]
  Comments: This is an official paper of the J-PAS collaboration.

- **Title:** Some disquisitions on cosmological 2-form dualities.
  Authors: Katsuki Aoki, Jose Beltrán Jiménez and David Figueruelo.

The list of research visits done during this PhD dissertation is the following:

- **Place:** Universidad Complutense de Madrid.
  Supervisor: Prof. Antonio López Maroto.
  Dates: 14/10/19 - 18/10/19.

- **Place:** Donostia International Physics Center.
  Supervisor: Dr. Raul Angulo.
  Dates: 12/07/21 - 23/07/21.

- **Place:** Institute of Theoretical Astrophysics of the University of Oslo.
  Supervisor: Prof. David F. Mota.
  Dates: 19/04/22 - 19/07/22.

- **Place:** Niels Bohr Institute.
  Supervisor: Dr. Jose María Ezquiaga.
  Dates: 11/02/23 - 11/03/23.

TABLE OF CONTENTS

INTRODUCTION

osmology is nothing but the attempt of adults to answer the question every child asks: what is that up in the skies and why does it work like it does? As Carl Sagan said: *The cosmos is within us. We are made of star-stuff. We are a way for the Universe to know itself.* The wish to understand the Cosmos has been with humanity since its beginning of times, since humans could be called humans. This should not come as a surprise to us. Although now ruined in the cities by light contamination, the breathtaking experience of being in the countryside, far from city lights, in a cloudless night looking up to the skies poses too many questions while making us very small in front of such a vast infinity. Maybe one of the first discovered evidences of those everlasting questions is at the caves of Lascaux, where the Pleiades were left for eternity by our ancestors. Temples astronomically oriented are another example that goes from the Stonehenge and the Pyramids in every culture to recent catholic churches. The ancients looked up to the sky in order to search for answers in the regular patterns that celestial objects have while they configured their lives, their harvests and ceremonies according to those patterns. Hence, Cosmology, as a science, is just the modern manifestation of such quest for answers humanity has been making since the dawn of mankind.

As any other science, Cosmology deals with a subject of study. In this case the Universe, also called the Cosmos from ancient Greek meaning order. Because of that, it is a peculiar science in the sense it deals with the origin, evolution and death of everything that was, is and will be, placing Cosmology in a complex interplay with philosophy and religion. In fact, some of the questions Cosmology tries to answer were addressed by all the different religions and, historically, the descriptions of the Cosmos came from religion not from science. What we may call Modern Cosmology relates to the pursuit of understanding how the Cosmos works under the scientific

method. The very first attempts in that way appeared when we first took our telescopes up to the sky, showing that there were more stars than those seen by naked eye, showing that some of them formed structures and discovering certain patterns. This historical event led to questioning our position in the Cosmos, thought to be in the centre, driving us to the Copernicus Principle. Even though technology progressed very fast in the subsequent centuries, we were only able to observe our very local Universe bringing, of course, enormous advances to Astrophysics. But this also implied theoretical progresses. For example, Kepler Laws or Newton Laws, which, although in principle applied to our Solar System dynamics, now we use them for several cosmological purposes. Despite all the previous progress, we may consider that the founding events leading to Modern Cosmology date back from the twentieth century. If we have to highlight some of them in this preface, we may split them into theoretical and observational events. In the theoretical realm, the appearance of General Relativity [1] stands out among the rest. Even if it was first applied to the dynamics of the Solar System as a new theory of gravity, quickly showed its value when applied to the whole Universe. In the observational domain, the discovery of other galaxies and the expansion of the Universe changed forever our conception of the Universe. Milky Way was no longer the only system but a vast number of galaxies began to appear. Moreover, the Cosmos was not static but evolving in time, making us wonder if there was a beginning and if there will be an end. Since those early century milestones, Cosmology took his own path to become a respectable science in its own right. But the process was not easy and we are yet on it. Although there was a large amount of remarkable events and discussions, we cannot comment all here but only some of them. For instance, the presence of the Cosmological Constant in our cosmological models in the last one hundred years. First considered in the pursuit of a closed and static Universe by Einstein, then intriguingly not observed when the expansion of the Universe was discovered and finally resurrecting when the expansion was observed to be accelerating. Dark Matter also has a turbulent history. Never detected in our Earth experiments, no theory able yet to explain it but cosmological experiments continuously indicating it is there, for instance with rotational curves of galaxies or when measuring the total matter abundance. The Cosmic Microwave Background is without any doubt the most amazing cosmological observational discovery in the twentieth century. Light emitted in the beginning of the Universe that travelled until now and containing an enormous amount of information. Up to now, it is the main cosmological observable and, ironically, it was discovered serendipitously by Penzias and Wilson. In their antenna they had a signal that they were unable to remove nor identify its origin, it was spread all around the sky, day and night. The next landmark arrived with the discovery of the accelerated expansion in the late nineties, changing completely the paradigm. In recent years, another turning point is happening as now we have a vast quantity of datasets with a percentage level of precision. This has been called the era of precision Cosmology, although such a name is now rather hackneyed. Nowadays, we have observations

from the Baryonic Acoustic Oscillations [2], the Cosmic Microwave Background both from Earth [3, 4] and extraterrestrial probes [5], Supernovae experiments [6], Large Scale Structure surveys [7], Gravitational Waves observations [8], Lyman-α data [9] or Cosmic Chronometers [10], to name just a few of the uncountable list of observations.

The previous process, from which we have just barely commented certain achievements, took place for more than one century and it concluded with the establishment of a concordance model: the so-called Λ Cold Dark Matter model (ΛCDM). It is able to account for most of our datasets. It explains, with the addition of the inflationary paradigm, how the very early, hot and dense Universe ended up in our current Cosmos. How different structures were formed. How the abundances of the different components balance. And, at the end, it gives us a coherent description of the Cosmos. Because of that, Chapter 2 will be solely dedicated to it. There, we will speak about the pillars ΛCDM is built upon, which description ΛCDM gives to the background and large scale cosmology and which formularisation gives to the perturbation sector. Finally, we will devote a section to explain the most important observables both for the concordance model and for this thesis. Nevertheless, we should not forget that ΛCDM model is nothing but an effective theory which, even though it is able to explain most of our Universe, is not ultimately perfect. Due to that, we will devote Chapter 3 to briefly explain which problems have appeared inside it in recent years in the form of tensions among datasets or inconsistencies in the process of formation of structures. That will allow us to motivate the main topic of this PhD dissertation: finding a better and well motivated alternative description of the Cosmos. In our case, we will focus on what is commonly called pure momentum transfer interactions. They basically consist in having some kind of coupling between certain components of the Universe which implies a momentum transfer between them with, however, no energy transfer. That will be Chapter 4. In that chapter, we will make use of the most updated datasets to fully analyse the models under consideration. Since the next years are enormously populated with new experiments, in Chapter 5 we will perform several forecasts for future surveys. Up to now, only linear analyses have been considered, thus in Chapter 6 we will analyse how the non-linear dynamics are when a pure momentum transfer is included. We will present our conclusions and future work in Chapter 7.

Notation and conventions

Here we want to fix the notation used in this thesis according to the following rules:

- Metric signature is $(-, +, +, +)$, unless specified.

- Indices with Greek letters represent both time and spatial coordinates while indices with Latin letters represent only spatial coordinates, unless specified.

- Having a subscript "0" in a cosmological quantity means it is measured today.

- Scale factor today is normalised to $a_0 = 1$.

- We denote the derivative with respect to cosmic time t by " $\dot{}$ " and with respect to conformal time τ by " $\prime$ ".

- $\Omega_i(a)$ represent the density evolution of the i-th component of the Universe in units the critical density, while having just Ω_i means $\Omega_i \equiv \Omega_{i0} \equiv \Omega(a_0)$

THE STANDARD COSMOLOGICAL MODEL

Since the discovery of the accelerated expansion of the Universe in the late nineties, cosmologists have established a concordance model to describe the Universe, called the Lambda Cold Dark Matter model (ΛCDM). It is able to explain the evolution of the Universe from the initial moments after the Big Bang to the current observable Universe with all the structures present in it, such as galaxies, clusters, superclusters, etc. With an astonishing simplicity, since it only needs six free parameters, it allows us to explain most of the observables we have, like the Cosmic Microwave Background, the Baryonic Acoustic Oscillations or the Large Scale Structure. The concordance model bases its success in three pillars: General Relativity, the Cosmological Principle and a Dark Sector. The first pillar, General Relativity, has been tested up to Solar Scales, with Gravitational Waves and, recently with the shadow of black holes. On the other hand, the Cosmological Principle is tested above 100 Mpc. However, the Dark Sector was an ingredient added to explain observations like the accelerated expansion of the Universe or the rotational curves of galaxies, but its nature remains completely elusive for us.

In this chapter, we want to show the basics of this model. For this purpose, our first stop of the journey will be the assumptions and mathematical tools required. After it, we will present and deepen into the ΛCDM model, firstly its constituents, then its parameters. When the background theory has been explained, we will analyse the perturbation regime around it to finish with the main observables.

2.1 Assumptions, foundations and mathematical tools

Before delving into the concordance model of Cosmology, the first step in the amazing journey of understanding the whole Universe ought to be defining what is Cosmology itself and under which assumptions our concordance model should be relied

upon. After that, we need to explain the main concepts we will deal with, so we can finally focus on the standard cosmological model.

Cosmology is the scientific field inside physics knowledge which tries to study the Universe as a whole, focusing on its composition, origin, evolution, dynamics and final fate. Gravity is one of the main rulers of the Universe and, hence, the first pillar of our concordance model is General Relativity as the standard theory to describe the gravitational interaction.

General Relativity is the geometrical theory of Gravitation developed by Albert Einstein [1] in the early twentieth century, which explains the gravitational force as an intrinsic property of the space-time itself, related to its curvature[1]. The construction of General Relativity can be summarised as follows. We want an action principle from which we can derive the equations of motion for our field and such that it respects all the symmetries required. As we are dealing with gravity, the metric $g_{\mu\nu}$ is the field in our theory. In principle, we usually work with second-order theories described by a Lagrangian that, as typically, is of first-order. By general covariance, our symmetry here, we want to write the Lagrangian as an unknown scalar of the metric times the volume form. But the metric is a 2-covariant tensor, thus contracting the metric with a derivative to have a first-order Lagrangian will not give us a scalar and, therefore, we cannot construct a first order Lagrangian as we wished. Unavoidably, we need a second-order Lagrangian. Now, considering second derivatives and linearity in them, we can construct the Ricci scalar and, thus, our theory emerges from

$$S = \frac{1}{2N} \int_V R \sqrt{-g}\, \mathrm{d}^4 x \ , \tag{2.1}$$

where N is a certain normalisation factor, R is the Ricci scalar and $g_{\mu\nu}$ is the metric and g its determinant. There is one subtlety that, at the end, will be strongly relevant as we will see. One can always add a constant to the Lagrangian, there is nothing preventing us from doing it. Thus, in principle, it is allowed from the theoretical point of view. Also, if there is matter its corresponding Lagrangian should appear. Consequently, the full description of Gravity is

$$S = \frac{1}{2N} \int_V (R - 2\Lambda) \sqrt{-g}\, \mathrm{d}^4 x \ + \ S_\mathrm{m} \ , \tag{2.2}$$

where numerical factors have been chosen by convenience. At the moment, Λ is just a constant but we will see through this PhD dissertation its crucial significance. Also, S_m corresponds to the action of the matter fields in the Universe.

For the purposes of this thesis, we can condense the General Relativity Theory into the Einstein Field Equations, which are derived from the previous equation (2.2), encoding the relation between the space-time geometry and the matter content in it,

---

[1]Although equivalent formulations can be done relating the gravitational force to torsion or non-metricity [11].

as follows:

$$R_{\mu\nu} - \frac{1}{2}g_{\mu\nu}R + \Lambda g_{\mu\nu} = 8\pi G\, T_{\mu\nu}\ ,\qquad\qquad (2.3)$$

where $R_{\mu\nu}$ is the Ricci tensor, Λ will be called the Cosmological Constant, G the gravitational constant and $T_{\mu\nu}$ the stress-energy tensor, related to the previous S_{m}. Although later we will explain it in detail, as a brief introduction the left-hand side of the equation describes the shape of the space-time while the right-hand side the energy and matter living in that space-time. In equation (2.3), we named for the first time one of the two main ingredients of the concordance model, the Cosmological Constant Λ, which from General Relativity ought to be understood just as one of its parameters. As a historical curiosity, it was introduced by Einstein to counteract gravity in his pursuit of a static and closed Universe, which was how the Universe was though to be in those days. He supported its inclusion in General Relativity even when astronomical data started to suggest the Universe was not static but expanding. At the end, under the overwhelming evidence of the expansion of the Universe, he finally accepted Λ was not there, describing its inclusion in the field equations as "*the greatest blunder of his life*", as reported by physicist George Gamow in his autobiography [12]. The reason for that strong statement was that he could have predicted the expansion of the Universe with his theory more than a decade before observations did. Consequently, the question in that moment was posed: if the cosmological constant is allowed in the theory, why is it not really there? Nevertheless, in the late nineties the Supernova Search Team [13] and the Supernova Cosmology Project Collaboration [14] discovered the accelerated expansion of the Universe. In a Universe only filled with matter nothing can prevent gravity to gradually decelerate its expansion. Therefore, this unexpected discovery led to the revival of the Cosmological Constant as the leading force of such accelerated expansion. Since that moment, we are trying to discover the underlying nature of *the greatest blunder* of Albert Einstein. Unfortunately, Einstein passed away in 1955, being unable to see his Cosmological Constant was really there at the end[2].

The second assumption in the building process of the ΛCDM model is the Cosmological Principle. It states the Universe is spatially homogeneous and isotropic for cosmological scales, that is scales larger than $100\,\mathrm{Mpc}$. We must be aware that the typical size of a galaxy is $1\,\mathrm{kpc}$ and the average distance between two galaxies is $1\,\mathrm{Mpc}$, while the size of the observable Universe is of the order of $10\,\mathrm{Gpc}$. Then, the Cosmological Principle rules over very large scales of the Universe, indicating there is no special place in the Universe and that we should see no privileged direction in the sky. Moreover, the isotropy is extended to any observer due to the homogeneity and, therefore, the sky one sees is the same wherever one looks to and from wherever one looks. The inclusion of "spatially" is necessary as we know, and inexorably

---

[2]Maybe at the end Λ is not there and what we are seeing is something else dubbed as Dark Energy in the cosmologist community. Dark Energy is an extension of ΛCDM model where a new fluid, maybe a new field, an undiscovered interaction, the consequences of a breakdown of General Relativity or something else we cannot even imagine provokes the accelerated expansion of the Universe or maybe the accelerated expansion of our region of the Universe.

feel, time has a privileged direction[3]. Finally, we should remark, as a historical fact, that the Cosmological Principle evolves from the Copernican Principle, which states we live in no particular place of the Universe.

Combining the previous assumptions one can find a solution of the Einstein Field Equations which is usually called the Friedman-Lemaître-Robertson-Walker metric (FLRW). This is a family of metrics, which of course are isotropic and homogeneous, of the form

$$ds^2 = -dt^2 + a^2(t) \left(\frac{dr^2}{1 - kr^2} + r^2\,d\theta^2 + r^2\sin^2\theta\,d\phi^2 \right) , \tag{2.4}$$

where t is the cosmic time and r, θ and ϕ are the comoving coordinates. Cosmic time t is not the sole definition of time we use in Cosmology. In fact, we usually speak about conformal time τ, both times related by $dt = a\,d\tau$. Thus, using conformal time the FLRW metric is

$$ds^2 = -a^2(\tau)\,d\tau^2 + a^2(\tau) \left(\frac{dr^2}{1 - kr^2} + r^2\,d\theta^2 + r^2\sin^2\theta\,d\phi^2 \right) . \tag{2.5}$$

In equation (2.4) we have two key objects to describe the Universe, the scale factor $a(t)$ and the spatial curvature k, described as:

- Scale factor $a(t)$: it accounts for the expansion of the Universe and, generally, it is normalised to be one today as $a(t = t_0) = a_0 = 1$[4]. We can use the scale factor to define the expansion rate of the Universe as $H = \dot{a}/a$, whose current value is the Hubble constant $H_0 = H(t = t_0)$.

- Spatial curvature k: it encodes the curvature of the spatial part of the metric. When $k = -1$ we have negative curvature (open Universe), $k = 0$ no curvature (flat Universe) and $k = 1$ positive curvature (closed Universe), as shown in Figure 2.1.

With the previous FLRW metric the left-hand side of equation (2.3) is fully characterised. Therefore, we have to study the right-hand side which tells us about the energy and matter budget of the Universe. We can define the stress-energy tensor as

$$T_{\mu\nu} \equiv \frac{-2}{\sqrt{-g}} \frac{\delta S_{\mathrm{m}}}{\delta g^{\mu\nu}} , \tag{2.6}$$

where g is the determinant of the metric and S_{m} is the action of each component of the Universe. It is customary to describe the matter fields as fluids whose elements are described by a unitary time-like field u, which is the 4-velocity. In the most general case, we can write the stress-energy tensor as

$$T_{\mu\nu} = (\rho + p)\,u_\mu u_\nu + p g_{\mu\nu} + q_\mu u_\nu + q_\nu u_\mu + \Pi_{\mu\nu} , \tag{2.7}$$

---

[3]There was a time when the Universe was thought to satisfy the Perfect Cosmological Principle, that is, the Universe was homogeneous and isotropic both in time and space. But the Hubble expansion was discovered [15] and Big Bang was proposed by Georges Lemaître [16].

[4]We remind here that all quantities with a sub-index 0 refer to today.
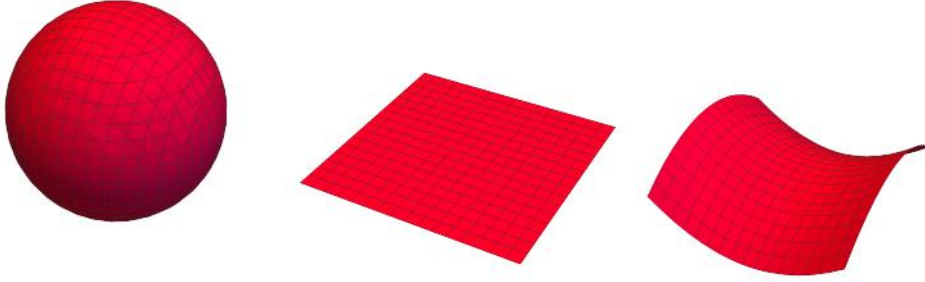
Figure 2.1: Geometries of the Universe according to their curvature k: closed Universe $k = 1$ (right), flat Universe $k = 0$ (centre) and open Universe $k = -1$ (left).

where ρ is the energy density, p the pressure, q_μ the heat flux and $\Pi_{\mu\nu}$ the anisotropic stress. Commonly, we work with no heat flux and no anisotropic stress, while we can relate the energy density and the pressure by an equation of state defined as $w \equiv p/\rho$. In that case, we are dealing with perfect fluids whose stress-energy tensor simply reads as

$$T_{\mu\nu} = (\rho + p)\, u_\mu u_\nu + p g_{\mu\nu}\,, \tag{2.8}$$

where u_μ is the 4-velocity of the fluid, which is $u_\mu = (1, 0, 0, 0)$ as we are in the comoving rest-frame in an isotropic and homogeneous Universe. Perfect fluids are expected to satisfy a conservation law of its stress-energy tensor $\nabla_\nu T^{\mu\nu} = 0$, which leads to the following conservation equation for the density evolution

$$\dot{\rho} + 3H(\rho + p) = 0\,. \tag{2.9}$$

We can characterise the different components of the Universe and its evolution according to the equation (2.9), provided we set the equation of state of each component. Thus, we can classify the energy budget of the Universe in three main categories, namely: matter, radiation and the Cosmological Constant. Each one has the following features:

- Matter: non-relativistic component of the Universe and, then, pressureless since $w = \frac{p}{\rho} \simeq \frac{T}{m} \ll 1$, thus one simply sets $w = 0$. From equation (2.9) one finds the solution $\rho \propto a^{-3}$. We are seeing nothing but matter energy density diluting with the volume of the expanding Universe as the scale factor a measures precisely the expansion, as illustrated in Figure 2.2.

- Radiation: relativistic component, similar to the Photon gas so we can model it with $w = \frac{1}{3}$. Solving equation (2.9) one finds it evolves as $\rho \propto a^{-4}$. The extra factor of the scale factor accounts for the dilution of the intrinsic wavelength as we are dealing with a relativistic component and then its energy is redshifted as $E \propto \frac{1}{\lambda} \propto \frac{1}{a}$.

11
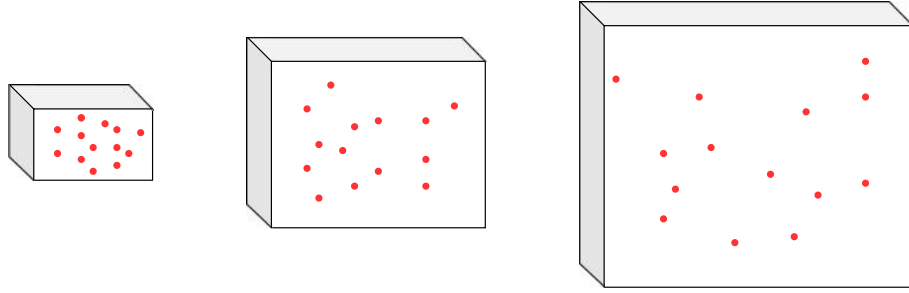
Figure 2.2: Schematic representation of the dilution of density of matter inside an expanding box of volume $V \propto a^3$. For radiation we should also take into account the dilution of its intrinsic wavelength.

- Cosmological constant: although we may argue Λ belongs to the geometric part of equation (2.3), it is completely equivalent to having an energy associated with the vacuum whose stress-energy tensor is $T_{\mu\nu} = -\frac{\Lambda}{8\pi G} g_{\mu\nu}$. In combination with the form of the stress-energy tensor for perfect fluids of equation (2.8), it naturally leads to $\rho = -p = \frac{\Lambda}{8\pi G}$, then in a cosmological fluid description its equation of state is $w = -1$. The name constant is perfectly reflected since from equation (2.9) we have $\dot{\rho}_\Lambda = 0$.

Once we have defined the geometric part of Einstein Field Equations via the FLRW metric and the energy/matter part via the stress-energy tensor, we can obtain the so-called Friedmann equations with the 0-0 and i-j components of Einstein Field Equations (2.3), leading to

$$\frac{\ddot{a}}{a} = -\frac{4\pi G}{3}(\rho + 3p) + \frac{\Lambda}{3} \, , \tag{2.10}$$

$$\left(\frac{\dot{a}}{a}\right)^2 = \frac{8\pi G\rho + \Lambda}{3} - \frac{k}{a^2} \, . \tag{2.11}$$

Finally, before delving into the concordance model, let us explain in some detail some concepts that will appear in next sections:

- Critical density ρ_{cr}: defined as $\rho_{\mathrm{cr}} = \frac{3H^2}{8\pi G}$. If the total density of the Universe is larger than the critical density we have a closed Universe, whereas the other way round it should be an open one. A Universe with the same density as the critical one is flat.

- Density parameter Ω: the energy density in units of the critical density ρ_{cr}, since $\Omega_i = \frac{\rho_i}{\rho_{\mathrm{cr}}}$. We can rewrite the Friedmann equations defining $\Omega_\Lambda \equiv \frac{\Lambda}{3H^2}$ and $\Omega_k \equiv -\frac{k}{H^2 a^2}$ as

$$\Omega_{\mathrm{k}} = 1 - \Omega \, . \tag{2.12}$$

- Redshift z: due to the expansion of the Universe the emitted wavelength λ_{e} will be shifted when observed λ_{o}. We can define the change of the wavelength with

the redshift due to the expansion as $z = \frac{\lambda_o - \lambda_e}{\lambda_e} = \frac{a_o}{a_e} - 1$. Then, provided we customarily set $a_0 = 1$, we have

$$a = (1 + z)^{-1}. \tag{2.13}$$

2.2 The ΛCDM model

As scientists, we usually tend to describe each area of physics by a standard or concordance model which should be able to describe all the physics involved. Or, in a more effective field perspective, all the physics involved in the relevant scales for the system under consideration. In the case of Cosmology, it is the Lambda Cold Dark Matter model (ΛCDM), which is considered by the cosmologist community as the concordance model because of its astounding capability of explaining the process of formation of structures from the very initial quantum fluctuation to the large scale structure we see today. This process extended for 13.8 billion years from the "*unique atom*"[5] until us, forcing the ΛCDM model, or any cosmological model, to be able to explain how a very non-structured, dense and hot Universe evolved during different cosmological eras until our current, structured, empty and cold Universe. Moreover, any cosmological model must be able to explain at the same time the extremely accurate observations we have today from a plethora of scales and times. In following sections, we will explain the foundational aspects of the Lambda Cold Dark Matter model and its astonishing capability of explaining almost everything of our elderly and vast Universe. We leave to Chapter 3 all the tensions, problems and disadvantages of the ΛCDM model, since that chapter will help us to motivate the search for new physics in the cosmological dynamics, which is the main aim of this PhD dissertation.

In the previous section, we explained how assuming General Relativity and the Cosmological Principle leads to a metric, called FLRW, which is able to describe the geometry of our Universe. Now, we should focus on the ingredients needed in our ΛCDM recipe of the Universe we live in. For the concordance model that recipe states the following constituents:

- Cosmological Constant: the perpetrator of the unexpected accelerated expansion of the Universe discovered in the late nineties. It is assumed to have an equation of state $w_\Lambda = -1$ leading to a negative pressure equal to minus its density $p_\Lambda = -\rho_\Lambda$ with a constant density parameter $\Omega_\Lambda(a) = \Omega_\Lambda$.

---

[5]In 1931, Georges Lemaître suggested in Ref. [16] the Universe should have started from an initial, unique and unstable atom with atomic weight as the total mass of the universe, which due to its instability will divide and divide into other atoms. Fred Hoyle called it jokingly Big Bang, a name that lasted until today although with a different meaning. Nowadays, Big Bang is thought to be the moment after inflation not that primordial atom.

- Cold Dark Matter: matter which only interacts gravitationally[6], hence it is neutral for the electromagnetic, weak nuclear and strong nuclear forces. It should cluster and be almost pressureless leading to an equation of state $w_{\mathrm{dm}} \simeq 0$. Solving equation (2.9), its fractional density should behave as $\Omega_{\mathrm{dm}}(a) = \Omega_{\mathrm{dm}} a^{-3}$.

- Baryons: here we refer to every type of matter described by the standard model of particle physics. Provided atomic nuclei are much more massive than Electrons, and Protons are the stable hadrons of the standard model of particle physics, the non-dark matter component of the Universe is mainly made up by Protons. Of course, it should cluster and be pressureless, which as before means non-relativistic matter. As before, its equation of state is $w_{\mathrm{b}} \simeq 0$ and, thus, its fractional density should evolve as $\Omega_{\mathrm{b}}(a) = \Omega_{\mathrm{b}} a^{-3}$.

- Radiation: we are dealing with a relativistic component which we can model using the Photon gas. Consequently, we have the Photon gas relation for the pressure and energy density $p_{\mathrm{r}} = \frac{1}{3}\rho_{\mathrm{r}}$, then its equation of state is $w_{\mathrm{r}} \simeq \frac{1}{3}$. Solving equation (2.9), the evolution of the radiation fractional density is given by $\Omega_{\mathrm{r}}(a) = \Omega_{\mathrm{r}} a^{-4}$.

Parameters of the concordance model

Once we have the ingredients, we can introduce the parameters of our concordance model. We can group the parameters involved in the concordance model in three different categories according to their role: free parameters, derived parameters and fixed parameters. The first group represents the minimum set of parameters required to explain all the observables we have, whose values will be determined by data. Only six parameters compose this group for the baseline model, although we can extend it allowing room for alternative models. From this previous group we obtain the derived parameters, which are completely determined once we have fitted the free parameters. Of course, we can interchange parameters between both free and derived groups since some of them are intrinsically related as we will see later. Finally, fixed parameters are set to a certain value due to the ΛCDM itself. Again, some extensions of the concordance model propose a different fixed value or even promoting certain parameters to the free parameters group.

As introduced before, the Lambda Cold Dark Matter model needs only six free parameters to fully explain all the observables we have from a wide range of scales and times. These free parameters are the fractional density today of Baryons and Cold Dark Matter denoted by Ω_{b} and Ω_{dm} respectively, the angular sound horizon scale at recombination θ_{s}, the primordial amplitude of scalar fluctuation A_{s} and the tilt of this initial power spectrum n_{s}; and the optical depth to reionization τ_{reio}. We summarise those parameters in Table 2.1 with the measured value by the Planck

---

[6]Among all the plethora of candidates of Dark Matter, some proposals like WIMPs (see Ref. [17] for a review) can interact weakly in addition to gravitationally.

Symbol	Description	Value from [5]
Ω_b	Baryon fractional density today	$\Omega_b h^2 = 0.02237 \pm 0.00015$
Ω_{dm}	Dark Matter fractional density today	$\Omega_{dm} h^2 = 0.1200 \pm 0.0012$
θ_s	Recombination angular scale	$100\theta_s = 1.04092 \pm 0.00031$
n_s	Spectral index of primordial fluctuations	0.9649 ± 0.0042
A_s	Primordial amplitude of scalar fluctuations	$\ln(10^{10} A_s) = 3.044 \pm 0.014$
τ_{reio}	Optical depth	0.0544 ± 0.0073

Table 2.1: The six free parameters of the concordance model, named Λ Cold Dark Matter model, with the measured value by the Planck experiment [5].

Symbol	Description	Value from [5]
H_0	Hubble parameter	$67.36 \pm 0.54 \ \mathrm{Km \ s^{-1} \ Mpc^{-1}}$
t_0	Age of the Universe	$13.797 \pm 0.023 \ \mathrm{Gyr}$
Ω_m	Total matter fractional density today	0.3153 ± 0.0073
Ω_Λ	Cosmological cta. fractional density today	0.6847 ± 0.0073
σ_8	Amount of clustering	0.8111 ± 0.0060
S_8	Amount of clustering	0.832 ± 0.013
z_{reio}	Reionization redshift	7.67 ± 0.73

Table 2.2: Derived parameters parameters of the concordance model, named Λ Cold Dark Matter model, with the measured value by the Planck experiment [5].

experiment [5] using the Cosmic Microwave Background. The previous set of parameters represents the minimum array of parameters needed to explain the data, but of course there are more parameters that contain valuable cosmological information For example, the so-called derived parameters, which once data have set the free parameters to certain values they will get fixed. In this group, we can highlight the current expansion parameter H_0 (also called Hubble constant), the age of the Universe t_0, the total current fractional density of matter Ω_m and of the Cosmological Constant Ω_Λ, the root mean square of matter fluctuation on spheres of $8h^{-1}$ Mpc radii denoted by σ_8 (or equivalently the parameter S_8) and the redshift of reionization z_{reio}. In Table 2.2, we summarise most of previous parameters with their value from the Planck experiment [5]. Finally, we have the so-called fixed parameters, representing those set to a certain and unique value by the ΛCDM model itself, although some extensions may give freedom to them. For example, we have the Dark Energy equation of state w, whose value is fixed to $w = -1$, or the spatial curvature of the Universe, fixed to $k = 0$. In this group, we gather the most important ones in Table 2.3 with the fixed value and some typical extensions.

To conclude, we want to explain the information each parameter carries and how they are related or derived according to the ΛCDM model, something we schematically present in Figure 2.3. Then we have:

Symbol	Description	fixed value
w	Λ equation of state	-1 typical extension: $w \in [-1, -1/3]$
k or Ω_{k}	Flat Universe	0
Ω	Total amount of matter today	1
N_{eff}	Relativistic d.o.f	3.046
$\sum m_\nu$	Massive Neutrinos	0 typical extension: $m_\nu = 0.06$ eV
T_0	CMB temperature	2.72548 ± 0.00057 K [18]

Table 2.3: List of fixed parameters in the ΛCDM model and values for typical extensions of ΛCDM.

- Hubble parameter and related quantities: the Hubble function $H(a) = \frac{\dot{a}}{a}$ measures the expansion of the Universe, then its current value is the Hubble parameter H_0. In certain situations, we prefer to use the reduced Hubble parameter h given by $H_0 = h\,100$. Moreover, we can also use the function $E(a)$, which is just defined as $E(a) \equiv \frac{H(a)}{H_0}$. Following the Friedmann equation (2.11), the Hubble function for the ΛCDM model is

$$H = H_0 \sqrt{\Omega_\Lambda + \Omega_{\mathrm{b}} a^{-3} + \Omega_{\mathrm{dm}} a^{-3} + \Omega_{\mathrm{r}} a^{-4}} \, . \tag{2.14}$$

From the very definition of the Hubble function $H(a) = \frac{1}{a}\frac{\mathrm{d}a}{\mathrm{d}t}$, one can easily relate it to time, then we have

$$t(a) = \int_0^a \frac{\mathrm{d}\bar{a}}{a H(\bar{a})} \, , \tag{2.15}$$

and, thus, the age of the Universe t_0 arises from $t_0 \equiv t(a = 1)$.

The angular scale of the comoving sound horizon at recombination θ_{s} measures the ratio between the sound horizon scale at last scattering r_{s} and the comoving angular diameter distance to last scattering D_A[7] as

$$\theta_{\mathrm{s}} = \frac{r_{\mathrm{s}}}{D_A(z_{\mathrm{s}})} \, , \tag{2.16}$$

where $z_{\mathrm{s}} \simeq 1100$ is the redshift of the last scattering surface and the angular distance is defined as

$$D_A(z) = \frac{1}{H_0(1+z)} \int_0^z \frac{\mathrm{d}\bar{z}}{E(\bar{z})} \, , \tag{2.17}$$

as explained in Appendix B.

---

[7]Consider a non-pointlike object with scale r in the sky that we need to cover all its amplitude (from extreme to extreme) an angle θ. One wants to calculate the distance from us to one of its extremes, that we call angular distance D. Provided objects in the Universe are very far away from us, we should see a small θ and, hence, the relation $\theta \simeq r/D$ holds.

- Cosmological constant related quantities: we can describe Λ by its fixed equation of state $w_\Lambda = -1$ and its fractional density today, whose value according to Planck 2018 experiment [5] is $\Omega_\Lambda = 0.6847 \pm 0.0073$. This result indicates that almost seventy percent of our current Universe is composed by an unknown component which we cannot measure in our laboratories and whose nature is a mystery to us.

- Fractional densities today Ω_i: in this group we have the Baryon Ω_b and Cold Dark Matter Ω_{dm} fractional densities as free parameters, the total matter Ω_m and the Cosmological Constant one Ω_Λ as derived parameters. They usually appear in the literature related to the reduced Hubble parameter as $\Omega_i h^2$ to avoid a degeneracy[8]. Commonly, one sets as free parameters to be fixed by data $\Omega_{dm} h^2$ and $\Omega_b h^2$ and, since the concordance model establishes the Universe is flat $k = 0$ ($\Omega_k = 0$), thus $\Omega = 1$, one can obtain the derived fractional densities as

$$\Omega_m = \Omega_{dm} + \Omega_b \,, \tag{2.18}$$

$$\Omega_\Lambda = 1 - \Omega_m - \Omega_r \,. \tag{2.19}$$

- Radiation related quantities: in this sector we have both Photons and Neutrinos. Despite the fact both are hot components of the Universe, that is relativistic components, they do not have the same evolution history. Firstly, Photons are massless particles but Neutrinos have mass[9]. As a consequence, Neutrinos become non-relativistic at some moment of the evolution history. Secondly, they decoupled at different epochs, therefore they are not affected by the same processes, for example the Electron-Positron annihilation into Photons increasing their density and, consequently, their temperature. Finally, they are not the same type of particles, Photons are bosons and they have only one family while Neutrinos are fermions with three different families according to the standard model of particles physics. Consequently, we study them separately:

  - Photons: with them it is customary to work with their temperature instead of the fractional density. The temperature of the Cosmic Microwave background, that is photons, is measured to be $T_0 = 2.72548 \pm 0.00057$ K [18]. By the Stefan-Boltzmann law we can relate the temperature and the density at any moment by

$$\rho_\gamma = \frac{\pi^2}{30} g \, T^4 \,, \tag{2.20}$$

---

[8]Consider an experiment that measures the Hubble function, which we know is $H \propto H_0 \sqrt{\sum_i \Omega_i(a)}$. Having the density parameters Ω_i a factor n^2 larger while having the Hubble constant H_0 a factor n smaller will give the same result for the Hubble function as with the original values of Ω_i and H_0, according to that experiment. Then, unless we have another experiment which can measure Ω_i and/or H_0 independently, usually called braking the degeneracy, we should use as parameters $\Omega_i h^2$ in order to avoid a biased result due to the explained degeneracy.

[9]In fact, the non-conservation of Neutrino flavour, so-called Neutrino oscillations, provides a strong proof for massive Neutrinos as it has been detected by several experiments from nuclear reactor experiments (e.g [19]), atmospheric experiments (e.g [20]) or solar physics experiments (e.g [21]).

with $g = 2$ as we have two Photon helicities, and one can recover the fractional density of Photons today as $\Omega_\gamma = \frac{\rho_{\gamma 0}}{\rho_{cr0}}$.

– Neutrinos: ΛCDM model does not contain massive Neutrinos and, therefore, we can model them as Photons in principle. However, we have to take into account they are fermions not bosons, the 3 generations of Neutrinos and absence of Electron-Positron annihilation[10]. Then, the Neutrino density is

$$\rho_\nu = 3\frac{7}{8}\left(\frac{4}{11}\right)^{4/3}\rho_\gamma \ , \tag{2.21}$$

and we can recover its fractional density today as $\Omega_{\nu 0} = \frac{\rho_\nu}{\rho_{cr0}}$. A very classic extension of the concordance model consists in adding one massive Neutrino, usually with mass $m_\nu = 0.06$, thus its fractional density today can be described by

$$\Omega_\nu = \frac{m_\nu(eV)}{94h^2\ eV} \ . \tag{2.22}$$

With the previous information about Photons and Neutrinos, one would naively consider that the radiation sector is described by a total energy density of the form

$$\rho_{\rm r} = \rho_\gamma\left[1 + 3\frac{7}{8}\left(\frac{4}{11}\right)^{4/3}\right] \ . \tag{2.23}$$

However, this is not true as we have to take into account the non-instantaneous decoupling of Neutrinos and the non-equilibrium corrections from early radiation dominated Universe. To account for it, we use the parameter $N_{\rm eff}$ as the effective number of relativistic degrees of freedom, inducing a correction of the form

$$\rho_{\rm r} = \rho_\gamma\left[1 + N_{\rm eff}\frac{7}{8}\left(\frac{4}{11}\right)^{4/3}\right] \ , \tag{2.24}$$

with $N_{\rm eff}$ fixed to $N_{\rm eff} = 3.046$, which accounts for all the previous deviations.

• Reionization parameters: when the first stars and quasars emerged they reionized the cosmic medium. We encode this process by the redshift when the Universe reionizes $z_{\rm reio}$ and the probability of a Photon being scattered between a past time and today, usually called optical depth $\tau_{\rm reio}$, defined as

$$\tau_{\rm reio} = \int_\tau^{\tau_0} n_e\,\sigma_{\rm T}\,a\,d\bar{\tau} \ , \tag{2.25}$$

where n_e is the Electron number density, $\sigma_{\rm T}$ is the Thomson cross-section and τ is the conformal time.

---

[10]The Electron-Positron annihilation provokes an increase of the Photon temperature, but as Neutrinos are decoupled from them they evolve independently. This leads to the following relation between Photon and Neutrino temperatures $\frac{T_\nu}{T_\gamma} = \left(\frac{4}{11}\right)^{1/3}$.
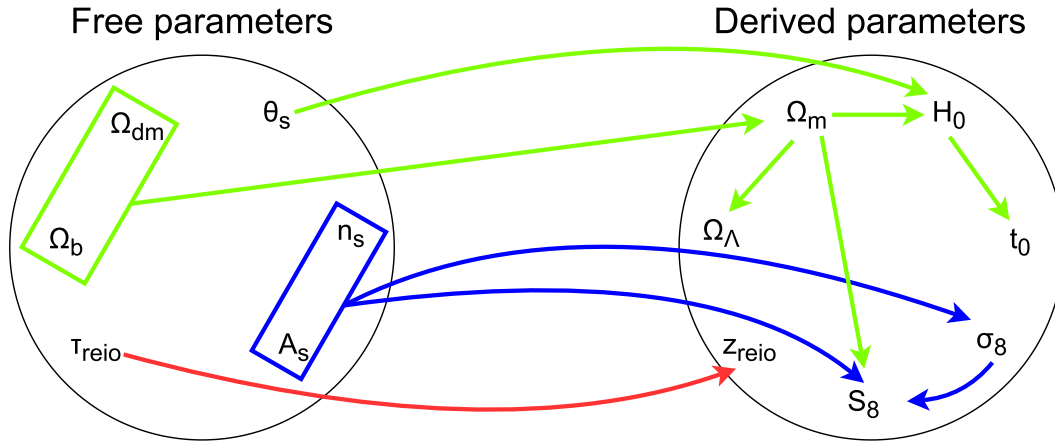
Figure 2.3: Main relations between free and derived parameters within the ΛCDM model. Green lines represent background relations, blue lines account for information from the perturbation sector while red line from reionization process.

- Primordial spectrum quantities: the primordial perturbations in the very early Universe are assumed to be adiabatic and mostly scalar. Simplest, but yet accurate, inflationary models suggest they can be described by an almost scale-invariant primordial spectrum of the form

$$P_{\mathrm{s}} = A_{\mathrm{s}} \left(\frac{k}{k_p} \right)^{n_{\mathrm{s}} - 1} , \qquad (2.26)$$

where k_p is the pivot scale. Consequently, A_{s} encodes the amplitude of scalar primordial perturbations while the spectral index n_{s} establishes the spectral tilt of such a initial spectrum.

- Parameters measuring clustering: both σ_8 and S_8 measure the amount of structures formed today inside certain scales. Specifically, σ_8 is defined as the root mean square of density fluctuations inside spheres of radius of $8h^{-1}\,\mathrm{Mpc}$ when using a top-hat filter

$$\sigma_8^2 = \frac{1}{2\pi^2} \int W_{\mathrm{s}}^2 \, k^2 \, P(k) \, \mathrm{d}k \qquad (2.27)$$

with W_{s} the top-hat filter function and $P(k)$ the Matter Power Spectrum[11]. However, as already explained with Ω_{i} and H_0, some experiments are not sensitive independently to σ_8 but a degeneration with Ω_{m} emerges. To avoid it, the parameter S_8 was defined as $S_8 \equiv \sigma_8 \left(\frac{\Omega_{\mathrm{m}}}{0.3} \right)^{0.5}$, following the direction of degeneracy in weak lensing measurements. As before, it is convenient to work with S_8 although other cosmological probes can break the degeneracy.

---

[11]Explained in Section 2.4.

19

2.3 Perturbations: from initial seeds to structures

So far our cornerstone was the isotropy and homogeneity of the Universe. Although that is an extremely good assumption for investigating the Universe as a whole, we know our Universe is not perfectly homogeneous nor isotropic. In fact, wherever we look in our local Universe we see structures in the form of planets, stars, galaxies, cluster, etc. Thus, the current Universe is not perfectly homogeneous. Also isotropy is broken around us. For example, we are moving toward the constellation of Leo, that is, we have a preferred direction. At the end, we are seeing nothing but the break of the symmetries of the Cosmological Principle for small scales[12].

As almost everything in physics this is an issue of scales, in this case a matter of spatial scales. When we look at scales larger than 100 Mpc we are under the mandate of the Cosmological Principle [22, 23]. When we consider smaller scales the Cosmological Principle is dethroned and we enter in the realm of perturbations. We see around us structures in several ways below 100 Mpc. The first question one may ask is where these structures have come from. The second is how they have evolved. Consequently, in this section we want to briefly explain how the very small, very early and very quantum initial perturbations evolved until forming the current lumpy Universe. The formalism for this purpose is called linear theory of scalar cosmological perturbations and, schematically, it describes the competition between gravitational instability leading to the collapse and pressure preventing it. We will focus only in scalar perturbations as they will be the ones used during this thesis. Also, we will remain in the linear regime as for most of the evolution and the scales of our Universe perturbations were small enough to be considered linear. However, we will devote a section of this thesis to non-linear regime and how the perturbations should be treated. Before starting that journey, we need to get the tools needed to work with perturbations.

Mathematical tool: metric perturbations and gauge

Following the same agenda as for the background, we first want to study the permutations in the space-time geometry, that is the left-hand side of equation (2.3). The geometry was set by the metric, in our case the Friedman-Lemaître-Robertson-Walker (FLRW) metric, then this is our first step.

Considering the general FLRW metric defined by the scale factor a in comoving coordinates x^i and conformal time τ

$$\mathrm{d}s^2 = -a^2(\tau)\,\mathrm{d}\tau^2 + a^2(\tau)\delta_{ij}\,\mathrm{d}x^i\mathrm{d}x^j \,, \tag{2.28}$$

---

[12]From a more philosophical and anthropic point of view, we all are the sons of the inhomogeneities since we would not be here to study the cosmos if the Universe were perfectly homogeneous and isotropic.

the most general perturbed definition of the FLRW metric can be written as

$$\mathrm{d}s^2 = -a^2(1+2A)\,\mathrm{d}\tau^2 + 2a^2 B_i\,\mathrm{d}x^i\mathrm{d}\tau + a^2\left[(1-2C)\delta_{ij} + \chi_{ij}\right]\mathrm{d}x^i\mathrm{d}x^j \ , \tag{2.29}$$

where A, B_i, C and χ_{ij} are general functions of time and space. Provided in the scalar-vector-tensor decomposition each type of perturbation does not mix with the others at linear order when studying their evolution, we can split B_i and χ_{ij} as

$$
\begin{aligned}
B_i &= \partial_i B + \hat{B}_i \ , \tag{2.30}\\
\chi_{ij} &= 2\partial_{[i}\partial_{j]}E + 2\partial_{(i}\hat{E}_{j)} + 2\hat{E}_{ij} \ , \tag{2.31}
\end{aligned}
$$

with $\hat{B}_i$ and $\hat{E}_i$ divergenceless $\partial^i\hat{B}_i = \partial^i\hat{E}_i = 0$ and $\hat{E}_{ij}$ divergenceless and traceless, $\partial^i\hat{E}_{ij} = 0$ and $\hat{E}^i_i = 0$. Then, we have ten degrees of freedom. However, we have not uniquely defined the metric perturbations as we need to fix the gauge to have the six degrees of freedom needed. In this thesis, we will mainly work with scalar perturbations and in the following gauges:

- Newtonian gauge: the perturbations are characterised by only two scalars Ψ and Φ, with Ψ being the gravitational potential in the Newtonian limit, such that
$$\mathrm{d}s^2 = -a^2(1+2\Psi)\,\mathrm{d}\tau^2 + a^2(1-2\Phi)\delta_{ij}\,\mathrm{d}x^i\mathrm{d}x^j \ . \tag{2.32}$$

- Synchronous gauge: we can define comoving observers with synchronous time, then perturbations are characterised by
$$\mathrm{d}s^2 = -a^2\,\mathrm{d}\tau^2 + a^2(\delta_{ij} + h_{ij})\,\mathrm{d}x^i\mathrm{d}x^j \ . \tag{2.33}$$

- Spatially-flat gauge: extremely useful when dealing with inflation, defined by
$$\mathrm{d}s^2 = -a^2(1+2A)\,\mathrm{d}\tau^2 + 2a^2 B_i\,\mathrm{d}x^i\mathrm{d}\tau + a^2\delta_{ij}\,\mathrm{d}x^i\mathrm{d}x^j \ . \tag{2.34}$$

Mathematical tool: matter perturbations and gauge

Once we have perturbed the space, inexorably we have to perturb the matter in it. For that purpose, we need to calculate the linear perturbations of the stress-energy tensor in the Newtonian and Synchronous gauges. Considering the stress-energy tensor $T_{\mu\nu}$ for a perfect fluid previously shown in equation (2.8)

$$T_{\mu\nu} = (\rho + p)\,u_\mu u_\nu + p g_{\mu\nu} \ , \tag{2.35}$$

if we consider perturbations of the perfect fluid as

$$
\begin{aligned}
\rho(\tau) &\rightarrow \rho(\tau) + \delta\rho(\vec{x}, \tau) \ , \tag{2.36}\\
p(\tau) &\rightarrow p(\tau) + \delta p(\vec{x}, \tau) \ , \tag{2.37}\\
u_\mu &\rightarrow u_\mu + \delta u_\mu(\vec{x}, \tau) \ , \tag{2.38}
\end{aligned}
$$

then the stress-energy tensor up to linear order $T^\mu{}_\nu \to T^\mu{}_\nu + \delta T^\mu{}_\nu$ has the following components:

$$\delta T^0{}_0 = -\delta\rho \,, \tag{2.39}$$

$$\delta T^0{}_i = -\delta T^i{}_0 = (\rho + p)\, v_i \,, \tag{2.40}$$

$$\delta T^i{}_j = \delta p\, \delta^i{}_j + \Sigma^i{}_j \,, \tag{2.41}$$

where ρ and p are the background density and pressure, v_i is the perturbed velocity defined as $v_i \equiv \frac{\mathrm{d}x_i}{\mathrm{d}\tau}$ and $\Sigma^i{}_j$ is the anisotropic shear perturbation, which satisfies $\Sigma^i{}_i = 0$.

Now we have all the tools to obtain and derive the linear theory of cosmological perturbations but, however, there would be no structures today without an initial seed. Then, in the very early Universe there should be a mechanism generating some kind of fluctuations and, at the same time, promoting them to the seeds of all the structures we see today in the Universe.

Inflation

When dealing with perturbations we cannot omit saying a few words about inflation as the underlaying thought phenomena giving birth to them. Before that, we may ask where does inflation come from as a theory. The answer is the horizon and the flatness problem. Regarding horizon problem, we see for example in the Cosmic Microwave Background areas that were not in causal contact at any moment, but they are now in thermodynamic equilibrium. In fact, having the same temperature in all the Cosmic Microwave Background cannot be explained naturally. On the other hand, the flatness problems relates to the fact that the total energy density is extremely close to the critical one, making the Universe flat. But, this extremely similar value should have been like that from the very early Universe or, otherwise, we could see certain departures with cosmic evolution.

Consequently, inflationary paradigm comes as a natural solution to both issues. It postulates that the Universe went through a brief but intense phase of exponential expansion in its very first moments. Because of that, what we consider our Universe was actually in that moment a small patch, which was small enough to have achieved both a thermal equilibrium and a curvature extremely close to zero due to its smallness. In its simplest form, inflation is conducted by the inflaton scalar field $\phi(t)$ which can only depend on time by the virtue of the Cosmological Principle. Given a standard scalar field, its density and pressure are simply

$$\rho_\phi = \frac{1}{2}\dot{\phi}^2 + V(\phi) \,, \tag{2.42}$$

$$p_\phi = \frac{1}{2}\dot{\phi}^2 - V(\phi) \,, \tag{2.43}$$

$$w_\phi = \frac{p_\phi}{\rho_\phi} \,. \tag{2.44}$$

Therefore, to have the inflationary paradigm we need that the potential energy dominates over the kinetic one, that is, we need the field to slow roll, so we have $w_\phi \to -1$ and, thus, expansion due to the inflaton field happens. However, to have the Universe with the structures we see today, ϕ cannot be slowly rolling perennially but it will reach at a certain moment to the bottom of the potential and oscillate around it, presumably generating the standard model particles in a process called reheating. For the purposes of the following derivations, there are certain consequences from standard inflation that we are interested in:

- Primordial perturbations have to be mainly adiabatic, gaussian and isotropic.

- The curvature perturbation $\mathcal{R}$ is conserved outside the horizon.

- Primordial perturbations spectrum should be close to a Harrison–Zeldovich one, that is, a scale invariant spectrum.

Where does the initial fluctuation come from?

As this PhD dissertation is not devoted to early Universe physics, we will only explain schematically how the initial seeds were created to, after it, focus on the evolution of such initial seeds into the structures we see today.

Consider a perturbation of comoving scale k^{-1} and the comoving Hubble horizon defined by $(aH)^{-1}$, whose evolution is symbolically represented in Figure 2.4 where the y-axis represents comoving scales and the x-axis time. In the very early Universe, we have inflation which in its simplest but yet accurate version is characterised by the inflaton field ϕ. This inflaton field should have some fluctuations[13] that, again in the simplest form, we characterise by $\delta\phi$ that depends on both time and space. Those perturbations were initially inside the horizon, but due to inflation itself they exit the horizon at a moment. When each mode k exits the horizon we can describe the perturbations $\delta\phi$ by the curvature perturbations $\mathcal{R}$[14]. It is a known result that appears in almost each Cosmology book (see for example [25]) that the relation between the inflaton fluctuations $\delta\phi$ and the curvature perturbations $\mathcal{R}$ in the spatially-flat gauge is

$$\mathcal{R} = -\frac{\mathcal{H}}{\phi'}\delta\phi \, . \tag{2.45}$$

We are interested in computing the variance of such perturbations, as that is the power spectrum which is formally defined for a quantity $a(\vec{k})$ as

$$\langle a(\vec{k})\, a^*(\vec{k'})\rangle = (2\pi)^3 P_a(k)\, \delta^3(\vec{k} - \vec{k'}) \, . \tag{2.46}$$

---

[13]In some sense, we are just the sons of the Uncertainty Principle postulated by Werner Heisenberg in his original paper [24], as all the current structures we see today have their origin in the initial perturbations in the early Universe, which belong to the quantum regime.

[14]The interpretation of $\mathcal{R}$ as a curvature perturbation can only be done in the comoving gauge. However, $\mathcal{R}$ is a gauge invariant quantity and, therefore, its meaning is preserved in any other gauge we may consider.
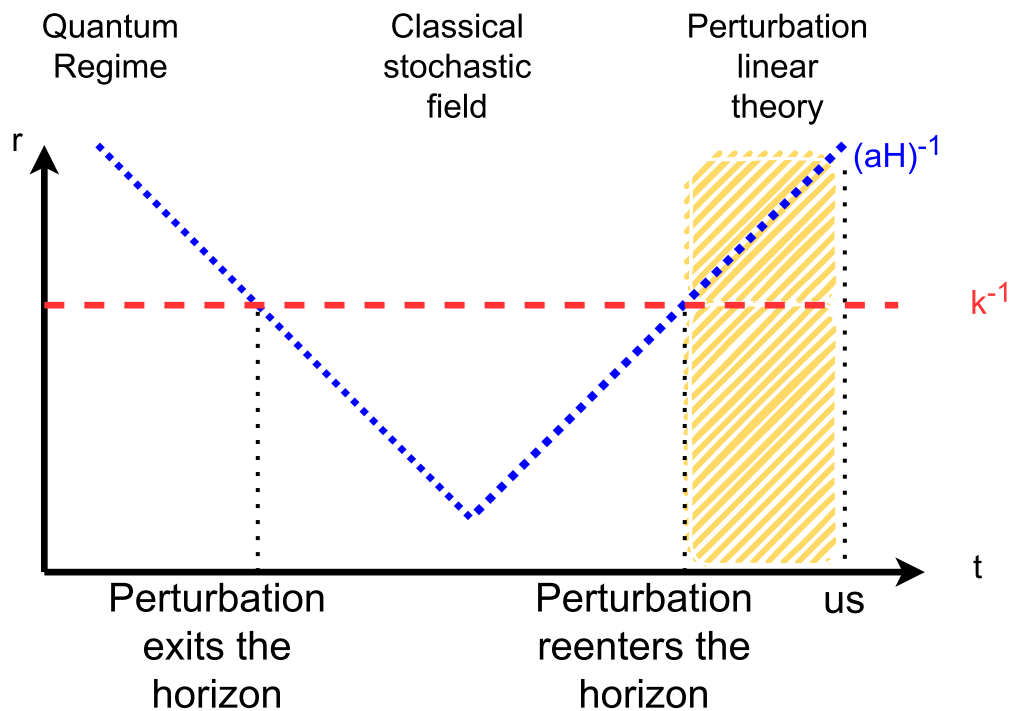
Figure 2.4: Schematic evolution of a perturbation compared to the horizon and the respective theory to study each regime.

Therefore, we simply have the following relation between the power spectrum of the very primordial quantum fluctuations of the inflaton field ϕ and the power spectrum of the curvature perturbation $\mathcal{R}$, that will be the initial conditions for the perturbation theory, as

$$P_{\mathcal{R}} = \left(\frac{\mathcal{H}}{\phi'}\right)^2 P_{\delta\phi} , \qquad (2.47)$$

which for scalar and adiabatic perturbations with a slow-roll inflation description one simply recovers the nearly scale-invariant primordial spectrum explained before in equation (2.26). However, this last sentence represents an enormous leap divided into two steps. First, we are assuming the inflaton field, which is intrinsically quantum, can be now described by a classical stochastic field represented by the curvature perturbation. This is provided by the horizon exit. Second, this power spectrum $P_{\mathcal{R}}$ is calculated for each mode k precisely when it exits the horizon, but the initial conditions for our perturbation linear theory have to be applied when each mode reenters the horizon. Then, connecting both times is only allowed by the conservation of the perturbations outside the horizon. As already mentioned, these two steps are well known results that appear in every Cosmology book and they are uncorrelated to the topics of this thesis, because of that we only mentioned them here without demonstrating.

Evolution of perturbations

Now, our purpose is to exhibit the formalism of how those perturbations evolved from when they reentered until us, which corresponds to the yellow region of the schematic Figure 2.4. Here, we will only consider the linear regime and scalar perturbations.

As done for the background, let us consider a cosmological perfect fluid described by its perturbed stress-energy tensor of the form $T_{\mu\nu} + \delta T_{\mu\nu}$. When in the previous section we applied the conservation of the stress-energy tensor $\nabla_\nu T^{\mu\nu} = 0$, we obtained the background continuity equation for the $\nu = 0$ component, depicted in equation (2.9), while the $v = i$ component was identically zero provided the definition of the 4-velocity. Now this is no longer true. The perturbed 4-velocity is

$$u^\mu = \left(\frac{1-\Psi}{a}, \frac{\vec{v}}{a} \right) \qquad \text{Newtonian gauge}, \qquad (2.48)$$

$$u^\mu = \left(\frac{1}{a}, \frac{\vec{v}}{a} \right) \qquad \text{Synchronous gauge}, \qquad (2.49)$$

with the 3-velocity defined as $\vec{v} \equiv \frac{\mathrm{d}\vec{x}}{\mathrm{d}\tau}$ in each gauge with the respective spatial coordinates. Before applying the conservation law, we have to set the dictionary of the linear theory of cosmological perturbations. It is customary to work with the density contrast δ and the velocity divergence θ instead of the density and velocity perturbation, both defined as

$$\delta = \frac{\delta\rho}{\rho}, \qquad (2.50)$$

$$\theta = i\vec{k} \cdot \vec{v}, \qquad (2.51)$$

where θ is defined in the Fourier space. Also, given the properties of the anisotropic shear perturbation Σ^i_j, we can define in Fourier space the following variable encoding the anisotropic stress perturbations $\sigma = -(k_i k_j - \frac{1}{2}\delta_{ij})\Sigma^i_j$. It is also preferred to use the equation of state w instead of the pressure p. Finally, as done with the equation of state which relates the density and the pressure, we have for the perturbations the sound speed, defined as

$$c_{\mathrm{s}}^2 = \left. \frac{\delta p}{\delta\rho} \right|_{restframe}, \qquad (2.52)$$

in the rest frame of the fluid to be gauge invariant. We can also define the adiabatic sound speed of the fluid as

$$c_{\mathrm{a}}^2 = \frac{p'}{\rho'} = w + \rho \frac{\mathrm{d}w}{\mathrm{d}\rho}, \qquad (2.53)$$

both being related in an arbitrary frame by [26]

$$\delta p = c_{\mathrm{s}}^2 \, \delta\rho + 3 \frac{\mathcal{H}(1+w)(c_{\mathrm{s}}^2 - c_{\mathrm{a}}^2)\, \rho\, \theta}{k^2}. \qquad (2.54)$$

25

Thus, applying the conservation of the perturbed stress-energy tensor, we obtain the following system of equations in the Newtonian Gauge

$$\delta' \;=\; -3\mathcal{H}\,(\frac{\delta p}{\delta \rho} - w)\,\delta - (1+w)\,\theta + 3(1+w)\,\Phi' \,, \tag{2.55}$$

$$\theta' \;=\; -\mathcal{H}\,(1-3w)\,\theta - \frac{w'}{1+w}\,\theta + \frac{\frac{\delta p}{\delta \rho}k^2}{1+w}\,\delta - k^2\sigma + k^2\Psi \,. \tag{2.56}$$

If we consider the Synchronous gauge, the previous system of differential equations reads as

$$\delta' \;=\; -3\mathcal{H}\,(\frac{\delta p}{\delta \rho} - w)\,\delta - (1+w)\,\theta - (1+w)\,\frac{h'}{2} \,, \tag{2.57}$$

$$\theta' \;=\; -\mathcal{H}\,(1-3w)\,\theta - \frac{w'}{1+w}\,\theta + \frac{\frac{\delta p}{\delta \rho}k^2}{1+w}\,\delta - k^2\sigma \,. \tag{2.58}$$

The previous equations should be adapted to each component of the Universe as follows:

- Dark Energy sector: for the Cosmological Constant Λ one sets the equation of state to $w = -1$ and $w' = 0$. If we consider a general Dark Energy fluid, one has $w = w(z) \neq -1$, while one may or not change also the sound speed but preserving $c_{\rm s}^2 \gg 0$ or otherwise it will cluster.

- Cold Dark Matter: given it is cold, that is, non-relativistic, one has $w \simeq 0$ and $w' \simeq 0$. As it clusters $c_{\rm s}^2 \simeq 0$ and one typically sets $\sigma = 0$. In the synchronous gauge, Cold Dark Matter particles are used to define synchronous observers, provided that if one sets $\theta(\tau_{\rm ini}) = 0$ it satisfies $\theta(\tau) = 0$ for any time.

- Baryons: also non-relativistic matter, then $w \simeq 0$, $w' \simeq 0$, $c_{\rm s}^2 \simeq 0$ and, again, one typically sets $\sigma = 0$. In the case of Baryons, there should be an additional term in the Euler equation due to the Thomson scattering with Photons as

$$\theta'_{\rm b} = -\mathcal{H}\theta_{\rm b} + \Gamma_{\rm T}(\theta_\gamma - \theta_{\rm b}) \,, \qquad \Gamma_{\rm T} \equiv \frac{4\rho_\gamma}{3\rho_{\rm b}}a n_e \sigma_{\rm T} \,, \tag{2.59}$$

  with n_e the abundance of free Electrons and $\sigma_{\rm T}$ the Thomson scattering cross section.

- Photons and Neutrinos: for the previous cases, Dark Matter, Baryons and Dark Energy, only having the first two equations for δ and θ was enough as they were non-relativistic. But now both have a relativistic nature during all (photons) or a large part of the cosmic evolution (neutrinos). Therefore, its description requires a differential equation for δ, a differential equation for θ and an infinite hierarchy of moment equations, for which we refer to classical papers like [27].

2.4 Cosmological observables

In the previous sections, we have introduced the model to describe the Universe on cosmological scales and up to first order in perturbation theory. However, theory without observations is empty space and, thus, we should now focus our attention on the observations that led to the establishment of the theoretical frame. Here, we will explain those which stand out among the plethora of observables by their enormous importance or by the utility in this thesis.

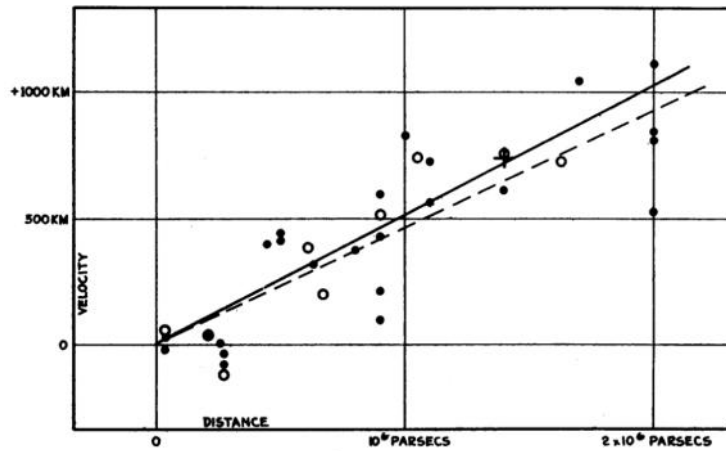**Expansion of the Universe**

Figure 2.5: Iconic figure from the original paper [15] where Edwin Hubble first discovered the relation between velocity (redshift) and distance.

In March 1929, Edwin Hubble published in the Proceedings of the National Academy of Sciences journal a paper [15] which stands as the first milestone of Modern Cosmology[15]. It left us for the eternity the Figure 2.5. Hubble proposed and measured using cepheids a proportionality factor between the distance island universes[16] were and the velocity they moved away from us. Modern measurements make use of the fact that spectral lines of galaxies are redshifted, that by the very definition of redshift can be written as

$$z = H_0 \, d \, , \tag{2.60}$$

where z is the redshift, H_0 is the Hubble constant and d is the distance to the galaxy. For the very local Universe $z \ll 1$, this can be interpreted as the Doppler effect of galaxies receding from us and, thus, $z \simeq v$. Spectral lines are relatively easy to

---

[15]It would be fair to also comment about the fact that Georges Lemaître published before this relation but in a french-tongue small journal and, when translating this part for the Royal Society, he omitted it as more recent and accurate results appeared in the meanwhile. Also, the work of Henrietta Leavitt on cepheids was essential for this discovery.

[16]At that time, there was a discussion on whether the nebulae or island universe were part of our galaxy or new galaxies.

measure, but not the distance. For measuring distance we have to resort to the so-called cosmic ladder. That means using overlapping measurement on redshift scales to calibrate the next observable. Also the definition of distance in Cosmology is not unique as we can see in Appendix B.

The most recent observations correspond to $H_0 = 73.04 \pm 1.04$ by Ref. [28] using the cosmic ladder for the local Universe, while to $H_0 = 67.4 \pm 0.5$ by Ref. [5] using the very early Universe measurement of the CMB integrated until us by using the standard cosmological model. This gruesome discrepancy is gaining a large attention in the field and it will be commented in Section 3.4.

Cosmic Microwave Background

Consider the very early Universe which was hot enough to have Photons interacting continuously with the matter (Baryons) forming a plasma in combination with Electrons. At the same time, Dark Matter was clustering as it had decoupled much earlier. Due to the expansion of the Universe itself, the density of this plasma decreases and, thus, its temperature. When the Universe was cold enough, Electrons and Protons formed atoms leading to a transparent Universe for Photons. This process is known as recombination. After that, the Photons free-stream until reaching us as the Cosmic Microwave Background (CMB), having with them a snapshot of the very Early Universe. Specifically, given temperature scales with expansion as $T_0 = \frac{T_{\text{rec}}}{1+z_{\text{rec}}}$ while $T_{\text{rec}} \simeq 2974\ K$, then CMB happened at $z_{\text{rec}} \simeq 1090$.

The Cosmic Microwave Background is a perfect black-body radiation spectrum with temperature $T_0 = 2.72548 \pm 0.00057$ K [18], showing inhomogeneities in the temperature field of order $\frac{\Delta T}{T_0} \sim 10^{-5}$ once the dipole due to our motion has been removed, hence supporting the Cosmological Principle. The characteristic shape of the spectrum of the anisotropies of the CMB is determined mainly by the primary anisotropy contributors, that is Acoustic Oscillations explained later in Section 2.4 and Diffusion Damping due to the increasing mean free path of Photons as the initial plasma rarefies with the expansion of the Universe, and the finite depth of the last scattering surface, that is, the set of places where decoupling occurred. The Acoustic Oscillations gave birth to the wiggle structure while the Diffusion Damping induced the damping tail for small scales.

Secondary anisotropies are related to the phenomena happening after recombination that may modify the shape of the CMB. As we will see, the most relevant ones to the topics of this thesis are:

- Thermal and Kinetic Sunyaev-Zeldovich effect: CMB Photons are scattered by unbound high energetic Electrons living in the Intergalactic Medium.

- Integrated Sachs-Wolfe effect: due to the time dependence of the gravitational potential along the line of sight.

The information of the CMB is mainly carried by its perturbations as from the black body background temperature we can only extract the time of decoupling. Perturba-

tions of the CMB are a photograph of the perturbations in the matter fields by the time of decoupling, given they have been less contaminated by gravitational instabilities. Since we are dealing with perturbations, we are no longer in the realm of the Cosmological principle and then we have that the temperature field can be described by

$$T(\hat{n}) = T_0 \left(1 + \frac{\delta T}{T_0}(\hat{n}) \right) \,, \tag{2.61}$$

where $\hat{n}$ is the direction of incoming Photons. In order to extract information from the anisotropies, it is customary to expand the temperature perturbations field in spherical coordinates θ and ϕ as follows

$$\frac{\delta T}{T_0}(\theta, \phi) = \sum_{\ell=1}^{\infty} \sum_{m=-\ell}^{\ell} a_{\ell m} Y_{\ell m}(\theta, \phi) \,, \tag{2.62}$$

where $Y_{\ell m}$ are the orthogonal basis of spherical harmonics. The expansion coefficients $a_{\ell m}$ are Gaussian random variables where the information of a cosmological model is encoded, and they are calculated as

$$a_{\ell m} = \int T(\vec{n}) Y_{\ell m}^* \mathrm{d}\Omega \,. \tag{2.63}$$

There are certain requirements that the coefficients of the expansion should fulfil:

- Zero mean $\langle a_{\ell m} \rangle = 0$: as deviation around the reference temperature ought to be zero on average.

- Statistical independence: $\langle a_{\ell m} a_{\ell m}^* \rangle = 0$ for $\ell \neq \ell'$ or $m \neq m'$, as the $a_{\ell m}$ are independent random variables.

- Isotropy: $\langle a_{\ell m} a_{\ell m}^* \rangle$ should be independent of m.

- Ergodicity hypothesis: an ensemble (the average $\langle \ \rangle$) of Universes should be the same as an ensemble of all independent points of one Universe. Applied to the CMB, this means that although we would like to study all the possible final configurations of the CMB in all possible universes, we can extract the same[17] information by studying the ensemble of all possible and independent patches of our realisation of the CMB.

Consequently, all the cosmological information of a model is encoded in the variance of the expansion coefficients, that we define as

$$\langle a_{\ell m} \, a_{\ell m}^* \rangle = \delta_{\ell \ell'} \delta_{mm'} \, C_\ell \,, \tag{2.64}$$

and we show in Figure 2.6 for the temperature spectrum[18]. The very same can be done for the polarisation, shown for example in Figure 2.7, or the cross correlation of temperature and polarisation as shown in Figure 2.8. The case of polarisation has

---

[17]Not exactly the same, cosmic variance will have an important effect on low l observations.

[18]In the plots, the customary prefactor is $\frac{\ell(\ell+1)}{2\pi}$ is used. However, if we plot it with $\frac{(2\ell+1)}{4\pi}$ or with $\frac{\ell(2\ell+1)}{4\pi}$ in ℓ linear or logarithm scale, the area under the curve is actually the temperature variance.
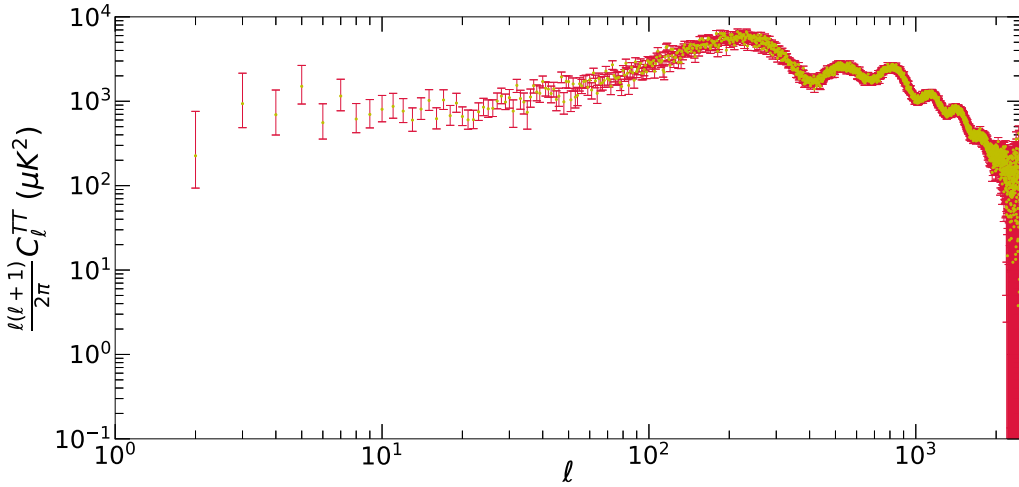
Figure 2.6: Cosmic Microwave Background as detected by Planck 2018 experiment [29]: Temperature

further complexities as we are dealing with a vector field rather than a scalar field, as it was with temperature. Any linear polarisation pattern can be decomposed in the Q and U Stokes parameters, but it is more convenient to work with the curl-free component, named the E-mode, and the divergence-free component, named the B-mode. To do so, we decompose the combination $(Q \pm iU)(\theta, \phi)$, which has a 2-spin behaviour, into the spherical harmonics as follows

$$(Q \pm iU)(\theta, \phi) = \sum_{\ell=0}^{\infty} \sum_{m=-\ell}^{\ell} a_{\ell m}^{(\pm 2)} Y_{\ell m}^{(\pm 2)}(\theta, \phi) \, , \tag{2.65}$$

where $Y_{\ell m}^{(\pm 2)}(\theta, \phi)$ are the ± 2-spin spherical harmonics. Defining the following linear combinations

$$a_{\ell m}^{E} = \frac{-1}{2}\left(a_{\ell m}^{(2)} + a_{\ell m}^{(-2)}\right) \, , \tag{2.66}$$

$$a_{\ell m}^{B} = \frac{i}{2}\left(a_{\ell m}^{(2)} - a_{\ell m}^{(-2)}\right) \, , \tag{2.67}$$

we obtain the curl-free E-mode and the divergence-free B-mode as

$$E(\theta, \phi) = \sum_{\ell=0}^{\infty} \sum_{m=-\ell}^{\ell} a_{\ell m}^{E} Y_{\ell m}(\theta, \phi) \, , \tag{2.68}$$

$$B(\theta, \phi) = \sum_{\ell=0}^{\infty} \sum_{m=-\ell}^{\ell} a_{\ell m}^{B} Y_{\ell m}(\theta, \phi) \, . \tag{2.69}$$
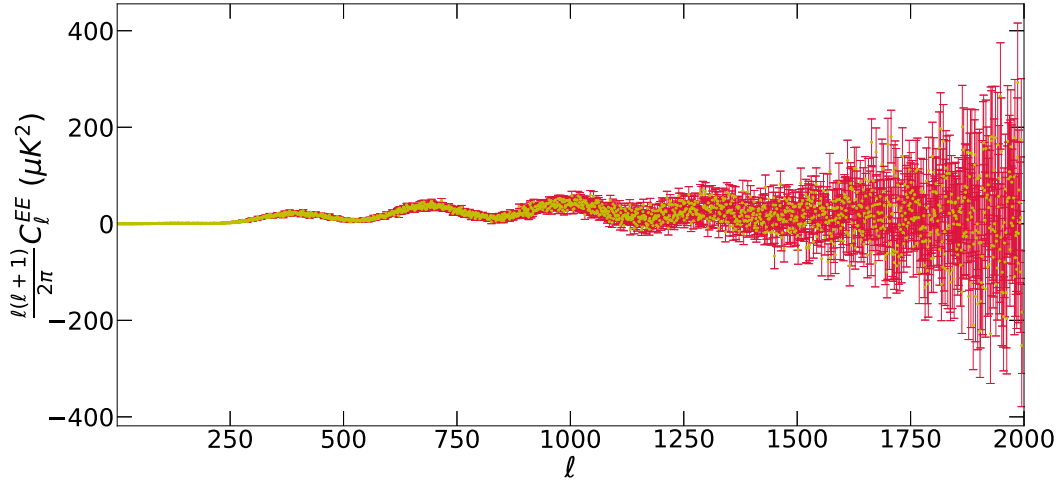
Figure 2.7: Cosmic Microwave Background as detected by Planck 2018 experiment [29]: Polarisation
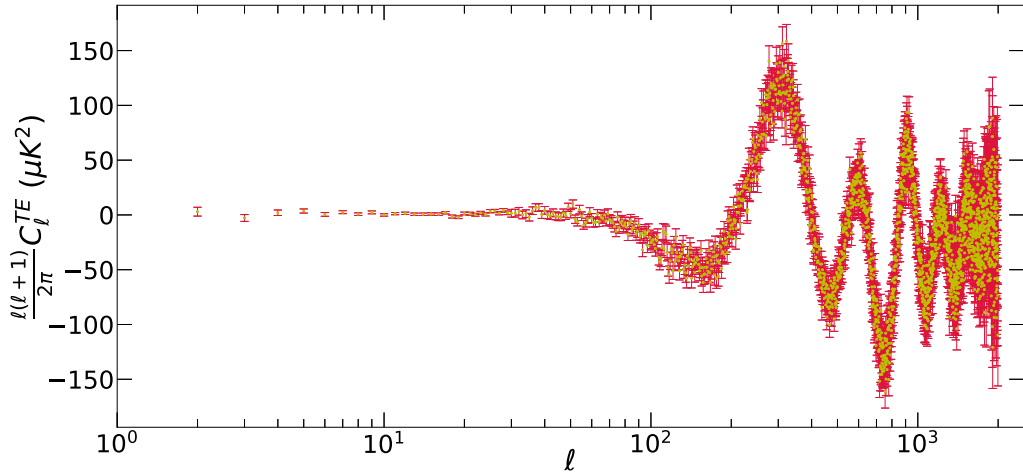

Figure 2.8: Cosmic Microwave Background as detected by Planck 2018 experiment [29]: Temperature-Polarisation

Planck-SZ data

Here we refer to the data from Ref. [30], which we devote a full explanation due to the importance along this PhD dissertation.

Consider a cluster which due to its temperature has hot gas with X-ray emission. This translates into very hot Electron gas emitting while having its internal motion. At the same time, we have the Photons of the CMB coming from all directions which were, at that moment structures formed, cold particles, that is, low frequency or low energy Photons. Inescapable, scattering happens. Then, the source of what is called

Thermal Sunyaev-Zeldovich effect is the change of frequency, that is temperature, of the CMB Photons due to the interaction with hot Electrons in the clusters. The interaction is an inverse Compton scattering, then producing a shift in the energy of the Photons and changing the shape of the CMB, as Thermal Sunyaev-Zeldovich constitutes one of the main contributors to the CMB secondary anisotropies.

The importance of this effect remains in its sensitivity to the total matter $\Omega_{\rm m}$ and to the parameter capturing the amount of perturbations σ_8, since the abundance and evolution of clusters depend on both parameters. As the sources of the Thermal Sunyaev-Zeldovich are the clusters, a good measurement of this signal can constrain them. Usually, both parameters are strongly degenerated and that is the reason why we defined the parameter S_8, as explained in Section 2.2. The data of Sunyaev-Zeldovich effect typically come as a likelihood of the form

$$\log \mathcal{L}_{S_8} = -\frac{(S_{8,\text{model}} - S_{8,\text{obs}})^2}{2\sigma_{S_8}^2} \,, \tag{2.70}$$

which of course constitutes an extremely oversimplified method. In particular, for the case of the Thermal Sunyaev-Zeldovich effect the value corresponds[19] to

$$S_{8,\text{SZ}} \equiv \sigma_8 \left(\Omega_{\rm m}/0.27\right)^{0.3} = 0.782 \pm 0.010 \,. \tag{2.71}$$

which appeared in Table 2 of Ref. [31] as obtained from the combination of data-sets `Planck2013+BAO+BBN` and for a fixed mass bias $1 - b = 0.8$. It is implemented in `MontePython` [32, 33] under the name of `Planck_SZ`. Even though it is a very simplified application of the observable, there are numerous papers showing how adding this likelihood leads to strong constraints inside the pure momentum transfer models. Hence, a question arises: why such oversimplified data can have such an enormous impact? In any case, in the following we should not forget that the analysis to obtain that value was done for the ΛCDM, while the models we will study alter the clustering already at the linear regime so a warning should be remarked.

Matter Power Spectrum

Consider each perturbation is defined as $\delta(\vec{x}, t)$ at a given time. The two-point correlation function for density perturbations at a certain moment is defined as

$$\xi(x) \equiv \langle \delta(\vec{x}) \, \delta(\vec{x}\,') \rangle \,. \tag{2.72}$$

However, it is more convenient to work in Fourier space. Then, for a given density perturbation at a certain time one can define the density perturbation in Fourier Space by just Fourier transforming $\delta(\vec{x}, t)$ into $\delta(\vec{k})$. Therefore, the power spectrum for the density perturbations is defined as the Fourier transform of the auto-correlation function as

$$P(k) \propto \langle |\delta(k)|^2 \rangle \,, \tag{2.73}$$

---

[19]A small variation compared to the typical definition of S_8 given by $S_8 \equiv \sigma_8 \left(\frac{\Omega_{\rm m}}{0.3}\right)^{0.5}$.
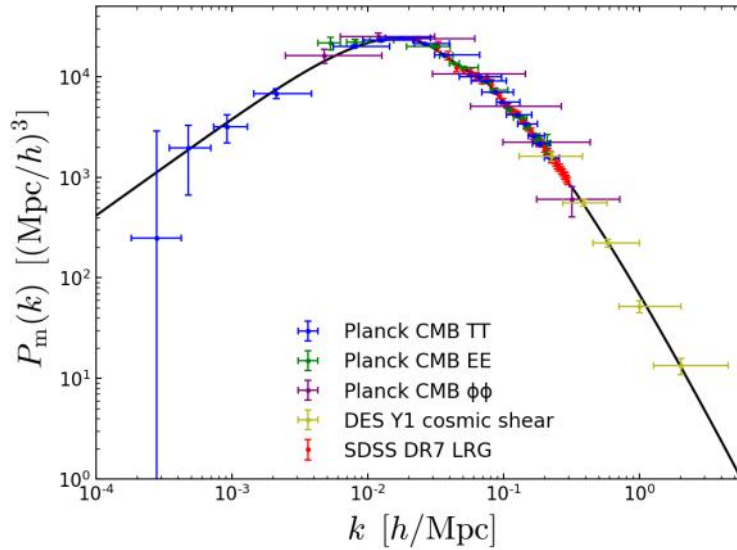
Figure 2.9: Last data available from Temperature (TT), polarisation (EE) and lensing ($\phi\phi$) of CMB experiment Planck [34], the Cosmic shear Dark Energy Survey (DES) data [35] and the galaxy clustering data from the Sloan Digital Sky Survey (SDSS) [36], using the Matter Power Spectrum figure tools developed in Ref. [37].

where the normalisation depends on the convention used. In Figure 2.9, we display the Matter Power Spectrum data available from Planck experiment [34], cosmic shear DES experiment [35] and clustering SDSS survey [36].

Supernovae type Ia

A Supernova constitutes the explosion of a star by some astrophysical process and it is nowadays one the most important standard candles we have. A standard candle is an object or process such that we know its energy emission per second, called the absolute luminosity L. As we can measure the energy received per area and per second, called the observed flux F, we can obtain from the relation between L and F the Luminosity distance D_L as

$$D_L^2 \equiv \frac{L}{4\pi F} \, , \tag{2.74}$$

to measure distances as explained in Appendix B.

The usual classification of Supernovae relies on the spectral properties of the emission associated with them. In our case, we here focus on type Ia Supernova, whose emission has no hydrogen lines associated, since the emitter star has burned all the hydrogen fuel, but a strong emission in the Silicon line II ($\lambda = 615$ nm). Supernovae Ia (SN Ia) are explained by the explosion of a white dwarf star which has evolved until a stage such that its interior pressure cannot counteract gravity leading to the explosion of the star. Until now, there are two mechanisms which can produce that stage. The first one is related to binary systems where the white dwarf is obtaining

matter from its companion until the mass exceeds a limit where the gravity overcomes the pressure, leading to the collapse of the star and, after that, its explosion. On the other hand, a merger of two white dwarf stars exceeding that mass limit would end up in the same explosion. SN Ia explosions constitute an extremely good standard candle as their luminosity curve should be similar, standarisable, for all events in the case of the binary systems. Provided that, we can use them to measure the expansion of the Universe since we can obtain the redshift from the spectrum.
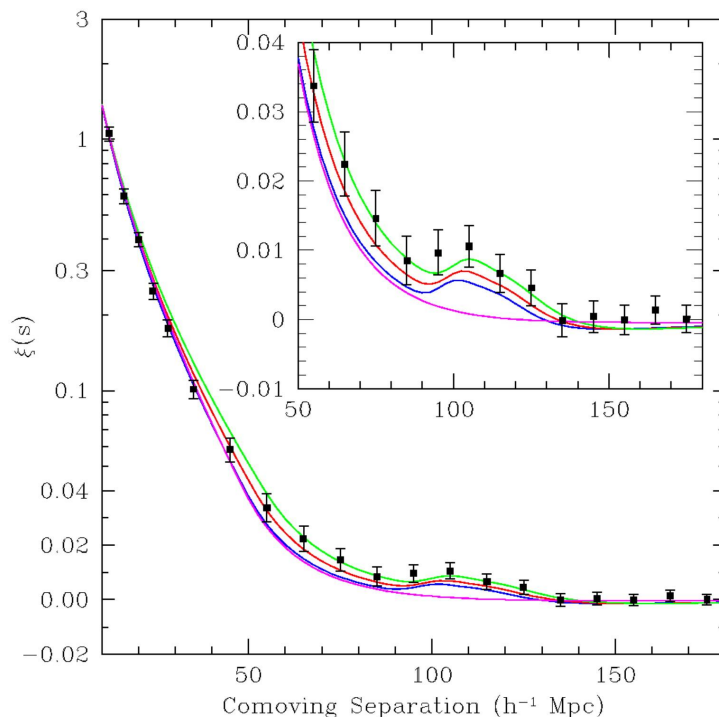
Baryonic Acoustic Oscillations

Figure 2.10: Iconic figure from the original paper [38] where the Sloan Digital Sky Survey (SDSS) firstly detected the BAO characteristic scale in the large scale redshift space correlation function of Luminous Red Galaxies. Lines correspond to different cosmological models with both Baryons and Dark Matter, except from magenta line which only includes Cold Dark Matter.

Baryonic Acoustic Oscillations, denoted by BAO, are the sequences of oscillations that appear in the CMB spectrum and in the Matter Power Spectrum, just evolved in time with the effects of gravity, which have a characteristic scale constituting a standard ruler. A standard ruler is an object of a known physical size R. As we can measure the actual angular size $\Delta\theta$ in the sky, we can relate both R and $\Delta\theta$ by the angular distance D_A as

$$D_A \equiv \frac{R}{\Delta\theta} = \frac{\chi(z)}{1+z} \, , \qquad (2.75)$$

to measure distances as explained in Appendix B.

Its origin comes from the epoch before recombination, where Baryons and Photons were strongly coupled while Cold Dark Matter was not. Consequently, as nothing prevented the clustering of Cold Dark Matter its perturbations started to grow by the gravitational instability, creating potential wells. On the other side, Baryons did have a repulsive force opposing gravity given by its coupled partner, Photons. Due to gravity Baryons fall into the Cold Dark Matter potential wells, getting compressed and, unavoidably, increasing the temperature of the Photon-Baryon plasma. Thus, increasing its radiation pressure which points outwards the potential well. The radiation pressure necessarily increases until at a certain moment it overcomes the gravitational attraction provoking an acoustic spherical expanding wave that expands the plasma, but not the Cold Dark Matter, beyond the potential well. This creates a shell of baryonic matter at a fixed radius, which is the sound horizon. The process may restart, then accreting more matter until another shock wave appears, and so forth until decoupling, when Baryons can no longer couple to Photons and fall irrevocably into the potential wells. This sequence of shock waves and the posterior action of gravity leaves an overdense peak with some echo shell around it for each perturbation. Something which can be seen clearly in the very shape of Cosmic Microwave Background as Photons after decoupling evolve mostly free preserving such shock waves in the form of oscillation in the perturbations of the temperate field. Also in the Matter Power Spectrum, although diluted since the Baryon distribution is erased by gravity trying to cluster everything, or in the correlation function as shown in Figure 2.10.

Galaxy Number Counts

Consider a mean density of galaxies per redshift and per steradian defined by $\bar{n}(z)$. Due to the isotropy and homogeneity of the Universe, it cannot depend on the position of the sky we are looking to, defined by $\vec{n}$, but only on the redshift. However, when having real data the observed density distribution of galaxies has fluctuations around the mean value that we can encode into a generic function $\Delta(\vec{n}, z)$. Therefore, the observed distribution of galaxies reads as

$$n(\vec{n}, z) = \bar{n}(z) \left[1 + \Delta(\vec{n}, z) \right] , \tag{2.76}$$

which, of course, now it depends on the patch of the sky we are looking to, along with the redshift. The contributors to the fluctuations are many and with varied origins, so we can decompose them as follows

$$\Delta(\vec{n}, z) = \Delta^{\mathrm{D}}(\vec{n}, z) + \Delta^{\mathrm{RSD}}(\vec{n}, z) + \Delta^{\mathrm{L}}(\vec{n}, z) + \Delta^{\mathrm{REL}} , \tag{2.77}$$

each one accounting for different effects:

- Density term Δ^{D}: it accounts for the pure contribution from the matter distribution in the sky but corrected by a certain function b, called the bias, which

encodes the differences induced by using a certain tracer for the underlaying matter field. We can write this term as

$$\Delta^{\mathrm{D}}(\vec{n}, z) = bD \ , \tag{2.78}$$

with D the growth function.

- Redshift-Space Distortions term Δ^{RSD}: it corresponds to the over and under-counted galaxies due to the distorted observed position of galaxies in redshift space caused by its peculiar velocity along the line of sight, defined as

$$\Delta^{\mathrm{RSD}}(\vec{n}, z) = \mathcal{H}^{-1}\partial_r^2 V \ , \tag{2.79}$$

with $\mathcal{H}$ the conformal Hubble function and V the velocity potential for the peculiar velocity in the longitudinal gauge.

- Lensing term Δ^{L}: it encodes the possible departures on the area and apparent magnitude of the different patches of the sky due to lensing effects on the Photons detected when performing the survey. It is defined as

$$\Delta^{\mathrm{L}}(\vec{n}, z) = -(2 - 5s)\kappa \ , \tag{2.80}$$

with s the magnification bias and κ the lensing convergence defined in Ref. [39] as

$$\kappa = \frac{3\Omega_{\mathrm{m}}H_0^2}{2} \int_0^{\chi(z)} \frac{\chi(\chi(z) - \chi)}{\chi(z)} \delta(\vec{n}\chi, \chi) \, \mathrm{d}\chi \ , \tag{2.81}$$

with $\chi(z)$ the comoving distance.

- Relativistic corrections Δ^{REL}: they correspond to corrections to the redshift in order to have a correct estimation of the physical depth and width of the redshift bins used. We will study them when speaking about the dipole of the power spectrum, otherwise we will neglect them.

Provided for a certain redshift $\Delta(\vec{n}, z)$ is just defined in the sphere, we can proceed as done with the CMB before. Hence, using the spherical harmonics we have that the fluctuations can decompose into

$$\Delta(\vec{n}, z) = \sum_{\ell=1}^{\infty} \sum_{m=-\ell}^{\ell} a_{\ell m}(z)Y_{\ell m}(\vec{n}) \ , \quad \text{with} \quad a_{\ell m}(z) = \int \Delta(\vec{n}, z)Y_{\ell m}^*(\vec{n}) \, \mathrm{d}\Omega \ . \tag{2.82}$$

which leads, as before, to the variance as the spectrum we are interested in, defined as

$$\langle a_{\ell m} \, a_{\ell m}^* \rangle = \delta_{\ell\ell'}\delta_{mm'} \, C_\ell(z) \ . \tag{2.83}$$

3

Problems in the ΛCDM model

In the previous chapter we presented the concordance model in Cosmology. We have shown the ability of the Λ Cold Dark Matter model to explain the evolution of the Universe from its initial stages until now, being able to match our observations. However, it would be presumptuous to think about the ΛCDM as the ultimate framework to describe the Universe we live in. Even before data can make a judgement, if we look at how the content of the Universe is shared we find that almost all the Universe today is made up of *something* that we do not know and that we have not detected in our laboratories. Even worse, our best description to the particle world has nothing to describe such dark part of our Universe. One may consider that our time is particular in some sense, but the situation persists in time. In any moment of our Universe there was, and there will be, around five times more Dark Matter than Baryons as both densities dilute with expansion in the same way[1], as $\rho_{\mathrm{dm}} \sim a^{-3}$ and $\rho_{\mathrm{b}} \sim a^{-3}$. In addition to Dark Matter we have the Cosmological Constant Λ, or in a more general description Dark Energy. According to General Relativity is just one parameter, but we do not understand its nature or its origin. When we try to describe it as a general fluid permeating the Universe, called Dark Energy, the situation does not improve since, then, we should have been able to see, detect or describe it, which has not happened yet. Both components have elusive properties as they are neutral for the electromagnetic or nuclear forces in a situation which resembles excessively to the postulated aether before modern physics solved the problem of light going through the space. Even if our datasets agree on most of the predictions of ΛCDM, some problems have emerged in the last years. Particularly when precise data appeared. We have some deviations from the structures predicted by the concordance model and, at the same time, different datasets give different

---

[1]In the concordance description, while there is no extra interaction changing how each fluid behaves.

values to the model parameters with a specific trend we will later comment.

In this chapter, we want to summarise most of the previous tensions of the model as a way to motivate the alternatives we have developed, something which is the main subject of this PhD dissertation. First, we will expose the elusive nature of the Dark Sector, to later on speak about how the Cosmological Constant dynamic seems to be strange to us. After that, we will enumerate the unexplained problems in the formation of structures detected when comparing the predictions of the standard model and the observations. Finally, we will focus on the tensions between datasets that have appeared with the very precise data of the last missions.

3.1 Dark Sector: unknown nature

Regarding Dark Matter, we infer it is there not because we have seen it directly but because of the gravitational effects on systems like galaxies or structure formation processes. We only know it must be *something* mainly non relativistic (cold), able to cluster and form structures and almost inert to standard model interactions. Moreover, when we go down to laboratory, or even Solar System dynamics, the influence of Dark Matter should be negligible. Even more intriguing is the fact that our concordance model for particle physics has no particle able to mimic Dark Matter or, on the other side, even some modifications of gravity have been proposed with limited success. However, the presence of such *something* is supported by several cosmological evidences. The classical example is the flatness of rotation curves of galaxies discovered by Rubin and Ford [40], but moderns probes have emerged in the last twenty years. For instance, CMB measuring Dark Matter density different from zero since $\Omega_{\mathrm{dm}}h^2 = 0.1200 \pm 0.0012$ [5]. Also, early Universe observations point towards a significant fraction of matter being dark to fulfil the requirements of Big Bang Nucleosynthesis (see for example Ref. [41]). Even visual evidences have appeared in the last years like gravitational lensing images or the bullet cluster. Notwithstanding the foregoing, no experiment has been able to directly detect Dark Matter. Different approaches have been considered, for example calorimeters like Cryogenic Rare Event Search with Superconducting Thermometers (CRESST) [42], Xenon detectors as XENON1T [43] or Argon detectors like ArDM [44]. All the previous experiments had limited success at directly detecting Dark Matter although with them we were able to exclude large portions of the parameter space, constraining at the end the possible properties of Dark Matter. Therefore, the first problem in ΛCDM model arises from one of its main ingredients as we both lack of a theoretical description and/or a direct observation of Dark Matter.

In the case of the Cosmological Constant, it was introduced in General Relativity by Einstein to counteract gravity and, hence, having a static and closed Universe as it was though to be at that moment. But when the expansion of the Universe was firmly demonstrated its role disappeared. However, General Relativity perfectly accommodates the presence of the Λ term and then its absence posed the question of

why it was not there. In the late nineties, the discovery of the accelerated expansion of the Universe brought the comeback of Λ. With this comeback, a new problem appeared: why its value is that small one compared to the radiative correction of vacuum energy? Again, we know nothing about its nature and we are unable to detect it directly but because of its effects in the expansion of the Universe. From the point of view of General Relativity, it is just a parameter of the theory with no further meaning. From the cosmological point of view where Λ lies into one of the possible descriptions of Dark Energy, it is the reason why the Universe entered recently in a phase of accelerated expansion and it should had been negligible in the rest of the epochs. Other attempts to explain such accelerated expansion invoked some modification of General Relativity but not great advances have been made. The discovery of the accelerated expansion by the Supernova Search Team [13] and the Supernova Cosmology Project Collaboration [14] constitutes the classical evidence for the Cosmological Constant. Also, modern observations, like the CMB, constrain its current magnitude to be $\Omega_\Lambda \equiv \frac{\Lambda}{3H_0^2} = 0.6847 \pm 0.0073$ [5].

With all the previous information we can conclude that the unknown intrinsic nature of the Dark Sector, which accounts for the 95% of the energy budget today of the Universe, constitutes the first flaw in the concordance model. Because of that, further descriptions of Dark Matter and Dark Energy are needed to discover their properties with the ultimate objective of unveiling the nature of such a mysterious Dark Sector.

3.2 Λ related problems

Even though we have no knowledge about the nature of the Cosmological Constant Λ, its measured value represents an enormous challenge in two different ways to our poor theoretical description. Either its observed value compared to the natural one is problematic, usually called the Cosmological Constant Problem, and its contribution today to the energy budget of the Universe as compared to the matter sector forces us to ask questions about the nature of Λ, called the Coincidence Problem. Let us start with the first one.

Consider again the Einstein Field Equations that we have already introduced in equation (2.3). But now we will reformulate them explicitly including the vacuum fluctuations that unavoidable gravitate as dictated by General Relativity. Then, we have

$$R_{\mu\nu} - \frac{1}{2} g_{\mu\nu} R + \Lambda g_{\mu\nu} = 8\pi G \left(T_{\mu\nu} + \langle T_{\mu\nu} \rangle \right) , \qquad (3.1)$$

where $\langle T_{\mu\nu} \rangle$ is the expected value of the stress-energy tensor for the vacuum fluctuations. Given the vacuum state must be invariant under any change of the observer, the expected value reads as

$$\langle T_{\mu\nu} \rangle = -\rho_{\rm v} \, g_{\mu\nu} , \qquad (3.2)$$

where $\rho_{\rm v}$ is the vacuum density. Consequently, the vacuum fluctuations contribute to the Cosmological Constant measured value or, equivalently, the Cosmological

Constant contributes to the measured value of vacuum energy as

$$\Lambda_{\text{obs}} = \Lambda + 8\pi G \rho_{\text{v}} \iff \rho_{\text{obs v}} = \rho_{\text{v}} + \frac{\Lambda}{8\pi G} \; . \tag{3.3}$$

The problem arrives when measuring the Cosmological Constant as its value should be inferred as

$$\Lambda_{\text{obs}} = 3\Omega_\Lambda H_0^2 \sim 10^{-83}\,\Omega_\Lambda h^2\,\text{GeV}^2 \iff \rho_{\text{obs v}} = \frac{\Lambda_{\text{obs}}}{8\pi G} \sim 10^{-48}\,\Omega_\Lambda h^2\,\text{GeV}^4 \tag{3.4}$$

where both the Cosmological Constant density and reduced Hubble parameter are order one as measured by Planck (or any other) experiment, as explained in Section 2.2. This value is enormously different form the value one would expect from the vacuum fluctuations encoded in ρ_{v}. A typical calculation using only the zeroth order diagrams would give contributions like $\rho \sim \lambda_{\text{cutoff}}^4$, where λ_{cutoff} is a cut-off scale of the effective theory we are dealing with. In our case, we could naively set this to correspond to the Planck scale which is to $m_{\text{Pl}} \sim 10^{19}$ GeV. Therefore, only a miraculous precise cancellation among all the different contributions to the vacuum from our laboratory scales up to the Planck scales would save us from the Cosmological Constant Problem. The previous calculation can be refined by considering the standard model contributions although the problems persist. For example, for the weak interaction $\rho \sim 10^6$ GeV^4 or for the strong interaction, quantum chromodynamics, the difference in order of magnitudes improves since $\rho \sim 10^{-6}$ GeV^4. However, still extremely inconsistent in both cases with the measured cosmological value unless a precise cancellation happens among all the contributions to the total vacuum energy.

Secondly, a quick analysis on the time evolution of each component of the Universe shows that the Cosmological Constant has no similarity with matter, baryonic or dark, or with radiation as it is constant for all the evolution of the Universe. However, today both matter and Dark Energy are of the same amount in the energy budget of the Universe[2]. In the future, matter will continue to dilute with the expansion of the Universe and, then, they will be no longer of the same order. This "coincidence" poses a maybe philosophical but also scientific question: why such different types of energy/matter are the same today?

There are other coincidences, less often commented in the literature. For example, the Dark Energy scale today is $\rho_{\text{de 0}} \sim \rho_{\text{cr 0}} \sim \text{meV}^4$ while the Neutrino scale is also $\sim \text{meV}^4$. Both coincidences may not just be a coincidence but a consequence. If an undetected interaction is acting between Dark Energy and Dark Matter or between Dark Energy and Neutrinos, the scale coincidence emerges naturally. We also have the coincidence between the Planck Mass M_{Pl}, the observed value of the Cosmological Constant ρ_Λ and the electro-weak scale M_{EW}, being the latter one the geometrical mean of the other two, since $M_{\text{EW}} \sim \sqrt{M_{\text{Pl}}\,\rho_\Lambda^{1/4}}$.

---

[2]However, it should be said that such Coincide Problem is strongly dependant on the time variable used since when we work with cosmic time the amount of time both fluids are of the same order enlarges.

3.3 Small scales related problems

When we go to smaller scales, that is $\lesssim 1$ Mpc, the observations from the matter distribution do not match perfectly with the predictions from the standard ΛCDM model. We should not forget here that Dark Matter governs how structures formed, although what we detect is baryonic matter. First, because in the early Universe the starter in the race to cluster was Dark Matter since Baryons were coupled through Thomson scattering to Photons. Consequently, the gravitational potentials were initially created by Dark Matter overdensities. After that, and looking to the abundance of both matter components, Dark Matter was and still is the main contributor to the gravitational potentials where structures form. Therefore, the following list of issues in the small scales regime can be understood as an alert of our enormous ignorance on the Dark Matter nature. The following list does not intend to be a full and self-explanatory list, but rather a short compendium of all the most important issues with a brief explanation to motivate the future alternative models. For more details, we refer to dedicated reviews like Refs. [45, 46].

Cusp-vs-core problem

N-body simulations where only Dark Matter is considered show that Dark Matter halos should have a density profile increasing around the centre of the halo. This is the well-known Navarro-Frenk-White density profile (NFW) [47], described by

$$\frac{\rho(r)}{\rho_{\mathrm{cr}}} = \frac{\delta_{\mathrm{c}}}{(r/r_{\mathrm{s}})(1 + r/r_{\mathrm{s}})^2} \, , \tag{3.5}$$

where δ_{c} and r_{s} are a characteristic density and a characteristic radius, respectively. Then, simulations predicts what is known as a "cusp" density profile. On the other hand, one can look at Dark Matter dominated galaxies to test these predictions. What it is found is that such galaxies have a "core" density profile, that is a constant density near the centre of the halo, which creates a conflict between core-like observations and cusp-like predictions. This problem has been with us for a long time, pointed out in the classical paper [48], with several proposed solutions like interacting models for Dark Matter. Despite it, we still miss an ultimately solution for it.

Missing-satellite problem

As before, we have that N-body simulations predict a large number of sub-halos structures per halo. In particular, simulations of the Milky Way-like halos predict a number of $\sim 100 - 1000$ sub-halos. However, our observations point to a number of $\sim 10 - 100$ sub-halos, that is an order of magnitude lower than expected as it was first noticed in Ref. [49]. Increasing observational capabilities, which help us to detect fainter and fainter galaxies, have reduced the tension but still a reasonable doubt is placed in the community.

Too-big-to-fail problem

Using the standard model, N-body simulations predict large massive satellite galaxies in our Local Group that have enough mass, they are "too big", to form a corresponding galaxy, that is, stars we can see. However, we cannot find enough of them around [50], which points to an erasing mechanism yet to be discover. This inconsistency has also been found in our Milky Way [51] and in Andromeda galaxy [52].

Other problems

The previous issues constitute the more challenging problems to the standard ΛCDM model emerging from small scales. However, they are not the only ones. Issues like the angular momentum catastrophe [53], the satellite planes problem [54] or certain inconsistencies in baryonic Tully-Fisher Relations [55] still seek for an explanation. Several solutions have been proposed. From increasing the capabilities of N-body simulations or a more rigorous inclusion of the feedback from Baryons to changing the nature of Dark Matter, like in the case of having a fraction of it as "warm", or even modifying General Relativity (see Ref. [56] for a review). The intrinsic nature of Dark Matter is completely unknown to us, despite the fact we know it clusters, a significant portion should be cold, interactions with standard model particles, if there, are strongly suppressed, its abundance today and with the current experiments we have been able to heavily constrain the parameter space ruling out several Dark Matter proposals. However, no Dark Matter particle or field has been detected and we have not developed any theory that fully explains Dark Matter. Thus, the previous small scales problems are merely the hallmark of our ignorance about the intrinsic nature of Dark Matter.

3.4 Cosmological tensions

In the last years, our technology has facilitated the development of a large number of very high precision experiments, entering in what is popularly called the era of precision Cosmology in the literature. This means we have an enormous collection of data with a precision never achieved before. However, having several very precise probes constraining the same parameters has brought some inconsistencies. It is not yet well delimited when an inconsistency between two different surveys is problematic or not, but generally we consider a tension when the inconsistency is 3σ or more and a crisis when the discrepancy rises to the 5σ level. Contemporaneously to this thesis, we are on the edge of a crisis as the discrepancy on the Hubble parameter is around 5σ, while we are on the verge of a tension with the σ_8 parameter. Maybe more important than the amount of discrepancy is the trend exhibited by both tensions. They are not a tension/crisis between two particular datasets, but a tension between two methods of measuring the parameters. For most of the observables, the value
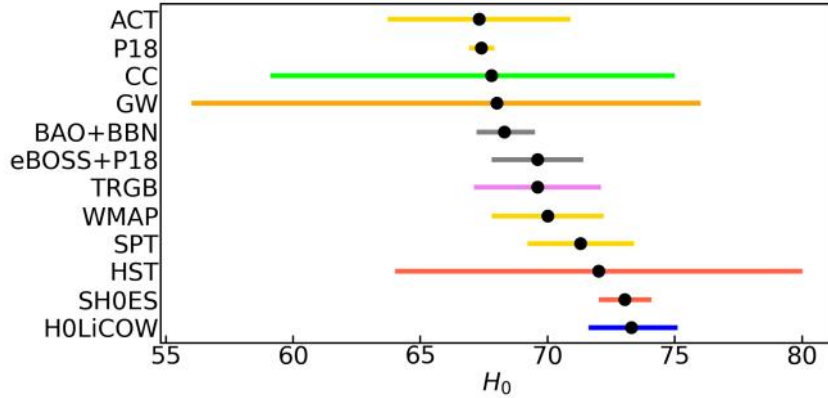
Figure 3.1: Cosmological constraints on the Hubble parameter from different surveys, namely: Atacama Cosmology Telescope (ACT) $H_0 = 67.3 \pm 3.6$ [3], Planck 2018 (P18) $H_0 = 67.4 \pm 0.5$ [5], Cosmic Chronometers method (CC) $H_0 = 66.5 \pm 5.4$ [57], Gravitational Waves method (GW) $H_0 = 68^{+12}_{-7}$ [8], Baryon Acoustic Oscillation and Big Bang Nucleosynthesis observables (BAO+BBN) $H_0 = 68.3^{+1.1}_{-1.2}$ [58], extended Baryon Oscillation Spectroscopic Survey with Planck 2018 best-fit (eBOSS+P18) $H_0 = 69.6 \pm 1.8$ [59], Tip of the Red Giant method (TRGB) $H_0 = 69.6 \pm 2.5$ [60], Wilkinson Microwave Anisotropy Probe (WMAP) $H_0 = 70.0 \pm 2.2$ [61], South Pole Telescope (SPT) $H_0 = 71.3 \pm 2.1$ [4], Hubble Space Telescope (HST) $H_0 = 72 \pm 8$ [62], the SH0ES team $H_0 = 73.04 \pm 1.04$ [28] and the H0LiCOW collaboration $H_0 = 73.3^{+1.7}_{-1.8}$ [63].

in each case depends on whether they are direct/local or indirect/early-Universe techniques, as we will explain now.

H_0 **tension**

The Hubble constant measures the expansion rate today. As explained in Section 2.2, it corresponds to the current value of the Hubble function $H_0 \equiv H(z = 0)$. We have two different methods to constrain its value as, on one hand, we have the distance ladder method which is based on the Hubble Law

$$z = H_0 \, d \, , \tag{3.6}$$

where d is the distance to any other object from us. In the local Universe, the redshift provides us a way to measure the velocity any object is receding from us since $z \simeq v$ and, hence, the Hubble parameter is just the proportional factor between the receding velocity and the distance to the object. On the other hand, we have the CMB which happened in the early Universe and, thus, we have to reconstruct the path of this primordial light from recombination to us, requiring necessarily the assumption of a cosmological model and obtaining from the fitting the value of H_0 in such fiducial model used. There are other methods like using the tip of the red-giant branch or even nowadays gravitational waves. However, different methods measure different values for H_0, having a tension among them, and of particular concern is the fact

that a trend seems to exist. Direct methods, which usually correspond to late and lo-cal Universe with less influence of the fiducial cosmology, tend to get larger values of the Hubble parameter. For example, the SH0ES team with $H_0 = 73.04 \pm 1.04$ [28] using the cosmic ladder. Indirect methods, which typically means early Universe observ-able and the requirement of a fiducial cosmology to extrapolate it until now, point to lower values. For example, the last Planck data report the value $H_0 = 67.4 \pm 0.5$ [5]. The discrepancy has grown in time and, today, we have a $\sim 5\sigma$ tension depending on the surveys compared as seen in Figure 3.1, which definitely calls for more at-tention, and may even suggest new physics is hidden.

In the literature, we have several proposals to answer this problem. For example, a miscalibration of the SH0ES collaboration avoiding universal colour–luminosity re-lation in Cepheids [64] may alleviate the tension or, although now ruled out, a local under-density [65]. Modifications on the pillars of Cosmology have been studied, for example all modified gravity theories (see Ref. [56] for a review) or questioning the FLRW metric [66]. Even the bases of particle physics have been revised, like having a not constant electron mass [67]. Also extensively studied, certain modifications in the ΛCDM model like wCDM or Early Dark Energy models [68] in the side of Dark Energy, and warm Dark Matter [69] or decaying Dark Matter [70] regarding Dark Matter. Also Dark Radiation has been proposed [71]. Interactions between different sectors of the Universe have been widely analysed, for example between Dark En-ergy and Dark Matter [72] or between Dark Energy and Baryons [73]. Changing the cosmology is a natural solution to the previous problem. The large impact of the chosen cosmology in indirect methods compared to direct methods made any devia-tion from the standard cosmological description a suitable escape hatch, reconciling both methods.

Despite the enormous ability of ΛCDM to fit most of our datasets, the H_0 ten-sion emerges as a disturbing consequence of our experimental precision. Therefore, a question should be asked: are there systematics spoiling certain results or are there new physics we have not accounted for? If not due to systematics, we should analyse all the possible alternatives to the standard model with our current and fu-ture datasets, with the ultimate duty of finding the most accurate description of our Universe.

σ_8 or S_8 tension

The parameter σ_8 encodes the root mean square of matter fluctuations on spheres of $8h^{-1}$ Mpc radii. This means it accounts for the amount of clustering of matter in the Universe, serving as a measure of the growth of structures. Again, we have two main methods of measuring the value of the parameter. We can use our local Universe to set a value for σ_8, then a direct method, or we can re-evolve the CMB be-tween today and recombination using a fiducial cosmology to set its value, thus an
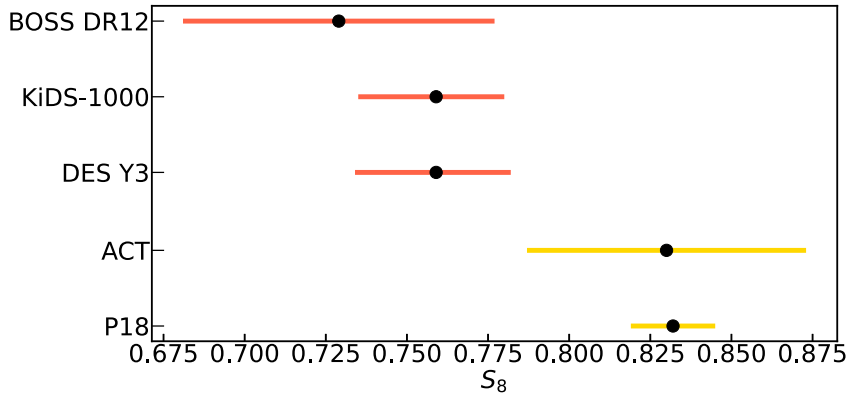
Figure 3.2: Cosmological constraints on the S_8 parameter from different surveys, namely: Baryon Oscillation Spectroscopic Survey (BOSS) $S_8 = 0.729 \pm 0.048$ [74], Kilo-Degree Survey (KiDS-1000) $S_8 = 0.759^{+0.024}_{-0.021}$ [75], Dark Energy Survey (DES Y3) $S_8 = 0.759^{+0.025}_{-0.023}$ [76], Atacama Cosmology Telescope (ACT) $S_8 = 0.830 \pm 0.043$ [77] and Planck 2018 (P18) $S_8 = 0.832 \pm 0.013$ [5].

indirect method. Again the same duality appears. Now, direct methods tend to give lower values while indirect methods have larger ones. Due to the strong degeneracy between Dark Matter current density Ω_m and the parameter σ_8 in weak lensing measurements as already said in Section 2.2, it is convenient to work with the parameter S_8 defined as

$$S_8 \equiv \sigma_8 \left(\frac{\Omega_m}{0.3} \right)^{0.5}. \tag{3.7}$$

Regarding S_8, local Universe probes like for example the Kilo-Degree Survey sets $S_8 = 0.759^{+0.024}_{-0.021}$ [75] while early Universe probes like Planck experiment has a different value $S_8 = 0.832 \pm 0.013$ [5]. This implies a $2-3\sigma$ tension as depicted in Figure 3.2. Although not as perturbing as the tension in H_0, certain attention is required.

There are several proposals in the literature to overcome this emerging tension. For example, a miscalibration due to the value of the optical depth used was suggested in Ref. [78], or due to the value of the mass bias used as explained in Ref. [79] and, even, massive Neutrinos with no positive result [80]. As before, extensions of the Dark Matter being not cold or decaying appear as alternatives as seen in Refs. [81, 82]. An enormous field of undiscovered interactions opened in the last years, for example Refs. [83, 84, 85, 86, 87, 88, 89, 89, 90, 91] or the review [72]. In particular, pure momentum transfer interactions have gained interest in the last years regarding the σ_8 tension (see Refs. [92, 93, 94, 95, 96, 97, 98, 99, 100, 101, 102, 103, 104]) as a possible solution. Part of this PhD dissertation is devoted to this type of interactions and its relation with the σ_8 tensions.

Although less disturbing than the H_0 tension, the σ_8 or S_8 tension also shows the same trend. Low redshift probes, that is in our local Universe, seem to prefer

lower values of the parameter in comparison with early Universe measurements. It is true that they require more control on the systematics, something that is not always achievable as with the CMB. But, on the other hand, the impact of a wrong modelling of the cosmology is less significant as they look into the local Universe, while early Universe methods have to extrapolate the observable until today with the chosen cosmology. Whether the current tension is due to systematics not under control, a bad fiducial model or something we are yet to discover, time alone will tell.

Other tensions

Previous H_0 and S_8 tensions get most of the attention nowadays. The two main reasons for that is the large difference in values, specially for H_0, and above all because of the notorious splitting between direct and indirect methods. However, they are not the only claimed tensions on the cosmological parameters.
The lensing amplitude parameter A_L, used by the Planck experiment [29], captures the effects of weak lensing on the CMB photons. If no lensing happens, it should vanish and for the lensed CMB spectrum it should be $A_L = 1$. However, the last result from the Planck Collaboration is $A_L = 1.180 \pm 0.065$ [5], clearly pointing towards $A_L > 1$. Also, the consideration of our Universe to be flat is not free from controversy. In the last years, there are claims of a closed Universe according to CMB data as explained in Ref. [105], which can be connected to the previous A_L results. Moreover, in Ref. [106] they also suggested a possible tension between Planck data [29] and Atacama Cosmology Telescope [77] regarding the spectral index n_s. Also, in the last years some studies found some redshift evolution of the parameters H_0 and Ω_m inside the standard model, see for example Ref. [107], which may indicate a bad modelling of the background dynamics.

Whether the previous tensions are simply systemics not under control, bad modelling, a wrong fiducial cosmology or new physics yet to be discovered, it is unavoidable that with the increase in precision of current and future surveys this type of tensions will exacerbate at the moment we miss something in the analyses. Moreover, if now being at the 1% precision in most of the parameters we have an almost 5σ tension, with future and more precise surveys the pressure will grow. Because of that, it is extremely important to study and analyse all possible alternatives to the current scenario, as we partially do in this PhD dissertation.

MOMENTUM TRANSFER INTERACTIONS

e have seen in the previous chapter that Cosmology is not perfectly pleased with its standard model. Certain theoretical and observational issues hover around our theoretical description of the Universe. In the theoretical sector, we have seen how those controversies might be related with our poor knowledge of the constituents of our Universe, while in the observational side future surveys will disentangle if such tensions are really there or just an act of statistics and mis-calibrations. Consequently, our duty is to test the current theoretical description against alternatives, analyse how data relate with tensions and how future surveys will shed light on the previous questions. We devote this Chapter to the first two questions in the realms of linear scales, while the third one is discussed in Chapter 5. A non-linear analysis is shown in Chapter 6.

In this thesis, the global and main aim is to transcend the current standard description of our Universe, called the ΛCDM model, to find a more suitable portrayal of it. However, we should not forget the great achievements of the ΛCDM model since it is able to accurately describe the whole evolution history or the formation of structures while matching most of the observables we have. Accordingly, we want to walk around the ΛCDM model and add something to it capable of correcting its small shortcomings while respecting its enormous achievements. Moreover, we do not want to wackily change the picture but we prefer to have a certain motivation to choose that modification. Because of that, we will study here a certain class of alternative models usually called pure momentum transfer interactions. The pivot idea here is the presence of a certain and yet undetected interaction involving the Dark Sector whose microphysics is invisible to us by the proper nature of the Dark Sector, but whose expressed effects in the large picture of the Cosmos are modelled by a momentum interchange, at the same time there is no energy transfer between

coupled fluids. The consequences of that exchange is a suppression of structures as we are adding some impulse to the pressureless matter, dark or not, by the momentum transfer and, thus, allowing matter to escape from gravitational potentials. A similar idea is already in our picture. In the Thomson Scattering where two fluids, one with pressure and one without it, have a certain interaction whose microphysics belongs to quantum electrodynamics. However, for the cosmological concerns the microphysics is not relevant, so we include it as a momentum exchange between the cosmological Baryon fluid and the cosmological Photon fluid.

Here, we will first explain the so-called Covariantised dark Thomson-like scattering which includes a Thomson-like interaction between Dark Energy and Dark Matter or Baryons, invoking the already commented pure momentum transfer between both fluids. After that, we will also explain the so-called Velocity-entrainment coupling model, which induces a more sophisticated momentum transfer and adds a new dark component in the form of radiation, all of these derived from a Lagrangian. In each case, we will explain the main effects on observables of the previous models and, then, explain the results from the Monte Carlo Markov Chain (MCMC) analyses using the latest available data.

This chapter is partially based on the following published papers:

- **Title:** On cosmological signatures of Baryons-Dark Energy elastic couplings.
  Authors: Jose Beltrán Jiménez, Dario Bettoni, David Figueruelo and Florencia A. Teppa Pannia.
  DOI: 10.1088/1475-7516/2020/08/020
  Published in: Journal of Cosmology and Astroparticle Physics 08 (2020), 020 [108].
  e-Print: 2004.14661 [astro-ph.CO]

- **Title:** J-PAS: Forecasts for Dark Matter - Dark Energy elastic couplings.
  Authors: David Figueruelo et al.
  DOI: 10.1088/1475-7516/2021/07/022
  Published in: Journal of Cosmology and Astroparticle 07 (2021), 022 [109].
  e-Print: 2103.01571 [astro-ph.CO]

- **Title:** Velocity-dependent interacting Dark Energy and Dark Matter with a Lagrangian description of perfect fluids.
  Authors: Jose Beltrán Jiménez, Dario Bettoni, David Figueruelo, Florencia A. Teppa Pannia and Shinji Tsujikawa.
  DOI: 10.1088/1475-7516/2021/03/085
  Published in: Journal of Cosmology and Astroparticle 03 (2021), 085 [110].
  e-Print: 2012.12204 [astro-ph.CO]

- **Title:** Probing elastic interactions in the Dark Sector and the role of S_8.
  Authors: Jose Beltrán Jiménez, Dario Bettoni, David Figueruelo, Florencia A.

Teppa Pannia and Shinji Tsujikawa.

4.1 Covariantised dark Thomson-like scattering: Dark Energy-Dark Matter

In this PhD dissertation, our purpose is to study alternative descriptions to our current concordance model explained in Chapter 2. To this end, we do not want to completely repudiate our current description of the Universe since its successes outweigh its failures. Regarding the description of the Dark Sector, here we will still consider a pressureless, non-relativistic dark component of matter. On the side of the other dark component, instead of just considering a Cosmological Constant we will treat it more generally as the so-called Dark Energy. In the concordance scenario no interaction in the Dark Sector is included, but we know the visible sector is fully populated with particle interactions with cosmological implications and effects. Then, it would be a mistake to not even consider the possibility of interactions taking place in the Dark Sector, even more so if we take into account all the issues of the concordance paradigm shown in Chapter 3. However, as the ΛCDM model has proven to be an extraordinary accurate description, we want to remain close to it. Thus, we want to preserve its background prescription as much as possible, while the modifications considered should have a motivation in some sense. Here is where Covariantised dark Thomson-like scattering belonging to the Dark Sector can help.

The philosophy of the Covariantised dark Thomson-like scattering is an interaction between Dark Energy and a matter fluid similar to the Thomson scattering prior to recombination. In that epoch, Dark Matter had already decoupled but the rest of components were part of a plasma where Photons and Electrons were coupled as they experience the Thomson scattering, that is the elastic scattering of Photons by the free charged Electrons present in that plasma. Because of this process, Baryons could not collapse to form bounded structures, while uncoupled Dark Matter was already clustering at that moment by the action of gravity, forming the seeds of the future halos. Then, whereas Thomson scattering was efficient, the radiation pressure of Photons counteracted the gravitational collapse of Baryons, preventing them from forming gravitational bounded structures. Here, the philosophy of this interaction is similar. If we have an interaction between Dark Energy and a matter fluid, the pressure of Dark Energy can counteract the gravitational collapse of the coupled matter component. This inevitably leads to less structures in the Universe. We know from Chapter 3 that late Universe experiments seem to prefer lower values of the parameter σ_8[1]. Hence, one would naturally expect a late-time mechanism that erases the extra structure predicted by early Universe measurements, leading to less structures as we measure today. This kind of interaction was firstly explored in Ref. [101], and then revisited in Refs. [109, 111] in order to expand its understanding. Moreover, this interaction is grouped into a more general group of couplings, dubbed as

---

[1]As explained in Section 2.2, the cosmological parameter σ_8 captures the amount of structures in the Universe today by measuring the root mean squared of mass fluctuation on spheres of $8h^{-1}$ Mpc radii.

pure momentum transfer models, provided the net effect of them is an interaction with no energy transfer but a momentum transfer between coupled fluids.

With this philosophy and the targeted problem in mind, the Covariantised dark Thomson-like scattering formalism commences from the non-conservation of the stress-energy tensor of the coupled components as

$$\nabla_\mu T_{\mathrm{dm}}^{\mu\nu} = Q^\nu \,, \qquad \nabla_\mu T_{\mathrm{de}}^{\mu\nu} = -Q^\nu \,, \qquad \text{with} \qquad Q^\nu = \bar\alpha \left(u_{\mathrm{de}}^\nu - u_{\mathrm{dm}}^\nu \right) \,, \qquad (4.1)$$

where Q^ν encodes the interaction and $\bar\alpha$ the coupling function controlling the strength of the interaction. The previous equations ensures the global conservation of the coupled system Dark Energy-Dark Matter, since we have $\sum_i \nabla_\mu T_{\mathrm{i}}^{\mu\nu} = 0$. It is convenient to work with adimensional couplings, then we can normalise it as

$$\alpha = \frac{8\pi G}{3H_0^3} \bar\alpha \,. \qquad (4.2)$$

Given the Covariantised dark Thomson-like scattering interaction is proportional to the relative velocity of the coupled fluids, the background evolution cannot be affected unless we violate the Cosmological Principle. As we have that the 4-vector describing an element of any fluid is the same for all components $u_i^\mu = u_j^\mu$, provided we are in the comoving rest-frame of an isotropic and homogeneous Universe, then $Q^\mu \propto u_{\mathrm{de}}^\nu - u_{\mathrm{dm}}^\nu \to 0$. However, when dealing with perturbations this is no longer true. Now the velocity takes the form $u^\mu = \frac{1}{a}(1 - \Psi, \vec{v})$ in the Newtonian Gauge[2], with $\vec{v} = \frac{\mathrm{d}\vec{x}}{\mathrm{d}\tau}$. When deriving the differential equations governing the linear perturbation dynamics as explained in Section 2.3, we will see the density contrast ones will remain unaltered, while modifications will take place only on the Euler equations of the coupled fluids. Nevertheless, there is a more sound theoretical explanation for this result as we are dealing with an interaction similar to the Thomson scattering. That means a low-energy interaction which does not alter the number of particles or the kinetic energy of the incident Photons, which translated to the cosmological description means no modification on related quantities to number or energy density. Therefore, having the continuity and the density contrast equations preserved while modifying the Euler equation emerges as a natural consequence of the Covariantised dark Thomson-like scattering. Consequently, the equations governing the background cosmology, that is Friedmann equations, continuity equations or the Hubble function, are the same explained in Chapter 2. There is only one subtle point here. We cannot use a ΛCDM model but a wCDM. As we will see later, the new term in the perturbation sector will be proportional to $\frac{\alpha}{1+w}$, then having a Cosmological Constant $w = -1$ would not be compatible with this interaction. It is important to highlight that preserving the background cosmology is an appealing property of this type of models as we know most of our datasets favour the concordance model

---

[2]The coupling is gauge independent as by a gauge transformation of the form $\delta x^\mu = \zeta^\mu$ the interaction transforms as $\delta Q^\mu = -\mathcal{L}_\zeta Q^\mu = 0$, where $\mathcal{L}$ is the Lie derivative and Q^μ is the background coupling. Thus, we do not need to care about the gauge for that explanation.

and, thus, we may only expect small deviations around it. Consequently, preserving its background evolution is a strongly supported advantage due to the success of the concordance model, although it will be a weak point regarding the H_0 tension.

In principle, the coupling parameter α can have time and/or scale dependence. As we will explain later, in the case of the Dark Energy-Dark Matter interaction we will explore a cut-off scale as a proxy of a scale dependence, finding no preferred scale at least for the scales explored by data. Regarding the time dependence, in this PhD dissertation we only consider the case such that α is constant in time. We can see such a simple case as a proof-of-concept of having a late-time efficient coupling able to erase structures and its relation with the σ_8 tension. In any case, we did try to investigate if a time dependence could be convenient in two different cases. First, we considered a power-law dependence with the scale factor as $\alpha(a) = \alpha_{\rm pl}\,a^n$ where the power n should keep the late time efficiency of the coupling. On the other side, a CPL-inspired or Taylor expansion around today given by $\alpha(a) = \alpha_0 + \alpha_1(1-a)$ was considered, having the parameters α_0 and α_1 such that they preserve the desired late-time behaviour. However, we found data is not enough precise to disentangle the possible scale factor dependence when doing MCMC analyses and, provided with both cases we can recover the constant case, we, therefore, keep those ideas for when future data will be available in the next generation experiments.

As the background evolution is the same as in a wCDM model, we shall focus now in the perturbation sector that emerges from this interaction. Given the perfect fluid description for each component of the Universe, with no anisotropic stress and same background evolution, one can obtain the equations governing the perturbation sector of the interacting components[3] by the non-conservation of the perturbed stress-energy tensor

$$\nabla_\mu(T_{\rm dm}^{\mu\nu} + \delta T_{\rm dm}^{\mu\nu}) = \bar{\alpha}\,(u_{\rm de}^\nu - u_{\rm dm}^\nu)\ , \qquad \nabla_\mu(T_{\rm de}^{\mu\nu} + \delta T_{\rm de}^{\mu\nu}) = -\bar{\alpha}\,(u_{\rm de}^\nu - u_{\rm dm}^\nu)\ , \qquad (4.3)$$

with u_i^ν the perturbed 4-velocity. Following the formalism of Ref. [27] and explained in Chapter 2.3, the equations governing the perturbation sector, that is the density contrast δ and the velocity variable θ, are in the Newtonian gauge

$$\delta_{\rm dm}' = -\theta_{\rm dm} + 3\Phi'\ , \qquad (4.4)$$

$$\theta_{\rm dm}' = -\mathcal{H}\theta_{\rm dm} + k^2\Phi + \Gamma(\theta_{\rm de} - \theta_{\rm dm})\ , \qquad (4.5)$$

$$\delta_{\rm de}' = -3\mathcal{H}\left(c_{\rm s}^2 - w\right)\delta_{\rm de} + 3(1+w)\Phi' - \theta_{\rm de}(1+w)\left(1 + 9\mathcal{H}^2\frac{c_{\rm s}^2 - w}{k^2}\right)\ , \qquad (4.6)$$

$$\theta_{\rm de}' = \left(-1 + 3c_{\rm s}^2\right)\mathcal{H}\theta_{\rm de} + k^2\Phi + \frac{k^2 c_{\rm s}^2}{1+w}\delta_{\rm de} - \Gamma R(\theta_{\rm de} - \theta_{\rm dm})\ , \qquad (4.7)$$

---

[3]The non-interacting components have the same equations as in the standard model explained in Section 2.3.

while in the synchronous gauge we have

$$\delta'_{\rm dm} = -\left(\theta_{\rm dm} + \frac{1}{2}h'\right) , \tag{4.8}$$

$$\theta'_{\rm dm} = -\mathcal{H}\theta_{\rm dm} + \Gamma(\theta_{\rm de} - \theta_{\rm dm}) , \tag{4.9}$$

$$\delta'_{\rm de} = -3\mathcal{H}\left(c_{\rm s}^2 - w\right)\delta_{\rm de} - (1+w)\left(\theta_{\rm de} + \frac{1}{2}h'\right) + 9(1+w)\mathcal{H}^2\frac{c_{\rm s}^2 - w}{k^2}\theta_{\rm de} , \tag{4.10}$$

$$\theta'_{\rm de} = \left(-1 + 3c_{\rm s}^2\right)\mathcal{H}\theta_{\rm de} + \frac{k^2 c_{\rm s}}{1+w}\delta_{\rm de} - \Gamma R(\theta_{\rm de} - \theta_{\rm dm}) , \tag{4.11}$$

with Γ the interaction rate between Dark Energy and Dark Matter and R the Dark Matter-to-Dark Energy ratio, both defined as

$$\Gamma \equiv \bar{\alpha}\frac{a}{\rho_{\rm dm}} , \tag{4.12}$$

$$R \equiv \frac{\rho_{\rm dm}}{(1+w)\rho_{\rm de}} . \tag{4.13}$$

As seen from previous equations, the interaction only introduces an additional term in the perturbed Euler equations, both for Dark Matter and Dark Energy, proportional to the relative perturbed velocity between both coupled fluids. We can clearly see the resemblance between the new term due to the interaction $\Gamma(\theta_{\rm de} - \theta_{\rm dm})$ and the Thomson scattering term[4] $\Gamma_{\rm T}(\theta_\gamma - \theta_{\rm b})$ where $\Gamma_{\rm T} \equiv \frac{4\rho_\gamma}{3\rho_{\rm b}}an_e\sigma_{\rm T}$ with n_e the abundance of free Electrons and $\sigma_{\rm T}$ the Thomson scattering cross section. However, the crucial differences between both interactions are the scales involved. For being efficient, the Covariantised dark Thomson-like scattering requires peculiar velocities between interacting components, or for $\theta_{\rm de} \sim \theta_{\rm dm}$ the coupling term necessarily vanishes, a feature shared with the Thomson scattering. Thus, the interaction is only efficient for small scales where peculiar velocities arise, as for large scale all components share the same rest-frame. But, regarding the time scales, the Thomson scattering needs a non negligible fraction of free charges as $\Gamma_{\rm T} \sim n_e$, something that only occurred in the early Universe before recombination or during reionization. On the other hand, Covariantised dark Thomson-like scattering becomes efficient at late-times for a constant coupling α as $\Gamma \sim a^4$. In fact, it dominates for a completely general coupling $\alpha(\tau, k)$ the dynamics of the Euler equations when $\Gamma > \mathcal{H}$.

In principle, the coupling can have a scale and/or time dependence $\alpha(\tau, k)$. Here, we will explore two scenarios, one with neither time nor scale dependence $\alpha(\tau, k) = \alpha$, and the other scenario with a cut-off scale of the form $\alpha(k) = \alpha\,e^{-k/k_{\rm s}}$, where $k_{\rm s}$ sets such cut-off scale[5]. From a very phenomenological point of view, this interaction was motivated as a late-time mechanism to erase structures with the goal of finding

---

[4]See equation (2.59) of Chapter 2.3.

[5]We may think of existing screening mechanisms like chameleon, symmetron, K-mouflage or Vainshtein mechanisms (see for instance [112]), but here we do not intend our previous parameterisation of the coupling to reproduce any of the previous mechanisms. With that parameterisation we only want to explore if cutting-off small scales from a certain $k_{\rm s}$ could improve the compatibility with data.

an agreement between early and late-time measurements of the parameter σ_8. As we said, the interaction becomes efficient when $\Gamma > \mathcal{H}$, then for the late Universe and assuming a Dark Energy equation of state not too far away from $w \to -1$ we need $\Gamma > \mathcal{H} \sim a$. Hence, a constant coupling parameter suits the purpose of this mechanism. Moreover, one can understand a constant coupling parameter as the zeroth order term of a CPL-like description for the coupling parameter, that is a Taylor expansion around us, since the σ_8 tension suggests a late-time interaction. From a bit more fundamental point of view, let us consider that we assume Dark Energy is described by a scalar field ϕ having an approximate shift symmetry, while a natural dependence for the interaction might be $\alpha \propto \dot{\phi}$, which is nothing but an interaction proportional to the gradient of the scalar field. From that, we can naturally expect $\phi \propto t$ and thus $\alpha \propto cte$ as we are supposing here. Moreover, this interaction can be the consequence of a $U(1)$ charge in the Dark Sector, that given its still unknown nature we are not able to detect directly, yielding to a Thomson-like scattering whose cosmological effects we might be able to spot. As commented, this is a late-time interaction departing then from Thomson scattering which was mainly active in the very early Universe. However, we know Thomson scattering reappeared later when reionization happened, so we could speculate our dark Thomson-like scattering might be mediated by a dark reionization taking place in the late Universe. Of course, the microphysics explanation to this interaction is still an open question. Until we do not detect the dark particles, if they exist, the previous discussion only belongs to the speculative world.

We include the different modifications due to the interaction in the Boltzmann code CLASS [113, 114] to obtain a full adapted code to the Dark Energy-Dark Matter Covariantised dark Thomson-like scattering. With that modified code we study the evolution of the density contrast δ and the velocity perturbation θ of the different components and we analyse the effects of the interaction in several observables. However, before delving into that, in Ref. [108] it was studied the different regimes of this interaction for the case Dark Energy-Baryons. Here, we will perform a similar analysis for the Dark Energy-Dark Matter scenario.

4.1.1 Regimes

Before analysing the effects of the interaction in observables like the Matter Power Spectrum or the CMB, it will be of particular interest trying to understand the different regimes and scales involved. We have already commented how this interaction can only be relevant for small scales regime where peculiar velocities arise as, otherwise, the coupling term vanishes since $\theta_{\mathrm{de}} \sim \theta_{\mathrm{dm}}$. We have also purposely chosen a constant coupling, then it appears as a late-time interaction which may naturally alleviate the σ_8 tension. Provided that, in this section we will analyse the different regimes to give a first taste so then we can fully understand the effects observed in the numerical codes when we compute certain observables.

Super-horizon modes

Let us consider the super-horizon regime, that is $\mathcal{H} \gg k$. For super-horizon modes, we can safely consider the gravitational potential is constant as those modes remain frozen until they reenter the horizon. Thus, provided $\frac{\mathcal{H}^2}{k^2} \gg 1$, the perturbation equations read as

$$\delta'_{\rm dm} = -\theta_{\rm dm} \,, \tag{4.14}$$

$$\theta'_{\rm dm} = -\mathcal{H}\theta_{\rm dm} + k^2\Phi + \Gamma(\theta_{\rm de} - \theta_{\rm dm}) \,, \tag{4.15}$$

$$\delta'_{\rm de} = -3\mathcal{H}\left(c_{\rm s}^2 - w\right)\delta_{\rm de} - (1+w)9\mathcal{H}^2\frac{c_{\rm s}^2 - w}{k^2}\theta_{\rm de} \,, \tag{4.16}$$

$$\theta'_{\rm de} = \left(-1 + 3c_{\rm s}^2\right)\mathcal{H}\theta_{\rm de} + k^2\Phi + \frac{k^2 c_{\rm s}^2}{1+w}\delta_{\rm de} - \Gamma R(\theta_{\rm de} - \theta_{\rm dm}) \,. \tag{4.17}$$

Firstly, we consider the interaction is not efficient which we can describe by the criterion $\Gamma \ll \mathcal{H}$ for Dark Matter and $R\Gamma \ll \mathcal{H}$ for Dark Energy. This accounts for most part of the evolution history choosing a constant coupling function $\alpha(\tau, k) = \alpha$, which gives rise to a very late-time interaction. In that case, the equations will be just as in the standard cosmological scenario with some very minimal deviation due to the required $w \neq -1$. Consequently, the evolution will not be modified and we refer to classical textbooks like [25, 115] where it is comprehensively described. On the other hand, if we consider the interaction is efficient, then late-time Universe according to the previous criterion, we again should expect no modification by just looking at the coupling term. For such very large super-horizon modes, peculiar velocities between components should not appear given they are in cosmological scales inside the realm of the Cosmological Principle. Although that argument might be enough, we can demonstrate it. Firstly, the interaction will act on Dark Energy provided $R\Gamma \gg \Gamma$ as $R \gg 1$. Then, in that scenario $R\Gamma \gg \mathcal{H} \gg \Gamma$ the Dark Matter equations will remain unaltered but for Dark Energy we would have

$$\delta'_{\rm de} = -3\mathcal{H}\left(c_{\rm s}^2 - w\right)\delta_{\rm de} - (1+w)9\mathcal{H}^2\frac{c_{\rm s}^2 - w}{k^2}\theta_{\rm de} \,, \tag{4.18}$$

$$\theta'_{\rm de} \simeq -\Gamma R\theta_{\rm de} + k^2\Phi + \Gamma R\theta_{\rm dm} \,, \tag{4.19}$$

with both equations having as homogeneous solution a decaying mode. Particularly, for Euler equation where the interaction explicitly appears we have $\theta_{\rm de}^{(\rm hom)} \propto e^{-\int \Gamma R d\tau}$ since $\Gamma R \gg 1$. Then, the only departure from non-interacting evolution might emerge from the inhomogeneous part of Dark Energy Euler equation but as it is mainly determined by the primordial spectrum which is purely adiabatic, thus same velocities for all components so vanishing interacting term. Then, we keep the behaviour unaltered as the coupling term is negligible for $\theta_{\rm de} \sim \theta_{\rm dm}$. Even later in time when $R\Gamma \gg \Gamma \gg \mathcal{H}$, we will continue to have the decaying modes in the homogeneous part and, hence, the scenario should be the same.

Tight coupling regime: Dark Energy

We now consider sub-horizon modes $\mathcal{H} \ll k$ at late-time Universe $z \lesssim 1$ and for scales where gravity does not control the dynamics $k^2\Phi \leq \mathcal{H}\theta$, where the interaction is efficient provoking a tight coupling between Dark Energy and Dark Matter leading to the exchange of momentum and then both velocities couple $\theta_{\rm dm} \to \theta_{\rm de}$. This scenario is similar to the Baryon-Photon tight coupling regime before recombination, which was induced by a Thomson scattering. Again, we clearly see the resemblance between this interaction and the Thomson scattering, motivating once again the possible presence of this coupling.

Consequently, we have for the zeroth order $\theta_{\rm dm}^{(0)} \simeq \theta_{\rm de}$ while using the Dark Matter Euler equation we can write the relative velocity up to first order corrections as

$$\theta_{\rm dm}^{(1)} \simeq \theta_{\rm de} - \frac{1}{\Gamma}(\theta_{\rm dm}' + \mathcal{H}\theta_{\rm dm} - k^2\Phi)\,. \tag{4.20}$$

In Section 4.1.2, we will numerically confirm how both, Dark Energy and Dark Matter, velocities will couple when the interaction becomes efficient. This will provoke that Dark Matter no longer follows Baryons and then it will not fall into the potential wells due to the interaction, at least for the scales where gravity is not the leading force. For that last scenario, we will see how even in such case the tight coupling will leave an imprint.

Once we have a first insight of the Dark Matter velocity divergence variable, we are now interested in understanding the Dark Energy density contrast evolution, which we will later confirm in Section 4.1.2. For this purpose, we first have to rewrite the equation (4.6) under the approximation considered for the sub-horizon modes, then

$$\delta_{\rm de}' \simeq -3\mathcal{H}\left(c_{\rm s}^2 - w\right)\delta_{\rm de} + 3(1+w)\Phi' - \theta_{\rm de}(1+w)\,. \tag{4.21}$$

In order to get a second order differential equation for $\delta_{\rm de}$, we obtain from equation (4.21) $\theta_{\rm de} = \theta_{\rm de}(\delta_{\rm de}', \delta_{\rm de}, \Phi)$ and its derivative $\theta_{\rm de}' = \theta_{\rm de}(\delta_{\rm de}'', \delta_{\rm de}', \delta_{\rm de}, \Phi)$, then we insert them into equation (4.7) including the approximation obtained before for $\theta_{\rm dm}$. Hence, the second order differential equation controlling the evolution under the previous approximation of $\delta_{\rm de}$ is

$$\delta_{\rm de}'' + \delta_{\rm de}'\mathcal{H}\left[1 - 3(w - c_{\rm eff}^2 R)\right] + \delta_{\rm de}\left[k^2 c_{\rm eff}^2 + m_{\rm eff}^2\right] \simeq (1+w)f(\Phi'', \Phi', \Phi)\,, \tag{4.22}$$

where $m_{\rm eff}^2$ and $c_{\rm eff}^2$ are the squared effective mass and squared effective sound speed, defined as

$$m_{\rm eff}^2 \equiv 3(c_{\rm s}^2 - w)\left[(1 - 3c_{\rm eff}^2)\mathcal{H}^2 + \mathcal{H}'\right]\,, \tag{4.23}$$

$$c_{\rm eff}^2 \equiv \frac{c_{\rm s}^2}{1 + R}\,, \tag{4.24}$$

while the function $f(\Phi'', \Phi', \Phi)$ depends just on the matter clustering. Given $R \gg 1$ we can further simplify the differential equation as

$$\delta_{\rm de}'' + \delta_{\rm de}'\mathcal{H}\left[1 - 3(w - c_{\rm s}^2)\right] + \delta_{\rm de}\left[\frac{k^2 c_{\rm s}^2}{R} + m_{\rm eff}^2\right] \simeq (1+w)f(\Phi'', \Phi', \Phi)\,, \tag{4.25}$$

which immediately invokes a damped oscillator with a certain force whose general equation is $\ddot{x} + A\dot{x} + Bx = F(t)$. Consequently, the competition between the effective mass m_{eff}^2 and the effective sound speed c_{eff}^2 sets the natural not damped not forced frequency of the system, while the clustering (mainly Dark Matter one) controls the force applied to the system. In any case, the clustering rate of Dark Energy should be negligible, then we can focus on the Dark Matter one.

Tight coupling regime: Dark Matter

For sub-horizon modes $\mathcal{H} \ll k$, the density contrast equations for Dark Matter and Dark Energy are

$$\delta'_{\text{dm}} = -\theta_{\text{dm}} + 3\Phi' , \tag{4.26}$$

$$\delta'_{\text{de}} = -3\mathcal{H}(c_s^2 - w)\delta_{\text{de}} + 3(1+w)\Phi' - (1+w)\theta_{\text{de}} . \tag{4.27}$$

As already done in Ref. [101], we can combine both equations to obtain the following coupled equation

$$\delta'_{\text{dm}} - \frac{\delta'_{\text{de}} + 3\mathcal{H}(c_s^2 - w)\delta_{\text{de}}}{1+w} = \theta_{\text{de}} - \theta_{\text{dm}} . \tag{4.28}$$

As a first approximation, just to get the idea of the implications due to the pure momentum transfer, we can neglect the second term in left-hand side provided Dark Energy barely clusters through all cosmic evolution and, then, those perturbations are extremely small and barely growing. Thus

$$\delta'_{\text{dm}} \propto \theta_{\text{de}} - \theta_{\text{dm}} . \tag{4.29}$$

Therefore, when the interaction couples both fluids $\theta_{\text{dm}} \sim \theta_{\text{de}}$, Dark Matter density perturbations get frozen leading to a reduction of structures in the late Universe and, then, one can expect a suppression on the Matter Power Spectrum for sub-horizon modes. As the final consequence, a lowering in the σ_8 parameter should appear, which may alleviate its related tension by this late-time mechanism which leaves the CMB physics untouched. We will numerically compute those observables in Section 4.1.2 to confirm the previous derivation.

Gravitational pull

The tight coupling regime was obtained assuming gravity was not the leading force but it was competing against the interaction. In other words, during tight coupling we have gravity trying to cluster Dark Matter while Dark Energy pressure is trying to put everything apart, as it did happen with Thomson scattering before recombination. Then, the final regime of interest would be what happens for smaller scales where gravity overcomes the interaction and becomes the leading force.

Considering again sub-horizon modes $\mathcal{H} \ll k$ for the late-time Universe when the interaction is only efficient as it needs $\Gamma \gg \mathcal{H}$, matter dominated epoch and very small

scales where gravity dominates $\theta_{\rm dm} \gg \theta_{\rm de}$, the Euler equation for Dark Matter is

$$\theta'_{\rm dm} = -\theta_{\rm dm}(\Gamma + \mathcal{H}) + k^2\Phi + \Gamma\theta_{\rm de} \implies \theta'_{\rm dm} + \Gamma\theta_{\rm dm} \simeq k^2\Phi \ . \tag{4.30}$$

It is more convenient to have the following change of variable $\mathrm{d}x = \Gamma\mathrm{d}\tau$ so that the previous equation can be rewritten as follows

$$\frac{\mathrm{d}\theta_{\rm dm}}{\mathrm{d}x} + \theta_{\rm dm} \simeq \frac{k^2\Phi}{\Gamma} \ , \tag{4.31}$$

which can be solved as the sum of the solution of the homogeneous differential equation plus a particular solution of the full equation

$$\theta_{\rm dm} \simeq Ce^{-x} + e^{-x}\int e^x \frac{k^2\Phi}{\Gamma}\mathrm{d}x \ , \tag{4.32}$$

where C is integration constant. Given we are in matter dominated epoch we have Φ is constant and $\Gamma = \Gamma_0\tau^8$ provided $a \sim \tau^2$, then we have that $x = \frac{1}{9}\Gamma_0\tau^9 = \frac{1}{9}\Gamma_0 a^{9/2} \gg 1$ which allows as to solve easily the integral in equation (4.32) since the exponential varies much faster than the Γ, then

$$\theta_{\rm dm} \simeq \frac{k^2\Phi}{\Gamma} = \frac{k^2\Phi}{\Gamma_0}a^{-4} \ , \tag{4.33}$$

where Γ_0 captures all the constant factors we are not interested in for this derivation. As in matter dominated epoch the gravitational potential is constant, we also have the density contrast from equation (4.5) as

$$\delta_{\rm dm} \simeq \bar{C} + \frac{k^2\Phi}{7\Gamma_0}a^{-7/2} \ , \tag{4.34}$$

where $\bar{C}$ is the integration constant giving the initial conditions. Here, we can clearly see the suppression of structures acting as the density contrast of Dark Matter rapidly saturates remaining constant from then.

Γ as starting shot of the interaction

We can perform the same trick done for Dark Energy with Dark Matter to obtain a second order differential equation for Dark Matter density contrast $\delta_{\rm dm}$. As before, using equation (4.4) we can obtain an equation of the form $\theta_{\rm dm} = \theta_{\rm dm}(\delta'_{\rm dm}, \Phi)$ and, then, $\theta'_{\rm dm} = \theta'_{\rm dm}(\delta''_{\rm dm}, \Phi)$ which can be plugged into equation (4.5) leading to

$$\delta''_{\rm dm} + \delta'_{\rm dm}(\mathcal{H} + \Gamma) = 3\Phi'' + 3(\mathcal{H} + \Gamma)\Phi' + k^2\Phi + \Gamma\theta_{\rm de} \ . \tag{4.35}$$

As a first approximation, one may consider $\theta_{\rm de}$ is negligible for the scales where clustering occurs and that the gravitational potential is mainly determined by Dark Matter not by Dark Energy. Then, the relevant departure from the non-interacting scenario can only take place when $\Gamma > \mathcal{H}$, which for a non-time dependent coupling function α only happens for the very late-time Universe, as already explained. This confirms what we already commented when presenting this interaction. The specific form of the coupling function $\alpha(\tau, k)$, that determines Γ, will mark the time scales when the Covariantised dark Thomson-like scattering is efficient and, in particular we need $\Gamma > \mathcal{H}$ to have deviation from the standard scenario.

Stability condition

In the implementation done in the numerical codes CLASS [113, 114] and CAMB [116], we found that negative values of the coupling parameter (along with Dark Energy equation of state $w > -1$) were numerically problematic to the code. In order to understand such situation, in this section we want to explore the potential emergence of instabilities provoked by the interaction.

Our first step is to derive the second order differential equations system for Dark Matter and Dark Energy density contrasts. We already have equation (4.35), although this time we will not neglect the velocity potential contribution of course. We will remain in the sub-horizon modes and in Dark Matter dominated epoch. We neglect the super-horizon potential instabilities as they cannot be caused by the interaction given its intrinsic properties. Now, we will use the Dark Energy Euler equation (4.6) in the sub-horizon regime to eliminate Dark Energy velocity as

$$\theta_{\text{de}} = -\frac{\delta'_{\text{de}}}{1+w} - \frac{3\mathcal{H}(c_{\text{s}}^2 - w)}{1+w}\delta_{\text{de}} + 3\Phi' \,. \tag{4.36}$$

Provided we consider the matter dominated epoch, we can use that Φ is constant and $k^2\Phi \simeq -\frac{3}{2}\mathcal{H}^2\delta_{\text{dm}}$, thus the second order differential equation reads as

$$\delta''_{\text{dm}} + \delta'_{\text{dm}}(\Gamma + \mathcal{H}) - \frac{\Gamma}{1+w}\delta'_{\text{de}} - \frac{3}{2}\mathcal{H}^2\delta_{\text{dm}} + 3\mathcal{H}\Gamma\frac{w - c_{\text{s}}^2}{1+w}\delta_{\text{de}} \simeq 0 \,. \tag{4.37}$$

We now need the corresponding equation for Dark Energy. Under the previous assumption of matter dominated epoch, considering equation (4.36) and its derivative, we can insert them in the Dark Energy Euler equation for sub-horizon modes

$$\theta'_{\text{de}} = \left(-1 + 3c_{\text{s}}^2\right)\mathcal{H}\theta_{\text{de}} + k^2\Phi + \frac{k^2 c_{\text{s}}^2}{1+w}\delta_{\text{de}} - \Gamma R(\theta_{\text{de}} - \theta_{\text{dm}}) \,, \tag{4.38}$$

using that in this regime $\delta'_{\text{dm}} \simeq -\theta_{\text{dm}}$ we obtain

$$\delta''_{\text{de}} + \delta'_{\text{de}}\left[(1 - 3w)\mathcal{H} + \Gamma R\right] + \delta_{\text{de}}\left[k^2 c_{\text{s}}^2 + 3\Gamma R\mathcal{H}(c_{\text{s}}^2 - w)\right] \simeq$$
$$\frac{3}{2}\mathcal{H}^2(1+w)\delta_{\text{dm}} + \Gamma R(1+w)\delta'_{\text{dm}} \,. \tag{4.39}$$

Hence, we can rewrite it in a more compact way as

$$\begin{bmatrix} \delta''_{\text{dm}} \\ \delta''_{\text{de}} \end{bmatrix} + \begin{bmatrix} \mathcal{H} + \Gamma & -\frac{\Gamma}{1+w} \\ -(1+w)\Gamma R & (1-3w)\mathcal{H} + R\Gamma \end{bmatrix} \begin{bmatrix} \delta'_{\text{dm}} \\ \delta'_{\text{de}} \end{bmatrix}$$
$$+ \begin{bmatrix} -\frac{3}{2}\mathcal{H}^2 & 3\frac{w - c_{\text{s}}^2}{1+w}\mathcal{H}\Gamma \\ -\frac{3}{2}(1+w)\mathcal{H}^2 & c_{\text{s}}^2 k^2 + 3(c_{\text{s}}^2 - w)\mathcal{H}R\Gamma \end{bmatrix} \begin{bmatrix} \delta_{\text{dm}} \\ \delta_{\text{de}} \end{bmatrix} \simeq 0 \,. \tag{4.40}$$

Our main concerns are not about UV Laplacian instabilities, given no change due to the interaction for high frequency modes with $k^2 \gg \max\{\mathcal{H}^2, R\Gamma\mathcal{H}\}$, neither with IR instabilities, since for very large scales the interaction term vanishes. But we do have

a new sound horizon scale induced in Dark Energy due to the modified prefactor in $\delta_{\rm de}$ of equation (4.39), which is

$$k_\star^2 = \left| 3 \left(1 - \frac{w}{c_{\rm s}^2} \right) R\Gamma\mathcal{H} \right| . \tag{4.41}$$

Let us consider only sub-Hubble modes that are inside this horizon when the interaction dominates the dynamics of the system, that is $\mathcal{H} \ll k \ll k_\star$. In that regime the mass matrix, the matrix accompanying the $\begin{bmatrix} \delta_{\rm dm} \\ \delta_{\rm de} \end{bmatrix}$ term, has

$$\det \hat{M} \simeq -\frac{9}{2}(c_{\rm s}^2 - w)R\Gamma\mathcal{H}^3 , \tag{4.42}$$

and, hence, its sign is determined by the sign of $\frac{\alpha}{1+w}$. To have the required unstable mode leading to collapse it has to obey $\det \hat{M} < 0$, so for $w > -1$ we need $\alpha > 0$. With these results and the numerical issues seen in CLASS, we will restrict our analyses to positive values of the coupling parameter α or, if negative, having $|\alpha|$ close to zero.

4.1.2 Linear effects

Once we have studied the interaction at certain regimes of interest, we should analyse with full detail the evolution of the perturbations and the possible effects on observables due to the pure momentum transfer. In this task, we have used the Boltzmann solver code CLASS [113, 114], which allows us to reproduce the evolution of the background cosmology and the linear perturbations while computing certain observables. We have created a modified version of CLASS which includes the Covariantised dark Thomson-like scattering scenario between Dark Energy and Dark Matter, both for a constant coupling parameter $\alpha(\tau, k) = \alpha$ and for the case with a scale cut-off $\alpha(\tau, k) = \alpha\, e^{-k/k_{\rm s}}$. This was achieved by including the new terms in the Euler equations (see equations (4.5) and (4.7)) and adding the new parameters, α or α and $k_{\rm s}$, to the code. We will first explore comprehensively the case where the coupling has neither time nor scale dependence, that is $\alpha(\tau, k) = \alpha$, as a very general proxy to study this type of interactions. After that, we will explore the main consequences of adding a cut-off scale using the coupling $\alpha(\tau, k) = \alpha\, e^{-k/k_{\rm s}}$.

For our analyses, we set the cosmological parameters to be $H_0 = 67.4$ Km/s/Mpc, $\Omega_{\rm b} h^2 = 0.0224$, $\Omega_{\rm dm} h^2 = 0.120$, $\tau_{\rm reio} = 0.054$, $A_{\rm s} = 2.1\ 10^{-9}$, $n_{\rm s} = 0.965$, $w = -0.98$ and $c_{\rm s}^2 = 1$, while any other parameter is set to the default value of the code. As previously explained, we are using as background cosmology a wCDM model as required by this interaction. Then, our reference model to compare the effects of the interaction should be also the wCDM model to avoid any degeneracy with the Dark Energy equation of state w equal to -1 or not. The implementation is done in the Newtonian gauge in CLASS code, but in Ref. [109] another complementary implementation was done but using the Synchronous gauge in the numerical code CAMB [116]. We found no difference between the results obtained in both codes with different gauges.
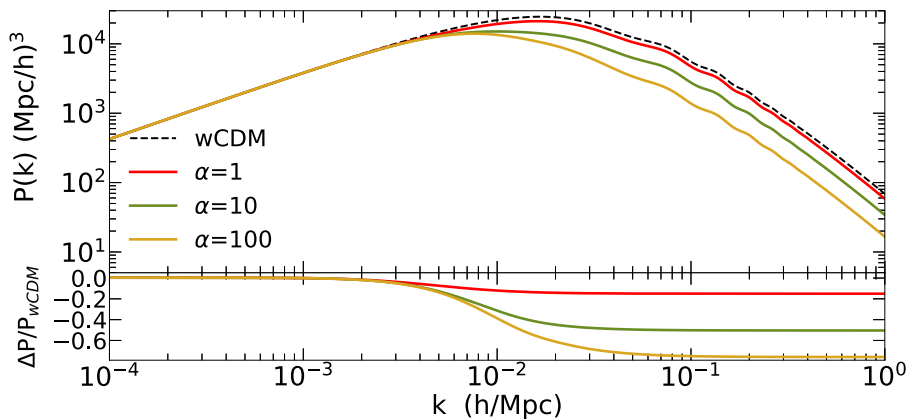
Figure 4.1: Matter Power Spectrum for different values of the coupling parameter α and its ratio with respect to the reference model.

As for the case $\alpha(\tau, k) = \alpha$ we are not introducing any new time or scale dependence, the interaction has to preserve the aforementioned properties. That is only small scales and late-time physics can be affected. Given the potential utility of this interaction in the σ_8 tension, one should look first at the clustering to infer any signal of the interaction. For that purpose, we explore how this interaction modifies the Matter Power Spectrum $P(k)$ for different values of the coupling parameter α, as shown in Figure 4.1. As expected, the interaction leaves no imprint on large scales, that is small k-modes, and only the small scale regime is affected where we see a suppression of the Matter Power Spectrum proportional to the value of the parameter α. We can trace back such suppression to the analytical study done in Section 4.1.1. There, we inferred how the Dark Matter perturbations stop growing when the interaction couples both, Dark Energy and Dark Matter, velocities. Moreover, the suppression exhibits two different regimes as inferred from the relative difference between the interacting Matter Power Spectrum and the wCDM one in the lower panel of Figure 4.1. For intermediate scales it shows a k-dependence, while when we go to smaller scales it saturates becoming k-independent. We can understand such saturation of the suppression since we are dealing with very small scales where gravity is the dominant force overcoming the interaction, something already suspected from the analysis of Section 4.1.1.

A remarkable property, with the capability of being a smoking gun for this interaction, is the shift of the turnover of the Matter Power Spectrum. Generally, its peak scale is determined by the matter-radiation equality time, as in the radiation dominated epoch density perturbations necessarily grow slower than in the matter dominated epoch. But here we are not modifying the background cosmology. This implies that we have the same values for the matter and radiation density as in the reference wCDM model, no matter which value of α we use. Hence, the shift of the peak of the Matter Power Spectrum is purely a feature of the pure momentum transfer. Moreover, this shift effect has an analogous origin to the previously explained
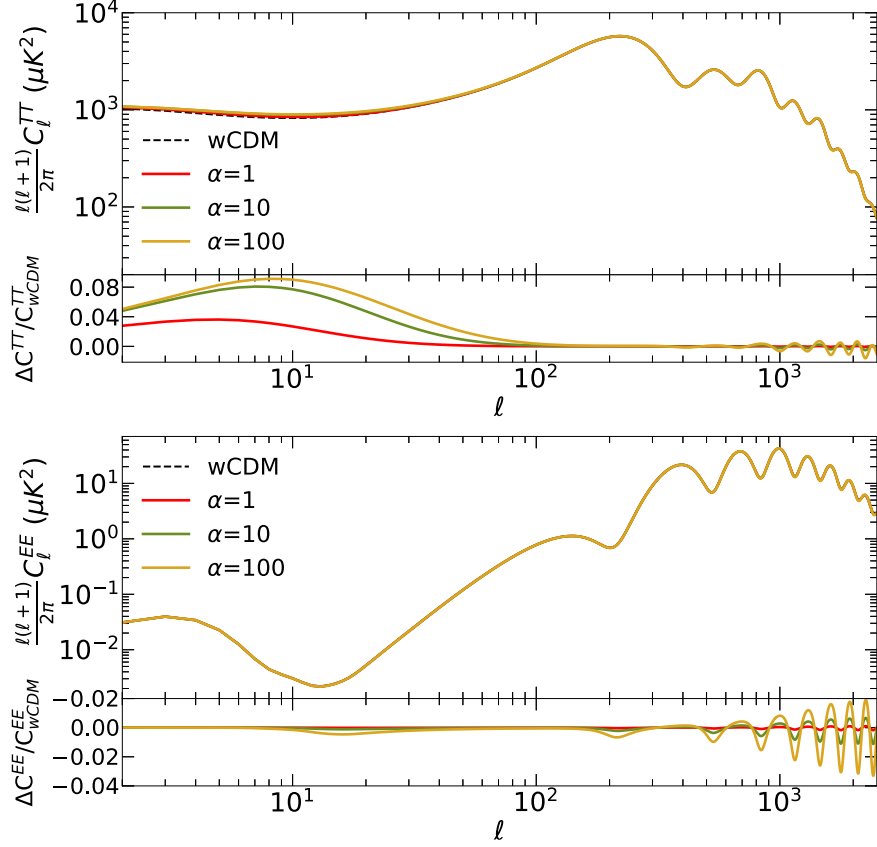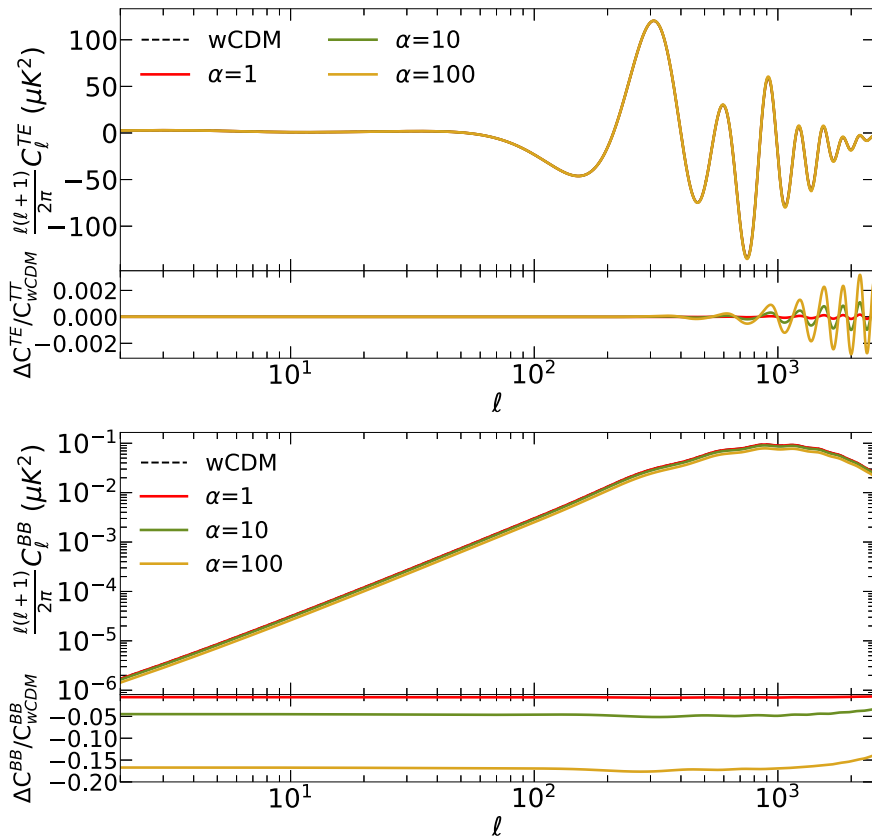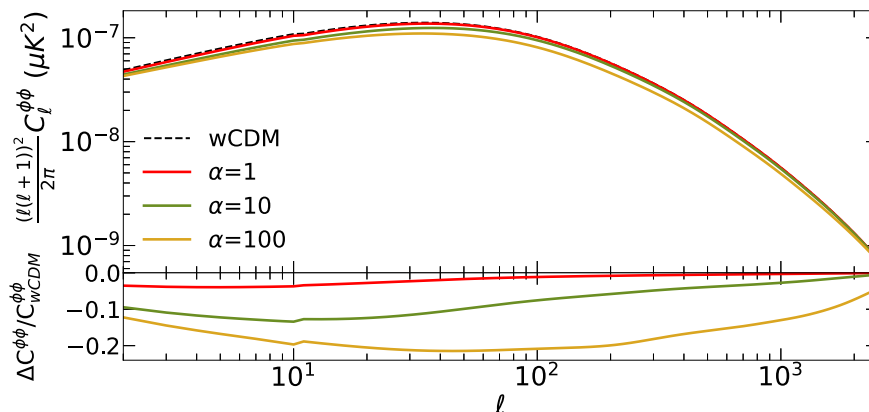
Figure 4.2: Cosmic Microwave Background (TT, TE) for different values of the coupling parameter α and its ratio with respect to the reference model.

radiation-matter equality time effect. Due to the interaction, when both Dark Energy and Dark Matter are coupled, the pressure of Dark Energy prevents the clustering of Dark Matter and, then, the density perturbations necessarily grow slower or even freeze as happened in the radiation dominated epoch. We will numerically confirm this when analysing the density contrast evolution.

Once we have seen the effects on the Matter Power Spectrum, we now focus our attention in the Cosmic Microwave Background. In Figures 4.2 and 4.3, we show the CMB power spectra for temperature TT, EE-polarization, its cross-correlation and BB-polarization for different values of α and for the reference model wCDM. In the case of the temperature power spectrum, the main signal of the interaction appears at large scales through a novel Integrated Sachs–Wolfe (ISW) effect. As expected, since the interaction is relevant at very late-times modifying the clustering and, then, modifying the evolution of the gravitational potential. The more it modifies the gravitational potential, that is the larger the value of α, the larger the late-time ISW effect is. There is also a small scale effect in the form of oscillations for very high-ℓ, but this effect is more notorious in the polarisation power spectrum and in the TE cross-correlated spectrum. It is worth mentioning that this effect only

66

Figure 4.3: Cosmic Microwave Background (EE and BB) for different values of the coupling parameter α and its ratio with respect to the reference model.

appears in the lensed power spectrum due to the modifications on lensing of this interaction and, thus, α controls the amplitude of the oscillations. In the case of the BB-power spectrum the interaction also induces a global correction proportional to the value of α. Also, since the coupling reduces the clustering of matter, the lensing potential decreases as α increases leading to less structures, as shown in the lensing spectrum of Figure 4.4, something already inferred from the Matter Power Spectrum.

In the previous paragraphs, we have explored the main consequences of the Co-variantised dark Thomson-like scattering on the observables Matter Power Spectrum and Cosmic Microwave Background. Those effects appear as consequence of the new term in the Euler equations of Dark Matter (4.5) and Dark Energy (4.7). Hence, in order to understand why those effects appeared, we should analyse the evolution of the perturbation equations due to the new terms. Now, we focus on the evolution of the density perturbation of Dark Matter whose equation remains formally invariant due to the interaction but, as it is coupled to the velocity equation where we have the new interacting term, it will have a different evolution. In the upper panel of Figure 4.5, we have the δ_{dm} evolution using different values of the coupling parameter α for three k-modes. For the very large scale mode $k = 0.001 \ h\mathrm{Mpc}^{-1}$, we see it remains

Figure 4.4: Cosmic Microwave Background ($\phi\phi$) for different values of the coupling parameter α and its ratio with respect to the reference model.

invariant as both fluids share the same rest-frame and, then, the coupling term vanishes leaving the Euler equations as in the reference wCDM model. For small scales modes, $k = 0.01\ h\mathrm{Mpc}^{-1}$ and $k = 1\ h\mathrm{Mpc}^{-1}$, we see how the density contrast gets frozen when the interaction becomes dominant. Again, we already inferred analytically this behaviour in Section 4.1.1. The larger the value of the coupling parameter, the earlier the mode stops growing since the earlier both velocities couple $\theta_{\mathrm{dm}} \sim \theta_{\mathrm{de}}$ and, then, $\delta'_{\mathrm{dm}} \to 0$. This freezing of the density contrast explains the suppression on the Matter Power Spectrum and its shift. When a mode enters the horizon, it does not grow due to the interaction while smaller scale modes have suffered such freezing for a very long time, as we see for example in the upper panel for the mode $k = 1\ h\mathrm{Mpc}^{-1}$. As a consequence of this late-time freezing, the gravitational potential is modified and, then, it acquires a time dependence which induces the late-time ISW effect we have seen in the temperature CMB power spectrum. Moreover, lensing will depart from the reference wCDM model leading to the suppressed lensing power spectrum and the oscillations which appeared in the TT, TE and EE-power spectrum of the CMB.

Provided the σ_8 tension induced us to conjecture about a late-time mechanism which could erase the extra structure, our next step is to analyse the value of σ_8 depending on the value of α. In the lower panel of Figure 4.5, we plot the value of σ_8 calculated by `CLASS` for different values of α with respect to the non-interacting case, as a first taste of the interaction effect on that parameter. We infer how values of the coupling parameter of order $\alpha \sim 10^{-2}$ or smaller provoke no change in σ_8. Nonetheless, larger values of α encode a significant amount of suppression of structures as the value of σ_8 decreases, until it saturates for values of the coupling parameter of order $\alpha \sim 10^4$. With this result, we can justify the normalisation done in equation (4.2) as a way to naturally obtain non-negligible and detectable effects with values of the adimensional coupling parameter of order $\alpha \sim 1$. Consequently, this interaction has the ability of lowering the value of the cosmological parameter
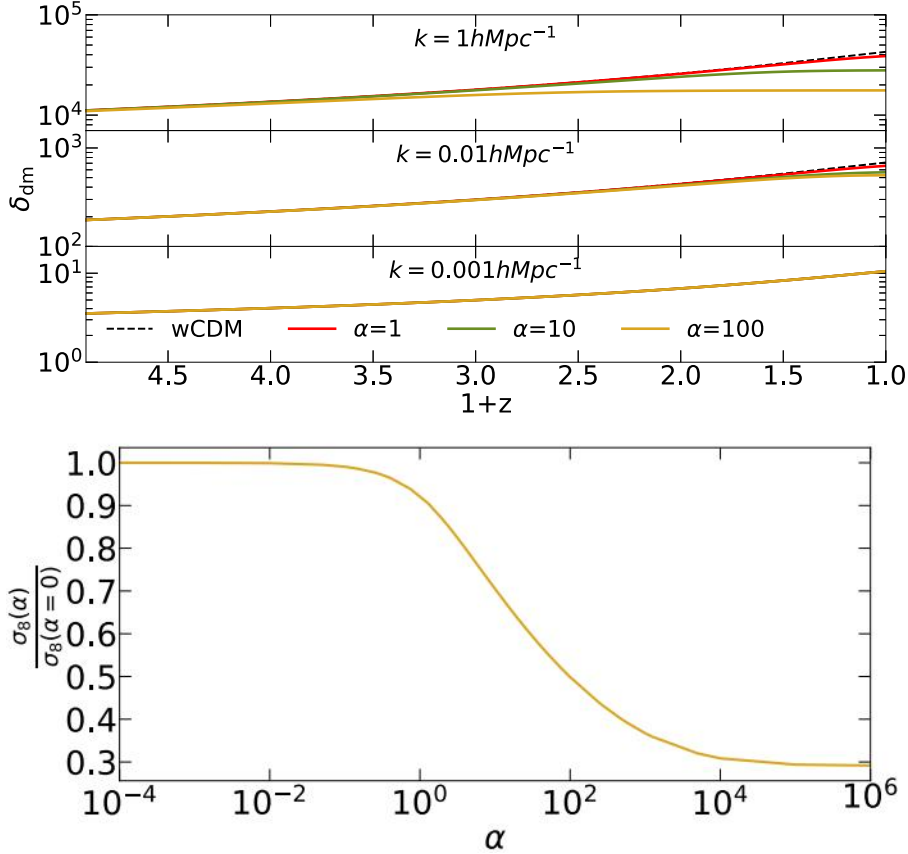
Figure 4.5: Upper panel: Dark Matter density contrast evolution for different values of the coupling parameter α.
Lower panel: ratio between the σ_8 parameter for different values of the coupling parameter α and its non-interacting value.

σ_8 by a late-time mechanism and without modifying the background cosmology or the matter content, leading to the potential alleviation of the σ_8 tension explained in Section 3.4. However, this result can only be confirmed when doing a proper Monte Carlo Markov Chain with real data, as we will do in Section 4.1.3. There, we will also study if the potential ability of this model to alleviate the σ_8 tension brings the worsening of other tensions, like the H_0 one, as it usually happens.

Finally, and given this interaction is dictated by the relative velocity between coupled fluids, the last thing we should study is how the evolution of the perturbed velocity θ departs from the reference wCDM model. In the upper panel of Figure 4.6, we have the relative velocity between Dark Energy and Dark Matter today for different values of the coupling parameter α. It indicates that the larger the value of the coupling α, the smaller the relative velocity between the interacting components. For larger scales, the reduction of the relative velocity is not relevant as it is already negligible provided both components share the same rest-frame. However, for smaller scales, the reduced relative velocity demonstrates how Dark Matter couples Dark
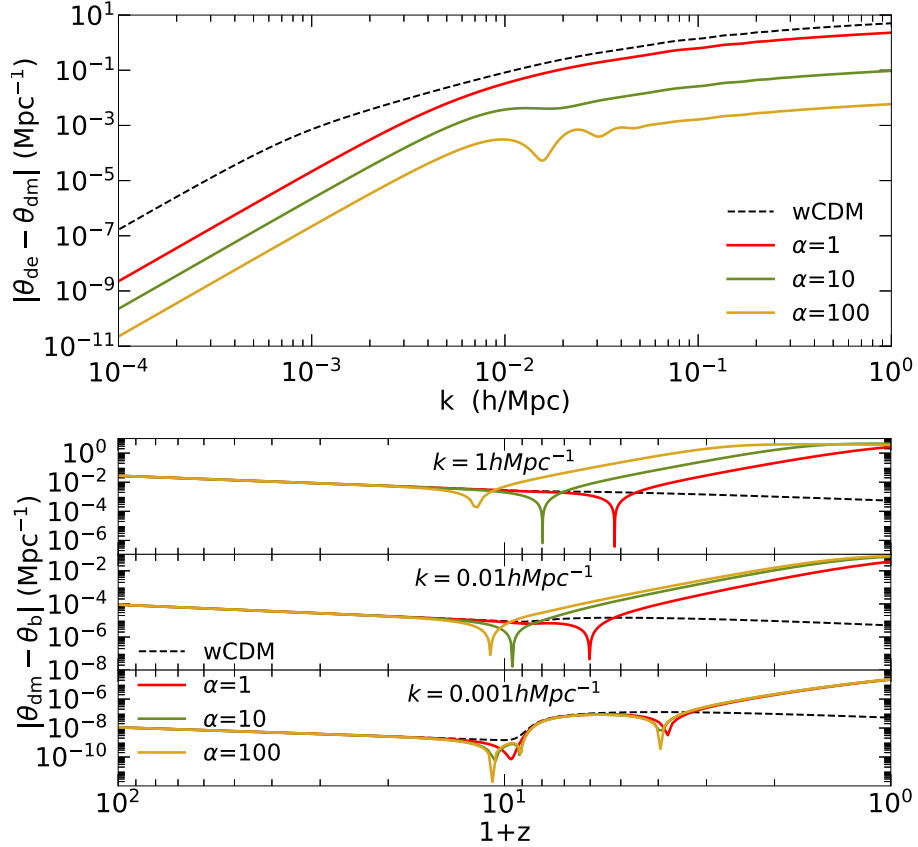
Figure 4.6: Upper panel: relative velocity between Dark Energy and Dark Matter for different values of the coupling parameter α.
Lower panel: relative velocity between Dark Matter and Baryons for different values of the coupling parameter α.

Energy due to the interaction, leading to $\theta_{\mathrm{de}} \sim \theta_{\mathrm{dm}}$ and then suppressing structures as $\delta'_{\mathrm{dm}} \sim (\theta_{\mathrm{de}} - \theta_{\mathrm{dm}}) \sim 0$, as analytically explained in Section 4.1.1 and numerically shown in the above paragraphs. This motivates the perception of the Covariantised dark Thomson-like scattering as a pure momentum transfer interaction leading to a coupling in velocities between both fluids. The consequence of this velocity coupling is even more noticeably seen in the relative velocity between Dark Matter and Baryons in lower panel of Figure 4.6. It is shown how Dark Matter and Baryons relative velocity is negligible no matter the scale (while we are in linear scales) as both fluids are falling into the gravitational potential wells created by the initial seeds. As anticipated, for the late-time Universe, when the interaction becomes efficient, this relative velocity has a kick which represents the Dark Matter no longer falling into the gravitational potential wells as Baryons, but coupling to Dark Energy due to the momentum transfer of this interaction. The pressure of Dark Energy induces a momentum transfer to Dark Matter, preventing it from falling into the potential wells. As a consequence, the Dark Matter density perturbation stops growing and then a
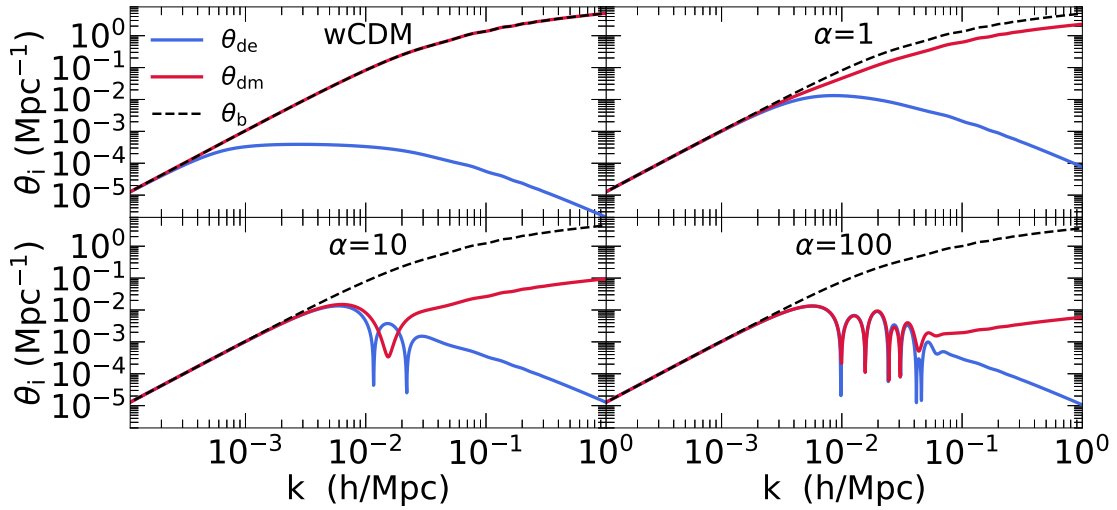
Figure 4.7: Velocity perturbation variable θ today of Dark Energy (blue), Dark Matter (red) and the non-interacting Baryons (black) for different values of the coupling parameter α.

suppression in the power spectrum should appear, as we already saw in previous figures. It is worth mentioning the oscillations that appear at the intermediate scales but, however, it is more illustrative to look at Figure 4.7 where we can infer the three regimes of this interaction to understand such oscillations. For very large scales all components, that is Dark Energy, Dark Matter and Baryons, have the same velocity, no matter the value of the coupling parameter α as all components of the Universe share the same rest-frame. When we deal with intermediate scales where the interaction becomes efficient, Dark Matter velocity no longer follows Baryons velocity, but it tries to couple the Dark Energy one. In this process, if the interaction is strong enough, the Dark Acoustic Oscillations appear. They are the imprint of Dark Energy pressure, trying to put everything apart, fighting with gravity, trying to collapse Dark Matter. As a consequence of this competition between gravity and pressure, the oscillations appear in a very similar process to the Baryons Acoustic Oscillations due to Thomson scattering before decoupling. In that early Universe process, radiation accounts for the pressure while now it is Dark Energy, and Baryons were the massive fluid while Dark Matter plays its role now. When we analyse very small scales, the gravitational pull overcomes the interaction drag and, then, Dark Matter velocity tries again to follow the potential wells.

Cut-off scale

In the previous section, we have shown how the Covariantised dark Thomson-like scattering naturally prevents any effect on very large scales but leaves freedom to modify the small scale regime. Provided this, we can study the possibility of having a screening mechanism which suppresses the interaction at some characteristic scale.
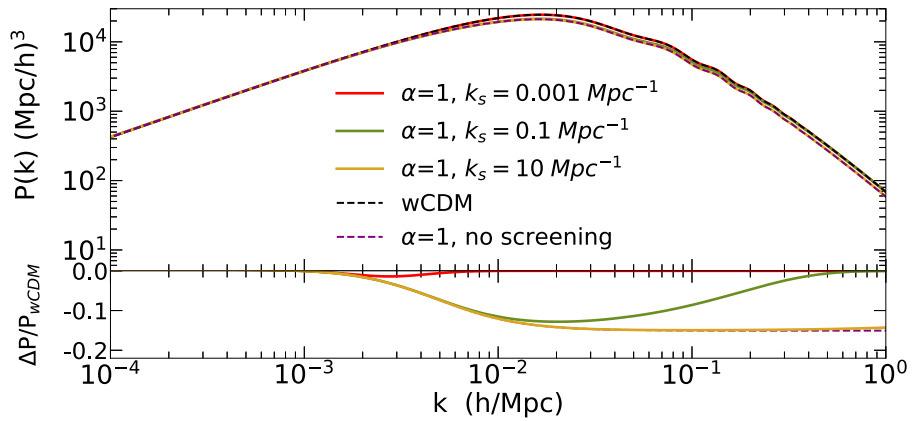
Figure 4.8: Matter Power Spectrum for different values of the cut-off scale parameter k_s fixing $\alpha = 1$, and its ratio with respect to the reference model.

Among all the plethora of possible scale dependencies, we will focus on a very general and phenomenological dependence defined by a cut-off scale k_s given by

$$\alpha(k) = \alpha \, e^{-k/k_s} \ . \tag{4.43}$$

Of course, we are aware of already known mechanisms like Vainshtein or chameleon screening that have a well defined theory behind. But here, with that cut-off, we are only interested in a very phenomenological description that can allow us to detect any relevant scale in this kind of models and/or improve the compatibility with current datasets. Given we are not modifying the time-scale dependence of the coupling, we do not expect any variation in the general mechanism driving this interaction. Moreover, the cut-off only introduces a suppression of the interaction for scales larger than the cut-off scale, that is $\alpha(k > k_s) \to 0$. Consequently, the evolution of the perturbation equations has to mimic the results of the previous section for $k < k_s$. Instead, for $k > k_s$, the evolution ought to follow the one in the reference wCDM model. To confirm our findings we will analyse the Matter Power Spectrum, while the value of σ_8 should reflect its consequences in the previously explained tension.

Regarding the Matter Power Spectrum in Figure 4.8, we plot it for a fixed value of the coupling parameter $\alpha = 1$, while we select different cut-off scales, namely $k_s = 0.001 \ \text{Mpc}^{-1}$, $k_s = 0.1 \ \text{Mpc}^{-1}$ and $k_s = 10 \ \text{Mpc}^{-1}$. We also plot the reference model and the previous case without cut-off scale for $\alpha = 1$. We can infer that for those modes smaller than the cut-off scale in each case $k < k_s$ the power spectrum tracks the results of the previous section with no cut-off scales, while for larger modes $k > k_s$ in each case the spectrum tends to the non-interacting case represented by the wCDM model.

In the case of the σ_8 parameter, we should keep in mind it measures the amount of clustering inside spheres $8 \ h^{-1}\text{Mpc}$ radii. Then, in Figure 4.9 we can see, for a fixed value of the coupling α, that when the cut-off scales are much smaller than the σ_8 characteristic scale its value is not affected by the cut-off. On the other case, when
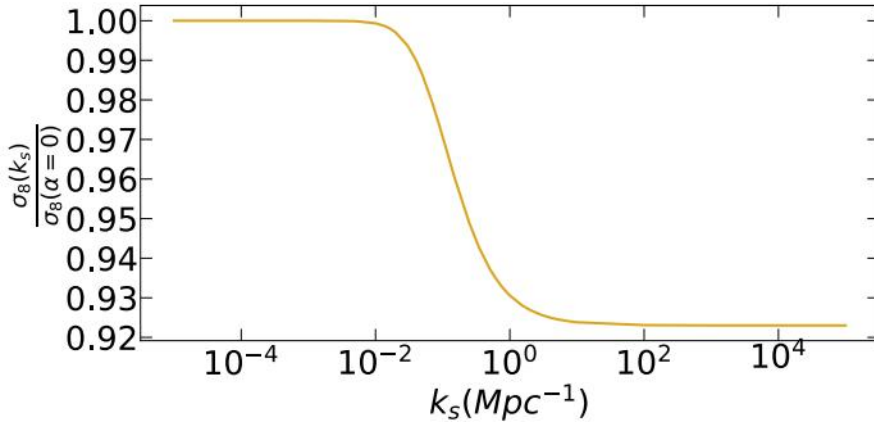
Figure 4.9: Ratio between the parameter σ_8 for different values of the cut-off scale $k_{\rm s}$ fixing $\alpha = 1$ and its non-interacting value.

the cut-off scale includes inside it the σ_8 scale, no lowering appears in the parameter.

The results found above were easily predictable before using the numerical code. However, the key point of adding such cut-off will appear when doing a MCMC analyses, since the goal is to find if a certain scale is preferred by the interaction or not.

Adding extra radiation via a free $N_{\rm eff}$

In all the previous analyses, we set the effective number of relativistic degrees of freedom $N_{\rm eff}$ to its standard model value $N_{\rm eff} = 3.046$. However, nothing prevents us from extending the model allowing for a varying $N_{\rm eff}$ that will be fixed by data. The goal of this extension is, on the one hand, see the possible degeneracy between the coupling parameter and $N_{\rm eff}$, since radiation also suppresses structures and, therefore, both the interaction and a larger value of $N_{\rm eff}$ would act similarly. On the other hand, we know this interaction cannot alleviate the H_0 tension as the background cosmology remains unchanged, but it is a known result that a larger $N_{\rm eff}$ implies a lower value of H_0. However, it is common in the literature that when one alleviates one of the tensions, σ_8 or H_0, the other gets worse, as it is the case with a larger $N_{\rm eff}$ to alleviate H_0 (see for example Figure 35 of Ref. [5]). Thus here, as we already have the momentum transfer dealing with σ_8, we want see if the easing of both tensions can happen simultaneously. Then, we want to study the behaviour of $N_{\rm eff}$ while the interaction is on under a MCMC analysis. Finally, as we will study another momentum transfer model in Section 4.3 where a new Dark Radiation emerges, we want to compare both models under similar conditions, that is, leaving room for extra radiation. Consequently, we will consider in our MCMC analyses this extra degree of freedom.

4.1.3 MCMC results

In the previous sections, we have fully characterised the evolution and main effects on observables due to this interaction both from an analytic point of view and using numerical codes. However, we are still completely blind to what the interaction really looks like in our Universe, given we are yet ignorant to the allowed cosmological and coupling parameters values when the Covariantised dark Thomson-like scattering is taken into account. To fulfil this purpose, we use the public code of Markov Chains Monte Carlo called `MontePython` [32, 33] applied to our modified `CLASS` code. We will not enter in the details of Bayesian statistics here to avoid loosing attention on the models studied. For that, we refer to Appendix A where the basics of Bayesian inference and Markov Chain Monte Carlo techniques, denoted by MCMC, are explained.

In our analyses, and unless specified otherwise, we use the full `Planck 2018` data [5, 29] compiling data from the high-ℓ and low-ℓ modes from the Cosmic Microwave Background (CMB) temperature (TT), polarisation (EE), cross-correlation of temperature and polarisation (TE) and the CMB lensing power spectra, the JLA survey with data from supernovae [117], the Baryonic Acoustic Oscillation data of Refs. [118, 119, 120], the `Planck_SZ` likelihood of the Planck Sunyaev-Zeldovich effect [30] and the weak lensing likelihood `CFHTLenS` [121]. The previous two datasets are implemented in `MontePython` as priors on $S_8^{\mathrm{SZ}} \equiv \sigma_8(\Omega_{\mathrm{m}}/0.27)^{0.3}$ and $S_8^{\mathrm{CFHTL}} \equiv \sigma_8(\Omega_{\mathrm{m}}/0.27)^{0.46}$ respectively. The use of Planck Sunyaev-Zeldovich data presents some caveats that we have already discussed when presenting the observable in Section 2.4. In any case, the value of the `Planck_SZ` likelihood can be found in Table 2 of Ref. [31] as obtained from the combination of `Planck2013+BAO+BBN` and for a fixed mass biased $1 - b = 0.8$. It is implemented under the name `Planck_SZ` in the likelihood gallery of `MontePython`. Although the previously explained caveats and the over-simplified prior method, this likelihood was used in Refs. [95, 97, 101, 103] where similar Thomson-like scatterings were analysed, giving equivalent results as we will see.

In our analyses and unless specified, we will set as cosmological parameter the following combination $\{\Omega_{\mathrm{b}}h^2, \Omega_{\mathrm{dm}}h^2, n_{\mathrm{s}}, A_{\mathrm{s}}.\tau_{\mathrm{reio}}, w, 100\theta_{\mathrm{s}}\}$ and, in addition to that, the model parameters in each case. We also consider as derived parameter the following list $\{z_{\mathrm{reio}}, H_0, \sigma_8, \Omega_{\mathrm{m}}\}$ and the nuisance parameter associated with each likelihood. We restrict ourselves to values of the Dark Energy equation of state fulfilling $w > -1$, while the coupling constant α should be positive or at least with not a large negative value for stability purposes, as explained in Section 4.1.1. We consider flat priors for all parameters and any parameter not mentioned here is set to its default value in `CLASS`. Our reference model will be a wCDM model rather than a ΛCDM one, as we want to avoid any effect of using an equation of state for Dark Energy $w = -1$ or not. Hence, any departure from the reference scenario must be solely attributed to the Covariantised dark Thomson-like scattering.

We will firstly analyse at length the case where there is no time or scale dependence as a proxy to understand how the interaction changes the picture. Later, we will analyse other scenarios around it.

Logarithm sampling $\log_{10} \alpha$

In order to provide the most unbiased approach to the model parameter α estimation, we firstly perform an analysis considering as a parameter $\log_{10} \alpha$ with a very large range of possible values as $\log_{10} \alpha \in [-8, 4]$. Such huge range is inspired by the results obtained in the previous Section 4.1.2 (for example in Fig. 4.5), where values of the coupling parameter such that $\alpha < 10^{-4}$ give no departure from the standard scenario and values fulfilling $\alpha > 10^4$ give completely unrealistic effects. We allow up to the very low limit $\alpha > 10^{-8}$ just to consider a non-interacting-like situation in our first analysis. In any case, we will later study when $\alpha = 0$ is consistently included into the allowed MCMC parameter space to fully discriminate if the interaction is allowed or not.

In Table 4.1 and Figure 4.10 we display the results obtained for the reference scenario wCDM and the Covariantised dark Thomson-like scattering when using as a coupling parameter $\log_{10} \alpha$ as explained. Here, the data used is the full `Planck 2018+JLA+BAO+CFHTLenS+Planck_SZ` combination, each one explained before.

With this analysis, we have confirmed the previously expected values of the coupling parameter $\alpha \sim \mathcal{O}(1)$, given the result is $\log_{10} \alpha = 0.003^{+0.15}_{-0.13}$. In principle, the posterior for the coupling parameter α indicates the interaction is preferred by data, as a non-interacting scenario preference would be represented by very small values of the coupling. However, the non-interacting scenario is not perfectly considered as $\alpha = 0$ is not allowed. Thus, our next step should be setting a narrower range of allowed values for α with the non-interacting scenario included. In this second approach, we will also analyse the shift in the other cosmological and derived parameters when the momentum transfer is considered.

Linear sampling α

Once the previous analysis has determined the coupling parameter is $\alpha \sim \mathcal{O}(1)$, we repeat the same analysis considering now the parameter α per se, inside the range $\alpha \in [-0.1, 100]$[6]. Thus, we do now consider the non-interacting case inside our parameter space, represented by $\alpha = 0$. We again consider the same datasets as before, that is the combination `Planck 2018+JLA+BAO+CFHTLenS+Planck_SZ`, and the result are shown in Table 4.2 and Figure 4.11.

The result for the coupling parameter is

$$\alpha = 1.005^{+0.26}_{-0.33} \, , \tag{4.44}$$

---

[6]We checked that the negative values of α up to $\alpha > -0.1$ remain numerically in the safe zone for not having the instabilities studied in Section 4.1.1.
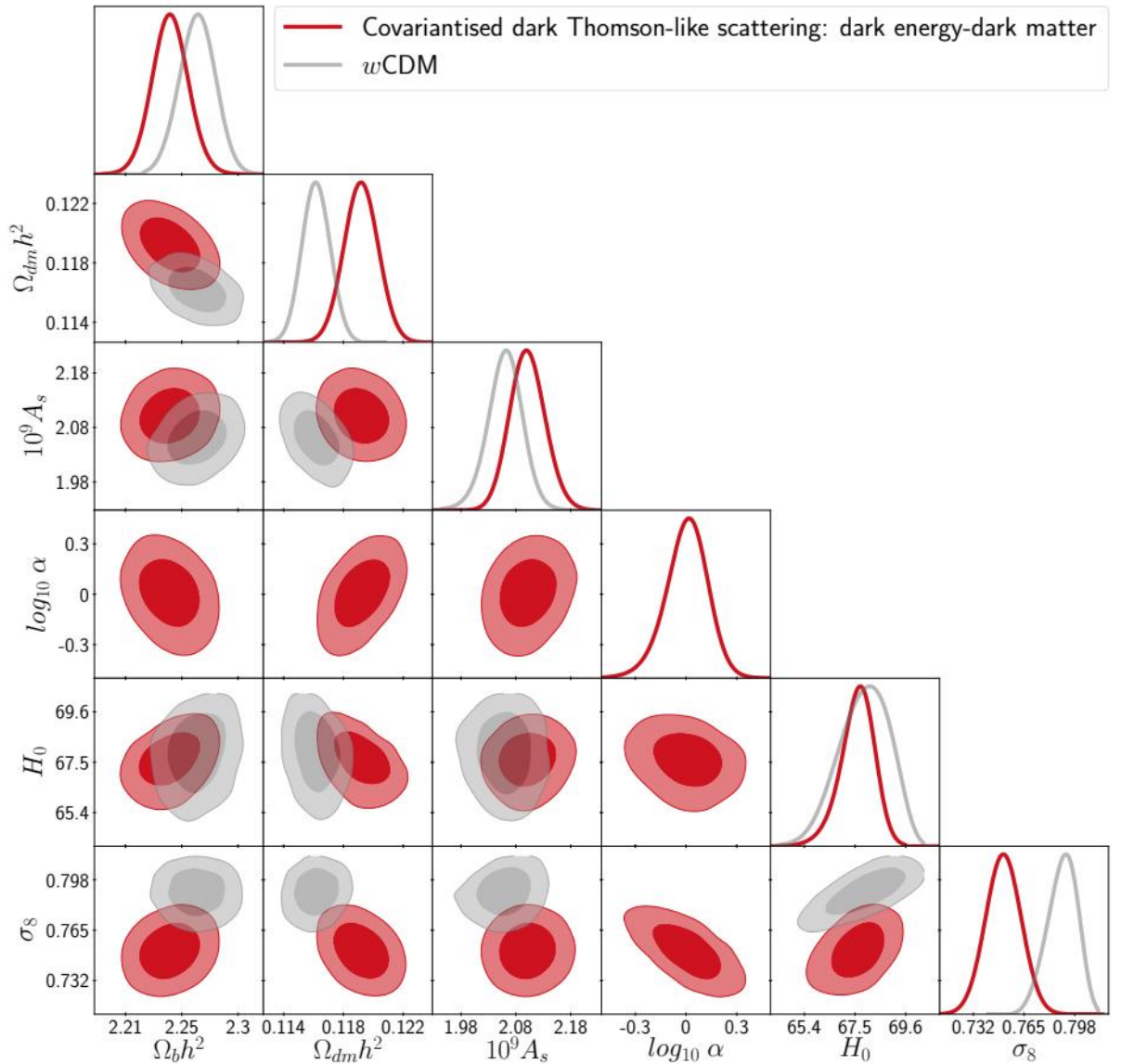
Figure 4.10: In this plot, we show the two-dimensional 1σ and 2σ posterior of several parameters for a wCDM model (gray) and for the interacting model using a logarithmic sampling on the coupling parameter α (red).

which points towards a possible detection of the interaction according to the data used, being one of the most notable results of this PhD dissertation. Even more, we find that the MCMC analysis indicates a more than 3σ detection of the interaction, provided $\alpha \underset{3\sigma}{\in} [0.25, 1.89]$. Regarding the parameter σ_8, we find a large shift on its value when compared to the reference wCDM model. Of course, this result is directly explained by a non-zero value of the coupling parameter α previously encountered. The connection between the interaction and the suppression of structures was explained in Section 4.1.2, and even in Figure 4.5 we already saw the direct connection

Param.	wCDM model			Elastic Interaction $\log_{10} \alpha$		
	mean$\pm\sigma$	2σ lower	2σ upper	mean$\pm\sigma$	2σ lower	2σ upper
$100\Omega_{\mathrm{b}}h^2$	$2.264^{+0.015}_{-0.015}$	2.235	2.295	$2.243^{+0.016}_{-0.016}$	2.211	2.275
$\Omega_{\mathrm{dm}}h^2$	$0.1163^{+0.0010}_{-0.0010}$	0.1143	0.1183	$0.1193^{+0.0012}_{-0.0013}$	0.1168	0.1218
n_{s}	$0.9721^{+0.0042}_{-0.0044}$	0.9638	0.9808	$0.9662^{+0.0044}_{-0.0046}$	0.9572	0.9753
$10^9 A_{\mathrm{s}}$	$2.063^{+0.034}_{-0.034}$	1.991	2.133	$2.105^{+0.033}_{-0.037}$	2.035	2.177
τ_{reio}	$0.0502^{+0.0087}_{-0.0087}$	0.0322	0.0686	$0.0562^{+0.0082}_{-0.0086}$	0.0392	0.0733
w	$-0.948^{+0.022}_{-0.043}$	-0.999	-0.888	$-0.979^{+0.0058}_{-0.021}$	-0.999	-0.939
$100\,\theta_{\mathrm{s}}$	$1.042^{+0.00031}_{-0.00032}$	1.041	1.043	$1.042^{+0.00033}_{-0.00032}$	1.041	1.043
z_{reio}	$7.14^{+0.99}_{-0.82}$	5.18	8.94	$7.84^{+0.83}_{-0.87}$	6.15	9.53
$H_0\ [\frac{\mathrm{km}}{\mathrm{s\,Mpc}}]$	$67.88^{+1.30}_{-0.99}$	65.70	69.98	$67.58^{+0.83}_{-0.73}$	65.97	69.19
σ_8	$0.790^{+0.011}_{-0.010}$	0.770	0.810	$0.752^{+0.012}_{-0.013}$	0.727	0.776
Ω_{m}	$0.302^{+0.0095}_{-0.012}$	0.281	0.323	$0.3104^{+0.0084}_{-0.0095}$	0.2925	0.3291
$\log_{10} \alpha$	$-$	$-$	$-$	$0.003^{+0.15}_{-0.13}$	-0.27	0.30

Table 4.1: In this table, we show the mean and 1σ values and the 2σ limits for the cosmological and derived parameters for a wCDM model (left) and for the interacting model using a logarithmic sampling on the coupling parameter α (right).

between the interaction and the amount of clustering, measured by the σ_8 parameter. This lowering should be highlighted, since in Section 3.4 we introduced the σ_8 tension that emerged between local and early Universe measurements. This possible extension of the concordance model alleviates such tension while not changing anything about the background cosmology. Moreover, it has a well sound motivation regarding its analogy with the already known Thomson scattering as previously explained.

Regarding the matter content, we find a small enhancement of Dark Matter and total matter abundance when comparing the cosmological Ω_{dm} parameter and the derived Ω_{m} parameter, due to the presence of the momentum transfer. On the other hand, there is a tiny lowering of Baryons abundance represented by Ω_{b}. The initial power spectrum is slightly more blue-tilted with a small increase of its amplitude.

However, all these shifts are not statistically relevant as they fall into the $1 - 2\sigma$ level. Other parameters, like the Hubble parameter, remain completely unmodified by this interaction as already expected. Consequently, the alternative Covariantised dark Thomson-like scattering provides, according to the data used, a mechanism to alleviate the so-called σ_8 tension without shifting the other parameters that are well constrained by current datasets. Of course, the H_0 tension cannot be addressed by the pure momentum transfer since the background remains absolutely unmodified.

Furthermore, we find a huge improvement of the χ^2 compared to the reference wCDM model $\Delta\chi^2 = 23.4$ which, using the information criterion explained in Appendix A, leads to $\Delta AIC = 21.4$. This indicates an extraordinary improvement of the fitting power of the Covariantised dark Thomson-like scattering as it strongly supports the new model compared to the reference wCDM model. Combined with the constraint for the coupling constant α that rules out the standard scenario, it calls for more attention in order to fully understand the results obtained. For that purpose, we will now analyse how each dataset used behaves when the interaction is turned on.

Analysing dataset per dataset

The huge improvement of the χ^2 value while strongly constraining the coupling parameter far away from the non-interacting scenario calls for more attention in order to fully understand the results. Regarding the tensions explained in Section 3.4 between different local and early Universe experiments, we will now analyse the impact of each dataset on the determination of the model parameter α. In previous analyses like in Ref. [109], we already determined that the key role for the detection was set by the weak lensing likelihood `CFHTLenS` [121] survey and, particularly, by the `Planck_SZ` likelihood of Planck Sunyaev-Zeldovich effect [30]. On the other hand, the `Planck 2018`, `BAO` and `JLA` data give similar results. Then, in Figure 4.12 we show the results when using the `Planck 2018+JLA+BAO` combination of datasets (green), `Planck 2018+JLA+BAO+CFHTLenS` (blue) and `Planck 2018+JLA+BAO+Planck_SZ` (purple). While most cosmological parameters converge to the same value no matter which datasets combination is used, the coupling parameter α is only fully constrained when the `Planck_SZ` likelihood is considered. When `Planck 2018+JLA+BAO` data, or adding `CFHTLenS` likelihood, we can only establish an upper limit for α.

As a consequence, the previously seen shift in σ_8 clearly responds to the value of α, as only when `Planck_SZ` likelihood is used (and then α is constrained) the σ_8 is solved. As a matter of fact, we should also highlight the behaviour of the `CFHTLenS` likelihood. In the one-dimensional constraint for $\log_{10}\alpha$, we see it also peaks around $\alpha \sim \mathcal{O}(1)$ although it is not able to put a lower constraint on it. This can be connected to the σ_8 two-dimensional posteriors, as for the `CFHTLenS` case a 2σ lower σ_8 value appears. We want to highlight here that we used as convergence criteria for the previous chains the Gelman-Rubin criteria satisfying $R - 1 < 0.01$ for all pa-
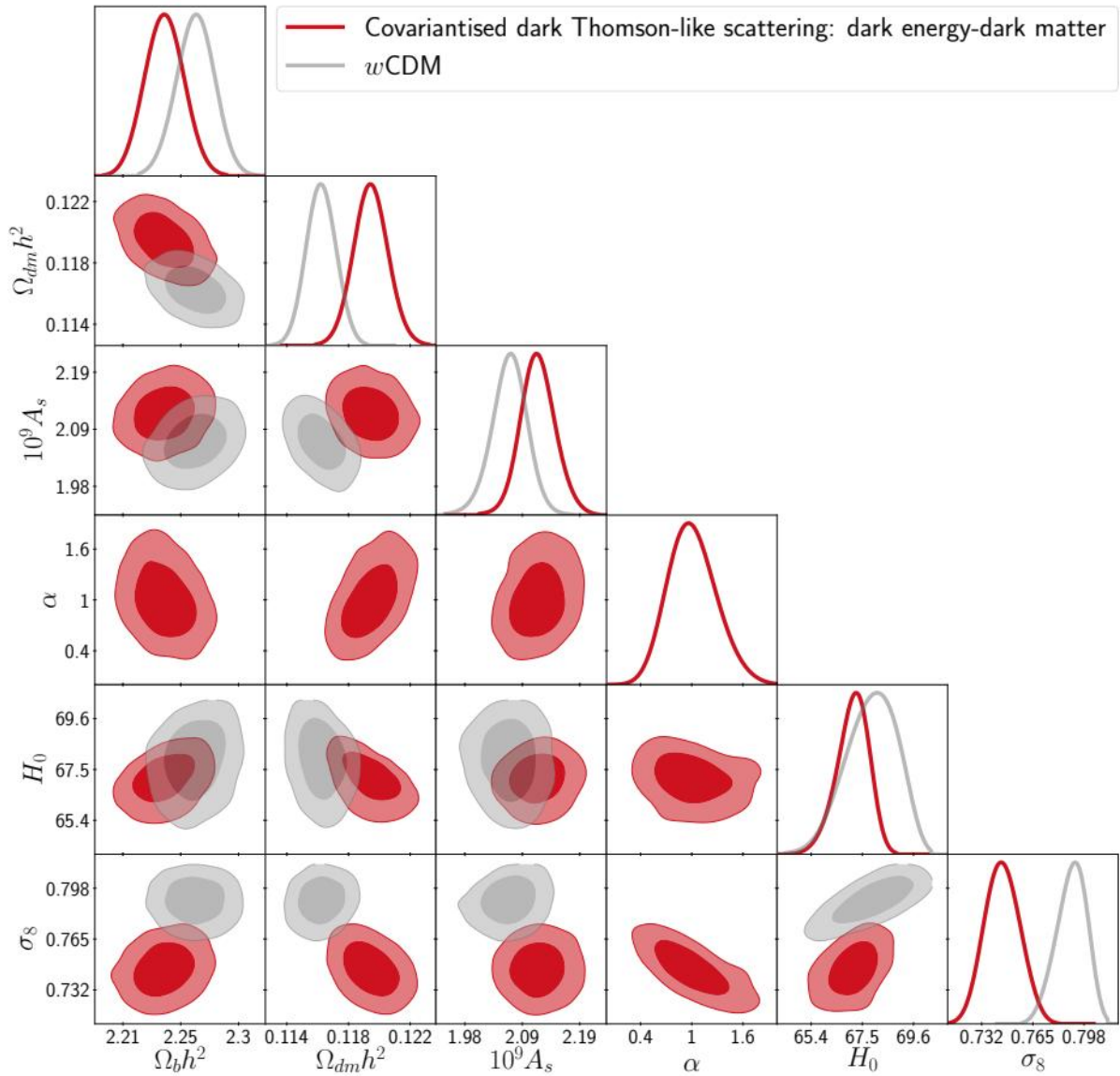
Figure 4.11: In this plot, we show the two-dimensional 1σ and 2σ posterior of several parameters for a wCDM model (gray) and for the interacting model (red).

rameters, as explained in Appendix A. Hence, the extended 2σ region has nothing to do with a problem in the convergence of the chains. Moreover, other momentum transfer models studied in the literature (see for example Refs. [95, 97, 103]) also point toward lower values of the σ_8 parameter. This general result can be explained by the dynamics of every Dark Sector momentum transfer and the local Universe likelihood measurements like `CFHTLenS` and `Planck_SZ`. Both likelihoods, and most local Universe measurements, indicate there are less structures than what early Universe surveys suggest. This is the so-called σ_8 tension explained in Section 3.4. In the Covariantised dark Thomson-like scattering, a late-time/small-scale mechanism

	wCDM model			Elastic Interaction α		
Param.	mean$\pm\sigma$	2σ lower	2σ upper	mean$\pm\sigma$	2σ lower	2σ upper
$100\Omega_{\rm b}h^2$	$2.264^{+0.015}_{-0.015}$	2.235	2.295	$2.241^{+0.015}_{-0.016}$	2.211	2.272
$\Omega_{\rm dm}h^2$	$0.1163^{+0.0010}_{-0.0010}$	0.1143	0.1183	$0.1194^{+0.0012}_{-0.0012}$	0.1171	0.1218
$n_{\rm s}$	$0.9721^{+0.0042}_{-0.0044}$	0.9638	0.9808	$0.9659^{+0.0042}_{-0.0045}$	0.9575	0.9748
$10^9 A_{\rm s}$	$2.063^{+0.034}_{-0.034}$	1.991	2.133	$2.115^{+0.032}_{-0.034}$	2.048	2.183
$\tau_{\rm reio}$	$0.0502^{+0.0087}_{-0.0087}$	0.0322	0.0686	$0.0582^{+0.0081}_{-0.0082}$	0.0415	0.0747
w	$-0.948^{+0.022}_{-0.043}$	-0.999	-0.888	$-0.981^{+0.004}_{-0.019}$	-0.999	-0.943
$100\,\theta_s$	$1.042^{+0.00031}_{-0.00032}$	1.041	1.043	$1.042^{+0.00032}_{-0.00032}$	1.041	1.043
$z_{\rm reio}$	$7.14^{+0.99}_{-0.82}$	5.18	8.94	$8.05^{+0.80}_{-0.78}$	6.46	9.69
$H_0\ [\frac{\rm km}{\rm s\,Mpc}]$	$67.88^{+1.30}_{-0.99}$	65.70	69.98	$67.10^{+0.77}_{-0.62}$	65.63	68.46
σ_8	$0.790^{+0.011}_{-0.010}$	0.770	0.810	$0.746^{+0.012}_{-0.012}$	0.722	0.769
$\Omega_{\rm m}$	$0.302^{+0.0095}_{-0.012}$	0.281	0.323	$0.3166^{+0.0075}_{-0.0087}$	0.3010	0.3338
α	–	–	–	$1.005^{+0.26}_{-0.33}$	0.44	1.65

Table 4.2: In this table, we show the mean and 1σ values and the 2σ limits for the cosmological and derived parameters for a wCDM model (left) and for the interacting model α (right).

appears erasing structures while Planck data is obtained integrating the very early Universe CMB signal until us using a ΛCDM model. Then, those late-time probes like `CFHTLenS` or `Planck_SZ` which already pointed toward a lower value of σ_8, can naturally accommodate a late-time mechanism that precisely erases structures and thus lowers σ_8.

The above explanation also accommodates the huge improvement of the χ^2 value, which should be capitalised by those surveys as they were already claiming for a lower value of σ_8. In order to summarise all this information, we display the main results in Table 4.3. With it, we reveal the crucial role of `Planck_SZ` likelihood on the detection (with some help of `CFHTLenS` likelihood) that clearly sets a lower limit on α while lowering the σ_8 parameter thanks to the interaction, since in the reference model this is not the case. We also show the Hubble parameter H_0 which, as expected, given this interaction cannot modify the background cosmology, it remains
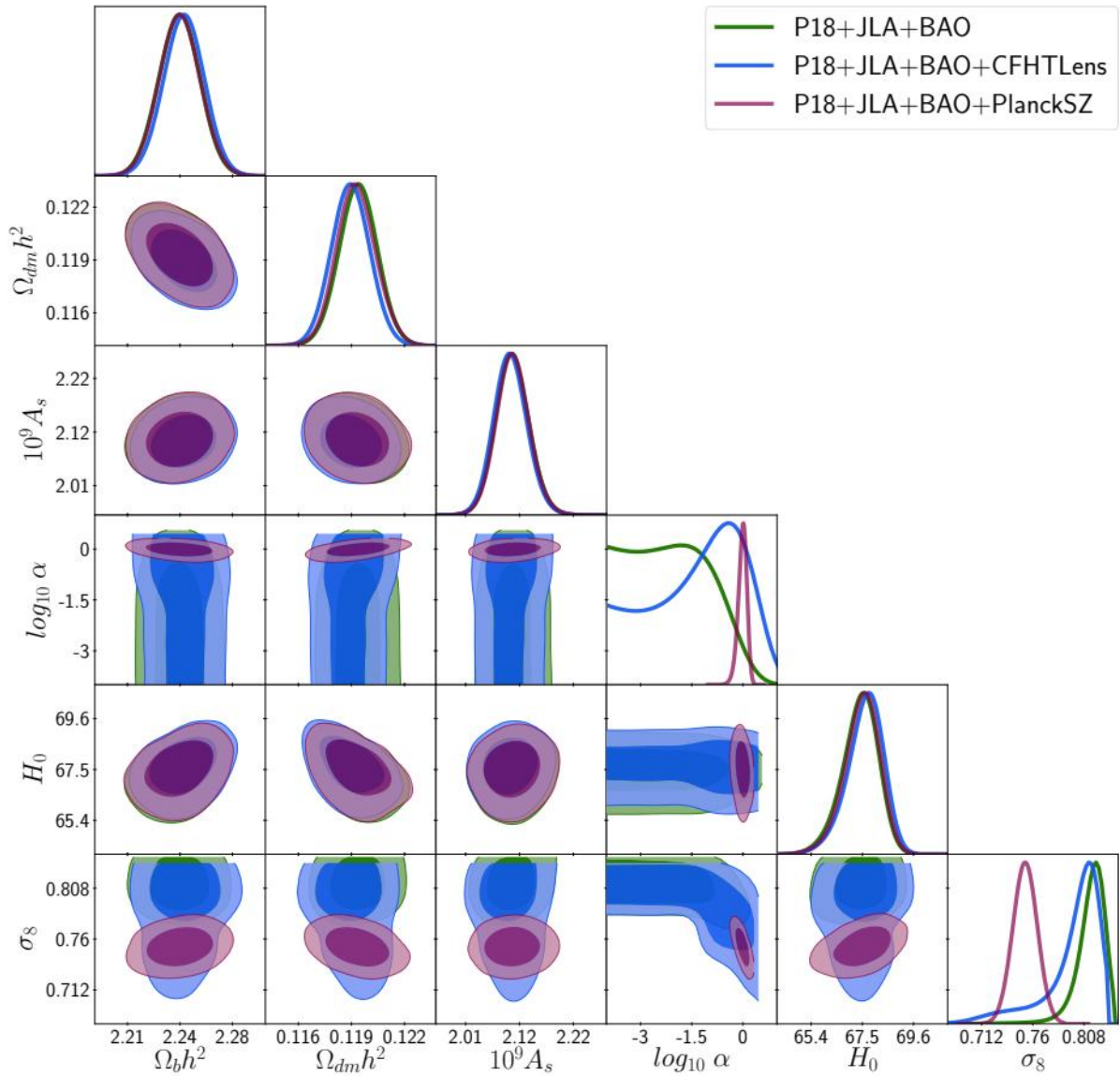
Figure 4.12: In this plot, we show the two-dimensional 1σ and 2σ posterior of several parameters for the Covariantised dark Thomson-like scattering, considering different datasets.

unchanged by the presence of the coupling.

As a conclusion, the presented interaction is able to erase structures by a late-time mechanism naturally explaining local probes measurements of σ_8 and, consequently, alleviating its related tension, while, however, it is blind to the H_0 tension.

	Planck2018	+JLA+BAO	+CFHTLenS	+Planck_SZ	All	All wCDM
$\log_{10} \alpha$	< -2.8	< -2.0	< 0.9	$-0.018^{+0.16}_{-0.13}$	$0.003^{+0.15}_{-0.13}$	$-$
σ_8	$0.797^{+0.035}_{-0.021}$	$0.812^{+0.038}_{-0.010}$	$0.798^{+0.046}_{-0.005}$	$0.753^{+0.013}_{-0.012}$	$0.752^{+0.012}_{-0.013}$	$0.790^{+0.011}_{-0.010}$
H_0	$65.25^{+2.80}_{-1.80}$	$67.4^{+0.89}_{-0.79}$	$67.6^{+0.95}_{-0.82}$	$67.47^{+0.87}_{-0.77}$	$67.58^{+0.83}_{-0.73}$	$67.88^{+1.30}_{-0.99}$

Table 4.3: In this table, we show the mean and 1σ values of certain parameters for the Covariantised dark Thomson-like scattering considering different datasets and for the reference model when all data is applied.

Cut-off scale

In Section 4.1.2, we have considered the possibility of having a screening mechanism for the coupling. Although there are several theories where screening mechanisms appear, we considered a very phenomenological approach defined by $\alpha(k) = \alpha \, e^{-k/k_s}$, where k_s was a certain cut-off scale. Then, we now consider this scenario in our MCMC analyses with the same previous combination of datasets defined by `Planck 2018+JLA+BAO+CFHTLenS+Planck_SZ`. We remind that the goal here is to infer if a certain characteristic scale is present in our model and if compatibility with data improves with it. If so, further theoretical investigations would be needed to explain why. Our bounds for the coupling parameter α are the already used $\alpha \in [-0.1, 100]$, while for the cut-off scale we will follow the same strategy considering first as parameter $\log_{10} k_s$ with extremely wide bounds defined by $\log_{10} k_s \in [-4, 21]$.

In Table 4.4, we show the constraints obtained for the coupling with the screening scale k_s. The cosmological and derived parameters are identical to the ones obtained for the constant coupling before, provided the differences appear inside the 1σ range in each one. The coupling parameter α is again more than 3σ away from a non-interacting value, while it has a slightly higher value compared to the previous case, although not statistically significant. The cut-off scale represented by the parameter k_s is sparsely constrained and pointing to very small scales. Those scales represent non-linear regimes where neither the code `CLASS` used nor the data considered in the MCMC analysis are reliable. Hence, one can conclude that for the linear scales of interest no cut-off scale is preferred by data and, consequently, neither a screening mechanism. Giving the vague constraints obtained, there is no need for an analysis using a linear sampling on k_s, since the results will not improve.

Adding extra radiation

As explained in Section 4.1.2, we may consider the scenario where the effective number of relativistic degrees of freedom N_{eff} is not fixed but acts as a free parameter. Apart from the already used data of `Planck 2018` CMB [5, 29] and the `Planck_SZ`

Param.	wCDM model			Elastic Interaction $\alpha e^{-k/k_{\mathrm{s}}}$		
	mean$\pm\sigma$	2σ lower	2σ upper	mean$\pm\sigma$	2σ lower	2σ upper
$100\Omega_{\mathrm{b}}h^2$	$2.264^{+0.015}_{-0.015}$	2.235	2.295	$2.240^{+0.015}_{-0.016}$	2.209	2.270
$\Omega_{\mathrm{dm}}h^2$	$0.1163^{+0.0010}_{-0.0010}$	0.1143	0.1183	$0.1196^{+0.0012}_{-0.0011}$	0.1172	0.1219
n_{s}	$0.9721^{+0.0042}_{-0.0044}$	0.9638	0.9808	$0.9656^{+0.0040}_{-0.0045}$	0.9574	0.9747
$10^9 A_{\mathrm{s}}$	$2.063^{+0.034}_{-0.034}$	1.991	2.133	$2.101^{+0.031}_{-0.036}$	2.036	2.169
τ_{reio}	$0.0502^{+0.0087}_{-0.0087}$	0.0322	0.0686	$0.0552^{+0.0076}_{-0.0085}$	0.0392	0.0722
w	$-0.948^{+0.022}_{-0.043}$	-0.999	-0.888	$-0.979^{+0.004}_{-0.021}$	-0.999	-0.943
$100\,\theta_s$	$1.042^{+0.00031}_{-0.00032}$	1.041	1.043	$1.042^{+0.00031}_{-0.00031}$	1.041	1.043
z_{reio}	$7.14^{+0.99}_{-0.82}$	5.18	8.94	$7.75^{+0.76}_{-0.84}$	6.13	9.38
$H_0\ [\frac{\mathrm{km}}{\mathrm{s\,Mpc}}]$	$67.88^{+1.30}_{-0.99}$	65.70	69.98	$67.44^{+0.73}_{-0.65}$	65.98	68.92
σ_8	$0.790^{+0.011}_{-0.010}$	0.770	0.810	$0.7483^{+0.011}_{-0.012}$	0.725	0.772
Ω_{m}	$0.302^{+0.0095}_{-0.012}$	0.281	0.323	$0.312^{+0.008}_{-0.009}$	0.295	0.329
α	$-$	$-$	$-$	$1.13^{+0.26}_{-0.33}$	0.53	1.78
$\log_{10} k_{\mathrm{s}}[\mathrm{Mpc}^{-1}]$	$-$	$-$	$-$	$8.5^{+5.2}_{-5.0}$	-1.1	16.6

Table 4.4: In this table, we give the obtained constraints for the cosmological and derived parameters for a wCDM model (left) and for the interacting model with the coupling parameter constant screened (right).

likelihood of Planck Sunyaev-Zeldovich effect [30], here we will promote the data of BAO and Supernovae to the most-updated data of BAO [2, 119, 120] and of Pantheon [6], which at the moment this investigation was performed was available. In Figure 4.13 and in Table 4.5, we display the main results. We find no significant difference with respect to our previous cases, which is translated into the new parameter N_{eff} that is compatible in all cases with the standard model value $N_{\mathrm{eff}} = 3.046$. The previous characteristic effect of the Sunyaev-Zeldovich data appears again, as the interaction is only detected once we add that dataset. Likewise, once we add the Sunyaev-Zeldovich data we have lower values of the σ_8 parameter alleviating its corresponding tension while the H_0 tension is barely alleviated by the free N_{eff}. In any case, the inconvenient effect of alleviating one of the tensions necessarily implying
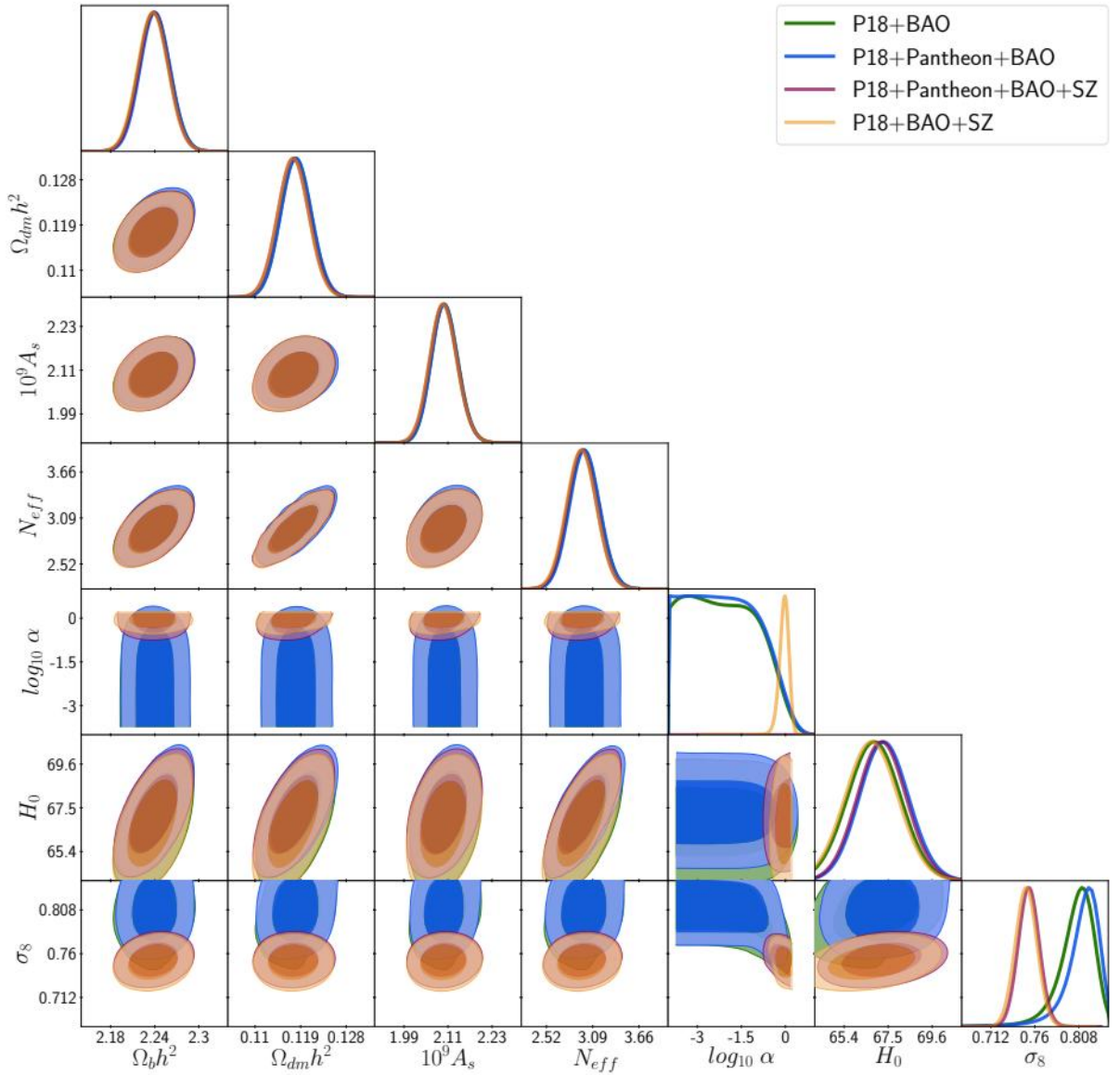
Figure 4.13: In this plot, we show the two-dimensional 1σ and 2σ posterior of several parameters for the Covariantised dark Thomson-like scattering, considering different datasets when we promote N_{eff} to be a free parameter.

the worsening of the other is not present in this model.

	P18+BAO	P18+Pantheon+BAO	P18+BAO+SZ	P18+Pantheon+BAO+SZ
$\log_{10} \alpha$	< -1.5	< -1.5	$-0.06^{+0.18}_{-0.16}$	$-0.05^{+0.45}_{-0.13}$
σ_8	$0.804^{+0.026}_{-0.015}$	$0.808^{+0.02}_{-0.019}$	$0.751^{+0.012}_{-0.013}$	$0.753^{+0.012}_{-0.012}$
H_0	$66.8^{+1.3}_{-1.4}$	$67.3^{+1.2}_{-1.3}$	$66.7^{+1.4}_{-1.3}$	$67.2^{+1.2}_{-1.2}$
N_{eff}	$2.99^{+0.19}_{-0.20}$	$2.99^{+0.19}_{-0.21}$	$2.96^{+0.19}_{-0.20}$	$2.96^{+0.19}_{-0.20}$

Table 4.5: In this table, we show the mean and 1σ values of certain parameters for the Covariantised dark Thomson-like scattering considering different datasets when N_{eff} is a free parameter.

4.2 Covariantised dark Thomson-like scattering: Dark Energy-Baryons

In the previous scenario, the interaction purely belongs to the Dark Sector. Nevertheless, the philosophy of this interaction is more general as it only implies a pressureless matter fluid interacting with a fluid whose pressure erases structure. Thus, we can now involve the cosmological Baryon fluid instead of the Dark Matter component. This work was partially motivated by Ref. [73] where a similar interaction was studied. There, however, they do not found any relevant effect on the cosmology neither in the observables. The key difference between their case and the one studied here is the time dependence of the coupling. In that case, it closely follows the Thomson scattering time dependence, then being not relevant for late times when precisely Dark energy is relevant. Here, we consider a time dependence which makes the interaction relevant by the time Dark Energy is also relevant for the cosmological evolution. Although it therefore departures from a Thomson scattering, since our interaction is mediated by Dark Energy it becomes natural to think its time dependence can correlate with the time when Dark Energy is non-negligible in the Universe. Under this logic, a dark reionization can activate the interaction as standard reionization does with Thomson scattering. Thus, only when Dark Energy is relevant in cosmological scales the interaction would be efficient and its effects seen. Of course, this is not a rigorous motivation. But since we have never detected a field of Dark Energy in our laboratories or we do not have any theory to explain its nature we can only speculate if an interaction associated to Dark Energy should appear when it is relevant in the Cosmic cake. In any case, further investigation must be performed.

As in the previous scenario nothing happens due to the interaction for the background cosmology, then our starting point is the non-conservation of the perturbed stress-energy tensor for the coupled system as

$$\nabla_\mu(T_{\rm b}^{\mu\nu} + \delta T_{\rm b}^{\mu\nu}) = \bar{\beta}\left(u_{\rm de}^\nu - u_{\rm b}^\nu\right) , \qquad \nabla_\mu(T_{\rm de}^{\mu\nu} + \delta T_{\rm de}^{\mu\nu}) = -\bar{\beta}\left(u_{\rm de}^\nu - u_{\rm b}^\nu\right) , \tag{4.45}$$

where now the coupling parameter is $\bar{\beta}$, which we again normalise to get the adimensional coupling parameter $\beta = \frac{8\pi G}{3H_0^3}\bar{\beta}$. As before, following the formalism of Ref. [27] and explained in Chapter 2.3, the equations governing the perturbation sector in the Newtonian gauge are

$$\delta_{\rm b}' = -\theta_{\rm b} + 3\Phi' , \tag{4.46}$$

$$\theta_{\rm b}' = -\mathcal{H}\theta_{\rm b} + k^2\Phi + \Gamma_{\rm T}(\theta_\gamma - \theta_{\rm b}) + \Gamma(\theta_{\rm de} - \theta_{\rm b}) , \tag{4.47}$$

$$\delta_{\rm de}' = -3\mathcal{H}(c_{\rm s}^2 - w)\delta_{\rm de} - (1+w)\left[1 + 9\frac{\mathcal{H}^2}{k^2}\left(c_{\rm s}^2 - w\right)\right]\theta_{\rm de} + 3(1+w)\Phi' , \tag{4.48}$$

$$\theta_{\rm de}' = (-1 + 3c_{\rm s}^2)\mathcal{H}\theta_{\rm de} + k^2\Phi + \frac{k^2 c_{\rm s}^2}{1+w}\delta_{\rm de} - \Gamma R(\theta_{\rm de} - \theta_{\rm b}) , \tag{4.49}$$

while in the synchronous gauge we have

$$\delta'_{\mathrm{b}} = -\left(\theta_{\mathrm{b}} + \frac{1}{2}h'\right) , \tag{4.50}$$

$$\theta'_{\mathrm{b}} = -\mathcal{H}\theta_{\mathrm{b}} + c_{\mathrm{s}}^2 k^2 \delta_{\mathrm{b}} + \Gamma_{\mathrm{T}}(\theta_\gamma - \theta_{\mathrm{b}}) + \Gamma(\theta_{\mathrm{de}} - \theta_{\mathrm{b}}) , \tag{4.51}$$

$$\delta'_{\mathrm{de}} = -(1+w)\left(\theta_{\mathrm{de}} + \frac{1}{2}h'\right) - 3\mathcal{H}(c_{\mathrm{s}}^2 - w)\delta_{\mathrm{de}} - 9(1+w)\left(c_{\mathrm{s}}^2 - w\right)\frac{\mathcal{H}^2}{k^2}\theta_{\mathrm{de}} , \tag{4.52}$$

$$\theta'_{\mathrm{de}} = \left(-1 + 3c_{\mathrm{s}}^2\right)\mathcal{H}\theta_{\mathrm{de}} + \frac{k^2 c_{\mathrm{s}}^2}{1+w}\delta_{\mathrm{de}} - \Gamma R(\theta_{\mathrm{de}} - \theta_{\mathrm{b}}) , \tag{4.53}$$

where Γ_{T} is the interaction rate due to the Photon-Baryon Thomson scattering defined as $\Gamma_{\mathrm{T}} \equiv \frac{4\rho_\gamma}{3\rho_b}an_e\sigma_{\mathrm{T}}$ with n_e the abundance of free Electrons and σ_{T} the Thomson scattering cross section. Now the interaction rate of the coupling studied here Γ and the Baryons-to-Dark Energy ratio R are

$$\Gamma \equiv \bar{\beta}\frac{a}{\rho_{\mathrm{b}}} , \tag{4.54}$$

$$R \equiv \frac{\rho_{\mathrm{b}}}{(1+w)\rho_{\mathrm{de}}} . \tag{4.55}$$

Given the previous results for the Dark Energy-Dark Matter case, here we will only study the case where the coupling has a constant value $\beta(\tau, k) = \beta$. Therefore, the interaction is relevant for small scales where peculiar velocities between components arise $\theta_{\mathrm{de}} \neq \theta_{\mathrm{b}}$ and, then, the new interacting term does not vanish. Moreover, the interaction is relevant for the late Universe when we have $\Gamma > \mathcal{H}$, provided β is constant. In equation (4.47) we can clearly see the analogy between this interaction and the Baryon-Photon Thomson scattering. As explained, both couplings have completely different time-scales due to the time dependence of the interaction rates, Γ and Γ_{T}, in each case. However, the process is similar leading to the analogue of Baryon Acoustic Oscillation, which we called Dark Acoustic Oscillations.

In the following sections, we will investigate the main effects of this coupling. As the similarities with the Dark Matter interacting case are obvious we will focus on the main differences.

4.2.1 Regimes

In this subsection, we could present a similar analysis as in the previous section 4.1.1 where we studied the model in different regimes. We could reproduce the same investigation here but the results will be similar to the previous case just replacing Dark Matter by Baryons. There is, however, one subtlety since in this case the gravitational potential can be treated as an external field mainly created by Dark Matter. However, we will see numerically that the effects in both cases are interchangeable and, thus, we can omit the same analyses here.

4.2.2 Linear effects

As done for the previous case, we have created a modified version of the Boltzmann solver code `CLASS` [113, 114] where the new interacting terms are included in the Euler equations for Baryons and for Dark Energy. At the same time, in Ref. [108] a version of the `CAMB` code was also created, finding no differences between both codes. Compared to the Dark Energy and Dark Matter case, here we have a subtlety due to modifying the evolution of the baryonic matter. Baryons are coupled via Thomson scattering to Photons beforehand, something particularly important for the early Universe before recombination and for the reionization process. Before recombination, Baryons and Photons formed a coupled system via their respective Euler equations, something which numerically can be extremely problematic when the different integrator algorithms are used. To avoid that, codes like `CLASS` or `CAMB` use the Tight Coupling Approximation (TCA) scheme which uses the approximations developed for the coupled Baryon-Photon system in Ref. [122]. Because of the Thomson scattering and the consequent TCA scheme, also radiation sector could be affected when we include our momentum transfer terms, even though the coupling is not to any radiation component. Photons are also treated under one approximation called the Radiation Streaming Approximation (RSA) scheme. Then, our first step has been to test how we should include the new terms in our equations and in the two different schemes, both fully explained in Ref. [114]. We found that no relevant difference appears if we consistently modify both schemes, TCA and RSA, propagating the new coupling terms through them, or if we only modify the equations for Baryons and for Dark Energy. The reason is that the coupling becomes relevant at low redshifts, where these approximations are not acting as we are significantly after recombination or reionization. Therefore, no matter if we propagate the terms through the schemes as they are not being used for the very late Universe when this interaction is acting. For our analysis, we set the same cosmological parameters as in the previous case, that is: $H_0 = 67.4$ Km/s/Mpc, $\Omega_b h^2 = 0.0224$, $\Omega_{dm} h^2 = 0.120$, $\tau_{reio} = 0.054$, $A_s = 2.1 \ 10^{-9}$, $n_s = 0.965$, $w = -0.98$ and $c_s^2 = 1$. Any other parameter is set to the default value of the code and our background cosmology is a wCDM model as required. Here, the implementation is done in the Newtonian gauge in `CLASS`, but the implementation in `CAMB` of Ref. [109] was done in the Synchronous one, with no differences found.

In Figure 4.14, we plot the Matter Power Spectrum for different values of the coupling parameter β and we compare it to the reference wCDM model. As before, we have a suppression for intermediate scales that saturates for smaller scales. The reason is the same as in the Dark Matter case and as analytically explained in Section 4.1.1. When the interaction is efficient, we have that both velocities couple $\theta_b \sim \theta_{de}$ and, since $\delta_b' \propto \theta_{de} - \theta_b$, the Baryons perturbations stop growing. That is reflected as a suppression in the Matter Power Spectrum. Again, we have a shift in the peak of the spectrum which no longer is only set by the equality time. The only
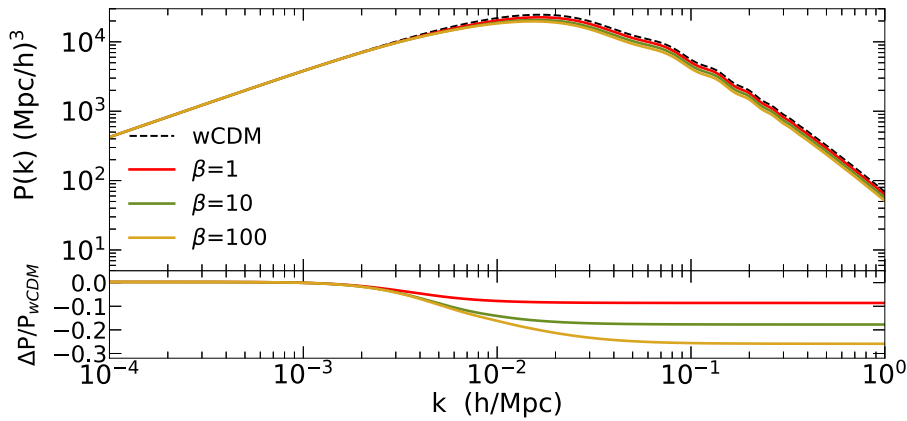
Figure 4.14: Matter Power Spectrum for different values of the coupling parameter β and its ratio with respect to the reference model.

difference compared to the case where Dark Matter was the interacting pressureless fluid is the amount of suppression. As $\Omega_{\mathrm{dm}}/\Omega_{\mathrm{b}} \sim 5$, we have proportionally less capability of suppression, which is clearly inferred if we compare both spectra for Dark Energy-Dark Matter of Figure 4.1 and for Dark Energy-Baryons of Figure 4.14.

Regarding now the Cosmic Microwave Background, we again have the additional Integrated Sachs-Wolf effect for low-ℓ in the TT-spectrum as shown in Figure 4.15. As before, the suppression of structures induces a time dependant gravitational potential which happens for very late times. We also find in the cross-correlated TE and EE-polarisation spectra the oscillations whose amplitude depends on the value of β, for the high-ℓ and only for the lensed spectra as depicted in Figures 4.15 and 4.16. The BB-polarisation spectrum also has a correction while, as shown in Figure 4.17, as there are less structures due to the coupling the lensing spectrum has a suppression proportional to the value of β.

One can understand the previous effects analysing the density perturbations of Baryons, shown in the upper panel of Figure 4.18. For late times and smaller scales, the Baryon density perturbation gets frozen in time once the interaction is efficient. This means we no longer have creation of structures, at least those associated with Baryons. However, one noticeable difference appears compared to the previous case. When we analysed the Dark Energy-Dark Matter interaction, the suppression started at $z \sim 2.5$ for very small scales $k = 1\ h\mathrm{Mpc}^{-1}$ and $\alpha = 100$. Now, for the case of Baryons and the same scales, for $\beta = 100$ we already have suppression at $z \sim 3.5$. The reason for that emerges from the definition of the interaction rate Γ in each case: $\Gamma_\alpha = \alpha\frac{a}{\rho_{\mathrm{dm}}}$ and $\Gamma_\beta = \beta\frac{a}{\rho_{\mathrm{b}}}$. Although both couplings have the same normalisation, for a given value such that $\alpha = \beta$ we have $\Gamma_\beta \sim 5\Gamma_\alpha$. Therefore, one naturally expects to modify earlier the evolution of the density perturbations in the case of Baryons. In the lower panel of Figure 4.18, we plot the value of the σ_8 parameter divided by its non-interacting value. We find that the larger the value of the coupling β, the stronger the suppression of structures, as reflected in the figure. Again, this
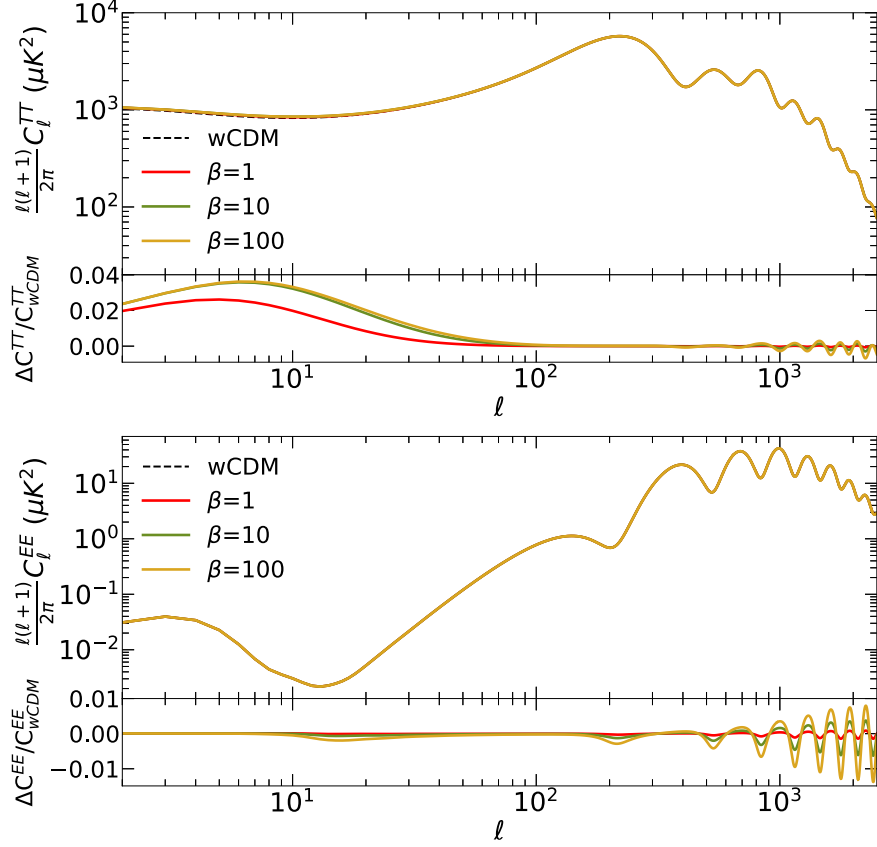
Figure 4.15: Cosmic Microwave Background (TT, TE) for different values of the coupling parameter β and its ratio with respect to the reference model.

result has powerful implications when dealing with the σ_8 or S_8 tension explained in Section 3.4, as this type of interactions can alleviate the tension as we will see.

Finally, we should look at how the velocity perturbation variable works. In the upper panel of Figure 4.19, we display the relative velocity today between Dark Energy and Baryons. As expected and analysed before, the interaction induces a strong coupling between both fluids which is translated into coupled velocities. Then, as a result, we see in the panel how the larger the value of the coupling β, the less the relative velocity. This confirms our expectations of $\theta_{\rm b} \to \theta_{\rm de}$ when the interaction becomes efficient and, consequently, the freeze of Baryons perturbations seen in Figure 4.18, since when the coupling dominates we have $\delta'_{\rm b} \propto \theta_{\rm de} - \theta_{\rm b} \to 0$. In the lower panel of Figure 4.19, we have the evolution of the relative velocity between both matter components, that is Baryons and Dark matter. For most of the time, its relative velocity is small as what we are seeing is both components falling into the potential wells at the same rate, as it should be expected from the Equivalence Principle. However, once the interaction is efficient, the relative velocity has a quick. This comes from the injection of pressure of Dark Energy into Baryons via a momentum transfer given by the interaction, which prevents Baryons from falling into the
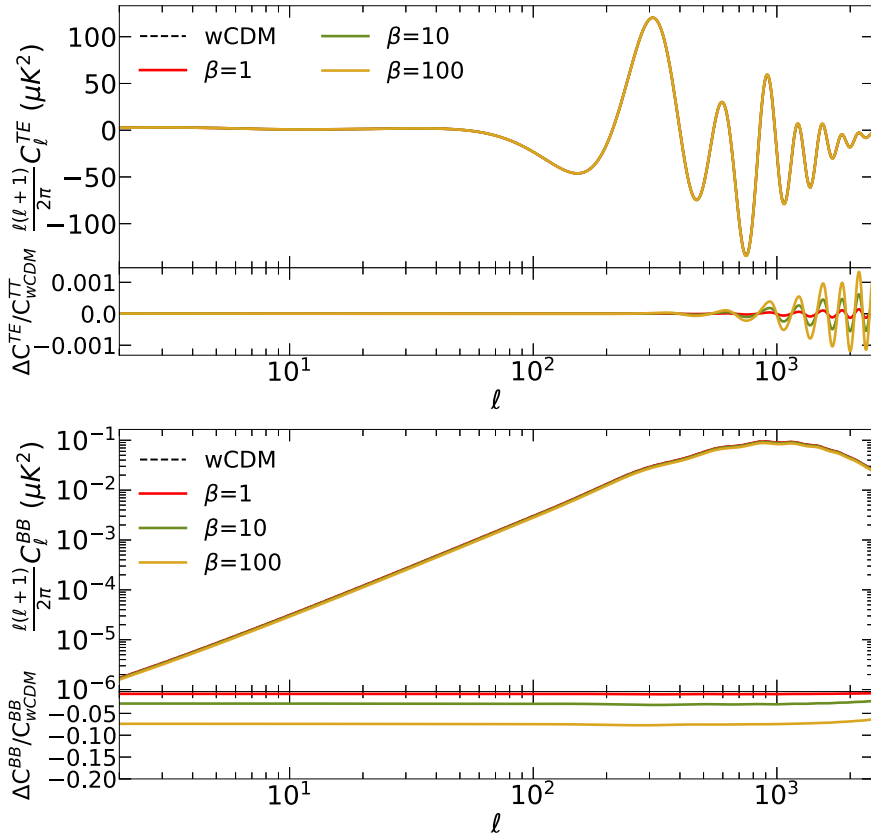
Figure 4.16: Cosmic Microwave Background (EE and BB) for different values of the coupling parameter β and its ratio with respect to the reference model.

potential wells. Even more clearly is seen in Figure 4.20. For the reference wCDM model, we have that both matter components are equivalent today no matter which scale we look into. If the interaction is there, the velocity of Baryons tries to couple Dark Energy velocity, although for very small scales gravity overcomes the coupling drag and, thus, Baryons also fall into the potential wells. As previously noticed, we have some oscillations which we can call here partially[7] Dark Acoustic Oscillations. As before, they reflect the competition between gravity trying to cluster Baryons and Dark Energy pressure trying to put everything apart. This is the very similar process as in the Dark Matter case and very similar to Baryons Acoustic Oscillations, but now the pressure is not due to Photons but due to Dark Energy.

4.2.3 MCMC results

As done in the previous case, we now want to see how data constrain the coupling parameter β and how the other cosmological parameters are modified due to the presence of the interaction. To do that, we apply to our modified version

---

[7]For the case of Dark Energy-Dark Matter they were Dark Acoustic Oscillations, but now one of the coupled components is Baryons.
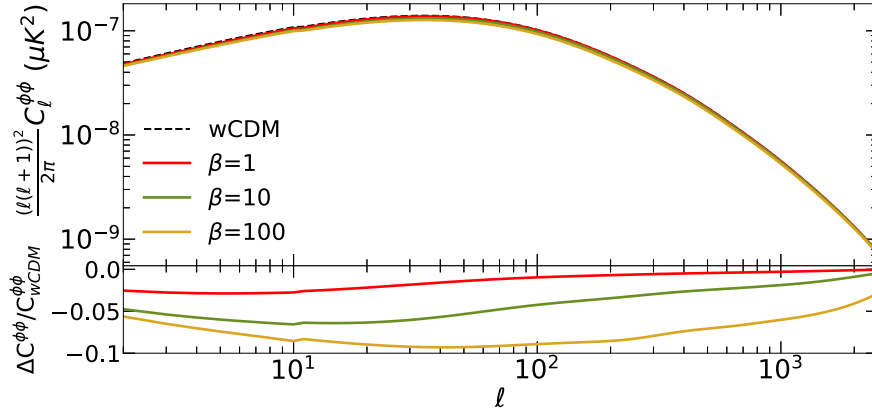
Figure 4.17: Cosmic Microwave Background ($\phi\phi$) for different values of the coupling parameter β and its ratio with respect to the reference model.

of `CLASS` the Bayesian statistics code `MontePython` [32, 33]. As already said, the basics of Bayesian inference and MCMC techniques are explained in Appendix A. To be consistent, we will use the same datasets as before, that is the full `Planck 2018` likelihood [5, 29] with data from the high-ℓ and low-ℓ from CMB temperature (TT), polarisation (EE), cross-correlation of temperature and polarisation (TE) and the CMB lensing power spectra ($\phi\phi$), the JLA survey with data from supernovae [117], the Baryonic Acoustic Oscillations data of Refs. [118, 119, 120], the `Planck_SZ` likelihood of Planck Sunyaev-Zeldovich effect [30] and the weak lensing likelihood `CFHTLenS` [121]. As parameters, we consider as cosmological parameters the following list $\{\Omega_b h^2, \Omega_{dm} h^2, n_s, A_s . \tau_{reio}, w, 100\theta_s\}$ and $\{z_{reio}, H_0, \sigma_8, \Omega_m\}$ as derived parameters. We also add the nuisance parameters corresponding to the previous likelihoods and our coupling parameter β. We consider flat priors for all the previous parameters, but we add a bound to the Dark Energy equation of state as $w > -1$, following the stability condition derived in Section 4.1.1, which should also hold in this case.

As done in the case of Dark Energy-Dark Matter, we will first perform an analysis sampling the logarithm of the parameter $\log_{10} \beta$ to set the expected order of magnitude.

Logarithm sampling $\log_{10} \beta$

In this first step, we want to establish the order of magnitude of the new parameter β, which controls the amount of momentum transfer. To do so, we consider a flat prior on $\log_{10} \beta$ over the large range $\log_{10} \beta \in [-8, 4]$. Although the non-interacting case, that is $\beta = 0$, is not properly considered, values of the coupling smaller than $\beta \leq 10^{-2}$ give no significant deviation from the non-interacting case. In any case, later we will consider that case properly.

We display in Table 4.6 and Figure 4.21 the results obtained for the Dark Energy-Baryons Covariantised dark Thomson-like scattering and the reference model for
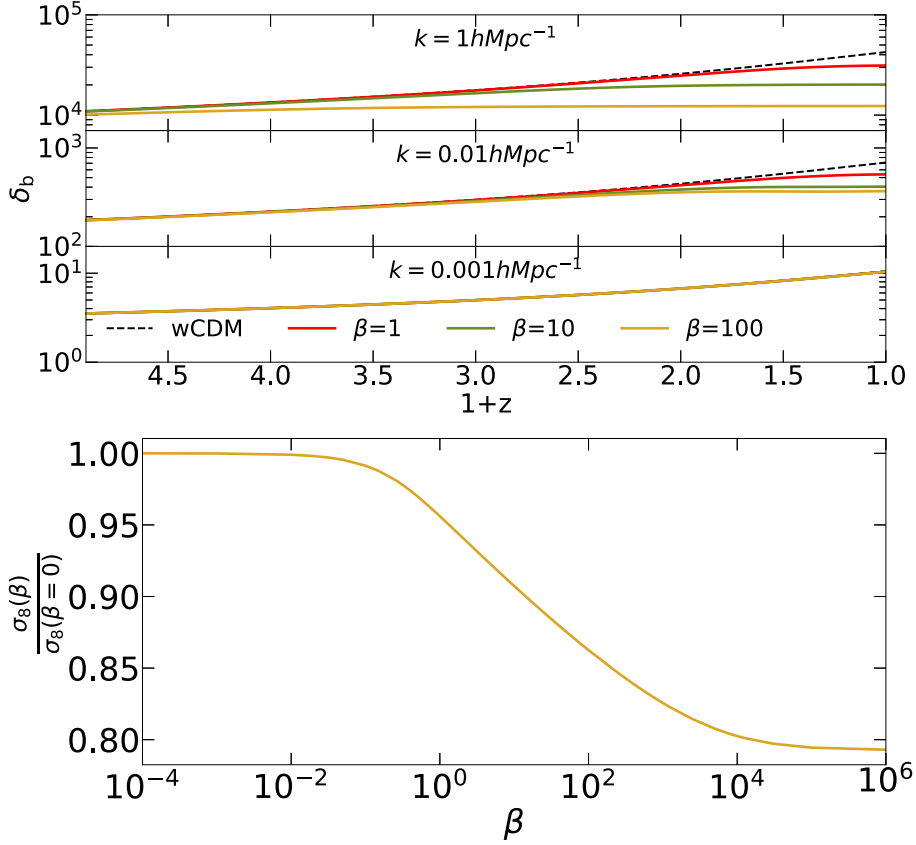
Figure 4.18: Upper panel: Dark Matter density contrast evolution for different values of the coupling parameter β.
Lower panel: ratio between the σ_8 parameter for different values of the coupling parameter β and its non-interacting value.

the combination of data `Planck 2018+JLA+BAO+CFHTLenS+Planck_SZ`. Regarding the constraints of the coupling parameter, we have $\beta \sim \mathcal{O}(1 - 10)$ given the result we obtain is $\log_{10} \beta = 0.63^{+0.39}_{-0.47}$, as expected by the normalisation chosen. This indicates we can move to a linear sampling of the parameter β to better constrain its value and, there, we will analyse how the other parameters are modified.

Linear sampling β

Once we have the order of magnitude, we repeat our experiment with a linear sampling of the coupling parameter β bounded inside the range $\beta \in [-0.01, 100]$. Thus, this time we do consider the non-interacting case. The results are shown in Table 4.6 and in Figure 4.21.
However, in this case we are not able to constrain the coupling parameter more than the 1σ region, as the 2σ upper limit is cut by the upper bound chosen and the very same happens for the lower limit. We did try with other bounds having no better results as shown in Ref. [108]. This implies that the data cannot set reliable limits
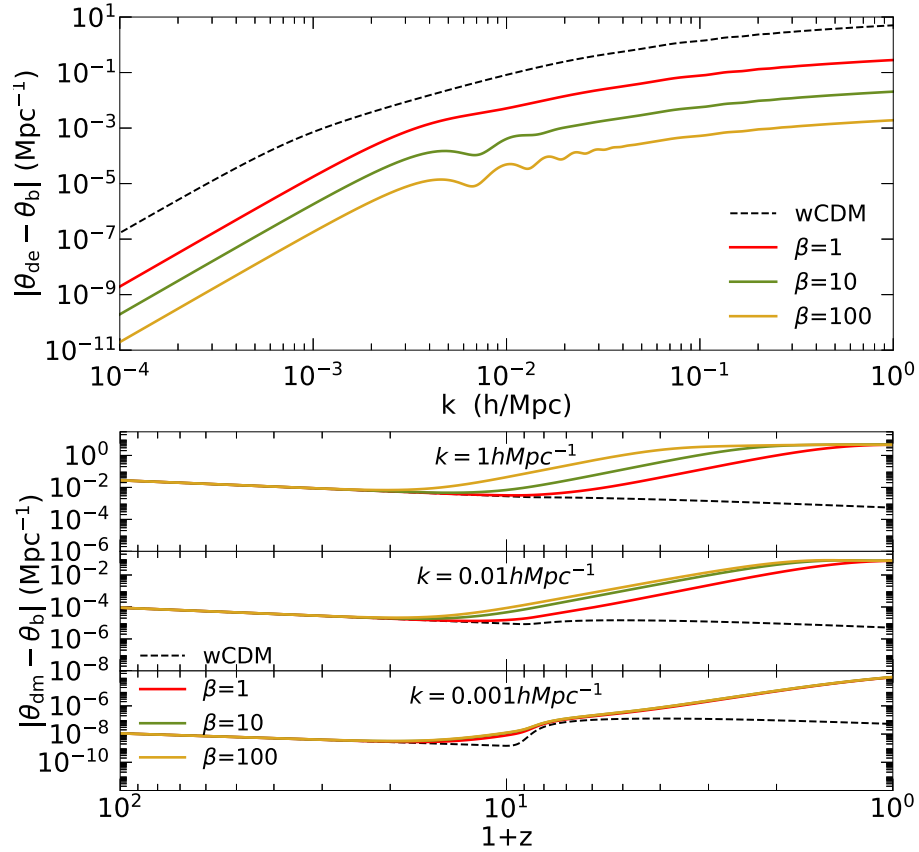
Figure 4.19: Upper panel: relative velocity between Dark Energy and Dark Matter for different values of the coupling parameter β.
Lower panel: relative velocity between Dark Matter and Baryons for different values of the coupling parameter β.

when the linear sampling on the parameter is used, while when we were setting just the scale in the logarithm case we were able to fit its value inside $\beta \underset{2\sigma}{\in} [0.63, 34.67]$ and even inside the 3σ region $\beta \underset{3\sigma}{\in} [0.25, 120.23]$. Regarding the other parameters, we find a strong shift to lower values in the σ_8 parameter. This results directly connects with the σ_8 or S_8 tension explained in Section 3.2 as, given the two trends in its value, a late-time mechanism which keeps the CMB unaltered but modifies the late-time clustering perfectly matches the problem. We can connect the lowering in the σ_8 parameter with the results obtained in Section 4.2.2. There, we found that the density perturbations of the matter fluid get frozen once the interaction is efficient, something that happens for the late Universe, as shown in the upper panel of Figure 4.18. This freezing has two consequences, the first one in the Matter Power Spectrum where we have a suppression for small scales, as shown in Figure 4.14. The second one is directly on the σ_8 parameter, as depicted in the lower panel of Figure 4.18. We found that the larger the amount of momentum, that is the larger the value of β, the lower the value of σ_8, since that parameter precisely captures the
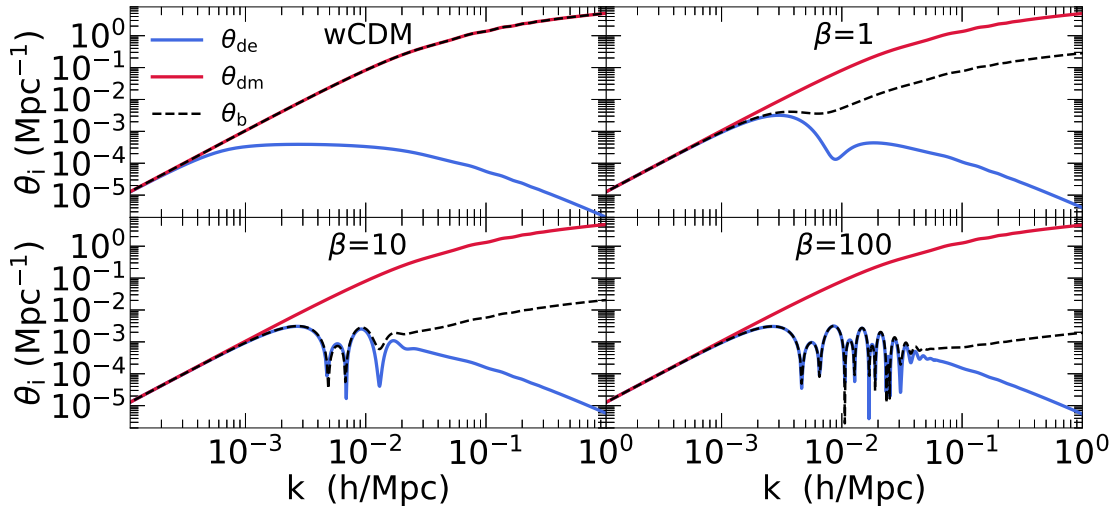
Figure 4.20: Velocity perturbation variable θ today of Dark Energy (blue), non-interacting Dark Matter (red) and the Baryons (black) for different values of the coupling parameter β.

amount of clustering. We also have some small shift in the density parameters, like a slight decrease in the Baryon density with an increase in the Dark Matter density but they remain well inside the 2σ region so not a remarkable effect.

Finally, we find a large improvement in the χ^2 value when comparing the reference wCDM model and our coupling. We have a $\Delta\chi^2 = 26$ improvement which translates into $\Delta AIC = 24$ and $\Delta BIC = 17$ using the information criteria explained in Appendix A. This indicates that both criteria strongly prefer the interaction as compared to the wCDM. One would wonder what happens when comparing with the pure ΛCDM model. We have to take into account two factors. First, the χ^2 of wCDM would be better or equal than the ΛCDM case as introducing an extra parameter, w, will always give better results than not introducing it. On the other hand, information criteria penalise adding new parameters. Our model compared to the ΛCDM has two extra parameters, w and β. However, comparing to the ΛCDM we have $\Delta AIC_{\Lambda CDM,\beta} = 22$ and $\Delta BIC_{\Lambda CDM,\beta} = 8$ that, although smaller evidence, we still have the interaction preferred by the criteria.

	wCDM model			Elastic Interaction $\log_{10} \beta$		
Param.	mean$\pm\sigma$	2σ lower	2σ upper	mean$\pm\sigma$	2σ lower	2σ upper
$100\Omega_{\rm b}h^2$	$2.264^{+0.015}_{-0.015}$	2.235	2.295	$2.243^{+0.016}_{-0.017}$	2.210	2.275
$\Omega_{\rm dm}h^2$	$0.1163^{+0.0010}_{-0.0010}$	0.1143	0.1183	$0.1193^{+0.0013}_{-0.0013}$	0.1166	0.1218
$n_{\rm s}$	$0.9721^{+0.0042}_{-0.0044}$	0.9638	0.9808	$0.9662^{+0.0047}_{-0.0046}$	0.9573	0.9757
$10^9 A_{\rm s}$	$2.063^{+0.034}_{-0.034}$	1.991	2.133	$2.107^{+0.034}_{-0.038}$	2.037	2.182
$\tau_{\rm reio}$	$0.0502^{+0.0087}_{-0.0087}$	0.0322	0.0686	$0.0567^{+0.0083}_{-0.0089}$	0.0391	0.0744
w	$-0.948^{+0.022}_{-0.043}$	-0.999	-0.888	$-0.981^{+0.005}_{-0.018}$	-0.999	-0.938
$100\,\theta_{\rm s}$	$1.042^{+0.00031}_{-0.00032}$	1.041	1.043	$1.042^{+0.00034}_{-0.00032}$	1.041	1.043
$z_{\rm reio}$	$7.14^{+0.99}_{-0.82}$	5.18	8.94	$7.88^{+0.82}_{-0.92}$	6.22	9.67
H_0 [$\frac{\rm km}{\rm s\,Mpc}$]	$67.88^{+1.30}_{-0.99}$	65.70	69.98	$67.65^{+0.80}_{-0.71}$	66.12	69.22
σ_8	$0.790^{+0.011}_{-0.0010}$	0.770	0.810	$0.756^{+0.011}_{-0.012}$	0.733	0.779
$\Omega_{\rm m}$	$0.302^{+0.010}_{-0.012}$	0.281	0.323	$0.3097^{+0.0079}_{-0.0093}$	0.2923	0.3272
$\log_{10} \beta$	-	-	-	$0.63^{+0.39}_{-0.47}$	-0.20	1.54

Table 4.6: In this table, we show the mean and 1σ values and the 2σ limits for the cosmological and derived parameters for a wCDM model (left) and for the interacting model using a logarithmic sampling on the coupling parameter β (right).
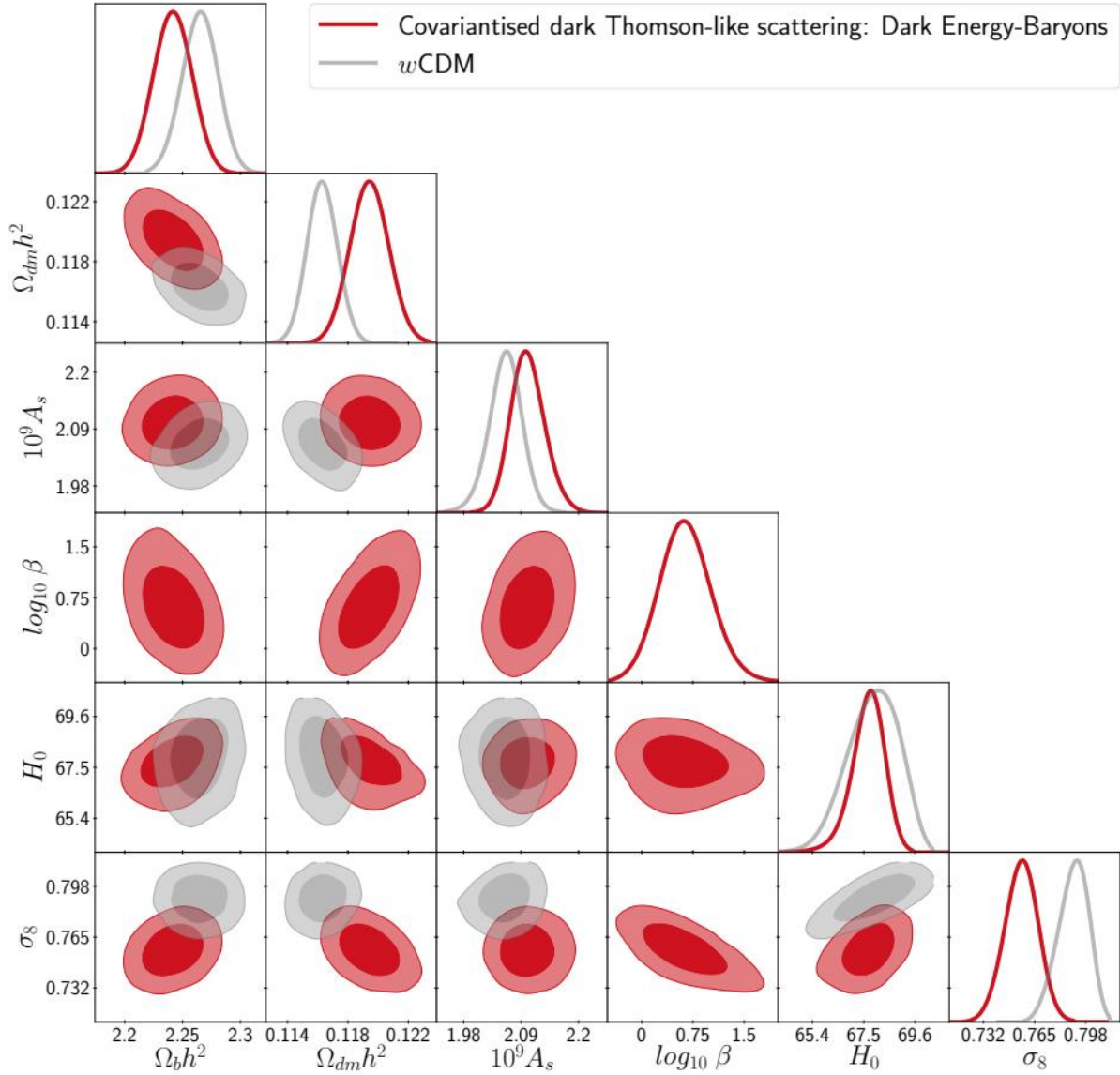
Figure 4.21: In this plot, we show the two-dimensional 1σ and 2σ posterior of several parameters for a wCDM model (gray) and for the interacting model using a logarithmic analysis on the coupling parameter β (red).

Param.	wCDM model			Elastic Interaction β		
	mean$\pm\sigma$	2σ lower	2σ upper	mean$\pm\sigma$	2σ lower	2σ upper
$100\Omega_\mathrm{b}h^2$	$2.264^{+0.015}_{-0.015}$	2.235	2.295	$2.237^{+0.015}_{-0.016}$	2.205	2.267
$\Omega_\mathrm{dm}h^2$	$0.1163^{+0.0010}_{-0.0010}$	0.1143	0.1183	$0.1200^{+0.0013}_{-0.0012}$	0.1175	0.1226
n_s	$0.9721^{+0.0042}_{-0.0044}$	0.9638	0.9808	$0.9647^{+0.0045}_{-0.0047}$	0.9554	0.9737
$10^9 A_\mathrm{s}$	$2.063^{+0.034}_{-0.034}$	1.991	2.133	$2.118^{+0.035}_{-0.041}$	2.045	2.194
τ_reio	$0.0502^{+0.0087}_{-0.0087}$	0.0322	0.0686	$0.0581^{+0.0084}_{-0.0093}$	0.0411	0.0761
w	$-0.948^{+0.022}_{-0.043}$	-0.999	-0.888	$-0.992^{+0.004}_{-0.008}$	-0.999	-0.961
$100\,\theta_\mathrm{s}$	$1.042^{+0.00031}_{-0.00032}$	1.041	1.043	$1.042^{+0.00032}_{-0.00035}$	1.041	1.043
z_reio	$7.14^{+0.99}_{-0.82}$	5.18	8.94	$8.05^{+0.84}_{-0.86}$	6.34	9.79
$H_0\ [\frac{\mathrm{km}}{\mathrm{s\,Mpc}}]$	$67.88^{+1.30}_{-0.99}$	65.70	69.98	$67.66^{+0.68}_{-0.60}$	66.32	68.97
σ_8	$0.790^{+0.011}_{-0.0010}$	0.770	0.810	$0.749^{+0.01}_{-0.012}$	0.728	0.771
Ω_m	$0.302^{+0.010}_{-0.012}$	0.281	0.323	$0.311^{+0.008}_{-0.008}$	0.295	0.327
β	-	-	-	$26.7^{+3.8}_{-26.0}$	$-$	≤ 100

Table 4.7: In this table, we show the mean and 1σ values and the 2σ limits for the cosmological and derived parameters for a wCDM model (left) and for the interacting model using a linear sampling on the coupling parameter β (right).
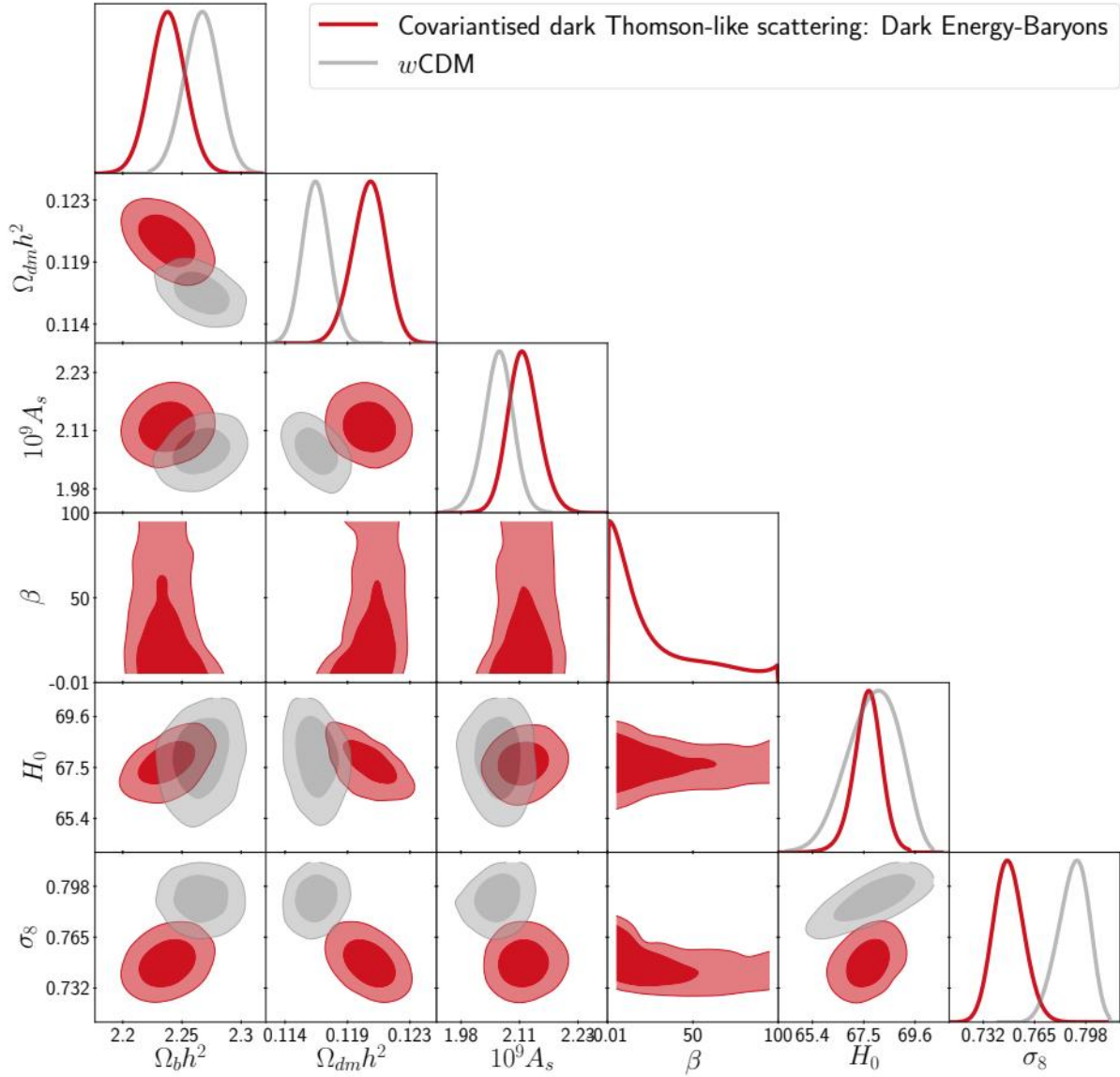
Figure 4.22: In this plot, we show the two-dimensional 1σ and 2σ posterior of several parameters for a wCDM model (gray) and for the interacting model using a linear sampling on the coupling parameter β (red).

4.3 Velocity-entrainment coupling

In the previous two models, our starting point was a broken conservation law for the individual coupled fluids, given by $\nabla^\nu T_{\mu\nu}^{(\mathrm{s})} \neq 0$, where (s) is the index representing each component. However, that was a very phenomenological approach and, therefore, we may think of a more systematic way of proceeding. Here, we consider an alternative model to the standard scenario with some sort of momentum transfer, but now from the point of view of a Lagrangian theory. Hence, from the Lagrangian we will derive the relevant equations, as before, to describe the cosmological dynamics both for the background cosmology and the linear perturbations.

We consider a general action taking into account the gravity sector in the standard way, that is General Relativity; the matter content including Dark Energy in the Schutz-Sorkin formalism [123, 124] and an interaction term described by, in principle, a general action S_{int}. Then we have

$$S = \frac{M_{\mathrm{pl}}^2}{2} \int \mathrm{d}^4x \sqrt{-g}\, R - \sum_{(\mathrm{s})=\mathrm{dm,de,b,r}} \int \mathrm{d}^4x \left[\sqrt{-g}\, \rho_{(\mathrm{s})}(n_{(\mathrm{s})}) + J_{(\mathrm{s})}^\mu \partial_\mu l_{(\mathrm{s})} \right] + S_{\mathrm{int}} \,, \qquad (4.56)$$

where the first term corresponds to the General Relativity action already explained in equation (2.1). The second term is the Schutz-Sorkin action for the different components in the Universe, namely: Dark Matter, Dark Energy, Baryons and the radiation part, respectively. We also have the energy density $\rho_{(\mathrm{s})}$, the number density $n_{(\mathrm{s})}$ and the current $J_{(\mathrm{s})}$, while $l_{(\mathrm{s})}$ are the Lagrange multipliers to ensure the particle number conservation. They satisfy the following relations for each fluid

$$n_{(\mathrm{s})} = \frac{\sqrt{g_{\mu\nu} J_{(\mathrm{s})}^\mu J_{(\mathrm{s})}^\nu}}{\sqrt{g}} \,, \qquad (4.57)$$

$$J_{(\mathrm{s})}^\mu = n\sqrt{-g}\, u_{(\mathrm{s})}^\mu \,, \qquad (4.58)$$

$$-1 = g_{\mu\nu} u_{(\mathrm{s})}^\mu u_{(\mathrm{s})}^\nu \,, \qquad (4.59)$$

where u^μ is the 4-velocity, as before.

Both, the General Relativity and the Schutz-Sorkin action, have been thoroughly studied in the literature, then we focus on the interaction encoded in the, so far, general action S_{int}. To begin with, we parameterise the interacting term with a general function f of a coupling variable that we will call Z, so that the action reads as

$$S_{\mathrm{int}} = \int \mathrm{d}^4x \sqrt{-g}\, f(Z) \,. \qquad (4.60)$$

In the previous scenarios, we considered an interaction between Dark Energy and Dark Matter and between Dark Energy and Baryons. But realising how the effects and detectability were larger in the first case, as of course expected since we have more structures due to Dark Matter than due to Baryons, here we will consider the interaction only belonging to the Dark Sector. In any case, the following derivation should be similar with Baryons instead of Dark Matter. Once settled the interacting

fluids, we want to build the scalar variable Z such that it encodes an interaction that carries momentum interchange in the Dark Sector. Although we can build in principle any order quantity, we will remain at lowest order and, thus, the following quantity emerges

$$Z \equiv g_{\mu\nu} \, u_{\mathrm{dm}}^{\mu} u_{\mathrm{de}}^{\nu} \,, \tag{4.61}$$

where u_{dm}^{μ}, u_{de}^{ν} are the 4-velocity of Dark Matter and Dark Energy respectively. The reason for this choice can be understood as follows. If one considers the Universe is homogeneous and isotropic at least for large scales, all fluids should have the same rest-frame and then $u_i^{\mu} \sim u_j^{\mu}$. This implies the coupling quantity Z satisfies equation (4.59) no matter we are considering different fluids as all have the same rest-frame. This translates into $u_i^{\mu} \sim u_j^{\mu}$ and, thus, $Z \to -1$ which keeps the dynamics unaltered for the background cosmology as we will see. Although we will derive this in detail, we are just following the same philosophy as in the Covariantised dark Thomson-like scattering. As before, no background quantity will be affected and when we consider perturbations where $u_i^{\mu} \sim u_j^{\mu}$ does not hold anymore we will have different dynamics related to the momentum exchange, as exactly happened before. For the convenience of the following calculations we can rewrite the coupling variable Z in terms of the currents $J_{(\mathrm{s})}$ and the number densities $n_{(\mathrm{s})}$, so it reads as

$$Z = -\frac{g_{\mu\nu} \, J_{\mathrm{dm}}^{\mu} J_{\mathrm{de}}^{\nu}}{g \, n_{\mathrm{dm}} n_{\mathrm{de}}} \,. \tag{4.62}$$

Now that we have the full action, we want to compute the equations of motion. Varying it with respect to the Lagrange multipliers we have

$$\frac{\partial \mathcal{L}}{\partial \, l_{(\mathrm{s})}} \;=\; 0 \,, \tag{4.63}$$

$$\frac{\partial \mathcal{L}}{\partial \, \partial_{\mu} \, l_{(\mathrm{s})}} \;=\; J_{(\mathrm{s})}^{\mu} \,, \tag{4.64}$$

and then we obtain the conservation rule for the currents of each fluid as the equations of motion are simply

$$\partial_{\mu} J_{(\mathrm{s})}^{\mu} = 0 \,, \tag{4.65}$$

which is an expected result as we do not want any non-conserved currents in our description. Moreover, we can also vary with respect to the currents having

$$\frac{\partial \mathcal{L}}{\partial \, \partial_{\sigma} J_{(\mathrm{s})}^{\mu}} \;=\; 0 \,, \tag{4.66}$$

$$\frac{\partial \mathcal{L}}{\partial J_{(\mathrm{s})}^{\mu}} \;=\; \partial_{\mu} l_{(\mathrm{s})} + \sqrt{-g} \, \frac{\partial \rho_{(\mathrm{s})}}{\partial n_{(\mathrm{s})}} \, \frac{\partial n_{(\mathrm{s})}}{\partial J_{(\mathrm{s})}^{\mu}} + \sqrt{-g} \, \frac{\partial f}{\partial Z} \, \frac{\partial Z}{\partial J_{(\mathrm{s})}^{\mu}} \,. \tag{4.67}$$

101

Using the previous relations we can compute each of the previous terms as

$$\frac{\partial n_{(s)}}{\partial J^{\mu}_{(s)}} = \frac{J_{(s)\,\mu}}{g\,n_{(s)}} \,, \tag{4.68}$$

$$\frac{\partial Z}{\partial J^{\mu}_{\mathrm{dm}}} = \frac{-1}{n_{\mathrm{dm}}\,g}\left(\frac{J_{\mathrm{de}\,\mu}}{n_{\mathrm{de}}} + \frac{Z\,J_{\mathrm{dm}\,\mu}}{n_{\mathrm{dm}}}\right) \,, \tag{4.69}$$

$$\frac{\partial Z}{\partial J^{\mu}_{\mathrm{de}}} = \frac{-1}{n_{\mathrm{de}}\,g}\left(\frac{J_{\mathrm{dm}\,\mu}}{n_{\mathrm{dm}}} + \frac{Z\,J_{\mathrm{de}\,\mu}}{n_{\mathrm{de}}}\right) \,. \tag{4.70}$$

Combining the previous equations and using that $J^{\mu}_{(s)} = n_{(s)}\sqrt{-g}\,u^{\mu}_{(s)}$, as depicted in equation (4.58), we have

$$\partial_{\mu}\ell_{\mathrm{dm}} = \frac{\partial\rho_{\mathrm{dm}}}{\partial n_{\mathrm{dm}}}\,u_{\mathrm{dm}\,\mu} + \frac{f_{,Z}}{n_{\mathrm{dm}}}\left(u_{\mathrm{de}\,\mu} + Z u_{\mathrm{dm}\,\mu}\right) \,, \tag{4.71}$$

$$\partial_{\mu}\ell_{\mathrm{de}} = \frac{\partial\rho_{\mathrm{de}}}{\partial n_{\mathrm{de}}}\,u_{\mathrm{de}\,\mu} + \frac{f_{,Z}}{n_{\mathrm{de}}}\left(u_{\mathrm{dm}\,\mu} + Z u_{\mathrm{de}\,\mu}\right) \,, \tag{4.72}$$

$$\partial_{\mu}\ell_{\mathrm{b}} = \frac{\partial\rho_{\mathrm{b}}}{\partial n_{\mathrm{b}}}\,u_{\mathrm{b}\,\mu} \,, \tag{4.73}$$

$$\partial_{\mu}\ell_{\mathrm{r}} = \frac{\partial\rho_{\mathrm{r}}}{\partial n_{\mathrm{r}}}\,u_{\mathrm{r}\,\mu} \,, \tag{4.74}$$

where we shorten the notation by defining $f_{,Z} \equiv \frac{\partial f}{\partial Z}$. These relations allow us to rewrite the Lagrange multipliers in terms of the energy and number density, the coupling and the velocity.

Background dynamics

We have now set the general action describing this model and then the next step corresponds to compute the field equations for the cosmology described. We will start by computing the background field equations which, in our case, will be composed of three different parts: General Relativity, Schutz-Sorkin matter description and the interacting term. In the case of the gravity part, its action will give the standard result as

$$\frac{2}{\sqrt{-g}}\frac{\delta\mathcal{L}_{\mathrm{GR}}}{\delta g^{\mu\nu}} = M_{\mathrm{pl}}^2\,G_{\mu\nu} \qquad \text{where} \qquad \frac{\delta\sqrt{-g}}{\delta g^{\mu\nu}} = -\frac{1}{2}\sqrt{-g}\,g_{\mu\nu} \,. \tag{4.75}$$

For the matter field part and the new interacting term $\mathcal{L}_{\mathrm{m}} + \mathcal{L}_{\mathrm{int}}$ we have

$$-\frac{2}{\sqrt{-g}}\frac{\delta(\mathcal{L}_{\mathrm{m}} + \mathcal{L}_{\mathrm{int}})}{\delta g^{\mu\nu}} = \sum_{\mathrm{(s)=dm,de,b,r}}\left(T^{(s)}_{\mu\nu}\right) + T^{\mathrm{int}}_{\mu\nu} \,, \tag{4.76}$$

where the stress-energy tensor for the standard part is just described by

$$T^{(s)}_{\mu\nu} = \left(\rho_{(s)} + p_{(s)}\right)u_{(s)\mu}\,u_{(s)\nu} + p_{(s)}\,g_{\mu\nu} \,. \tag{4.77}$$

Thus, we penned all the new terms in the corresponding stress-energy tensor $T^{\mathrm{int}}_{\mu\nu}$, which reads as

$$T^{\mathrm{int}}_{\mu\nu} = g_{\mu\nu}\,f(Z) + f(Z)_{,Z}\left[u^{\mathrm{dm}}_{\mu}\,u^{\mathrm{de}}_{\nu} + \frac{Z}{2}\left(u^{\mathrm{dm}}_{\mu}\,u^{\mathrm{dm}}_{\nu} + u^{\mathrm{de}}_{\mu}\,u^{\mathrm{de}}_{\nu}\right)\right] \,, \tag{4.78}$$

where we have used that

$$\frac{\delta Z}{\delta g^{\mu\nu}} = u_\mu^{\rm dm}\, u_\nu^{\rm de} + \frac{Z}{2}\left(u_\mu^{\rm dm}\, u_\nu^{\rm dm} + u_\mu^{\rm de}\, u_\nu^{\rm de}\right)\,. \tag{4.79}$$

Finally, the gravitational equations of motion read as

$$M_{\rm pl}^2\, G_{\mu\nu} = \sum_{\rm (s)=dm,de,b,r} T_{\mu\nu}^{\rm (s)} + T_{\mu\nu}^{\rm (int)}\,. \tag{4.80}$$

Consequently, we are introducing new terms to the field equations proportional both to $f(Z)$ and to $f(Z)_{,Z}$, which no longer preserve the background untouched. However, we will see later how those new terms can be absorbed by a redefinition of the Dark Energy sector when we assume the Universe is both homogeneous and isotropic.

We can further simplify our equations since for the background cosmology, where isotropy and homogeneity are preserved, we have that all fluids share the same rest-frame. This translates into having

$$J_{\rm (s)}^0 = n_{\rm (s)}a^3\,, \tag{4.81}$$

$$J_{\rm (s)}^i = 0\,. \tag{4.82}$$

The conservation rule obtained before in equation (4.65) for the currents of each fluid simply translates into

$$J_{\rm (s)}^0 = n_{\rm (s)}a^3 = {\rm constant} \equiv \mathcal{N}_{\rm (s)}\,, \tag{4.83}$$

which is nothing but the conservation of the number particle of each fluid. As it is more convenient to speak about the energy density, we can expand the previous conservation equation as follows

$$\partial_\mu J_{\rm (s)}^\mu = \partial_\mu\left(n_{\rm (s)}\,\sqrt{-g}\,u_{\rm (s)}^\mu\right) = \sqrt{-g}\,u_{\rm (s)}^\mu\,\partial_\mu n_{\rm (s)} + n_{\rm (s)}\,\sqrt{-g}\,\nabla_\mu u^\mu = 0\,, \tag{4.84}$$

where we used in the last equality that $\nabla_a u^a = \frac{1}{\sqrt{g}}\partial_a\left(\sqrt{g}\,u^a\right)$. Introducing the relations to energy density and pressure density as $\frac{\partial\rho_{\rm (s)}}{\partial n_{\rm (s)}}\,u_{\rm (s)}^\mu\,\partial_\mu n_{\rm (s)} = u_{\rm (s)}^\mu\,\partial_\mu\rho_{\rm (s)}$ and as $p_{\rm (s)} = n_{\rm (s)}\frac{\partial\rho_{\rm (s)}}{\partial n_{\rm (s)}} - \rho_{\rm (s)}$, we rewrite it as

$$u_{\rm (s)}^\mu\,\partial_\mu\rho_{\rm (s)} + \left(\rho_{\rm (s)} + p_{\rm (s)}\right)\nabla_\mu u_{\rm (s)}^\mu = 0\,, \tag{4.85}$$

which in our case simply reduces to the standard conservation equation for each fluid

$$\dot\rho_{\rm (s)} + 3H\left(\rho_{\rm (s)} + p_{\rm (s)}\right) = 0\,. \tag{4.86}$$

Although here we have formally the same expression as in the standard case, the Einstein Field Equations have new terms as we have seen before. Thus, we are

unavoidably modifying the background cosmology as now we have

$$3M_{\text{pl}}^2 H^2 \quad = \quad \sum_{(\text{s})=\text{dm,de,b,r}} \rho_{(\text{s})} - f \, , \tag{4.87}$$

$$M_{\text{pl}}^2 \left(2\dot{H} + 3H^2 \right) \quad = \quad - \sum_{(\text{s})=\text{dm,de,b,r}} p_{(\text{s})} - f \, , \tag{4.88}$$

where we should remark that no $f(Z)_{,Z}$ terms appear from equation (4.78) as for the background with $Z = -1$ all fluids are comoving at the background level. This implies that the modifications in the Field Equations are only proportional to the general function $f(Z)$, which now is constant, for the background cosmology. Therefore, we can reabsorb it by the following redefinition of the Dark Energy density and pressure as a term acting like a cosmological constant since

$$\hat{\rho}_{\text{de}} \quad = \quad \rho_{\text{de}} - f \, , \tag{4.89}$$

$$\hat{p}_{\text{de}} \quad = \quad p_{\text{de}} + f \, . \tag{4.90}$$

which represents nothing but a shift in the value of the cosmological constant and, therefore, it will not alter the conservation rule previously obtained in equation (4.86), but now for $\hat{\rho}_{\text{de}}$.

Perturbations dynamics: general description

Now the background cosmology is described, we turn our attention to the perturbation sector. Due to the complexity required by the following calculations to obtain the equations governing the perturbations, the software of symbolic computations `Maple` [125] was required.

As we have seen with the background, provided $Z = -1$ we have no deviation from the standard scenario. This continues with the philosophy of the momentum transfer models where no background deviations appear due to the interaction. Also for the perturbation part, pure momentum transfer manifests explicitly only by a modification on the Euler equation that is proportional to the relative velocity of the interacting fluids. Here, we want to preserve those properties.

For the convenience of the following, we consider a FLRW perturbed metric without choosing a particular gauge of the form

$$\text{d}s^2 = -(1 + 2\alpha)\,\text{d}t^2 + 2\partial_i\chi\,\text{d}t\text{d}x^i + a^2(t)\left[(1 + 2\zeta)\delta_{ij} + 2\partial_i\partial_j E\right]\text{d}x^i\text{d}x^j \, , \tag{4.91}$$

and, in principle, we will work with a general function $f(Z)$ to remain as general as possible. We can define the perturbations for the previous variables in the following way:

$$J_{(\text{s})}^\mu \quad = \quad \left(\mathcal{N}_{(\text{s})} + \delta J_{(\text{s})} \, , \, \frac{1}{a^2(t)} \delta^{ik}\,\partial_k \delta j_{(\text{s})} \right) \, , \tag{4.92}$$

$$n_{(\text{s})} \quad = \quad \bar{n}_{(\text{s})} + \delta n_{(\text{s})} \, , \tag{4.93}$$

$$\rho_{(\text{s})} \quad = \quad \bar{\rho}_{(\text{s})} + \delta\rho_{(\text{s})} \, , \tag{4.94}$$

$$f(Z) \quad = \quad \bar{f} + \delta f = f + f_{,Z}\delta Z \, , \tag{4.95}$$

where we have denoted with a bar the background quantities although we will simplify the notation in the next steps. With the definition of $n_{(\mathrm{s})}$ in equation (4.57) and the relation of equation (4.58), we have now that the perturbations in the number and energy density, in the velocity and in the perturbation variable Z are

$$
\delta n_{(\mathrm{s})} = \frac{\mathcal{N}_{(\mathrm{s})}}{a^3} \left[\frac{\delta\rho_{(\mathrm{s})}}{\rho_{(\mathrm{s})} + p_{(\mathrm{s})}} - \frac{\delta\rho_{(\mathrm{s})}}{\rho_{(\mathrm{s})} + p_{(\mathrm{s})}} \left(3\zeta + \partial^2 E \right) \right.
$$
$$
\left. - \frac{(\partial\delta j_{(\mathrm{s})} + \mathcal{N}_{(\mathrm{s})}\partial\chi)^2}{2\mathcal{N}_{(\mathrm{s})}^2 a^2} - \frac{1}{2}(\zeta + \partial^2 E)(3\zeta - \partial^2 E) \right] , \qquad (4.96)
$$

$$
\delta\rho_{(\mathrm{s})} = \frac{\rho_{(\mathrm{s})} + p_{(\mathrm{s})}}{\mathcal{N}_{(\mathrm{s})}} \left[\delta J_{(\mathrm{s})} - \mathcal{N}_{(\mathrm{s})} \left(3\zeta + \partial^2 E \right) \right] , \qquad (4.97)
$$

$$
u_{\mu(\mathrm{s})} = \left(-1 - \alpha \, , \, -\partial_i v_{(\mathrm{s})} \right) \quad \text{where} \quad v_{(\mathrm{s})} = -\frac{\delta j_{(\mathrm{s})}}{\mathcal{N}_{(\mathrm{s})}} - \chi \, , \qquad (4.98)
$$

$$
\delta Z = -\frac{1}{2a^2} \left(\partial_i v_{\mathrm{de}} - \partial_i v_{\mathrm{de}} \right)^2 . \qquad (4.99)
$$

Now that we have all the physical variables expanded, we only need to do the same with the Lagrangian multipliers defined in equations (4.71)-(4.74). As we have that for the background cosmology where all fluids are comoving $\dot{\bar{l}}_{(\mathrm{s})} = -\frac{\partial\bar{\rho}_{(\mathrm{s})}}{\partial n_{(\mathrm{s})}}$, we rewrite the multipliers as

$$
\ell_{\mathrm{dm}} = -\int^t \frac{\partial\rho_{\mathrm{dm}}}{\partial n_{\mathrm{dm}}} \mathrm{d}\tilde{t} - \frac{\partial\rho_{\mathrm{dm}}}{\partial n_{\mathrm{dm}}} v_{\mathrm{dm}} - \frac{f_{,Z}}{n_{\mathrm{dm}}} (v_{\mathrm{de}} - v_{\mathrm{dm}}) , \qquad (4.100)
$$

$$
\ell_{\mathrm{de}} = -\int^t \frac{\partial\rho_{\mathrm{de}}}{\partial n_{\mathrm{de}}} \mathrm{d}\tilde{t} - \frac{\partial\rho_{\mathrm{de}}}{\partial n_{\mathrm{de}}} v_{\mathrm{de}} - \frac{f_{,Z}}{n_{\mathrm{de}}} (v_{\mathrm{dm}} - v_{\mathrm{de}}) , \qquad (4.101)
$$

$$
\ell_{\mathrm{b}} = -\int^t \frac{\partial\rho_{\mathrm{b}}}{\partial n_{\mathrm{b}}} \mathrm{d}\tilde{t} - \frac{\partial\rho_{\mathrm{b}}}{\partial n_{\mathrm{b}}} v_{\mathrm{b}} , \qquad (4.102)
$$

$$
\ell_{\mathrm{r}} = -\int^t \frac{\partial\rho_{\mathrm{r}}}{\partial n_{\mathrm{r}}} \mathrm{d}\tilde{t} - \frac{\partial\rho_{\mathrm{r}}}{\partial n_{\mathrm{r}}} v_{\mathrm{r}} . \qquad (4.103)
$$

$$
\qquad (4.104)
$$

With the previous relations expanded for the perturbations we can write a perturbed

up to quadratic order action, which as before we will decompose as follows:

$$
\begin{aligned}
L_{\mathrm{GR}} &= \frac{aM_{\mathrm{pl}}^2}{2}\Bigg[2\{3a^2H(2\dot{\zeta}+3H\zeta)-2H\partial^2\chi-2\partial^2\zeta\}\alpha - 3a^2(2\dot{\zeta}^2+3H^2\alpha^2) \\
&\quad + 2(\partial_i\zeta)^2 + 3H^2(\partial_i\chi)^2 + 4\dot{\zeta}\partial^2\chi \Bigg] \\
&\quad + a^3M_{\mathrm{pl}}^2\Big[2\ddot{\zeta}+2H(3\dot{\zeta}-\dot{\alpha})\Big]\partial^2 E \\
&\quad + \frac{a^3M_{\mathrm{pl}}^2}{2}\Big(2\dot{H}+3H^2\Big)\big[3\zeta^2 + \partial^2 E(2\zeta-2\alpha-\partial^2 E)\big] \ ,
\end{aligned}
\tag{4.105}
$$

$$
\begin{aligned}
L_{\mathrm{m}} &= \sum_{(\mathrm{s})=\mathrm{dm,de,b,r}} a^3\Bigg[(\dot{v}_{(\mathrm{s})}-3Hc_{(\mathrm{s})}^2 v_{(\mathrm{s})}-\alpha)\delta\rho_{(\mathrm{s})} - \frac{c_{(\mathrm{s})}^2}{2(\rho_{(\mathrm{s})}+p_{(\mathrm{s})})}\delta\rho_{(\mathrm{s})}^2 \\
&\quad - \frac{\rho_{(\mathrm{s})}+p_{(\mathrm{s})}}{2a^2}\partial_i v_{(\mathrm{s})}\left(\partial_i v_{(\mathrm{s})}+2\partial_i\chi\right) - \frac{\rho_{(\mathrm{s})}}{2a^2}(\partial_i\chi)^2 + \frac{\rho_{(\mathrm{s})}}{2}\alpha^2 \\
&\quad + \frac{p_{(\mathrm{s})}}{2}\left(\zeta+\partial^2 E\right)\left(3\zeta-\partial^2 E\right) \\
&\quad + \left\{(\rho_{(\mathrm{s})}+p_{(\mathrm{s})})\left(\dot{v}_{(\mathrm{s})}-3Hc_{(\mathrm{s})}^2 v_{(\mathrm{s})}\right)-\rho_{(\mathrm{s})}\alpha\right\}\left(3\zeta+\partial^2 E\right)\Bigg] \ ,
\end{aligned}
\tag{4.106}
$$

$$
\begin{aligned}
L_{\mathrm{int}} &= \frac{f}{2}a\left[(\partial_i\chi)^2 + a^2\left\{2(3\zeta+\partial^2 E)\alpha - \alpha^2 + (\zeta+\partial^2 E)(3\zeta-\partial^2 E)\right\}\right] + \frac{f,_Z}{2}a\left(\partial_i v_{\mathrm{de}}-\partial_i v_{\mathrm{dm}}\right)^2 \\
&\quad - a^3 f,_Z\left[\dot{v}_{\mathrm{de}}-\dot{v}_{\mathrm{dm}}+3H(v_{\mathrm{de}}-v_{\mathrm{dm}})\right]\left(\frac{\delta\rho_{\mathrm{de}}}{\rho_{\mathrm{de}}+p_{\mathrm{de}}}-\frac{\delta\rho_{\mathrm{dm}}}{\rho_{\mathrm{dm}}+p_{\mathrm{dm}}}\right) \ .
\end{aligned}
\tag{4.107}
$$

Varying the action with respect to α, χ, $v_{(\mathrm{s})}$, E and ζ we can obtain the following equations

$$
\begin{aligned}
6HM_{\mathrm{pl}}^2\left(H\alpha-\dot{\zeta}\right) + \frac{2M_{\mathrm{pl}}^2}{a^2}\left(\partial^2\zeta+H\partial^2\chi-a^2H\partial^2\dot{E}\right) \\
+ \sum_{(\mathrm{s})=\mathrm{dm,de,b,r}}\delta\rho_{(\mathrm{s})} = 0 \ ,
\end{aligned}
\tag{4.108}
$$

$$
2M_{\mathrm{pl}}^2\left(H\alpha-\dot{\zeta}\right) - \sum_{(\mathrm{s})=\mathrm{dm,de,b,r}}\left(\rho_{(\mathrm{s})}+p_{(\mathrm{s})}\right)v_{(\mathrm{s})} = 0 \ ,
\tag{4.109}
$$

$$
\begin{aligned}
\dot{\delta\rho}_{(\mathrm{s})} + 3H\left(1+c_{(\mathrm{s})}^2\right)\delta\rho_{(\mathrm{s})} + 3\left(\rho_{(\mathrm{s})}+p_{(\mathrm{s})}\right)\dot{\zeta} \\
-\frac{1}{a^2}\left(\rho_{(\mathrm{s})}+p_{(\mathrm{s})}\right)\left(\partial^2 v_{(\mathrm{s})}+\partial^2\chi-a^2\partial^2\dot{E}\right) = 0 \ ,
\end{aligned}
\tag{4.110}
$$

$$
\begin{aligned}
\ddot{\zeta} + 3H\dot{\zeta} - H\dot{\alpha} - \left(3H^2+\dot{H}\right)\alpha \\
-\frac{1}{2M_{\mathrm{pl}}^2}\sum_{(\mathrm{s})=\mathrm{dm,de,b,r}}\left(\rho_{(\mathrm{s})}+p_{(\mathrm{s})}\right)\left(3Hc_{(\mathrm{s})}^2 v_{(\mathrm{s})}-\dot{v}_{(\mathrm{s})}\right) = 0 \ ,
\end{aligned}
\tag{4.111}
$$

$$
\alpha + \zeta + \dot{\chi} + H\chi - a^2\left(\ddot{E}+3H\dot{E}\right) = 0 \ ,
\tag{4.112}
$$

which remain unaltered due to the interaction. As in the previous scenarios studied,

the only modification will appear in the Euler equations that now read as

$$\dot{v}_{\rm dm} - 3Hc_{\rm dm}^2 v_{\rm dm} - \alpha - c_{\rm dm}^2 \frac{\delta\rho_{\rm dm}}{\rho_{\rm dm} + p_{\rm dm}}$$
$$+ \frac{f_{,Z}}{\rho_{\rm dm} + p_{\rm dm}} \left[\dot{v}_{\rm de} - \dot{v}_{\rm dm} + 3H \left(v_{\rm de} - v_{\rm dm} \right) \right] = 0 \,, \quad (4.113)$$

$$\dot{v}_{\rm de} - 3Hc_{\rm de}^2 v_{\rm de} - \alpha - c_{\rm de}^2 \frac{\delta\rho_{\rm de}}{\rho_{\rm de} + p_{\rm de}}$$
$$- \frac{f_{,Z}}{\rho_{\rm de} + p_{\rm de}} \left[\dot{v}_{\rm de} - \dot{v}_{\rm dm} + 3H \left(v_{\rm de} - v_{\rm dm} \right) \right] = 0 \,, \quad (4.114)$$

$$\dot{v}_{\rm b} - 3Hc_{\rm b}^2 v_{\rm b} - \alpha - c_{\rm b}^2 \frac{\delta\rho_{\rm b}}{\rho_{\rm b} + p_{\rm b}} = 0 \,, \quad (4.115)$$

$$\dot{v}_{\rm r} - 3Hc_{\rm r}^2 v_{\rm r} - \alpha - c_{\rm r}^2 \frac{\delta\rho_{\rm r}}{\rho_{\rm r} + p_{\rm r}} = 0 \,. \quad (4.116)$$

From the previous equations, we can infer that the same formal structure that with the Covariantised dark Thomson-like scattering appears. All the formal structures remain unaltered except the Euler equations, which for the interacting fluids have a new term depending on the relative velocity and acceleration between both fluids. However, now the interacting term in Euler equations does depend on the relative acceleration between fluids, something that in the Thomson-like scattering was not happening. We will see later how this will be translated into a momentum transfer as before.

However, the previous equations are not invariant under gauge transformations. For example, under the coordinate transformation defined by $t \to t + \xi^0$ and $x^i \to x^i + \delta^{ij}\partial_j \xi$. To do that, following the definitions of Ref. [126], we have the following gauge-invariant variables

$$\Psi = \alpha + \frac{\mathrm{d}}{\mathrm{d}t} \left(\chi - a^2 \dot{E} \right) \,, \quad (4.117)$$

$$\Phi = -\zeta - H \left(\chi - a^2 \dot{E} \right) \,, \quad (4.118)$$

$$\delta\rho_{\rm (s)N} = \delta\rho_{\rm (s)} + \dot{\rho}_{\rm (s)} \left(\chi - a^2 \dot{E} \right) \,, \quad (4.119)$$

$$v_{\rm (s)N} = v_{\rm (s)} + \chi - a^2 \dot{E} \,, \quad (4.120)$$

which lead to the final result we were searching for. A general gauge invariant set of

equations governing the perturbations dynamics for our interacting model as

$$6HM_{\mathrm{pl}}^2\left(\dot\Phi+H\Psi\right)+\frac{2k^2}{a^2}M_{\mathrm{pl}}^2\Phi+\sum_{(\mathrm{s})=\mathrm{dm,de,b,r}}\delta\rho_{(\mathrm{s})\mathrm{N}}=0\ ,\tag{4.121}$$

$$2M_{\mathrm{pl}}^2\left(\dot\Phi+H\Psi\right)-\sum_{(\mathrm{s})=\mathrm{dm,de,b,r}}\left(\rho_{(\mathrm{s})}+p_{(\mathrm{s})}\right)v_{(\mathrm{s})\mathrm{N}}=0\ ,\tag{4.122}$$

$$\dot{\delta\rho}_{(\mathrm{s})\mathrm{N}}+3H\left(1+c_{(\mathrm{s})}^2\right)\delta\rho_{(\mathrm{s})\mathrm{N}}-3(\rho_{(\mathrm{s})}+p_{(\mathrm{s})})\dot\Phi+\frac{k^2}{a^2}\left(\rho_{(\mathrm{s})}+p_{(\mathrm{s})}\right)v_{(\mathrm{s})\mathrm{N}}=0\ ,\tag{4.123}$$

$$\ddot\Phi+3H\dot\Phi+H\dot\Psi+\left(3H^2+\dot H\right)\Psi+\frac{1}{2M_{\mathrm{pl}}^2}\sum_{(\mathrm{s})=\mathrm{dm,de,b,r}}\left(\rho_{(\mathrm{s})}+p_{(\mathrm{s})}\right)\left(3Hc_{(\mathrm{s})}^2v_{(\mathrm{s})\mathrm{N}}-\dot v_{(\mathrm{s})\mathrm{N}}\right)$$

$$=0\ ,\tag{4.124}$$

$$\dot v_{\mathrm{dmN}}-3Hc_{\mathrm{dm}}^2v_{\mathrm{dmN}}-\Psi\tag{4.125}$$
$$-\frac{(\rho_{\mathrm{de}}+p_{\mathrm{de}})[c_{\mathrm{dm}}^2\delta\rho_{\mathrm{dmN}}+3Hf_{,Z}\{(1+c_{\mathrm{dm}}^2)v_{\mathrm{dmN}}-(1+c_{\mathrm{de}}^2)v_{\mathrm{deN}}\}]-f_{,Z}(c_{\mathrm{dm}}^2\delta\rho_{\mathrm{dmN}}+c_{\mathrm{de}}^2\delta\rho_{\mathrm{deN}})}{(\rho_{\mathrm{dm}}+p_{\mathrm{dm}})(\rho_{\mathrm{de}}+p_{\mathrm{de}})-f_{,Z}(\rho_{\mathrm{dm}}+p_{\mathrm{dm}}+\rho_{\mathrm{de}}+p_{\mathrm{de}})}$$
$$=0\ ,$$

$$\dot v_{\mathrm{deN}}-3Hc_{\mathrm{de}}^2v_{\mathrm{deN}}-\Psi\tag{4.126}$$
$$-\frac{(\rho_{\mathrm{dm}}+p_{\mathrm{dm}})[c_{\mathrm{de}}^2\delta\rho_{\mathrm{deN}}+3Hf_{,Z}\{(1+c_{\mathrm{de}}^2)v_{\mathrm{deN}}-(1+c_{\mathrm{dm}}^2)v_{\mathrm{dmN}}\}]-f_{,Z}(c_{\mathrm{dm}}^2\delta\rho_{\mathrm{dmN}}+c_{\mathrm{de}}^2\delta\rho_{\mathrm{deN}})}{(\rho_{\mathrm{dm}}+p_{\mathrm{dm}})(\rho_{\mathrm{de}}+p_{\mathrm{de}})-f_{,Z}(\rho_{\mathrm{dm}}+p_{\mathrm{dm}}+\rho_{\mathrm{de}}+p_{\mathrm{de}})}$$
$$=0\ ,$$

$$\dot v_{\mathrm{bN}}-3Hc_{\mathrm{b}}^2v_{\mathrm{bN}}-\Psi-\frac{c_{\mathrm{b}}^2}{\rho_{\mathrm{b}}+p_{\mathrm{b}}}\delta\rho_{\mathrm{bN}}=0\ ,\tag{4.127}$$

$$\dot v_{\mathrm{rN}}-3Hc_{\mathrm{r}}^2v_{\mathrm{rN}}-\Psi-\frac{c_{\mathrm{r}}^2}{\rho_{\mathrm{r}}+p_{\mathrm{r}}}\delta\rho_{\mathrm{rN}}=0\ ,\tag{4.128}$$

$$\Psi=\Phi\ .\tag{4.129}$$

With the previous set of equations we have fully characterised the dynamics for the general action of equation (4.56), both for the background dynamics and the perturbations sector. Now we will focus on a particular case that continues with the philosophy of the interaction studied across this document. But other cases for different functions $f(Z)$ can be derived following the previous equations at will.

Perturbations dynamics: particular example

In the previous derivation we considered a general function $f(Z)$, which is a general interaction that is dependant on the previous variable Z. However, we already commented about the particular case satisfying $f(Z=-1)=0$. This is nothing more than a standard background keeper interaction, as we want in this PhD dissertation.

For the perturbation sector, this implies a new parameter defined as

$$b \equiv \left. \left(f_{,Z} \right) \right|_{Z=-1} , \qquad (4.130)$$

which is a constant parameter capturing all the previous family of functions. For the energy content, we will consider a departure from the standard scenario. In the case of Dark Matter, however, we will follow the standard definition, that is

$$\rho_{dm}(n_{dm}) = m_{dm}\, n_{dm} , \qquad (4.131)$$

$$w_{dm} \simeq 0 , \qquad (4.132)$$

$$c_{dm}^2 = 0 , \qquad (4.133)$$

$$p_{dm} \simeq 0 , \qquad (4.134)$$

where m_{dm} is a constant. But for the Dark Energy sector we will consider it is made up of a Cosmological Constant part plus a time dependant component. Consequently, we can parameterise it as

$$\rho_{de}(n_{de}) = \rho_\Lambda \left(1 + r_0\, n_{de}^{1+c_s^2} \right) , \qquad (4.135)$$

$$w_{de} = -\frac{1 - c_s^2\, r_0\, n_{de}^{1+c_s^2}}{1 + r_0\, n_{de}^{1+c_s^2}} , \qquad (4.136)$$

$$c_{de}^2 = c_s^2 , \qquad (4.137)$$

$$p_{de} = -\rho_\Lambda \left(1 - c_s^2\, r_0\, n_{de}^{1+c_s^2} \right) , \qquad (4.138)$$

where r_0 and c_s^2 are positive constants corresponding to the fraction of the extra dark component to the Dark Energy sector and to the propagation speed squared of the whole Dark Energy sector, respectively. Considering the evolution of the equation of state of the new Dark Sector, given Dark Energy number density n_{de} should satisfy the conservation of particle number $\mathcal{N}_{(s)} \equiv n_{(s)} a^3$, we need $n_{de} \propto a^{-3}$. Then, the equation of state will evolve from $w_{de} = c_s^2$ to a Cosmological Constant behaviour, that is $w_{de} = -1$, at late times. Consequently, we have to specify the value of the propagation speed. Regarding a potential effect on the H_0 tension[8] explained in Section 3.4, we will choose

$$c_{de}^2 = c_s^2 = \frac{1}{3} . \qquad (4.139)$$

With that choice, the previous equations are rewritten as

$$\rho_{de} = \rho_\Lambda \left(1 + r\, a^{-4} \right) , \qquad (4.140)$$

$$p_{de} = -\rho_\Lambda \left(1 - \frac{r}{3}\, a^{-4} \right) , \qquad (4.141)$$

$$w_{de} = -\frac{1 - r\, a^{-4}/3}{1 + r\, a^{-4}} , \qquad (4.142)$$

---

[8]The σ_8 tension is already addressed by the momentum transfer directed by the new parameter b.

where $r \equiv r_0 n_{\mathrm{de0}}^{4/3}$ and n_{de0} is the current Dark Energy number density. Then, the parameter r accounts for the ratio of abundances between the extra component and the cosmological constant part, thus $\Omega_{\mathrm{dr}} = r\Omega_{\Lambda}$. It is clear from equation (4.140) that the Dark Energy sector is composed by the standard Cosmological Constant given by ρ_{Λ} and by a "Dark Radiation" given its time dependence $\propto a^{-4}$. In principle any choice of the propagation speed c_{s} is acceptable. But with ours, and a reasonable amount of extra Dark Radiation Ω_{dr}, we are adding an extra early radiation to the Universe which, as known, tends to alleviate the H_0 tension since it reduces the sound horizon at recombination implying a larger value of the Hubble constant to keep unaltered the position of the acoustic peaks of the Cosmic Microwave Background. This choice was one of the reasons to study in the Covariantised dark Thomson-scattering the case with free N_{eff}, as the idea is to have an extra radiation in the early Universe alleviating the H_0 tension without worsening the σ_8 tension, which is addressed in both cases by the momentum transfer.
Now for the perturbation equations we have

$$\delta'_{\mathrm{dmN}} = 3\Phi' - \theta_{\mathrm{dmN}} , \qquad (4.143)$$

$$\delta'_{\mathrm{deN}} = -3\mathcal{H}\left(c_{\mathrm{de}}^2 - w_{\mathrm{de}}\right)\delta_{\mathrm{deN}} + 3(1 + w_{\mathrm{de}})\Phi' - (1 + w_{\mathrm{de}})\theta_{\mathrm{deN}} , \qquad (4.144)$$

$$\theta'_{\mathrm{dmN}} = -\mathcal{H}\theta_{\mathrm{dmN}} + k^2\Phi \qquad (4.145)$$
$$+ b\frac{3\mathcal{H}(1 + w_{\mathrm{de}})\rho_{\mathrm{de}}\left[\theta_{\mathrm{dmN}} - (1 + c_{\mathrm{de}}^2)\theta_{\mathrm{deN}}\right] - k^2 c_{\mathrm{de}}^2 \rho_{\mathrm{de}}\delta_{\mathrm{deN}}}{(1 + w_{\mathrm{de}})\rho_{\mathrm{de}}(\rho_{\mathrm{dm}} - b) - b\rho_{\mathrm{dm}}} ,$$

$$\theta'_{\mathrm{deN}} = \mathcal{H}(3c_{\mathrm{de}}^2 - 1)\theta_{\mathrm{deN}} + k^2\Phi \qquad (4.146)$$
$$+ \frac{\rho_{\mathrm{dm}}\left[k^2 c_{\mathrm{de}}^2 \rho_{\mathrm{de}}\delta_{\mathrm{deN}} + 3\mathcal{H}b\{(1 + c_{\mathrm{de}}^2)\theta_{\mathrm{deN}} - \theta_{\mathrm{dmN}}\}\right] - k^2 b c_{\mathrm{de}}^2 \rho_{\mathrm{de}}\delta_{\mathrm{deN}}}{(1 + w_{\mathrm{de}})\rho_{\mathrm{de}}(\rho_{\mathrm{dm}} - b) - b\rho_{\mathrm{dm}}} ,$$

which are written in the same form as the previous models so we can implement them into our numerical codes.

Once we have derived the equations controlling the dynamics in this case, we can proceed with the numerical analyses. For that, we will resort to numerical codes as we have already done in previous sections.

4.3.1 Linear effects

Once we have developed the theoretical description for the background and the perturbations, we should focus our attention on the effects of the interaction in observables. To do so, a numerical code was required as before. A modified version of the Boltzmann solver code CLASS [113, 114] was created, although it was unable to reproduce faithfully this model or suitably accommodate our modified version of the Dark Sector[9], since the analytical solutions previously found gave different results. However, a modified and correctly working version of CAMB [116] was developed by

---

[9]Although it is still not clear where the problem came from, it had some relation with having a Dark Energy related component being significant for the early Universe. It was also spotted a bug in the initial conditions module in the version of CLASS in use that, however, was already solved in the posterior version v2.9.
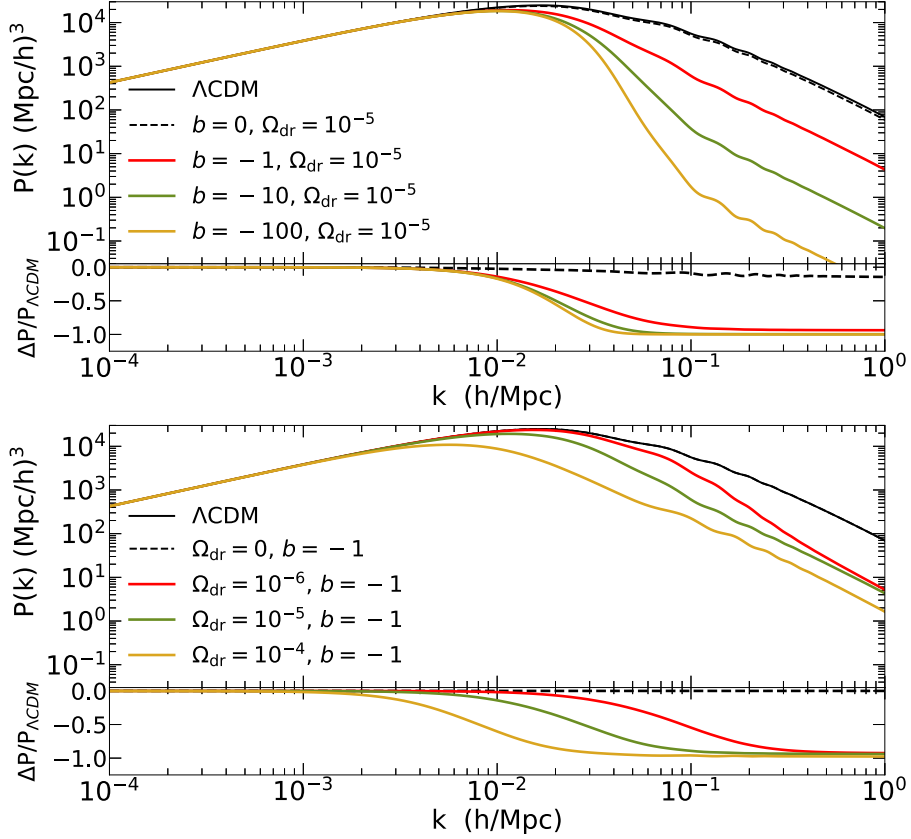
Figure 4.23: Matter Power Spectrum for several values of the coupling parameter b (top) and the extra Dark Radiation Ω_{dr} (bottom) and its ratio with respect to the reference model.

a collaborator in our group, Florencia Anabella Teppa Pannia. In that code, the new terms in the Euler equations alongside with the extra Dark Radiation were included. The outcomes of the code were tested against analytical solutions confirming the validity of this code.

For our analyses, we choose the cosmological parameters to be $H_0 = 67.4$ Km/s/Mpc, $\Omega_b h^2 = 0.0224$, $\Omega_{dm} h^2 = 0.120$, $\tau_{reio} = 0.054$, $A_s = 2.1 \; 10^{-9}$ and $n_s = 0.965$, which represent the same cosmology as before. Any other parameter is set to the default value of the code. This time our reference model is a truly ΛCDM instead of a wCDM as before, since now we have no incompatibility with our model provided the Dark Energy sector does behave as a Cosmological Constant for late times. Given now we have two parameters, the momentum transfer parameter b and the amount of Dark Radiation Ω_{dr}, we will study separately how each one modifies the different observables. Finally, we normalise b as we have done before, so we will work with the adimensional parameter as follows

$$b \rightarrow \frac{b}{\rho_{cr}} \; . \tag{4.147}$$

Regarding the Matter Power Spectrum shown in Figure 4.23 both for different

111
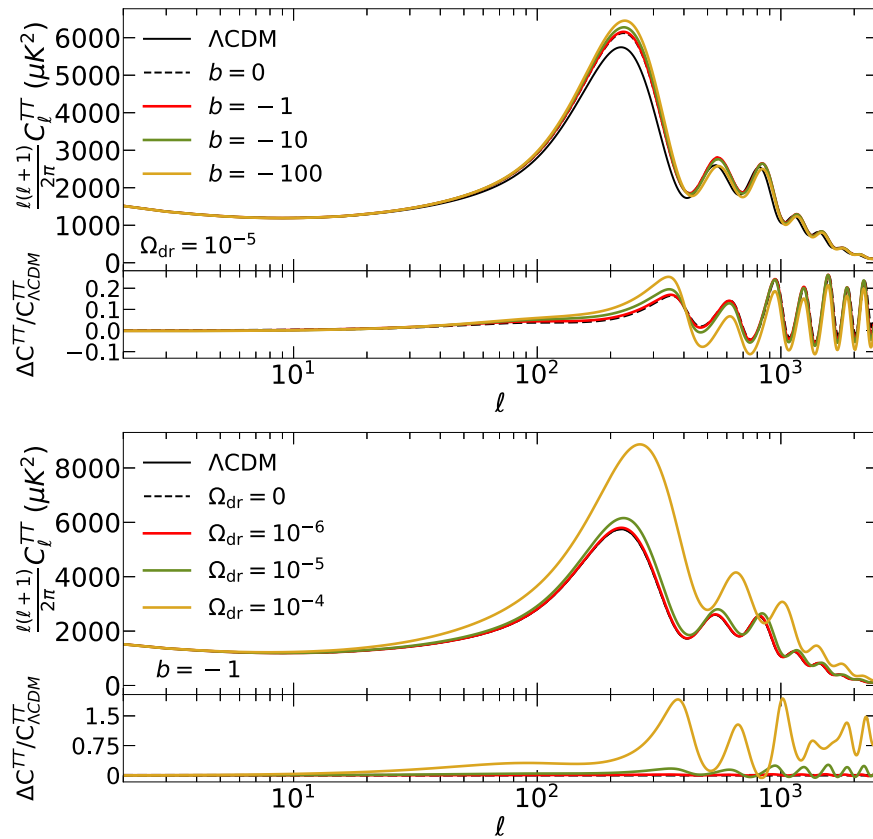
Figure 4.24: Cosmic Microwave Background (TT) for several values of the coupling parameter b (top) and the extra Dark Radiation Ω_{dr} (bottom) and its ratio with respect to the reference model.

values of the coupling parameter b and amount of Dark Radiation Ω_{dr}, we see how the interaction suppresses structures mainly for small scales. Specifically, the parameter b controls the amount of suppression, being larger for larger $|b|$, while the amount of Dark Radiation Ω_{dr} sets the largest scale suppressed. We also have a shift in the peak of the Power Spectrum, but in this case it is an expected result. Now we are modifying the amount of radiation by adding an extra dark one Ω_{dr} which precisely modifies the matter-radiation equality time, something that did not happen in the previous two models. The role of b is the same as in the previous cases with α or β. It encodes the amount of momentum transfer and, consequently, it controls the amount of suppression. Again, we see three different regimes. For very large scales, where both fluids share the same rest-frame, nothing happens while for smaller scales, where peculiar velocities emerge, the coupling induces a k-dependant suppression until it saturates for very small scales.

In the case of the Cosmic Microwave Background, we display it for the temperature and polarisations in Figures 4.24, 4.25, 4.26 and 4.27. In each figure we
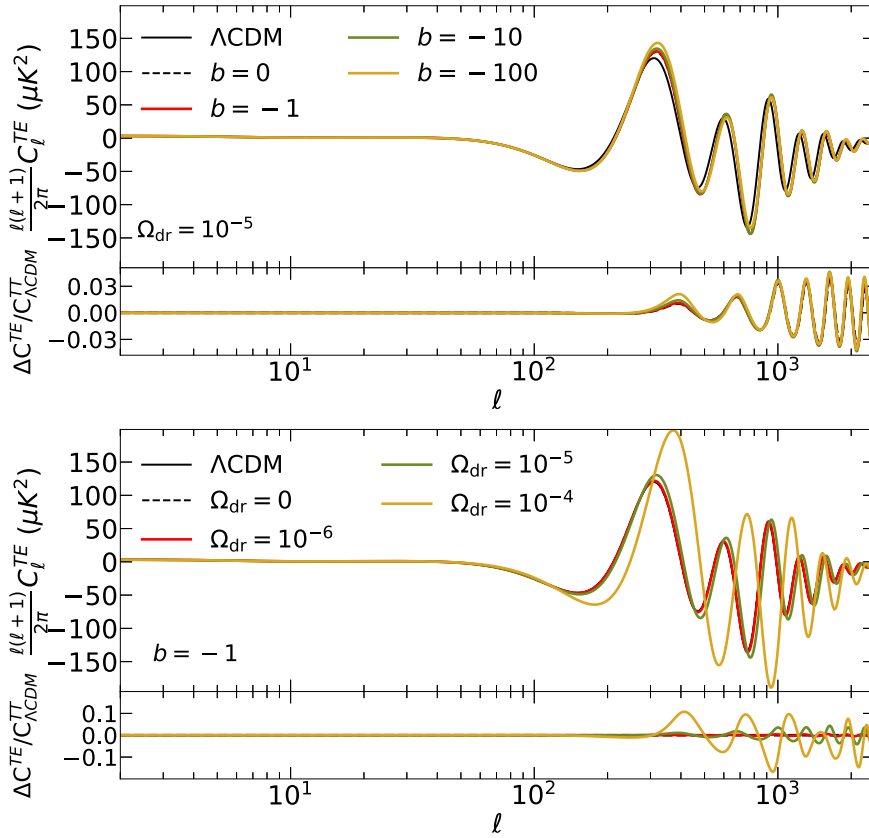
Figure 4.25: Cosmic Microwave Background (TE) for several values of the coupling parameter b (top) and the extra Dark Radiation Ω_{dr} (bottom) and its ratio with respect to the reference model.

have the temperature, cross-correlation between temperature and E-polarisation, E-polarisation and B-polarisation spectrum, respectively. We clearly see how only small scales are modified, as expected by the nature of the interaction. The main modification emerges from the extra Dark Radiation represented by Ω_{dr}, shifting and changing the amplitude of the peaks, as one would expect. We are changing the balance of components by adding an extra radiation that is non-negligible in the early Universe, that is by the time of recombination when, precisely, CMB was emitted. Also, there is a certain modulation of the amplitude of the CMB peaks by the momentum transfer parameter b, which as before it reflects the erasure of structures due to the momentum interchange.

In Figure 4.28, we show the ratio between the value of the parameter σ_8 and the ΛCDM value for different values of the coupling parameter b in three different cases with extra Dark Radiation, namely $\Omega_{dr} = 10^{-4}$, 10^{-5} and 10^{-6}. The larger the absolute value of b, the lower its value as we are suppressing more structures as seen before in the Matter Power Spectrum. On the other hand, also having more Dark Radiation implies less structures as expected.
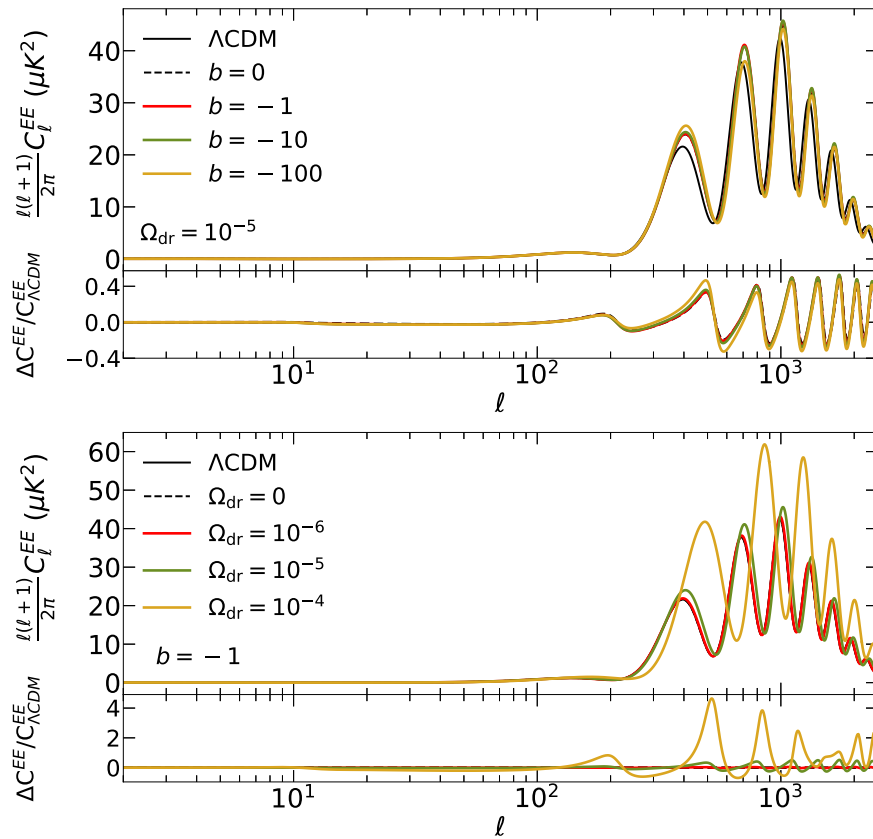
Figure 4.26: Cosmic Microwave Background (EE) for several values of the coupling parameter b (top) and the extra Dark Radiation Ω_{dr} (bottom) and its ratio with respect to the reference model.

At the moment, we have analysed the potential effects of the interaction studied here and the addition of extra Dark Radiation. We did it for several values of the parameters involved in this model, the one controlling the momentum transfer b and the other the amount of extra Dark Radiation Ω_{dr}. Hence, now it is the moment to set the allowed values for b and Ω_{dr} according to available data. For this task, we will resort to MCMC codes as we did before with the other models studied.

4.3.2 MCMC results

Until now, we have analysed the modifications due to the interaction and its imprints in different observables. However, we have no information about the value of the model parameter b and Ω_{dr}. Therefore, here we will perform Bayesian statistical analyses using the Markov-Chain Monte-Carlo code `CosmoMC` [128, 129] to the modified version of `CAMB` previously created. The data will correspond to the full `Planck` `2018` likelihood [5, 29] compiling data from the high-ℓ and low-ℓ from Cosmic Mi-
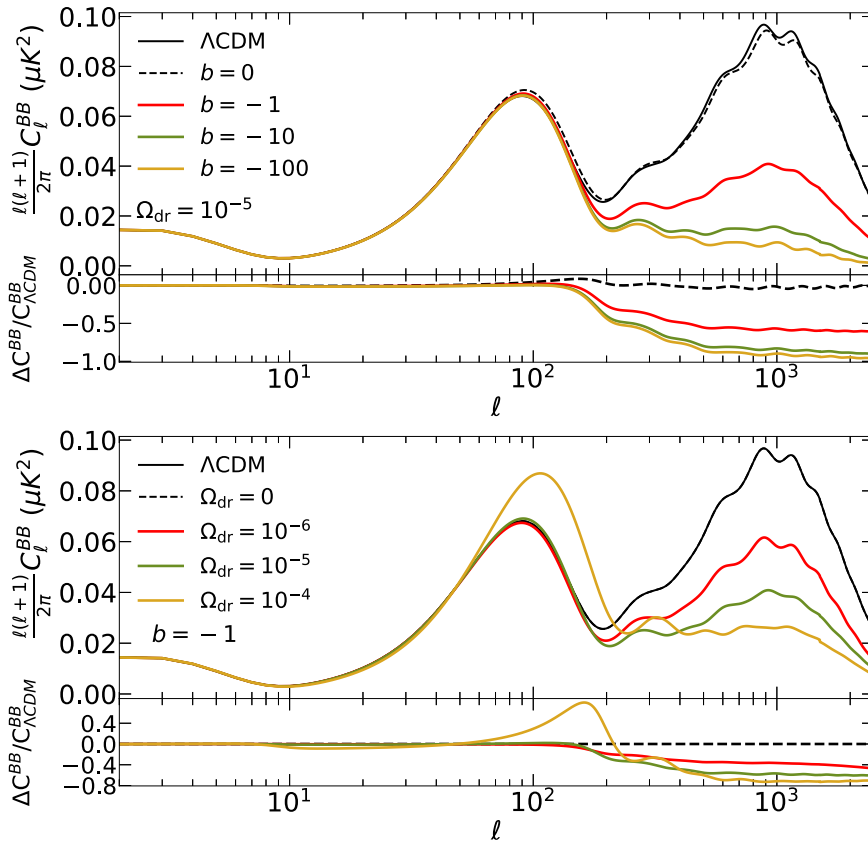
Figure 4.27: Cosmic Microwave Background (BB) for several values of the coupling parameter b (top) and the extra Dark Radiation Ω_{dr} (bottom) and its ratio with respect to the reference model.

crowave Background (CMB) temperature (TT), polarisation (EE), cross-correlation of temperature and polarisation (TE) and the CMB lensing power spectra, the `Pantheon` survey with data from supernovae [6], the Baryonic Acoustic Oscillation (BAO) data of Refs. [2, 119, 120] and the `Planck_SZ` likelihood of Planck Sunyaev-Zeldovich effect [30]. We consider the following list $\{100\Omega_{\mathrm{b}}h^2, \Omega_{\mathrm{dm}}h^2, n_{\mathrm{s}}, 10^9 A_{\mathrm{s}}.\tau_{\mathrm{reio}}, w_{\mathrm{de}}, 100\theta_{\mathrm{s}}\}$ as cosmological parameters and $\{z_{\mathrm{reio}}, H_0, \sigma_8, \Omega_{\mathrm{m}}\}$ as derived parameters. Moreover, we add the nuisance parameters corresponding to the likelihoods used in each case and our model parameters b and Ω_{dr}. We set flat priors for all the parameters with bounds in the model ones given by $\log_{10}|b| \in [-4, 0]$ and $\Omega_{\mathrm{DR}} \in [10^{-8}, 10^{-5}]$.

The results obtained for the different combinations of datasets are shown in Table 4.8 and Figure 4.29. When no Sunyaev-Zeldovich data are applied we cannot constrain the coupling parameter b, while we do observe that larger values of the Hubble constant H_0 are now allowed compared to the standard ΛCDM model. The reason for that is the presence of extra radiation, in this case a dark one, encoded in the variable Ω_{dr}. From the Figure 4.29, we infer that the larger the value of Ω_{dr}, the larger the parameter H_0, getting closer to the local Universe measurements and,
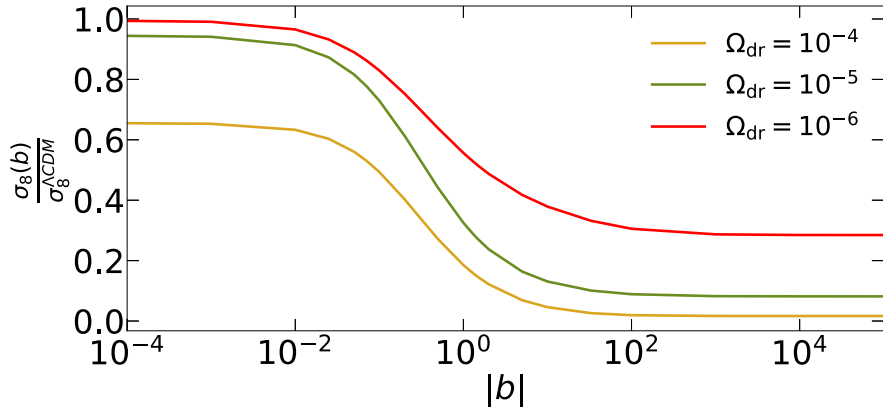
Figure 4.28: Ratio between the parameter σ_8 for different values of the coupling parameter b and the extra Dark Radiation Ω_{dr} and its non-interacting value.

thus, alleviating the H_0 tension explained in Section 3.4. In the case of σ_8 and without `Planck_SZ` data, its central value closely follows the early Universe measurements although we do have an enlargement of the lower limit allowed, therefore alleviating the σ_8 or S_8 tension at a certain extent.

Once we add the local Universe `Planck_SZ` data the picture completely changes. Now we do have a detection of the coupling parameter b around values of $|b| \sim \mathcal{O}(10^{-1})$. A proper analysis would require using b instead of $\log_{10}|b|$, but we did not find the data were precise enough to be used in that scenario. In any case, this is a very similar scenario to the one with the dark Covariantised Thomson-like scattering where firstly the logarithm samplings served us to set the order of magnitude and later, only if data allowed us, the linear samplings set the precise value. Because of that, we can conclude here that the interaction is preferred by data compared to the standard scenario, something also strongly suggested by the AIC criteria shown in Table 4.8. In any case, future surveys will be crucial to precisely establish its constraints, allowing us to perform the appropriate linear sampling on the coupling parameter b. Regarding the other parameters, we see that the value of σ_8 is now lowered as already expected by previous examples and as one can infer from figure 4.28. Therefore, the σ_8 or S_8 tension is alleviated when the interaction is on, since this interaction provokes a momentum transfer that erases structures in the late Universe. As before, the H_0 tension is also alleviated as the extra Dark Radiation induces larger values of the Hubble parameter. There is a remarkable result here. It is a known result that when alleviating one of the tension the other tends to increase, but here and thanks to the combination of extra radiation in the early Universe and a late-time erasing mechanism, we avoid such behaviour. Consequently, both tensions can be alleviated to some extent although not simultaneously, since the region in the σ_8-H_0 plot where both would is not allowed at the 2σ level.

116
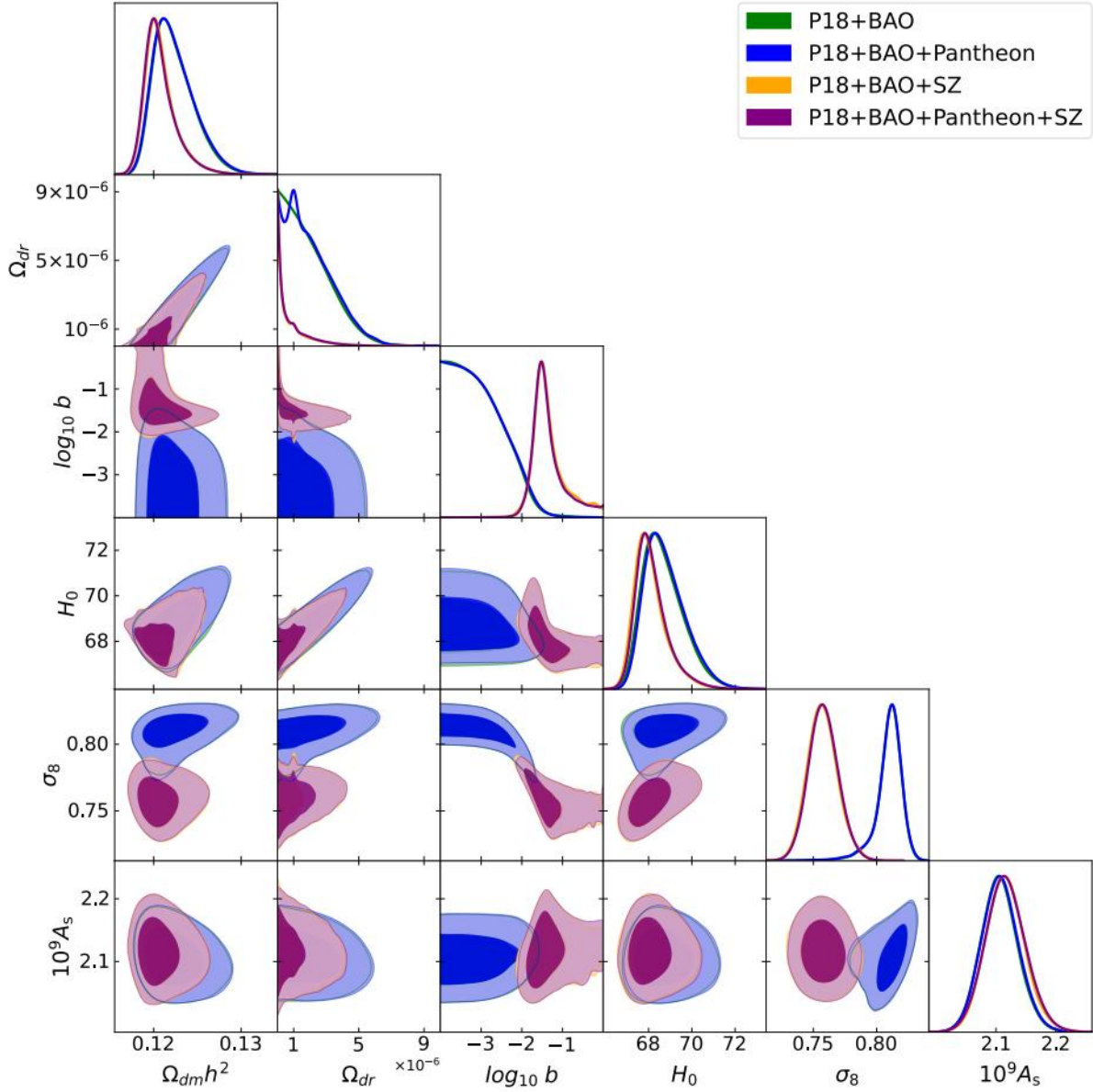
Figure 4.29: In this plot, we show the two-dimensional 1σ and 2σ posterior of several parameters for the interacting model using different datasets, namely `Planck 2018` and `BAO` data (green), `Planck 2018`, `BAO` and `Pantheon` data (blue), `Planck 2018`, `BAO` and `Planck_SZ` data (yellow) and all the previous datasets (purple). This figure was obtained using the code `GetDist` [127].

117

Λ**CDM**	P18+BAO	P18+BAO+Pantheon	P18+BAO+SZ	**All**
$H_0 \frac{\mathrm{km}}{\mathrm{s\,Mpc}}$	$67.62^{+0.42+0.83}_{-0.42-0.85}$	$67.67^{+0.41+0.81}_{-0.41-0.81}$	$68.58^{+0.39+0.76}_{-0.39-0.76}$	$68.58^{+0.38+0.75}_{-0.38-0.75}$
σ_8	$0.811^{+0.006+0.012}_{-0.006-0.012}$	$0.811^{+0.006+0.012}_{-0.006-0.012}$	$0.795^{+0.005+0.01}_{-0.005-0.010}$	$0.795^{+0.005+0.010}_{-0.005-0.010}$
Ω_{m}	$0.312^{+0.006+0.012}_{-0.006-0.011}$	$0.311^{+0.006+0.011}_{-0.006-0.011}$	$0.299^{+0.005+0.010}_{-0.005-0.010}$	$0.299^{+0.005+0.010}_{-0.005-0.009}$
S_8	$0.827^{+0.011+0.021}_{-0.011-0.021}$	$0.826^{+0.011+0.020}_{-0.011-0.021}$	$0.793^{+0.008+0.016}_{-0.008-0.016}$	$0.793^{+0.008+0.015}_{-0.008-0.015}$

b**CDM**	P18+BAO	P18+BAO+Pantheon	P18+BAO+SZ	**All**
$H_0 \frac{\mathrm{km}}{\mathrm{s\,Mpc}}$	$68.70^{+0.69+1.90}_{-1.12-1.64}$	$68.79^{+0.67+1.92}_{-1.13-1.63}$	$68.09^{+0.42+1.68}_{-0.87-1.30}$	$68.14^{+0.45+1.67}_{-0.86-1.32}$
σ_8	$0.810^{+0.010+0.018}_{-0.006-0.020}$	$0.810^{+0.010+0.019}_{-0.006-0.020}$	$0.757^{+0.011+0.023}_{-0.011-0.022}$	$0.758^{+0.011+0.024}_{-0.012-0.022}$
Ω_{m}	$0.309^{+0.006+0.012}_{-0.006-0.012}$	$0.308^{+0.006+0.012}_{-0.006-0.012}$	$0.311^{+0.006+0.012}_{-0.006-0.013}$	$0.31^{+0.006+0.012}_{-0.006-0.013}$
S_8	$0.822^{+0.013+0.025}_{-0.011-0.025}$	$0.821^{+0.012+0.024}_{-0.010-0.024}$	$0.770^{+0.010+0.020}_{-0.010-0.020}$	$0.770^{+0.010+0.020}_{-0.010-0.020}$
$\Omega_{\mathrm{dr}} \cdot_{10^{-6}}$	$< 2.0^{+0.6+2.6}$	$< 2.1^{+0.5+2.7}$	$< 1.0^{+0.1+2.3}$	$< 0.9^{+0.1+2.3}$
$\log_{10}|b|$	$< -3.1^{+0.3+1.1}$	$< -3.1^{+0.3+1.1}$	$-1.3^{+0.2+1.1}_{-0.4-0.6}$	$-1.3^{+0.2+1.1}_{-0.4-0.6}$
$\Delta\chi^2$	-2	-3	16	15
ΔAIC	-6	-7	12	11

Table 4.8: In this table, we show the mean, the 1σ values and the 2σ limits of certain parameters for the interacting model using different datasets as labelled.

4.4 Discussion and final comments on momentum transfer interactions

In this chapter, we have studied three different cosmological models which share a common property: the presence of a pure momentum transfer between one of the matter components and the Dark Energy sector. The momentum transfer models studied were characterised by an interaction between the coupled fluids that was mainly proportional to their relative velocity. In particular, we considered the following three different scenarios:

- Covariantised dark Thomson-like scattering between Dark Energy and Dark Matter.

- Covariantised dark Thomson-like scattering between Dark Energy and Baryons.

- Velocity-entrainment coupling between a modified Dark Energy sector and Dark Matter.

In all the previous scenarios, we have first presented and motivated the model under consideration to later perform an analytical derivation. After that, we made use of the linear Boltzmann solver codes `CLASS` and/or `CAMB` to further expand our knowledge of the models. To that end, we had to first modify the codes to add the new terms required. Once that was done, we have comprehensively studied the effects of each model in different observables. The general conclusion we obtained was that this kind of models tend to erase structures and, hence, reduce the clustering. Combining the analytical and numerical investigations performed, we know that the general mechanism of these models acts as follows. First, the interaction in each case is non-efficient for early times. When it does become efficient, at late times, the pressurefull interacting fluid couples the other pressureless partner, which previously to that moment was falling into the potential wells due to gravity. The pressure of the pressurefull fluid counteracts the gravitational force acting in the pressureless fluid which was provoking its clustering. This results in a substantial pure momentum exchange from the pressurefull fluid to the pressureless one. Consequently, the second fluid is no longer falling into the potential wells and, thus, the density perturbations stop growing. The final result is a reduced clustering rate which translates into less structures in the Cosmos.

The previous mechanism was proposed as a way to alleviate the well-known σ_8 or S_8 tension. As already explained in the first chapters of this PhD dissertation, the tension appears between early measurements, which have to be extrapolated until today, and the local/late Universe measurements. Therefore, having an interaction that erases structures would naturally accommodate both measurements to a compatible value of σ_8/S_8. Precisely, the previous mechanism acts in that way. For the considered scenarios, the interactions become efficient in the very late Universe and, as explained, they act reducing the clustering, that is, erasing structures. Moreover,

we also tried to address the other well-known tension, the H_0 tension. In this respect, we introduced extra radiation in our cosmologies, as a free N_{eff} parameter in the case of the Covariantised dark Thomson-like scattering and as an extra Dark Radiation making up the Dark Energy sector for the velocity-entrainment model. It is a well-known discouraging fact that when one tries to alleviate one of the previous tensions the other gets worse.

In our MCMC analyses, we first demonstrated that those previous models considered tend to ease only one tension at a time as the sweet spot in the $H_0 - \sigma_8$ plane where both tensions would be simultaneously alleviated was outside the 2σ region. However, a remarkable accomplishment was achieved: the typical property of worsening one of them while alleviating the other tension is not present here anymore. Apart from H_0 or σ_8, the other cosmological parameters remained virtually unchanged. However, the case of the coupling parameters constraints is noteworthy. When we used data from CMB, BAO and Supernovae Ia, only an upper bound was given by the data to α, β or b in each case. In contrast, when we also added the Sunyaev–Zeldovich cluster counts data from Planck experiment, in an oversimplified Gaussian likelihood, the situation dramatically changes. In the first model, the Covariantised dark Thomson-like scattering between Dark Energy and Dark Matter, we did find a more than 3σ evidence for the interaction being detected by data. Moreover, the information criteria used also claimed for a strong support of such a detection. In the second scenario presented, the same coupling as before but with Baryons, the results were similar although less constrained due to the fact there are less Baryons to interact with. Similar results were inferred from the third scenario, the velocity-entrainment coupling, as the interacting parameter was only constrained when we added the Sunyaev–Zeldovich data. Indeed, this prominent relation between momentum transfer models and local Universe data, like the case of Sunyaev–Zeldovich one, has been found in several research works in the last years, with different models but all of them sharing the presence of momentum exchange like in Refs. [95, 103, 108, 130]. These results, in combination with ours, invoke for more investigation to be performed related to pure momentum transfer models.

To summarise, we have studied three different scenarios theoretically and numerically, and later we have tested them with latest available data, where a momentum transfer interaction happens. We have proven how those momentum exchanges provoke a reduction of the clustering, having as a result the alleviation of the σ_8 tension without worsening the H_0 tension as a side effect. Finally, we have shown the remarkable relation between those models and the local Universe data on σ_8/S_8 parameter, no matter the specificities of each model, leading to a significant detection of this kind of interactions.

FORECASTS WITH PURE MOMENTUM TRANSFER INTERACTIONS

In the previous chapter, we studied different alternatives to the standard ΛCDM model which can describe in more appealing ways our Cosmos and can reveal the nature or some novel properties of the unknown Dark Sector of the Universe, that is the majority of our current cosmic pie. The motivations were varied, but the ultimate step was always to see what data could tell us about those models, if they were preferred or not. Until now, the main tool when constraining the cosmological, or our model, parameters has been the Cosmic Microwave Background. With the Planck experiment [5], most of the standard model parameters were fitted with uncertainties below the 1% level, a precision never reached before. But each pro has it cons, and with such high precision the cosmological tensions emerged, as explained in Section 3.4.

Contemporaneously to this thesis and in the future, several experiments are planned or already on-going which will shed light on the dynamics and the content of the Cosmos. With those surveys, we expect to go below the 1% level of precision in the measurement of the cosmological parameters and, even more importantly, clarify those tensions and problems that we already spoke about in Chapter 3. There are plenty of different techniques in those upcoming experiments, but we will start with the galaxy surveys, which study the galaxy distribution. We can classify the galaxy surveys in two types depending on the technique used. Spectroscopic surveys rely on the decomposition in wavelengths of the light emitted by an object, then getting its intensity in the different wavelengths, that is a spectrum. As advantage they are able to obtain the spectroscopic redshift with very accurate precision. As downside, they obtain no lensing information as they are insensitive to the shape of the objects observed. Examples of this type are the Baryon Oscillation Spectroscopic Survey (BOSS) [131] and Dark Energy Spectroscopic Instrument (DESI) [132]. On the

other hand, photometric experiments base their utility on passing the emitted light through filters getting the intensity of the wavelength allowed by the filters used. They have the advantage of detecting a larger amount of objects due to the filter system carrying also shape information but, on the other hand, they are less sensitive to the redshift. As examples, we have the Dark Energy Survey (DES) [133] and the Large Synoptic Survey Telescope (LSST) [134]. There is a third alternative called spectro-photometric surveys which operate with a combination of broad, medium and narrow band filters to have photometry in several wavelength. Then, they are able to produce a pseudo-spectrum and, at the same time, having larger samples and shape information. Experiments with this technique are the Physics of the Accelerating Universe survey (PAU) [135], the Javalambre Photometric Local Universe Survey (J-PLUS) [136] and the Javalambre Physics of the Accelerating Universe Astrophysical Survey (J-PAS) [137]. On the other side we have the radiotelescopes. Instead of mapping the Universe distribution of matter by its emission in the optic or in the infrared, they search for radio sources. With the detected radio emitters, they reconstruct the matter distribution in the same way as galaxy surveys do. As an example we have the Square Kilometre Array experiment (SKA) [138].

The goal of this chapter is to perform forecast analyses for future surveys. This means, we will simulate with how much precision a future survey is able to constrain certain parameters, analysing how the configuration of the survey will affect, how different surveys behave, which signals are more important and/or how neglecting certain contributions to the modelling of the observable will change the results. In a forecast, a certain fiducial cosmology needs to be assumed. In our case, we will use the Covariantised dark Thomson-like scattering for the case of Dark Energy and Dark Matter interaction. This particular model constitutes a general proxy for studying the pure momentum transfer, as we have seen in previous Chapter 4 and in the literature, since very different models lead to the same conclusions when data is confronted with them. Moreover, its simplicity and similarity to the standard model make it the ideal candidate to test as alternative, since we can use most of the work already done and, at the same time, test a departure from the standard scenario. In particular, we have three different general analyses: galaxy surveys (clustering and lensing), dipole of the power spectrum and cluster counts. In each analysis, a certain survey will be the reference one.

This chapter is partially based on the following published papers:

- **Title:** J-PAS: Forecasts for Dark Matter - Dark Energy elastic couplings.
  Authors: David Figueruelo et al.
  DOI: 10.1088/1475-7516/2021/07/022
  Published in: Journal of Cosmology and Astroparticle 07 (2021), 022 [109].
  e-Print: 2103.01571 [astro-ph.CO]

- **Title:** Momentum transfer in the Dark Sector and lensing convergence in upcoming galaxy surveys.
  Authors: Wilmar Cardona and David Figueruelo.
  DOI: 10.1088/1475-7516/2022/12/010
  Published in: Journal of Cosmology and Astroparticle 12 (2022), 010 [139].
  e-Print: 2209.12583 [astro-ph.CO]

And partially based on the following pre-print:

- **Title:** A smoking gun from the power spectrum dipole for elastic interactions in the Dark Sector.
  Authors: Jose Beltrán Jiménez, Enea Di Dio and David Figueruelo.
  e-Print: 2212.08617 [astro-ph.CO] [140].
  Sent to: Journal of Cosmology and Astroparticle.

5.1 Galaxy survey and J-PAS

The first forecast analysis is devoted to clustering and lensing observations in the context of the J-PAS survey [137], since we are part of its working group of Theoretical Cosmology and Fundamental Physics. J-PAS is a spectro-photometric survey installed in Pico del Buitre in the Sierra de Javalambre, Teruel, Spain. The facilities in the Observatorio Astrofísico de Javalambre (OAJ) consist of a 2.5m diameter telescope equipped with the 7 square degree Field of View Javalambre Panoramic Camera (JP-Cam). As a spectro-photometric survey, it has a total of 54 narrow-band filters and 2 broad-band filters covering all the optical wavelength range as shown in Figure 5.1. The expected area covered by the survey is 8000 square degrees of sky in the northern hemisphere.

Here, we will study both the clustering and weak lensing data, the latter being possible provided J-PAS is a spectro-photometric experiment. In order to compare the future results of J-PAS, we will perform the same analysis for DESI experiment [132] in the case of clustering (not being possible the lensing counterpart as DESI is a spectroscopic survey) and both clustering and lensing for EUCLID experiment [141]. For our analysis, we will follow the formalism of Ref. [142] and use the numerical code for galaxy survey Fisher Matrix[1] computations `FARO` [143], obtaining the cosmological functions from our modified version of `CLASS` for the case of the Covariantised dark Thomson-like scattering between Dark Energy and Dark Matter, explained in Section 4.1.

5.1.1 Modelling the clustering

The first step consists in analysing how the data from clustering will constrain the model parameter α. Basically, it consists of measuring the matter perturbations through different times using as tracers to do so the galaxy positions in redshift space, rather than real space. When having a galaxy survey measuring the galaxies distribution per redshift, the observed spectrum is given by [144]

$$P_{ij}(k_r, \mu_r, z) = \frac{D_{A\,r}^2 E}{D_A^2 E_r} \left(b_i D + f D \mu^2 \right) \left(b_j D + f D \mu^2 \right) P(k)\, e^{-\frac{k_r^2 \mu_r^2 \sigma_i^2}{2}} e^{-\frac{k_r^2 \mu_r^2 \sigma_j^2}{2}} , \qquad (5.1)$$

where subindices i and j set the different tracers used while r means that the quantity is evaluated in the fiducial cosmology. The term $b_i D + f D \mu^2$ encodes the density perturbations and the redshift space distortions, with b the bias, D the growth function, f the growth rate and μ the angle of separation with the line of sight. The Matter Power Spectrum is $P(k)$ and the exponential accounts for the photometric redshift error δz inside σ_i, defined as $\sigma_i = \delta z_i (1+z)/H(z)$. The prefactor $\frac{D_{A\,r}^2 E}{D_A^2 E_r}$, where D_A is the angular distance and E the normalised to today's value Hubble function, accounts for the Alcock-Paczynski effect. Such a effect is the induced distortions in the galaxy distribution positions obtained due to having a wrong geometry, that is

---

[1]See Appendix A.
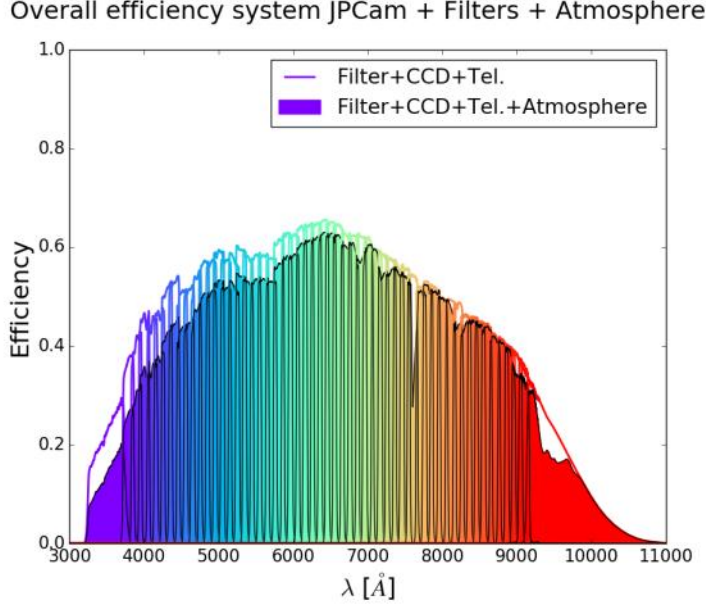
Figure 5.1: Filter distribution along with its efficiency for the J-PAS experiment [137].

a wrong cosmology. Also due to the Alcock-Paczynski effect, we have the following relations

$$k = Q k_r \quad \text{and} \quad \mu = \frac{E}{E_r Q} \mu_r \quad \text{with} \quad Q = \frac{\sqrt{D_A^2 \chi^2 \mu_r^2 - D_{Ar}^2 \chi_r^2 (\mu_r^2 - 1)}}{D_{Ar} \chi} , \quad (5.2)$$

being χ the comoving distance explained in Appendix B.

Then, the Fisher matrix for two different tracers at a certain redshift for two parameters a and b is [142]

$$F_{ab}^C(z_{\rm s}) = \frac{V_s}{8\pi^2} \int_{-1}^{1} {\rm d}\mu \int_{k_{\min}}^{\infty} {\rm d}k k^2 \frac{\partial P_{ij}(k,\mu,z_{\rm s})}{\partial a}\bigg|_r C_{jl}^{-1} \frac{\partial P_{lm}(k,\mu,z_{\rm s})}{\partial b}\bigg|_r C_{mi}^{-1} e^{-k^2 \Sigma_\perp^2 - k^2 \mu^2 (\Sigma_\parallel^2 - \Sigma_\perp^2)} ,$$

$$(5.3)$$

where V_s is the volume of each redshift bin $V_s = \frac{4\pi}{3} f_{\rm sky} \left[\chi\left(z_s\right)^3 - \chi\left(z_{s-1}\right)^3 \right]$ with $f_{\rm sky}$ the fraction of sky covered by the survey and $k_{\min} = 0.007\ h{\rm Mpc}^{-1}$. The covariance matrix is defined as $C_{ij} = P_{ij} + \frac{\delta_{ij}}{n_i(z_{\rm s})}$, with $n_i(z_{\rm s})$ the mean galaxy density in the s-th redshift bin for the i-tracer. The exponential acts as a cut-off scale to avoid non-linear physics contamination. We should bear in mind that we are using our modified version of CLASS and, then, only linear scales are obtained for functions like the Matter Power Spectrum. Therefore, non-linear scales are not properly calculated. For our cut-off prescription, one would need a proper characterisation of the non-linear dynamics, but given the similarities of this model to the standard one we will adopt the same prescription as in the ΛCDM model. This choice would not be appropriate when dealing with real data, where a full non-linear analysis is required as we pioneer in Chapter 6. However, when performing a Fisher analysis this will not be relevant.

Then, the ΛCDM prescription is given by

$$\Sigma_\perp(z) \;=\; 0.785 D(z)\Sigma_0 \;, \tag{5.4}$$

$$\Sigma_\parallel(z) \;=\; 0.785 D(z)\Big[1 + f(z)\Big]\Sigma_0 \;, \tag{5.5}$$

where $\Sigma_0 = 11\,\mathrm{Mpc}/h$.

5.1.2   Modelling the weak lensing

The second observable we use is the weak lensing signal. It is one of the main consequences of General Relativity as it consists of the distortion of light paths due to the presence of gravitational potentials between the emitter and the observer, which can be latter used to reconstruct the distribution of matter as those gravitational potentials are generated by that matter. Consequently, only photometric or spectro-photometric surveys are sensitive to it. For this effect, the observed convergence power spectrum under the Limber and flat-sky approximation is [145]

$$P_{ss'}(\ell) = \frac{9 H_0^3 \Omega_{\mathrm{m}}^2}{4} \int_0^\infty \frac{D(z)^2 (1+z)^2}{E(z)} \, g_s(z)\, g_{s'}(z)\, P\left(\frac{\ell}{\chi(z)}\right) \mathrm{d}z \;, \tag{5.6}$$

where indices s and s' indicate the redshift bin while the corresponding multipole is ℓ and the scale k, which are simply related by $k = \ell/\chi(z)$. As we want to analyse the weak lensing tomographically, we use the window functions g_s as follows

$$g_s(z) = \int_z^\infty \left(1 - \frac{\chi(z)}{\chi(z')}\right) n_s(z')\, \mathrm{d}z' \;, \tag{5.7}$$

where $n_s(z)$ is the galaxy density function in the s-th redshift bin defined as

$$n_s(z) \propto \begin{cases} \int_{\bar z_{s-1}}^{\bar z_s} n(z') e^{-\frac{(z'-z)^2}{2\sigma_s^2}} \, dz & \text{inside} \quad s\text{-bin} \\[2mm] 0 & \text{outside} \quad s\text{-bin} \end{cases} \quad \text{with} \quad n(z) = \frac{3}{2 z_p^3} z^2 e^{-(z/z_p)^{3/2}} \;, \tag{5.8}$$

such that it should satisfy the normalisation condition $\int_0^\infty n_s(z)\,dz = 1$ and where we have $z_p = z_{\mathrm{mean}}/\sqrt{2}$, with z_{mean} the mean redshift of each survey.

Then, the Fisher matrix for two different parameters a and b is [142]

$$F_{ab}^\kappa = f_{\mathrm{sky}} \sum_\ell \Delta\ln\ell \, \frac{(2\ell+1)\ell}{2} \, \frac{\partial P_{ss'}(\ell)}{\partial a}\bigg|_r \, C_{s'p}^{-1} \, \frac{\partial P_{pp'}(\ell)}{\partial b}\bigg|_r \, C_{p's}^{-1} \;, \tag{5.9}$$

where we sum from $\ell_{\mathrm{min}} = 5$ to $\ell_{\mathrm{max}} = 906$ with a step $\Delta\ln\ell = 0.1$. The matrix $C_{ss'}$ is defined as $C_{ss'} = P_{ss'} + \gamma_{\mathrm{int}}^2 \hat n_s^{-1} \delta_{ss'}$, with the intrinsic ellipticity $\gamma_{\mathrm{int}} = 0.22$, and the number of galaxies per steradian

$$\hat n_s = n_\theta \, \frac{\int_{\bar z_{s-1}}^{\bar z_s} n_s(z)\, \mathrm{d}z}{\int_0^\infty n_s(z)\, \mathrm{d}z} \;, \tag{5.10}$$

where n_θ is the areal galaxy density of the survey.

J-PAS			
z	LRG	ELG	QSO
0.3	226.6	2958.6	0.45
0.5	156.3	1181.1	1.14
0.7	68.8	502.1	1.61
0.9	12.0	138.0	2.27
1.1	0.9	41.2	2.86
1.3	0	6.7	3.60
1.5	0	0	3.60
1.7	0	0	3.21
1.9	0	0	2.86
2.1	0	0	2.55
2.3	0	0	2.27
2.5	0	0	2.03
2.7	0	0	1.81
2.9	0	0	1.61
3.1	0	0	1.43
3.3	0	0	1.28
3.5	0	0	1.14
3.7	0	0	0.91
3.9	0	0	0.72

DESI				
z	BGS	LRG	ELG	QSO
0.1	2240	0	0	0
0.3	240	0	0	0
0.5	6.3	0	0	0
0.7	0	48.7	69.1	2.75
0.9	0	19.1	81.9	2.60
1.1	0	1.18	47.7	2.55
1.3	0	0	28.2	2.50
1.5	0	0	11.2	2.40
1.7	0	0	1.68	2.30

Table 5.1: Galaxy densities are in units of $10^{-5} \ h^3\text{Mpc}^{-3}$ for the surveys J-PAS and DESI.

5.1.3 Modelling of the forecast

Once we presented the two observables we will use, we want to summarise all the details concerning the surveys specifications used and how we set the fiducial cosmology. We consider as parameters to analyse in our forecast the model parameter α, which controls the strength of interaction, and the total matter density today Ω_m. Then, we compute the Fisher Matrix[2] as

$$F = \begin{pmatrix} F_{\alpha\alpha} & F_{\alpha\Omega_\text{m}} \\ F_{\Omega_\text{m}\alpha} & F_{\Omega_\text{m}\Omega_\text{m}} \end{pmatrix} \ . \tag{5.11}$$

As said, we focus on the J-PAS survey [137], but we also use the DESI [132] and EUCLID [141] experiments for completeness and as a way to compare the capabilities of the different surveys. The tracers are the Luminous Red Galaxies (LRG), Emission Line Galaxies (ELG), Quasars (QSO) and Bright Galaxies (BGS), with the galaxy densities distributed as shown in Table 5.1 for J-PAS and DESI and in Table 5.2 for EUCLID.

For the bias prescription we perform two different analyses. First, we consider the standard bias prescriptions for J-PAS and DESI given in Ref. [142] for each tracer

---

[2]See Appendix A for a description of Fisher techniques.

EUCLID$_{\rm ph}$	
z	ELG
0.3	7440
0.5	6440
0.7	5150
0.9	3830
1.1	2670
1.3	1740
1.5	1070
1.7	620
1.9	341
2.1	178
2.3	88.3
2.5	41.8

EUCLID$_{\rm sp}$	
z	ELG
1.0	68.6
1.2	55.8
1.4	42.1
1.6	26.1

Table 5.2: Galaxy densities are in units of $10^{-5}\ h^3{\rm Mpc}^{-3}$ for spectroscopic EUCLID and photometric EUCLID.

as

$$b_{\rm LRG} = \frac{1.7}{D(z)}\,, \tag{5.12}$$

$$b_{\rm ELG} = \frac{0.84}{D(z)}\,, \tag{5.13}$$

$$b_{\rm QSO} = 0.53 + 0.289(1+z)^2\,, \tag{5.14}$$

$$b_{\rm BSG} = \frac{1.34}{D(z)}\,, \tag{5.15}$$

while for EUCLID, that only has ELG as a tracer, we have the following prescription [141]

$$b_{\rm ELG} = \sqrt{1+z}\,. \tag{5.16}$$

After that, we will also perform a second analysis where we marginalise the bias as a free parameter in each redshift bin $z_{\rm s}$. The reason for this second analysis is to avoid that a plausible modification in the bias, due to the different clustering provoked by the interaction, can spoil our results.

For the photometric redshift error δz, in the case of the clustering analysis we have $\delta z = 0.003$ for LRG, ELG and QSO in the case of J-PAS survey, $\delta z = 0.0005$ for BGS, LRG and ELG and $\delta z = 0.001$ for QSO in the case of DESI, while for EUCLID is $\delta z = 0.001$ for ELG. In the lensing analysis, $\delta z = 0.03$ for J-PAS and $\delta z = 0.05$ for Euclid. The mean redshift for each survey is $z_{\rm mean} = 0.5$ for J-PAS and $z_{\rm mean} = 0.9$ for Euclid. The areal galaxy density is $n_\theta = 12$ for J-PAS and $n_\theta = 30$ for EUCLID.

For the binning, in the case of the clustering analysis of the different scales k and angle of the line of sight μ, we have $k \in [0.007, 10]\ h{\rm Mpc}^{-1}$ with 20 bins logarithmically equispaced and $\mu \in [-1, 1]$ with 200 bins linearly equispaced. For the case of the lensing analysis, we consider $\ell \in [5, 906]$ with $\Delta \ln \ell = 0.1$. For the redshift binning, we

	$\alpha = 0$		$\alpha = 1$	
Survey	$\Delta_{1\sigma}\Omega_{\mathrm{m}}$	$\Delta_{1\sigma}\alpha$	$\Delta_{1\sigma}\Omega_{\mathrm{m}}$	$\Delta_{1\sigma}\alpha$
J-PAS	0.0022	0.132	0.0014	0.061
Euclid	0.0015	0.176	0.0011	0.052
DESI	0.0015	0.111	0.0010	0.054

Table 5.3: Marginalised errors for the forecasted parameters Ω_{m} and α using clustering data and having the bias fixed to the one in ΛCDM for J-PAS, Euclid and DESI surveys.

follow the ones of Tables 5.1 and 5.2.

Our analyses require the choice of a certain fiducial cosmology. Following previous results of Section 4.1, we take the Covariantised dark Thomson-like scattering for the case of the Dark Energy and Dark Matter interaction. We use as cosmological parameters $\Omega_{\mathrm{m}} = 0.310$, $h = 0.6774$, $w = -0.98$ and $n_{\mathrm{s}} = 0.96$ while the coupling parameter $\alpha = 1$. In addition to that, we also consider the case with $\alpha = 0$ for completeness and following results of Section 4.1 that suggested Sunyaev-Zeldovich data is the culprit of such detection.

5.1.4   Results

Once we have all the formalism presented we can perform the forecast. We consider the model parameter α, which sets the strenght of the momentum transfer, and the cosmological parameter Ω_{m} as the parameters to be forecasted. Making use of our modified version of the cosmological Boltzmann solver `CLASS`, we obtain the relevant functions required by the Fisher Matrix code `FARO` [143] to obtain the projected uncertainties in each experiment. We consider three scenarios, namely: clustering signal when bias follows the standard prescription, clustering when we marginalise the bias in each redshift bin and, finally, weak lensing signal.

Clustering: standard bias prescription

In our first analysis, we have the case of clustering data following the prescriptions of Section 5.1.1 for the three surveys, that is J-PAS, DESI and EUCLID. Our tracers are Luminous Red Galaxies (LRG), Emission Line Galaxies (ELG), Quasars (QSO) and Bright Galaxies (BGS).

In Figure 5.2 and Table 5.3 we summarise the results obtained. If the cosmology is the one obtained when adding the Sunyaev-Zeldovich data, that is $\alpha = 1$, the expected errors for the three surveys are around $\sim 5 - 6\%$ for the model parameter. Comparing this result with the already obtained in Section 4.1.3 $\alpha = 1.005^{+0.26}_{-0.33}$ for the combination of `Planck 2018+JLA+BAO+CFHTLens+PlanckSZ` data, the forecasted error considerably enhances the previous constraints and, then, future surveys will be capable of further detecting the interaction. When our fiducial cosmology
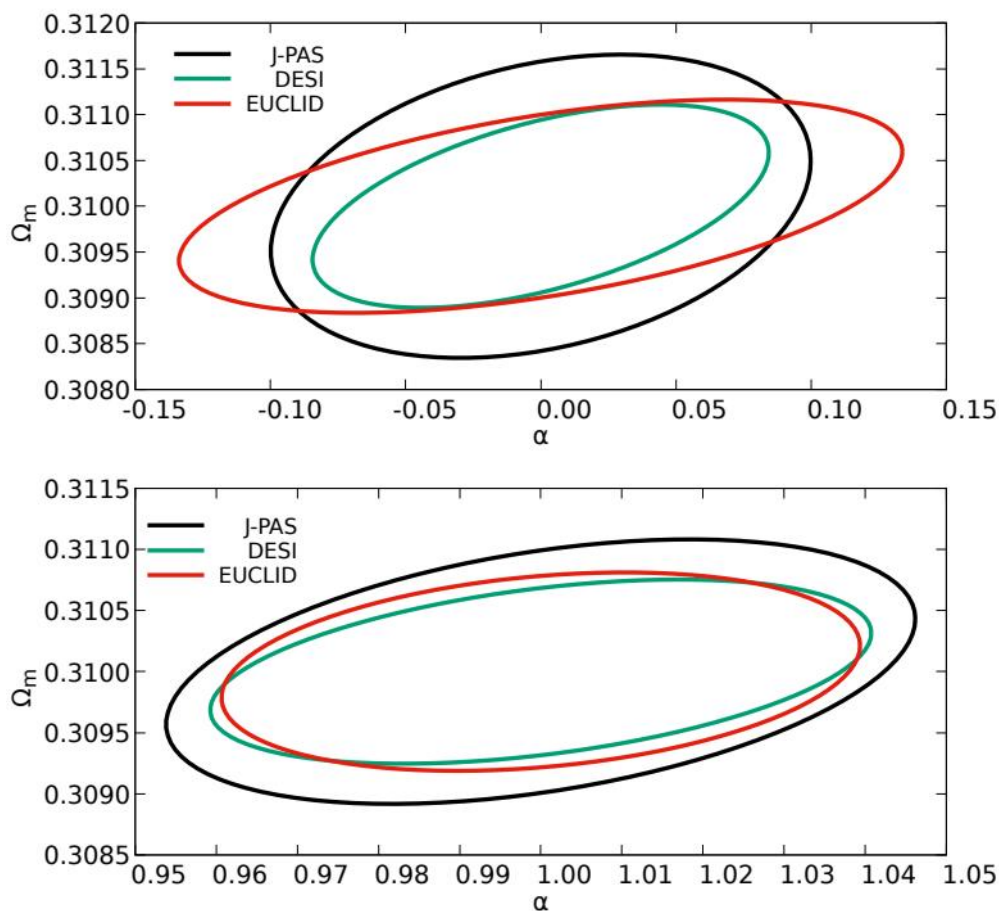
Figure 5.2: For the case of clustering signal, here we show the 1σ contour errors for Ω_{m} and α using as fiducial cosmology $\alpha = 0$ (top) and $\alpha = 1$ (bottom), while fixing the bias to the standard model one of equation (5.15).

is the standard one $\alpha = 0$, the future constraints show how the three surveys will be able to strongly reduce the values of α allowed. These outcomes indicate that a future survey will serve to discriminate the presence or not of this interaction. The comparison between surveys demonstrates how J-PAS experiment will be as capable as the other surveys considered.

Clustering: marginalising the bias

Now, we perform the same analysis but not using the standard bias prescriptions displayed in Section 5.1.1. Instead of that, we marginalise the bias in each redshift bin for the three experiments. The logic behind this is to avoid any possible bias because of a wrong election of the bias. Previous prescriptions were developed for the standard model from different numerical simulations where non-linear scales were studied. Then, a proper modelization of such scales when using another model is required. In Chapter 6 we commence the desirable study, but here we adopt a
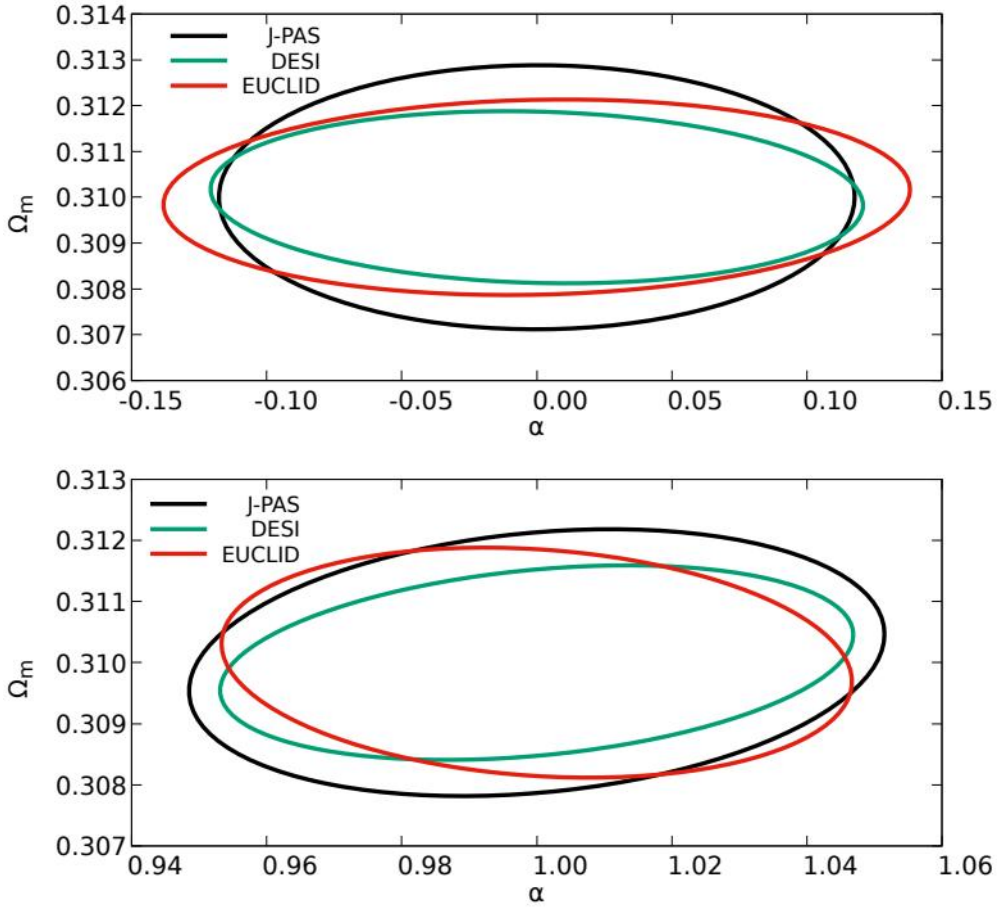
Figure 5.3: For the case of clustering signal, here we show the 1σ contour errors for Ω_{m} and α using as fiducial cosmology $\alpha = 0$ (top) $\alpha = 1$ (bottom), while marginalising the bias.

	$\alpha = 0$		$\alpha = 1$	
Survey	$\Delta_{1\sigma}\Omega_{\mathrm{m}}$	$\Delta_{1\sigma}\alpha$	$\Delta_{1\sigma}\Omega_{\mathrm{m}}$	$\Delta_{1\sigma}\alpha$
J-PAS	0.0038	0.155	0.0029	0.068
Euclid	0.0028	0.182	0.0025	0.062
DESI	0.0025	0.159	0.0021	0.062

Table 5.4: Marginalised errors for the forecasted parameters Ω_{m} and α using clustering data and marginalising the bias in each redshift bin for J-PAS, Euclid and DESI surveys.

very conservative perspective. As we marginalise over the bias in each redshift, we are avoiding any possible incorrect information coming from it. As drawback, we unavoidable increase the expected uncertainty due to the marginalisation.

We summarise the results in Figure 5.3 and Table 5.4 and, again, we obtain very

	$\alpha = 0$		$\alpha = 1$	
Survey	$\Delta_{1\sigma}\Omega_{\mathrm{m}}$	$\Delta_{1\sigma}\alpha$	$\Delta_{1\sigma}\Omega_{\mathrm{m}}$	$\Delta_{1\sigma}\alpha$
J-PAS	0.0070	0.55	0.0239	2.24
Euclid	0.0021	0.26	0.0070	0.74

Table 5.5: Marginalised errors for the forecasted parameters Ω_{m} and α using lensing data for J-PAS and Euclid surveys.

similar results. If the cosmology is $\alpha = 1$, each future survey will be capable of detecting the interaction with strong significance, while if $\alpha = 0$ strong constraints on the model parameter will be established. Finally, J-PAS is as competitive as the other surveys considered.

Weak lensing

Finally, we consider the case of lensing data from future surveys as explained in the previous Section 5.1.2. Now only J-PAS and EUCLID are considered since for weak lensing we need shape information, something only photometric surveys have.

In Figure 5.4 and Table 5.5 we summarise the results obtained. Although the cosmological parameter Ω_{m} is well constrained, the model parameter α is poorly constrained, as errors are much larger than what we already obtained with current data. Particularly, J-PAS will not be able to distinguish the presence of the interaction while the results from EUCLID, although better, will not be competitive. The cause of these results is that the interaction modifies the weak lensing signal slightly. When the interaction becomes efficient, which happens in the very late Universe, perturbations get frozen and then structure formation stops. As a consequence of this, gravitational potentials are altered but not enough to change considerably the signal. Also, no anisotropy is induced due to this interaction. We have already seen the small impact in lensing when studying the CMB in Section 4.1, where we saw how lensed CMB spectra have some oscillations depending on the model parameter but they were small compared to the other modifications. Moreover, the $C_\ell^{\phi\phi}$ spectrum was very slightly modified, at least for realistic values.

Consequently, this interaction affects stronger the clustering than the lensing and, thus, future galaxy survey signal from clustering will be key to confirm or rule out the detection of this interaction.

5.1.5 Final discussion

Cosmology is now living in the era of very high precision surveys. Already finished missions, like the Planck satellite, have established strong constraints on the allowed values for the cosmological parameters. Moreover, a myriad of ongoing and planned surveys for this decade will establish even lower constraints. Having such future precision data will unavoidable rule out a large number of alternative models.
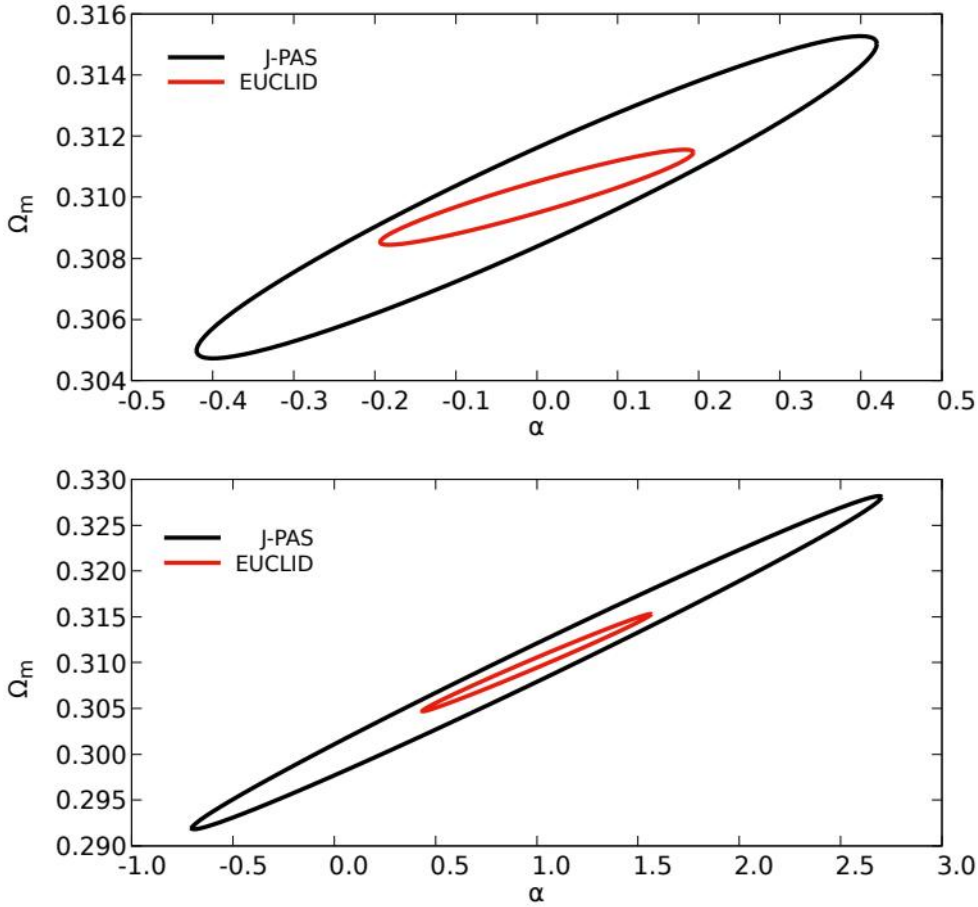
Figure 5.4: For the case of weak lensing signal, here we show the 1σ contour errors for Ω_{m} and α using as fiducial cosmology $\alpha = 0$ (top) and $\alpha = 1$ (bottom).

But, at the same time, new tensions may emerge motivating different alternatives, as it is now happening with the tensions explained in Section 3.4.

In the previous sections, we have tested the future abilities of J-PAS, DESI and EUCLID surveys to constrain the coupling parameter α of the model studied in Section 4.1. In our analyses, we have considered two different signals, namely the clustering and the weak lensing signal. In the case of clustering, we studied two different cases. Either we consider the bias prescriptions of each survey and tracer are not altered by the interaction or we include the possible modifications in the bias by marginalising it in each redshift bin. In both cases, we found that J-PAS will be able to establish strong constraints in the parameters leading rapidly to a more than a 3σ detection of the interaction in future data. Moreover, a 10σ detection of the interaction will be achieved, if the interaction is there, when the mission will come to an end. Even more remarkable is the fact that with only ~ 1000 square degrees J-PAS will find a 5σ detection of the coupling, as inferred from $\sigma_{\mathrm{b}} = \sqrt{\deg_{\mathrm{a}}^2 / \deg_{\mathrm{b}}^2}\, \sigma_{\mathrm{a}}$.

We have seen comparable results with both EUCLID and DESI, which denotes the future capabilities of the survey J-PAS. The previous results improve by a factor ~ 4 previous constraints with current data and, then, J-PAS or the other surveys will be able to confirm or rule out the Covariantised dark Thomson-like scattering.

In the case of weak lensing, results were not promising. In particular, J-PAS, but also EUCLID, will give very large errors in comparison with clustering and not even better that those with current data. Therefore, and as explained before, we can deduce lensing signal is not a powerful tool when dealing with a pure momentum transfer model like this one.

In conclusion, we have shown firstly that clustering signal in future surveys will be capable of detecting or ruling out a pure momentum transfer interaction. Secondly, we have proven that J-PAS survey is as powerful as other future surveys like DESI or EUCLID when dealing with this pure momentum transfer model. We have to remark here that this result should not be considered only in the realms of this particular model but, as it was a general proxy for pure momentum transfer models, similar outcomes should emerge when considering other momentum transfer models of the literature.

5.2 Dipole of the power spectrum and SKA

The Einstein equivalence principle is one of the cornerstones of our current understanding of the gravitational interaction inside the General Relativity theory. It states that all bodies, independently of their intrinsic compositions, should fall at the same rate given a gravitational field. In other words and applied to cosmology, the movement of Dark Matter and Baryons has to follow the same geodesics, provided of course there are no extra interactions. Therefore, detecting any departure between both movements indicates a violation of that principle unless an interaction is acting on one of them, since for cosmological scales we only know about gravity. The alternative answer would be some yet undetected interaction, in our case, for example, a pure momentum transfer acting on Dark Matter following the Covariantised dark Thomson-like scattering developed in Section 4.1. In previous literature [146, 147, 148], it has been shown how the dipole of the Matter Power Spectrum is useful for measuring violations of the equivalence principle. Since future surveys like the Square Kilometre Array experiment (SKA) [138] will measure the dipole of the Matter Power Spectrum, here we try to compute the potential ability of a SKA-like experiment to detect the Covariantised dark Thomson-like scattering by using the dipole.

The Square Kilometre Array experiment is a ground-based probe consisting of two different facilities, one in South Africa and the other in Australia, whose first-light of the observatory is planned to be in 2027. It consists of a giant distribution of small radiotelescopes in both sites that, once combined, will mimic a single giant radiotelescope with a collecting area of around one square kilometre.

5.2.1 Modelling the dipole of the Matter Power Spectrum

In section 2.4, we explained how the spectrum of Galaxy Number Counts was described. Its last term corresponded to the relativistic corrections and was negligible for our previous purposes. Here, however, it will acquire a core role as we will explain. As the other terms were already explained there, let us focus on it and, then, as a starting point, the general description of the relativistic contribution reads as

$$\Delta^{\mathrm{REL}} = \mathcal{H}^{-1} \partial_r \Psi + \left(\frac{5s - 2}{\chi \mathcal{H}} - \frac{\mathcal{H}'}{\mathcal{H}^2} - 5s - f_{evo} \right) \vec{v} \cdot \vec{n} + \mathcal{H}^{-1} \vec{v}\,' \cdot \vec{n} \,, \qquad (5.17)$$

where Ψ corresponds to the gravitational potential in the Newtonian gauge, s is the magnification bias, χ is the comoving distance and f_{evo} is the evolution bias. We denote by $\vec{v}$ the peculiar velocity of the matter distribution while $\vec{n}$ is the unit vector pointing from the source to the observer. We are now going to further simplify the full spectrum of number counts fluctuation by doing the following. First, we work with the radial velocity field defined by $v_{||} = \vec{v} \cdot \vec{n}$, up to linear order in $\mathcal{H}/k$ and, now, neglecting lensing contributions. We use the Euler equation to simplify the spectrum

and, finally, we move to Fourier space[3] as we are interested in the power spectrum. Given the fact we use the Euler equation as stated, for the velocity field of galaxies it reads simply as

$$\vec{v}\,' + \mathcal{H}\vec{v} + \nabla\Psi = 0 \ . \tag{5.19}$$

in the standard scenario. However, in our case we have a modification of Euler equation due to the momentum transfer. In fact, the only relevant change due to our model takes place here. Thus, we first have to derive our new Euler equation. Recalling from Section 4.1, we had

$$\theta'_{\mathrm{dm}} = -\mathcal{H}\theta_{\mathrm{dm}} + k^2\Psi + \Gamma(\theta_{\mathrm{de}} - \theta_{\mathrm{dm}}) \ , \tag{5.20}$$

where we have applied that there is no anisotropic stress and, then, $\Phi = \Psi$. If we consider small enough scales, where precisely this interaction is efficient, and under realistic values of the coupling parameter, $\alpha \sim \mathcal{O}(1)$, Dark Energy velocity is negligible compared to the Dark Matter one (see Figure 4.7 of Section 4.1). Thus, we simplify the previous equation as

$$\theta'_{\mathrm{dm}} \simeq -\mathcal{H}\theta_{\mathrm{dm}} + k^2\Phi - \Gamma\theta_{\mathrm{dm}} \ . \tag{5.21}$$

Provided $\theta = i\vec{k}\cdot\vec{v}$ with $v_{||} = \vec{v}\cdot\vec{n}$, we have

$$v_{||}{}' + \mathcal{H}\left(1 + \Theta\right)v_{||} - \partial_r\Phi \simeq 0 \, , \tag{5.22}$$

where the deviation from the standard scenario is only encoded in the variable Θ, following the notation of Ref. [146]. In our case, it reads as

$$\Theta \equiv \frac{\Gamma}{\mathcal{H}} = \alpha\frac{aH_0}{\Omega_{\mathrm{dm}}(a)\mathcal{H}} \ . \tag{5.23}$$

However, a big conceptual step is pending. The velocity of equation (5.22) is the Dark Matter radial peculiar velocity but as a SKA-like, or any other survey, only measures galaxies, we need to connect the Dark Matter one to the galaxy peculiar velocity. Here, for completeness, we consider two extreme and opposed scenarios leading to two conceptual assumptions as follows:

- Dark Matter tracers: galaxies comove with Dark Matter (for example Refs. [146, 147, 149]), meaning galaxies are faithful tracers of the Dark Matter velocity field.

- Gravitational potential tracers: galaxies move according to the linear geodesic equation, so they move according to the gravitational potential (see Ref. [150]).

---

[3]We use the following convention

$$\tilde{f}(\vec{k}) = \int f(\vec{x})\,e^{i\vec{k}\cdot\vec{x}}\,\mathrm{d}^3x \qquad \text{and} \qquad f(\vec{x}) = \int \tilde{f}(\vec{k})\,e^{-i\vec{k}\cdot\vec{x}}\,\frac{\mathrm{d}^3k}{(2\pi)^2} \ . \tag{5.18}$$

Finally, assuming the flat-sky approximation, we can define the estimator of the dipole as

$$\hat{P}_1^{AB}(k) = \frac{3}{2V} \int \frac{d\Omega_{\hat{\mathbf{k}}}}{2\pi} \, \mu \, \Delta^A(\mathbf{k}) \, \Delta^B(-\mathbf{k}) \ , \tag{5.24}$$

where V is the survey volume.

Dark Matter tracers

Assuming the galaxy velocity field perfectly matches the Dark Matter velocity, then we have $v_{||}{}^{\text{gal}} = v_{||}{}^{\text{dm}}$. This situation is expected by the following reasoning. The structures, galaxies, formed much earlier than the time this interaction is efficient. Then, following the standard scenario, galaxies have formed at the bottom of the gravitational potential due to Dark Matter. But, once this interaction becomes efficient, it acts as a friction term avoiding structures of Dark Matter to grow but not being able to detach them from Baryons under realistic value of α. Thus, they follow the Dark Matter gravity field. Therefore, under all the previous assumptions discussed, the relativistic number counts spectrum of galaxies is described by

$$\Delta(\mathbf{x}) = b\delta + \mathcal{H}^{-1}\partial_r v_{||} + \left(\frac{\mathcal{H}'}{\mathcal{H}^2} + \frac{2-5s}{\chi\mathcal{H}} + 5s - f_{\text{evo}} + \Theta\right)v_{||} + \mathcal{O}\left(\mathcal{H}^2/k^2\right) \ . \tag{5.25}$$

Given we do not modify the continuity equation, we can use that

$$\partial_r v_{||}{}^{\text{dm}} = f_{\text{dm}}\mathcal{H}\mu^2\delta_{\text{dm}} \qquad \text{and} \qquad v_{||}{}^{\text{dm}} = -i\mu f_{\text{dm}}\delta_{\text{dm}}\mathcal{H}/k \ , \tag{5.26}$$

with $\mu = \hat{\mathbf{x}} \cdot \hat{\mathbf{k}}$. Then, our expression for the number counts spectrum reads as

$$\Delta(\mathbf{k}) = b\delta(\mathbf{k}) + \left[f_{\text{dm}}\mu^2 - i\mu f_{\text{dm}}\frac{\mathcal{H}}{k}\mathcal{R}\right]\delta_{\text{dm}}(\mathbf{k}) \ , \tag{5.27}$$

where

$$\mathcal{R} = \frac{\dot{\mathcal{H}}}{\mathcal{H}^2} + \frac{2-5s}{\chi\mathcal{H}} + 5s - f_{\text{evo}} + \Theta \ , \tag{5.28}$$

$$\Theta \equiv \frac{\Gamma}{\mathcal{H}} = \alpha\frac{aH_0}{\Omega_{\text{dm}}(a)\mathcal{H}} \ . \tag{5.29}$$

However, here we face one inconsistency as we have δ and δ_{dm}, where the extra Baryon or Dark Energy density contrasts make the difference between both variables. To overcome it, we assume the ratio $\delta_{\text{dm}}/\delta$ is almost constant for the scales and redshifts of interest. This was numerically tested as we show in Fig. 5.5. Provided that, we finally get our answer for the spectrum of Galaxy Number Counts fluctuation in Fourier space

$$\Delta(\mathbf{k}) = \left[b + f_{\text{dm}}\mu^2 - i\mu f_{\text{dm}}\frac{\mathcal{H}}{k}\mathcal{R}\right]\delta(\mathbf{k}) \ . \tag{5.30}$$

Now we have the full power spectrum for two different populations called A and B
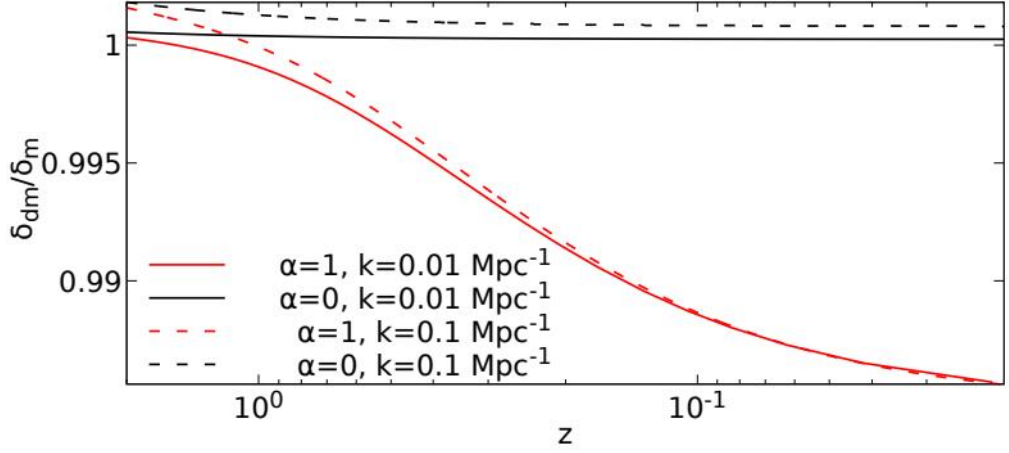
Figure 5.5: In this figure, we plot the ratio of the density contrasts of the Dark Matter component and the total matter (Dark Matter plus Baryons). We can see that the error of assuming that the ratio $\delta_{\rm dm}/\delta$ is constant and scale independent is below the 1% level, which, as we will see, is below the sensitivity for the measurement of the interaction parameter α. This justifies our assumption since including this effect will lead to a correction smaller than the precision of the measurement.

as

$$
P^{AB}(\mathbf{k}) = \left[b_A + f_{\rm dm}\mu^2 - i\mu f_{\rm dm}\frac{\mathcal{H}}{k}\mathcal{R}_A \right]
$$
$$
\times \left[b_B + f_{\rm dm}\mu^2 + i\mu f_{\rm dm}\frac{\mathcal{H}}{k}\mathcal{R}_B \right] P(k) \ . \tag{5.31}
$$

which we can expand into the multipoles and different redshift bins as

$$
P_0^{AB}(k,z) = \left[b_A b_B + \frac{1}{3}(b_A + b_B)f_{\rm dm} + \frac{f_{\rm dm}^2}{5} \right] P(k,z) + \mathcal{O}\left(\mathcal{H}^2/k^2\right) \ , \tag{5.32}
$$

$$
P_1^{AB}(k,z) = -if_{\rm dm}\frac{\mathcal{H}}{k}\left[\frac{3}{5}f_{\rm dm}(\mathcal{R}_A - \mathcal{R}_B) + (b_B\mathcal{R}_A - b_A\mathcal{R}_B) \right] P(k,z)
$$
$$
+ \mathcal{O}\left(\mathcal{H}^2/k^2\right) \ , \tag{5.33}
$$

$$
P_2^{AB}(k,z) = \left[\frac{2}{3}f(b_A + b_B) + \frac{4f_{\rm dm}^2}{7} \right] P(k,z) + \mathcal{O}\left(\mathcal{H}^2/k^2\right) \ , \tag{5.34}
$$

$$
P_3^{AB}(k,z) = -\frac{2}{5}if_{\rm dm}^2\frac{\mathcal{H}}{k}\left[\mathcal{R}_A - \mathcal{R}_B \right] P(k,z) + \mathcal{O}\left(\mathcal{H}^2/k^2\right) \ , \tag{5.35}
$$

$$
P_4^{AB}(k,z) = \frac{8}{35}f_{\rm dm}^2 + \mathcal{O}\left(\mathcal{H}^2/k^2\right) \ . \tag{5.36}
$$

As one infers from the previous expressions, relativistic effects only appear at linear order in the odd multipoles while their contributions to the even multipoles go as $\mathcal{O}\left(\mathcal{H}^2/k^2\right)$ and, then, negligible for our purposes here. Once the decomposition into the different multipoles is done, the only thing we still need is the variance of the

dipole. Following the definition of equation (5.24), its variance is

$$
\begin{aligned}
\langle \hat{P}_1^{AB}(k)\, \hat{P}_1^{*AB}(q)\rangle_c &= \frac{9}{4V^2}\int \frac{d\Omega_{\hat{\mathbf{k}}}}{2\pi}\frac{d\Omega_{\hat{\mathbf{q}}}}{2\pi}\mu_k\mu_q\langle \Delta^A(\mathbf{k})\,\Delta^B(-\mathbf{k})\,\Delta^A(-\mathbf{q})\,\Delta^B(\mathbf{q})\rangle \\
&= \frac{9}{4V^2}\delta_D^{(3)}(0)\,(2\pi)^6\int \frac{d\Omega_{\hat{\mathbf{k}}}}{2\pi}\frac{d\Omega_{\hat{\mathbf{q}}}}{2\pi}\mu_k\mu_q\big[P^{AA}(\mathbf{k})\,P^{BB}(-\mathbf{k})\,\delta_D(\mathbf{k}-\mathbf{q}) \\
&\qquad\qquad +P^{AB}(\mathbf{k})\,P^{BA}(-\mathbf{k})\,\delta_D(\mathbf{k}+\mathbf{q})\big] \\
&= \frac{9}{4}\frac{(2\pi)^6}{V^2}\frac{\delta_D^{(3)}(0)}{2\pi}\frac{\delta_D(k-q)}{k^2} \\
&\quad\times \sum_{\ell_1\ell_2}\Big[P_{\ell_1}^{AA}(k)\,P_{\ell_2}^{BB}(k)-P_{\ell_1}^{AB}(k)\,P_{\ell_2}^{BA}(k)\Big]\int d\mu\,\mu^2\mathcal{L}_{\ell_1}(\mu)\,\mathcal{L}_{\ell_2}(-\mu) \\
&= \frac{\delta_D^{(3)}(0)}{2\pi}\frac{(2\pi)^6}{V^2}\frac{\delta_D(k-q)}{k^2}\bigg[\frac{9}{5}(b_B\mathcal{R}_A-b_A\mathcal{R}_B)^2 \\
&\quad +\frac{18}{7}f_{\rm dm}(\mathcal{R}_A-\mathcal{R}_B)(b_B\mathcal{R}_A-b_A\mathcal{R}_B)+f_{\rm dm}^2(\mathcal{R}_A-\mathcal{R}_B)\bigg]\frac{\mathcal{H}^2}{k^2}f_{\rm dm}^2P^2(k) \\
&= \frac{(2\pi)^2}{V}\frac{\delta_D(k-q)}{k^2}\bigg[\frac{9}{5}(b_B\mathcal{R}_A-b_A\mathcal{R}_B)^2 \\
&\quad +\frac{18}{7}f_{\rm dm}(\mathcal{R}_A-\mathcal{R}_B)(b_B\mathcal{R}_A-b_A\mathcal{R}_B)+f_{\rm dm}^2(\mathcal{R}_A-\mathcal{R}_B)\bigg]\frac{\mathcal{H}^2}{k^2}f_{\rm dm}^2P^2(k)\;. \quad (5.37)
\end{aligned}
$$

where we have used that $\delta_D^{(3)}(0)\simeq V/(2\pi)^3$ for a finite volume survey. We also need to include the shot-noise contribution. Only the monopole of the auto-correlation power spectra have a non-vanishing shot-noise contribution, therefore we need to add the following term

$$
\begin{aligned}
P_{\ell_1}^{AA}(k)\,P_{\ell_2}^{BB}(k) &\rightarrow \big(P_{\ell_1}^{AA}(k)+\delta_{\ell_10}N_A\big)\big(P_{\ell_2}^{BB}(k)+\delta_{\ell_20}N_B\big) \\
&= P_{\ell_1}^{AA}(k)\,P_{\ell_2}^{BB}+\delta_{\ell_20}P_{\ell_1}^{AA}N_B+\delta_{\ell_10}P_{\ell_1}^{BB}N_A+\delta_{\ell_10}\delta_{\ell_20}N_AN_B\;,
\end{aligned}
$$

(5.38)

where N_A and N_B are the shot-noise power spectra of the populations A and B respectively. Combining all together, we find the following variance for the dipole of

the power spectrum

$$
\begin{aligned}
\langle \hat{P}_1^{AB}(k)\, \hat{P}_1^{*AB}(q) \rangle_c &= \\
&= \left\{ \left[\frac{9}{10} \left(b_B \mathcal{R}_A - b_A \mathcal{R}_B \right)^2 + \frac{9}{7} f_{\rm dm} \left(\mathcal{R}_A - \mathcal{R}_B \right) \left(b_B \mathcal{R}_A - b_A \mathcal{R}_B \right) \right. \right. \\
&\qquad \left. + \frac{f_{\rm dm}^2}{2} \left(\mathcal{R}_A - \mathcal{R}_B \right)^2 \right] \frac{\mathcal{H}^2}{k^2} f_{\rm dm}^2 P^2(k) \\
&\quad + \left[\frac{3}{2} \left(b_A^2 N_B + b_B^2 N_A \right) + \frac{9}{5} f_{\rm dm} (b_A N_B + b_B N_A) + \frac{9}{14} f_{\rm dm}^2 (N_A + N_B) \right. \\
&\qquad \left. \left. + \frac{9}{10} f_{\rm dm}^2 \frac{\mathcal{H}^2}{k^2} \left(N_B \mathcal{R}_A^2 + N_A \mathcal{R}_B^2 \right) \right] P(k) + \frac{3}{2} N_A N_B \right\} \frac{(2\pi)^2}{V} \frac{\delta_D(k-q)}{k^2} \\
&= \left\{ -\frac{9}{5} \left(P_1^{AB}(k) \right)^2 - \frac{23}{35} \left(P_3^{AB}(k) \right)^2 - \frac{36}{35} P_1^{AB}(k)\, P_3^{AB}(k) \right. \\
&\quad + 3 \left[\left(\frac{1}{2} P_0^{BB}(k) + \frac{1}{5} P_2^{BB}(k) \right) N_A + \left(\frac{1}{2} P_0^{AA}(k) + \frac{1}{5} P_2^{AA} \right) N_B \right. \\
&\qquad \left. \left. + \frac{1}{2} N_A N_B \right] \right\} \frac{(2\pi)^2}{V} \frac{\delta_D(k-q)}{k^2} \\
&= \sigma_{P_1}^2(k) \frac{(2\pi)^2}{V} \frac{\delta_D(k-q)}{k^2} \; . \tag{5.39}
\end{aligned}
$$

Gravitational potential tracers

In the second scenario, we consider that galaxies are just test particles moving in geodesics controlled by an external gravitational field of matter distribution. Then, the interaction is not directly acting on galaxies. This has a first consequence, the density contrast perturbation now is all the matter perturbation and, thus, $f_{\rm dm} \to f_{\rm dm+b+de}$[4] that we simply denote by f for simplicity of the notation. The second consequence is that we should set in previous equations $\Theta = 0$ and, thus, the dipole is sensitive only through modification in cosmological functions involved in the multipoles. In our case, only in the growth rate f and growth function D, the gravitational potential, the Matter Power Spectrum and the σ_8 parameter. Just by the equivalence principle, we get the Euler equation in ΛCDM as galaxies are now test particles with no extra interaction acting directly on them[5]. Of course the interaction is there but, as it is acting on Dark Matter, galaxies only feel it through a different gravitational potential sourcing the geodesics.

5.2.2   Modelling of the forecast

In this case, we will follow a Fisher analysis[6] for unveiling the detectability of the coupling parameter for a SKA-like survey. We consider that SKA will measure tomo-

---

[4]The additions coming from Dark Energy are negligible both to the density contrast, as Dark Energy does not form structure, and to the growth rate as the clustering of Dark Energy is strongly suppressed by its own nature.

[5]See Appendix C of Ref. [140] for the full derivation.

[6]See Appendix A.

graphically a redshift range from $z_{\min} = 0.1$ to $z_{\max} = 2$, and we divide such redshift range into nineteen bins of width $\Delta z = 0.1$, having in each bin the galaxy bias and the number density reported in Table 5.6, following data of Ref. [151]. Considering two populations, A and B, we set the bias for each one as

$$
\begin{aligned}
b_A(z) &= b(z) + 0.25\,, & \text{(5.40)} \\
b_B(z) &= b(z) - 0.25\,, & \text{(5.41)}
\end{aligned}
$$

such that $b_A(z) - b_B(z) = 0.5$, as reported in Ref. [146]. For the number density of each population, we simply use the prescription $n_A(z) = n_B(z) = n(z)/2$. In principle, we will make our forecast setting for simplicity $f_{\mathrm{evo}} = 0$ and $s = 0$ for both populations. This is a very simplistic prescription, but we should remember that the larger the difference between both populations, the better the detectability by relativistic effects sourcing the dipole. Thus, having a very simplistic but equal prescription for both populations will give us the worst scenario on detectability terms. For the shot-noise spectrum we use $N_A = 1/n_A$ and $N_B = 1/n_B$. The volume of each redshift bin is

$$
V_i = \frac{4\pi}{3} f_{\mathrm{sky}} \left[\chi(z_{\max})^3 - \chi(z_{\min})^3 \right]\,, \tag{5.42}
$$

where $\chi(z)$ is the comoving distance to redshift z and f_{sky} is the fraction of the sky covered, that for SKA [152] survey is $f_{\mathrm{sky}} = 30000/(360^2/\pi)$. Finally, we set our fiducial cosmology to be $\alpha = 1$ inside the Covariantised dark Thomson-like scattering between Dark Matter and Dark Energy, with the other cosmological parameters set to $\Omega_{\mathrm{b}} h^2 = 0.02264$, $\Omega_{\mathrm{dm}} h^2 = 0.1163$, $n_{\mathrm{s}} = 0.9721$, $A_{\mathrm{s}} = 2.063\ 10^{-9}$, $\tau_{\mathrm{reio}} = 0.0502$, $w = -0.948$ and $h = 0.6788$.

Considering a general redshift bins splitting without correlations between different bins, in Fourier space from a $k_{\min}$ to $k_{\max}$ and two parameters a and b, the corresponding Fisher element is

$$
F_{ab} = \sum_i \frac{V_i}{4\pi^2} \int \mathrm{d}k k^2 \left(\frac{\partial P_1(k, z_i)}{\partial a} \right) \left(\frac{\partial P_1(k, z_i)}{\partial b} \right)^* \sigma_{P_1}^{-2}(k, z_i)\,, \tag{5.43}
$$

where the summation is on the different bins considered. In principle, one should compute the Fisher element for Θ but as both, α and Θ, are simply related by

$$
\Theta = \frac{H_0}{\Omega_{\mathrm{dm}}(z)\mathcal{H}(z)(1+z)}\, \alpha\,, \tag{5.44}
$$

and since the interaction has no impact on background quantities, both Fisher elements $F_{\Theta\Theta}$ and $F_{\alpha\alpha}$ are directly related. Also, no correlations with the background parameters need to be considered when passing from $F_{\Theta\Theta}$ to $F_{\alpha\alpha}$. Consequently, the Fisher element for the model parameter is simply

$$
F_{\alpha\alpha} = \sum_i \frac{V_i}{4\pi^2} \int \mathrm{d}k\, k^2 \left| \frac{\partial P_1(k, z_i)}{\partial \alpha} \right|^2 \sigma_{P_1}^{-2}(k, z_i)\,. \tag{5.45}
$$

143

z_{min}	z_{min}	$n(z)$ [Mpc^{-3}]	$b(z)$
0.1	0.2	$6.20\ 10^{-2}$	0.623
0.2	0.3	$3.63\ 10^{-2}$	0.674
0.3	0.4	$2.16\ 10^{-2}$	0.730
0.4	0.5	$1.31\ 10^{-2}$	0.790
0.5	0.6	$8.07\ 10^{-3}$	0.854
0.6	0.7	$5.11\ 10^{-3}$	0.922
0.7	0.8	$3.27\ 10^{-3}$	0.996
0.8	0.9	$2.11\ 10^{-3}$	1.076
0.9	1.0	$1.36\ 10^{-3}$	1.163
1.0	1.1	$8.70\ 10^{-4}$	1.257
1.1	1.2	$5.56\ 10^{-4}$	1.360
1.2	1.3	$3.53\ 10^{-4}$	1.472
1.3	1.4	$2.22\ 10^{-4}$	1.594
1.4	1.5	$1.39\ 10^{-4}$	1.726
1.5	1.6	$8.55\ 10^{-5}$	1.870
1.6	1.7	$5.20\ 10^{-5}$	2.027
1.7	1.8	$3.12\ 10^{-5}$	2.198
1.8	1.9	$1.83\ 10^{-5}$	2.385
1.9	2.0	$1.05\ 10^{-5}$	2.588

Table 5.6: Galaxy bias $b(z)$ and number density used, following Table 3 of Ref. [151] for SKA.

and, then, we have

$$\Delta_{1\sigma}\alpha = \frac{2}{F_{\alpha\alpha}^{1/2}}\ , \tag{5.46}$$

as explained in Appendix A. Once the procedure has been explained, we will show the results obtained in the different scenarios commented before.

5.2.3   Results

Now we have all the tools developed, we take our modified version of CLASS code [113, 114] explained in Section 4.1 including the Dark Energy-Dark Matter Covariantised dark Thomson-like scattering to compute the numerical quantities required in previous equations. With it, we have created a forecast FORTRAN code to compute the corresponding Fisher elements. In each case, we compute the forecasted error for the coupling parameter α under the conditions of the scenario considered and all results are compressed into Figures 5.6 and 5.7.

Dark Matter tracers

Here we have assumed that galaxies are perfect tracers of the underlaying total matter distribution and then $v_{||}{}^{\rm gal} = v_{||}{}^{\rm dm}$. In this case, we obtain the expected uncertainty for the coupling parameter using the dipole in a SKA-like survey would be

$$\Delta_{1\sigma}\,\alpha = 0.198\,,\tag{5.47}$$

where we have assumed $\alpha = 1$. Comparing it to the constraints with current data obtained in Section 4.1.3, namely $\alpha = 1.005^{+0.26}_{-0.33}$, the forecasted error considerably enhances the previous constraints. Therefore, we can conclude the following: should the interaction be there, a SKA-like survey will detect it through the dipole of the Matter Power Spectrum. This conclusion should be extended to any similar model with pure momentum transfer as here we are only using this model because of its simplicity and similarity to the ΛCDM model, combined with its capabilities of alleviating the σ_8 or S_8 tension. Therefore, this calls for more attention in future experiments as the dipole of the Matter Power Spectrum can be a smoking gun for this interactions in the Dark Sector of the Universe.

We can go one step further and consider different prescriptions. In our case, we keep the same magnification bias $s_i = 0$ but now we follow for the evolution bias the one of Ref. [153], given by $f_{\rm evo} = (b-1)f\delta_c$, as a simple proxy to test the implications. The expected result is an improvement of the forecasted error since now both populations have different $f_{\rm evo}$, provided $b_A\,(z) - b_B\,(z) = 0.5$. We should remember that the relativistic effects were sourced in the dipole (or any odd multipole) weighted by the difference in the two populations considered. Another issue one may wonder is which value of the critical spherical collapse density should be used here. Although some corrections from the interaction may appear to the standard model value $\delta_c \simeq 1.686$, we ought to remember this is a late-time interaction and, then, for most of the structure formation process δ_c remains unaffected. Once we have real data, a precise analysis on the corrections will be required but, for our forecast purposes, we use the standard value. By doing that, the uncertainty lowers to

$$\Delta_{1\sigma}\,\alpha = 0.166\,.\tag{5.48}$$

In all the previous cases, most of the information is coming from linear scales as clearly depicted in Figure 5.7 where we can interpret that no extra constraining power emerges from scales larger than $k_{\rm max} \sim 0.1\ h/{\rm Mpc}$.

Gravitational potential tracers

Now we consider the movement of galaxies is fully determined by the gravitational potential, which is affected by the interaction via the Dark Matter contribution. Then, galaxies just follow the corresponding geodesics. In that case, the forecasted uncertainty is

$$\Delta_{1\sigma}\,\alpha = 1.30\,.\tag{5.49}$$

145
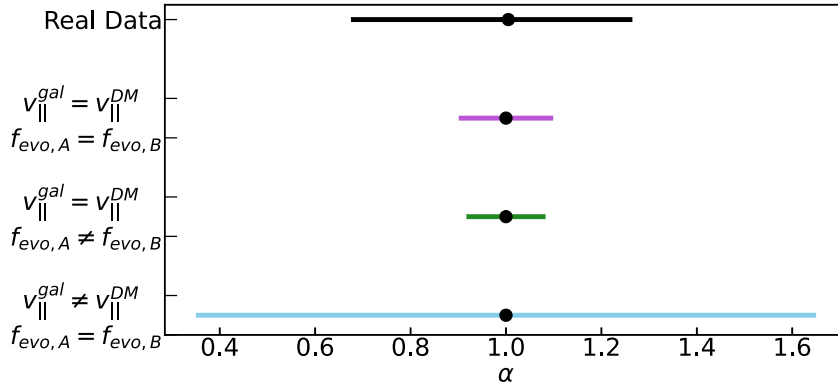
Figure 5.6: Constraining power for the case when Dark Matter halos and galaxies are comoving with $f_{\mathrm{evo,A}} = f_{\mathrm{evo,B}} = 0$ (purple), with $f_{\mathrm{evo,I}} = (b_I - 1)f\delta_c$, $I = A, B$ (green) and the case when galaxies are just test particles moving with the gravitational potential created by Dark Matter halos (blue). The black line corresponds to the constraints obtained with real data for this model, as shown in Chapter 4.

This result indicates that if galaxies just move in the geodesics, a future SKA-like survey will not be capable enough by the means of the dipole of the Matter Power Spectrum, at least compared with current constraints. The paradigm is, then, completely different from the first case studied. One can understand these results as follows. In the previous cases, galaxies directly feel the interaction as their velocity was attached to the Dark Matter velocity, that was completely modified by the interaction. But now this is not the case since the velocity of galaxies is no longer directly attached to the Dark Matter one but to the geodesic movement. It is true that the geodesics are sourced by the gravitational potential which is mainly determined by Dark Matter, but now the effect is diluted. First, Dark Energy has to change Dark Matter velocity by transferring momentum, this reduces the clustering of Dark Matter, then gravitational potentials change due to the different clustering. Consequently, geodesics for galaxies, that are sourced by the gravitational potentials, change.

Degeneracy between α and f_{evo}

Recall the form of the Galaxy Number Counts fluctuations shown in equation (5.25) as

$$\Delta\left(\mathbf{k}\right) = \left[b + f_{\mathrm{dm}}\mu^2 - i\mu f_{\mathrm{dm}}\frac{\mathcal{H}}{k}\left(\frac{\dot{\mathcal{H}}}{\mathcal{H}^2} + \frac{2-5s}{\chi\mathcal{H}} + 5s - f_{\mathrm{evo}} + \Theta\right)\right]\delta\left(\mathbf{k}\right) , \qquad (5.50)$$

where we have used the definition of $\mathcal{R}$ of equation (5.28). From its apparent functional dependence, one can expect a degeneracy between Θ and f_{evo} that might spoil our results and, thus, a more detailed analysis is required.

To do so, we now compute the Fisher matrix for the parameter of the model α and
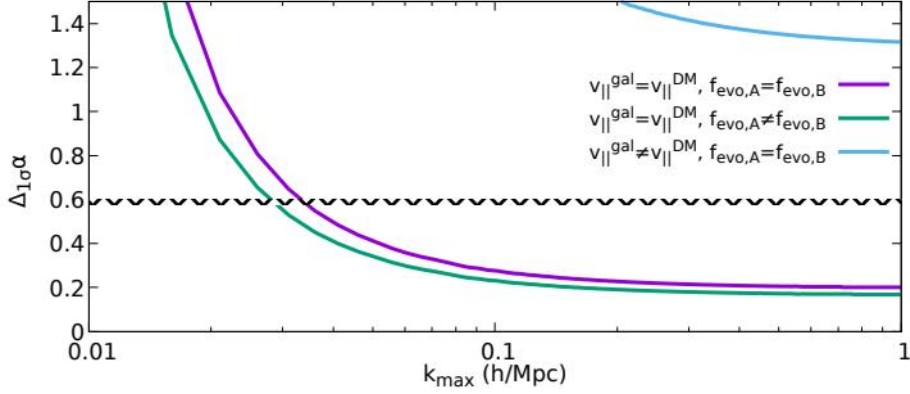
Figure 5.7: Constraining power as a function of the k_{max} used for the case when Dark Matter halos and galaxies are comoving with $f_{\mathrm{evo,A}} = f_{\mathrm{evo,B}} = 0$ (purple), with $f_{\mathrm{evo,I}} = (b_I - 1)f\delta_c$, $I = A, B$ (green) and the case when galaxies are just test particles moving with the gravitational potential created by Dark Matter halos (blue). The black region corresponds to the constraints obtained with actual data for this model, as shown in Chapter 4.

the evolution bias f_{evo} as follows

$$F = \begin{pmatrix} F_{\alpha\alpha} & F_{\alpha f_{\mathrm{evo}}} \\ F_{f_{\mathrm{evo}}\alpha} & F_{f_{\mathrm{evo}}f_{\mathrm{evo}}} \end{pmatrix} \, , \tag{5.51}$$

where the element $F_{\alpha\alpha}$ was already calculated in equation (5.45), while the new ones $F_{\alpha f_{\mathrm{evo}}}$ and $F_{f_{\mathrm{evo}}f_{\mathrm{evo}}}$ read as

$$F_{\alpha f_{\mathrm{evo}}} = \sum_i \frac{V_i}{4\pi^2} \int \mathrm{d}k \, k^2 \frac{\partial P_1(k, z_i)}{\partial \alpha} \left(\frac{\partial P_1(k, z_i)}{\partial f_{\mathrm{evo}}} \right)^* \sigma_{P_1}^{-2}(k, z_i) \, , \tag{5.52}$$

$$F_{f_{\mathrm{evo}}f_{\mathrm{evo}}} = \sum_i \frac{V_i}{4\pi^2} \int \mathrm{d}k \, k^2 \left| \frac{\partial P_1(k, z_i)}{\partial f_{\mathrm{evo}}} \right|^2 \sigma_{P_1}^{-2}(k, z_i) \, . \tag{5.53}$$

In the case of the $F_{\alpha\alpha}$, the derivatives inside it were not analytical as α modifies not only $\mathcal{R}$ but also the power spectrum $P(z, k)$ or the growth rate f. But now the derivative of the dipole P_1 with respect to the evolution bias f_{evo} is fully analytical, since $\frac{\partial \mathcal{R}}{\partial f_{\mathrm{evo}}} = -1$ and $b_A(z) - b_B(z) = 0.5$. Thus we have

$$\frac{\partial P_1(k, z_i)}{\partial f_{\mathrm{evo}}} = -if \frac{\mathcal{H}}{2k} P(k, z) \, . \tag{5.54}$$

Therefore, we can just get the forecasted error for the model parameter by marginalising over the evolution bias as

$$\Delta_{1\sigma} \alpha = 2\sqrt{F_{\alpha\alpha}^{-1}} = 0.242 \, , \tag{5.55}$$

where we have considered the case of Dark Matter tracers with $f_{\mathrm{evo}} = 0$ for simplicity. Moreover, we can also compute the marginalised error for the evolution bias as

$\Delta_{1\sigma} f_{\text{evo}} = 2\sqrt{F^{-1}_{f_{\text{evo}} f_{\text{evo}}}} = 0.553$. Consequently, we conclude the possible degeneracy is not there and results are not spoiled. The reason is clearly seen in Figure 5.8. If one considers only one redshift bin, no matter which one, the degeneracy is very strong leading to the impossibility of measuring both f_{evo} and α at the same time. But the direction of the degeneracy rotates with the redshift bin such that when combining all the bins the constraints are smaller. We can find the answer to that in the combination of two facts. The first thing is the different redshift dependence, as one deduces from Figure 5.8. The parameter α is only strongly constrained by the lower redshift bins as that is precisely the time when the interaction is efficient. This is not true for f_{evo}. The second fact comes from the other elements that depend on the model parameter α, as for example the Matter Power Spectrum. Both combined lead to the break of the degeneracy.

5.2.4 Final discussion

Regarding the discussed detection of the interaction using current data of Section 4.1, finding a probe that can act as a smoking gun for detecting the interaction would be crucial. Here is where a survey like SKA can help. SKA will be able to measure the dipole of the power spectrum with enough precision to test the equivalence principle. Then, if the principle holds Dark Matter and Baryons (or any other mass) have to follow the same geodesic. If a departure is found there are two possible answers, either the equivalence principle does not operate on the Dark Sector or an interaction we are not counting is happening. In this part of the thesis we have explored this last possibility.

Taken the Dark Energy-Dark Matter Covariantised dark Thomson-like scattering, we have investigated the future constraining power of a SKA-like experiment to detect the imprints of the interaction in the dipole of the Matter Power Spectrum. This type of interaction modifies the Euler equations as shown, leading to a correction in the relativistic contribution to the Galaxy Number Counts spectrum. We considered two scenarios. In the first one, named "Dark Matter tracers", we have assumed Dark Matter and galaxies comove and thus galaxies are perfect tracers of the Dark Matter peculiar velocity field. In that case, the forecasted uncertainty is $\Delta_{1\sigma} \alpha = 0.198$, which not only improves the results from current data but also indicates SKA will serve as a smoking gun for this kind of interactions. In the second scenario, called "gravitational potential tracer", we have considered galaxies move according to their geodesic equation sourced by the gravitational field, that is affected by the interaction via its Dark Matter part. In that case, results demonstrate no competitive capabilities of detecting the interaction. Finally, we should comment that, although our results were obtained under the model of Section 4.1, they can be understood as general remarks on the future abilities of detecting pure momentum transfer interactions.
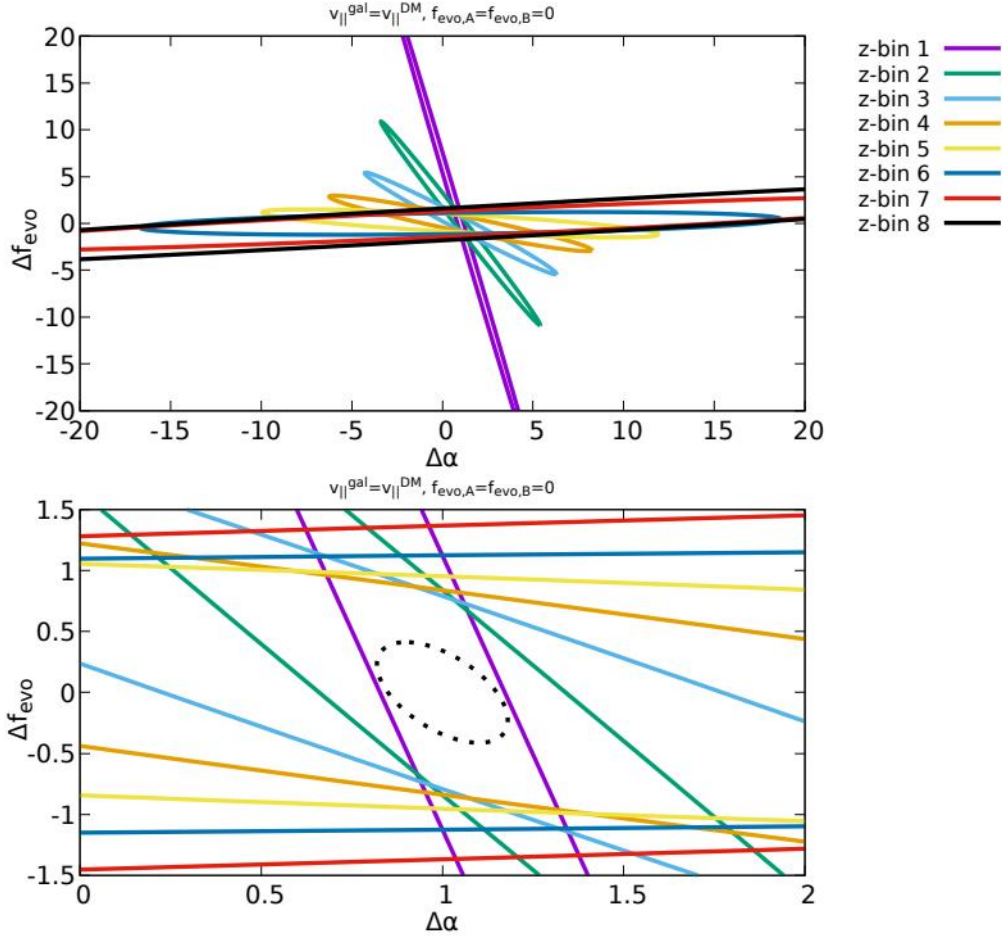
Figure 5.8: We show the 2-dimensional contour plot for the evolution bias $f_{\rm evo}$ and the parameter α. Different colours refer to individual redshift bins. In the bottom panel, we zoom in to see how the different degeneracies, generated by the redshift evolution of α, strongly reduce the error-bars in $f_{\rm evo}$ and α. We can also see that most of the information is carried by the lower redshift bins, where the dipole amplitude is larger.

To conclude, upcoming surveys like SKA will have a definitive role on ruling out or not several alternative model to the standard ΛCDM one. In particular, for pure momentum transfer models which alleviate the σ_8 tension and are under debate if current data have already detected them, the dipole of the Matter Power Spectrum can act as a smoking gun since their effects leave a measurable imprint on it as shown in this section.

5.3 Cluster Counts and EUCLID

When performing a clustering survey there are two main useful tools. Either one can use the Matter Power Spectrum in Fourier space or the angular Matter Power Spectrum, both explained in the corresponding subsections of 2.4. In other parts of this thesis we have proceeded with the Matter Power Spectrum $P(z, k)$ for our purposes but, however, there are some advantages of using the angular one, usually denoted as $C_\ell(z, z')$, since

- It is a direct observable as we can measure the distribution of galaxies in the sky as a function of the angles.

- It has been demonstrated its frame independence property, while the Matter Power Spectrum does depend [154].

- It can accommodate relativistic effects and different codes have been developed for this purpose, for example the CLASSgal [155] which is now implemented inside the CLASS code [113, 114].

Even though relativistic effects can be included, it is customary in the literature to neglect some contributions when computing it. In particular, here we focus on the lensing convergence contribution that, although we had already explained before in subsection 2.4, encodes the modification of the area and magnitude of the different regions of the sky due to lensing effects. Other previous works [39, 156, 157, 158, 159] have shown that when new and more precise surveys will start to operate, a careful inclusion of lensing convergence will be crucial to avoid biased constraints in certain cosmological parameters. Then, our purpose here is to investigate such potential biased results under the pure momentum transfer models. In particular, we focus on the Covariantised dark Thomson-like scattering in the Dark Energy and Dark Matter momentum transfer case. There are two reasons to consider this model appropriate for this kind of analyses: its simplicity and its similarity with the standard model. By one side, having a forecast for a model which has identical background and very similar perturbation dynamics to ΛCDM until very late times would allow us to confirm previous results on the importance of not neglecting lensing convergence. Moreover, results obtained here should not be understood as only belonging to the realm of the Covariantised dark Thomson-like scattering, but as a general warning. On the other side, the simplicity of the model, with only one new parameter, enables us to avoid multiple complicated degeneracies with the lensing part and, consequently, we may achieve a more clear conclusion on the importance of including lensing convergence in future surveys.

In this part, we will focus on the EUCLID survey[7], which is a forthcoming space-based experiment developed by the European Space Agency (ESA) planned to be launched contemporaneously to the publication of this thesis. When launched to the outer space, it will be placed in the L2 lagrangian point of the system Earth-Sun, that

---

[7]Taking its name from one of the most famous mathematician of the ancient world Euclides of Alexandria.

is, in opposition to the sun in the straight line that connects the Earth and the Sun. The survey is planned to operate for six years with a planned covering extension of the sky of 15000 deg^2 and a redshift range up to $z = 2$. The satellite is equipped with two main instruments, the near-infrared spectrometer and photometer (NISP) and the visible imager (VIS), that will focus on unveiling the secrets of Dark Energy and Dark Matter with a precision never reached before. For such purpose, it will map the galaxy distribution in the sky by measuring weak lensing, Baryonic Acoustic Oscillations (BAO) and Redshift Space Distortions (RSD). In the following, we will attach to the survey specifications explained in Refs. [141, 160].

5.3.1 Modelling the Galaxy Number Counts

Let us start by explaining how we model the angular power spectrum of number counts fluctuations in the forthcoming calculations. As starting point, we have what we already explained in the subsection 2.4, where the galaxy cluster counts were introduced. Considering a EUCLID-like survey, we divide the redshift range into several redshift bins so we can compute auto- and cross-correlations among them. We consider the spectrum, denoted by $C_l^{\mathrm{A,ij}}$, which is the sum of three terms as

$$C_\ell^{\mathrm{A,ij}} = C_\ell^{\mathrm{ij}} + E_\ell^{\mathrm{ij}} + \mathcal{N}\delta^{\mathrm{ij}} \,, \tag{5.56}$$

where the indices have the following meaning: i and j denote the redshift bins while A corresponds to what we call the observed (obs) or the theoretical (th) spectrum. The observed power spectrum $C_\ell^{\mathrm{obs,ij}}$ is calculated using `CLASS` only once for very high precision parameters for the chosen fiducial cosmology with all the different contributions to it, namely: lensing convergence, density perturbations and redshift space distortions. On the other hand, in the forecast analyses using MCMC techniques the theoretical spectrum $C_\ell^{\mathrm{th,ij}}$ is calculated with lower precision parameters, that is in shorter time so MCMC analyses can be performed. Moreover, since here we are interested in the relevance of lensing convergence, we compute the theoretical angular power spectrum $C_\ell^{\mathrm{th,ij}}$ in two situations

- Consistent computation where $C_\ell^{\mathrm{th,ij}}$ includes lensing convergence along with density perturbations and redshift space distortions.

- Approximate computation where lensing convergence is neglected in the computation of $C_\ell^{\mathrm{th,ij}}$.

Returning to the three contributors to the spectrum as depicted in equation (5.56), we have

- C_ℓ^{ij}: it represents the angular power spectrum of number counts fluctuations computed directly by the Boltzmann solver `CLASS`.

- E_ℓ^{ij}: given the previous computation of C_ℓ^{ij} is done under the linear regime, some non-linear contamination is happening. Non-linear options are available in `CLASS` but they are computationally expensive in time and, then, activating

Parameter	Value
$H_0 \left(\frac{\mathrm{km}}{\mathrm{s \cdot Mpc}} \right)$	67.38
$\Omega_{\mathrm{b}} h^2$	0.02247
$\Omega_{\mathrm{dm}} h^2$	0.1193
τ_{reio}	0.0543
n_{s}	0.9679
$\ln 10^{10} A_{\mathrm{s}}$	3.044
b_0	1
$\sum m_\nu$ (eV)	0.031
w	-0.98
α	0.0723

Table 5.7: Parameters defining the fiducial model used in this forecast.

them would ruin our MCMC analyses. As a modest but well posed solution, here we add this term which is defined as the difference when the non-linear `HALOFIT` prescription option is on or off in our Boltzmann solver, then

$$E_\ell^{\mathrm{ij}} = C_\ell^{\mathrm{ij,HALOFIT\ ON}} - C_\ell^{\mathrm{ij,HALOFIT\ OFF}} .$$
(5.57)

This term is only calculated once, for high precision parameters and for the fiducial cosmology including all the contribution to the number counts.

- $\mathcal{N}$: it accounts for the shot-noise contribution due to the discreteness of our sample and it will be survey-dependant.

Once we have the recipe to model the Galaxy Number Counts, we now focus on the specifications required for a EUCLID-like survey. Regarding the galaxy bias, this time we assume a scale-independent prescription of the form

$$b(z) = b_0 \sqrt{1+z} ,$$
(5.58)

where the parameter b_0 is a constant and will enter in our MCMC analyses. In the case of the magnification bias, our prescription follows the one of Ref. [161]

$$s(z) = 0.1194 + 0.2122z - 0.0671z^2 + 0.1031z^3 .$$
(5.59)

Several arguments can be said against the previous prescriptions as they were obtained in the canonical way for a ΛCDM model, while here we have a different cosmology. However, such criticism, which will be relevant when dealing with real data, has less impact when performing a forecast. Therefore, as a proof-of-concept here we stick to them as the topic of this specific part of the thesis is to highlight the necessity of considering lensing convergence for future surveys.

On the other hand, we model the number of galaxies per redshift and per steradian from the distribution

$$\frac{\mathrm{d}N}{\mathrm{d}z \mathrm{d}\Omega} = 3.5 \times 10^8 z^2 \exp \left[- \left(\frac{z}{z_0} \right)^{\frac{3}{2}} \right] ,$$
(5.60)

Parameter	$C_\ell^{\mathrm{obs,ij}}$	$C_\ell^{\mathrm{th,ij}}$ Top-hat		$C_\ell^{\mathrm{th,ij}}$ Gaussian	
	All	5 bins	10 bins	5 bins	10 bins
l_switch_limber_for_nc_local_over_z	20000	20000	20000	20000	20000
l_switch_limber_for_nc_los_over_z	1000	1000	1000	1000	1000
selection_sampling_bessel	3	1.2	1.2	1.2	1.2
q_linstep	0.3	2.5	1.65	40	10
k_max_tau0_over_l_max	15	2	2	2	2

Table 5.8: Precision parameters used in CLASS to compute the angular power spectrum of number counts fluctuations. For the observed spectrum $C_\ell^{\mathrm{obs,ij}}$, we use parameters yielding to a high precision computation. For the theoretical spectrum $C_\ell^{\mathrm{th,ij}}$, we adapt the precision parameters for each configuration in order to keep the error due to using lower precision parameters bound to $\Delta\chi^2 \le 0.2$ in the likelihood used.

where the parameter z_0 is defined as $z_0 = \frac{z_{\mathrm{mean}}}{1.412}$ and the mean redshift for the EUCLID survey is $z_{\mathrm{mean}} = 0.9$. Also, the galaxy density is set to $d = 30$ arcmin^{-2} and the fraction of the sky covered is $f_{\mathrm{sky}} = 0.364$. Finally, we model the shot-noise spectrum due to the discreteness of the sample as

$$\mathcal{N} = N_{\mathrm{bins}} \frac{1}{3600\, d\, (\frac{180}{\pi})^2} \ . \tag{5.61}$$

A strongly delicate point is the shape and redshift distribution of the survey. Because of that, and with the ultimate goal of not biasing our results we will use four different configurations as follows. For the redshift bins distribution, we consider two possible answer as $N_{\mathrm{bins}} = 5, 10$. In the case of the shape of each bin, we will use a Gaussian and a top-hat distribution for each case. In the four possible combinations we make sure the number of galaxies per redshift bin is evenly distributed. Finally, the fiducial cosmology corresponds to the Dark Energy-Dark Matter Covariantised dark Thomson-like scattering fully explained in Section 4.1, with the values of the cosmological parameters defined in Table 5.7.

5.3.2 Modelling of the forecast

Once the modelling of the number counts and survey is done, we should comment how we assess the importance or not of lensing convergence. In our case, we will follow a MCMC approach as we will explain now, using the public code of Bayesian statistics MontePython [32, 33].
Our first point is to calculate only once the observed number count spectrum $C_\ell^{\mathrm{obs,ij}}$. Then, we use the fiducial cosmology of Table 5.7 with high precision parameters of Table 5.8 in CLASS considering all contributions to the number counts, namely: lensing convergence, density perturbations and redshift space distortions. Once we

have it, we include it in a MCMC analyses through a likelihood prescription as

$$\Delta\chi^2 = \sum_{\ell=2}^{\ell_{max}} (2l+1) f_{sky} \left(\ln \frac{d_\ell^{th}}{d_\ell^{obs}} + \frac{d_\ell^{mix}}{d_\ell^{th}} - N_{bins} \right) + \sum_{i,j} (x_i - x_i^{fid}) C_{ij}^{-1} (x_j - x_j^{fid}) \,, \quad (5.62)$$

where $d_\ell^A = \det(C_\ell^{A,ij})$ and d_ℓ^{mix} are calculated as d_ℓ^{th} but substituting in each term of the determinant one factor by $C_\ell^{obs,ij}$. The theoretical spectrum $C_\ell^{th,ij}$ is calculated in each case, including lensing or neglecting lensing, with lower precision given by the parameters of Table 5.8. Nevertheless, we require that the possible error when calculating $C_\ell^{th,ij}$ due to the lower precision is bound to be $\Delta\chi^2 \leq 0.2$. To avoid contamination from non-linear scales, we bound the previous likelihood to $\ell_{max} = 400$. In order to speed up the calculations, we add the second term, a gaussian prior, where $\vec{x}^{fid}$ denotes parameters of the fiducial model as $\vec{x} = (\Omega_b h^2, \Omega_{dm} h^2, n_s, \ln 10^{10} A_s, \tau_{reio}, H_0, w, \alpha)$ and $\mathbf{C}$ is its covariance matrix that was calculated for such fiducial cosmology in Ref. [139].

The previous likelihood was encoded in a python script and added to the `MontePython` code as another likelihood to be used.

5.3.3 Results

The previous implemented likelihood of equation (5.62) measures the departure from the fiducial cosmology when computing the theoretical spectrum $C_\ell^{th,ij}$ in a certain cosmology and with a certain contribution or precision. As we have chosen the precision parameters of `CLASS` to satisfy $\Delta\chi^2 \leq 0.2$, the departure of the likelihood will account for how we compute the spectrum. Here, using the four possible configurations already explained, we perform in each case a MCMC analysis in the two following situations:

- Consistent computation of $C_\ell^{th,ij}$: including lensing convergence, density perturbations and redshift space distortions. Thus, we expect to recover the fiducial values of the cosmological parameters as the result of the MCMC for all four configurations and with $\Delta\chi^2 \rightarrow 0$.

- Approximate computation of $C_\ell^{th,ij}$: only with density perturbations and redshift space distortions. If in a EUCLID-like survey neglecting lensing can bias the results, the fiducial cosmology will not be recover from the MCMC analysis. If not, we will recover the fiducial cosmology.

The following figures have been obtained using the code `GetDist` [127].

Top-hat: 5 redshift bins

The outcomes of the MCMC analyses for both cases, consistently including lensing and neglecting it, are reflected in Table 5.9 and in Figure 5.9. As expected, when lensing convergence is considered the constrained parameters are identical to the fiducial cosmology, represented by the black dashed and dotted lines. Of course,

i) Consistently including lensing: $\Delta\chi^2 = 0$					
Parameter	Mean	Best fit	σ	shift: Mean	shift: Best fit
$\Omega_\mathrm{b}h^2$	0.02244	0.02248	0.00011	0.2σ	0.1σ
$\Omega_\mathrm{dm}h^2$	0.1195	0.1193	0.0006	0.3σ	0.1σ
n_s	0.9681	0.9691	0.0029	0.1σ	0.4σ
$\ln 10^{10}A_\mathrm{s}$	3.045	3.049	0.013	$< 0.1\sigma$	0.4σ
τ_reio	0.0544	0.0570	0.0059	$< 0.1\sigma$	0.5σ
$H_0 \left(\frac{\mathrm{km}}{\mathrm{s\cdot Mpc}}\right)$	67.29	67.40	0.42	0.2σ	$< 0.1\sigma$
w	-0.9781	-0.9794	0.01	$< 0.1\sigma$	0.1σ
b_0	1.007	0.999	0.011	0.7σ	0.1σ
$\sum m_\nu$ (eV)	0.0758	0.0357	0.05	0.9σ	$< 0.1\sigma$
α	0.0718	0.0708	0.01	$< 0.1\sigma$	0.1σ

ii) Neglecting lensing: $\Delta\chi^2 = 1636$					
Parameter	Mean	Best fit	σ	shift: Mean	shift: Best fit
$\Omega_\mathrm{b}h^2$	0.02240	0.02238	0.00012	0.5σ	0.7σ
$\Omega_\mathrm{dm}h^2$	0.1198	0.1196	0.0008	0.6σ	0.3σ
n_s	0.9673	0.9684	0.0029	0.2σ	0.2σ
$\ln 10^{10}A_\mathrm{s}$	3.0398	3.041	0.014	0.3σ	0.2σ
τ_reio	0.0523	0.0516	0.0060	0.3σ	0.4σ
$H_0 \left(\frac{\mathrm{km}}{\mathrm{s\cdot Mpc}}\right)$	66.67	66.72	0.47	1.5σ	1.4σ
w	-0.9608	-0.9613	0.014	1.2σ	1.2σ
b_0	1.0503	1.0499	0.012	4.2σ	4.2σ
$\sum m_\nu$ (eV)	0.276	0.273	0.056	4.3σ	4.3σ
α	0.0686	0.0683	0.011	0.3σ	0.4σ

Table 5.9: The statistical results and the respective shifts with respect to the fiducial cosmology when we consider all the contributions to the angular power spectrum of number counts fluctuation (up) and when we neglect lensing convergence (down) for a 5 redshift bins top-hat galaxy density distribution.

they coincide with the gaussian prior as both used the same fiducial cosmology. This is strongly imprinted in the shifts on the mean and on the best-fit values with respect to the fiducial cosmology used, reflected in the upper part of Table 5.9, where all the parameters are well inside the 1σ region and, thus, no deviation occurs. Also the relative χ^2 is zero as expected.

Nonetheless, when we neglect lensing convergence this is no longer true. Even if we have added a gaussian prior on the Dark Energy equation of state w and on the Hubble parameter H_0, they have a $\sim 1-2\sigma$ shift with respect to the fiducial cosmology, both in the mean and best fit values. In the case of the bias parameter b_0 and the neutrino mass $\sum m_\nu$, which were not affected by the gaussian prior, the shifts with respect to the fiducial cosmology used are $\sim 4\sigma$, pointing towards the importance in future surveys of considering lensing convergence. It is nonetheless disturbing that in the case of the neutrino mass we have obtained a spurious detection, since
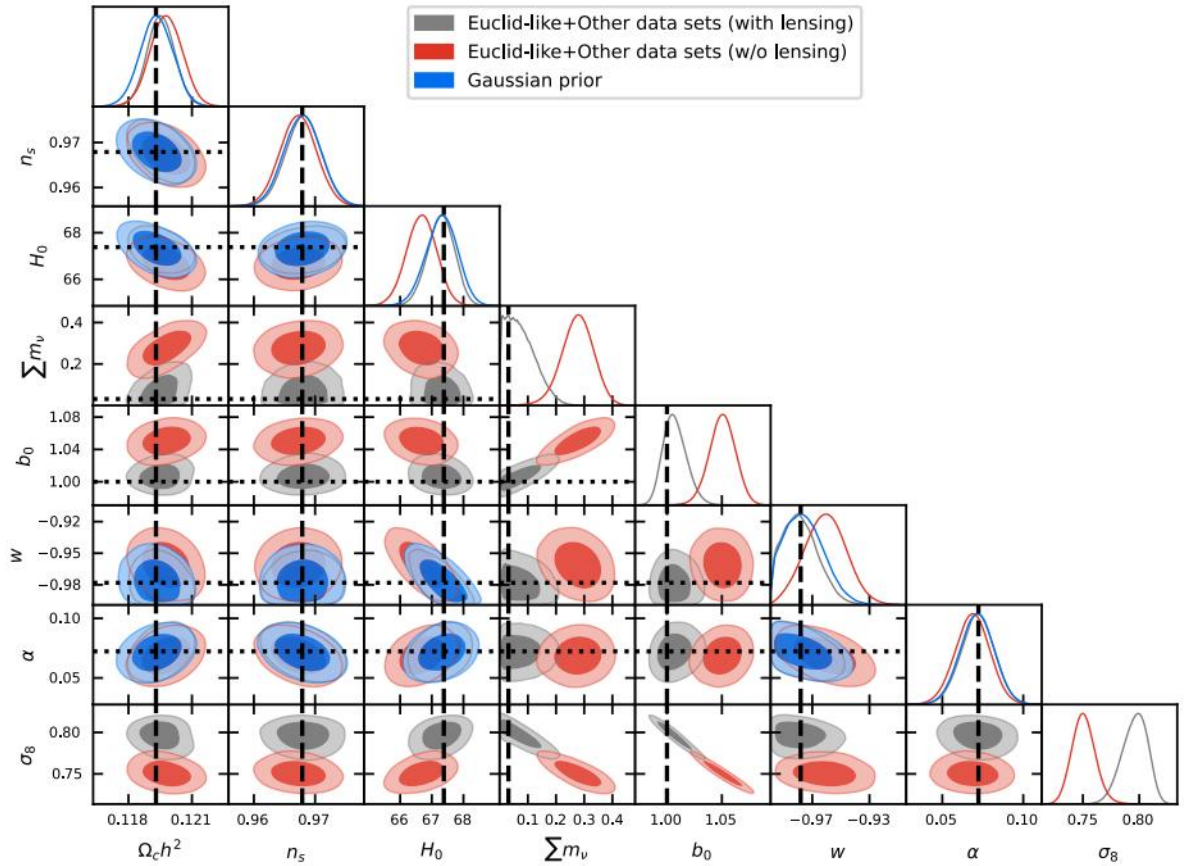
Figure 5.9: The 1-D and 2-D posteriors for the cosmological survey and model parameters. Here the analysis uses a 5 redshift bins top-hat galaxy density distribution. Gray (red) contours indicate results when lensing convergence is included (neglected), whereas in blue we show the Gaussian prior distribution. Black, dashed, vertical and black, dotted, horizontal lines indicate the values of the fiducial model.

when lensing is neglected we have a lower bound to it. This unavoidably remarks the importance of considering lensing convergence or completely biased results will be obtained.

Finally, we can see the strongly deviated value obtained for the σ_8 parameter when lensing is neglected. The value obtained indicates a lower clustering in the Universe, something that was one of the trademarks of pure momentum transfer models. However, in this case, we see the coupling parameter α remains unaltered when neglecting lensing and, then, the shift in σ_8 is uncorrelated to the model. Relating this to the σ_8 tension explained in Section 3.4, future surveys have to take care of properly modelling the galaxy cluster counts or known tension will exacerbate.

The outcome of this first configuration with a top-hat distribution of each of the five redshift bins has a clear message: lensing convergence in future surveys, like a EUCLID-like one, must be considered or strongly errors will appear in the con-

i) Consistently including lensing: $\Delta\chi^2 = 0$					
Parameter	Mean	Best fit	σ	shift: Mean	shift: Best fit
$\Omega_{\rm b}h^2$	0.02244	0.02247	0.00011	0.3σ	$< 0.1\sigma$
$\Omega_{\rm dm}h^2$	0.1195	0.1193	0.0006	0.4σ	$< 0.1\sigma$
$n_{\rm s}$	0.9678	0.9679	0.0028	0.1σ	$< 0.1\sigma$
$\ln 10^{10}A_{\rm s}$	3.043	3.044	0.013	0.1σ	$< 0.1\sigma$
$H_0 \left(\frac{\rm km}{\rm s\cdot Mpc}\right)$	67.27	66.38	0.4	0.3σ	$< 0.1\sigma$
$\sum m_\nu$ (eV)	0.06	0.03	0.04	0.6σ	$< 0.1\sigma$
b_0	1.006	1.000	0.011	0.5σ	$< 0.1\sigma$
w	-0.98	-0.98	0.01	$< 0.1\sigma$	$< 0.1\sigma$
$\tau_{\rm reio}$	0.0539	0.0543	0.0056	0.1σ	$< 0.1\sigma$
α	0.0730	0.0723	0.0096	0.1σ	$< 0.1\sigma$
ii) Neglecting lensing: $\Delta\chi^2 = 1835$					
Parameter	Mean	Best fit	σ	shift: Mean	shift: Best fit
$\Omega_{\rm b}h^2$	0.02240	0.02240	0.00012	0.6σ	0.6σ
$\Omega_{\rm dm}h^2$	0.1197	0.1196	0.0007	0.5σ	0.4σ
$n_{\rm s}$	0.9670	0.9680	0.0030	0.3σ	$< 0.1\sigma$
$\ln 10^{10}A_{\rm s}$	3.039	3.035	0.014	0.4σ	0.6σ
$H_0 \left(\frac{\rm km}{\rm s\cdot Mpc}\right)$	66.31	66.42	0.47	2.3σ	2.0σ
$\sum m_\nu$ (eV)	0.25	0.26	0.04	4.9σ	5.1σ
b_0	1.060	1.064	0.012	5.2σ	5.5σ
w	-0.95	-0.95	0.01	2.2σ	2.0σ
$\tau_{\rm reio}$	0.0516	0.0493	0.061	0.4σ	0.8σ
α	0.0650	0.0689	0.0107	0.7σ	0.3σ

Table 5.10: The statistical results and the respective shifts to the fiducial cosmology when we consider all the contributions to the angular power spectrum of number counts fluctuation (up) and when we neglect lensing convergence (down) for a 5 bins Gaussian galaxy density distribution.

straints of the cosmological parameters. As we will see, we will extend this warning in the other configurations.

Gaussian: 5 redshift bins

Now we change the galaxy distribution to a gaussian one, while keeping the five redshift bins. Results are shown in Figure 5.10 and the statistical information in Table 5.10 with the same labels as in the previous case. Again when lensing convergence is included, fiducial cosmology is recovered.

However, when we neglect lensing convergence we have $\sim 2\sigma$ biased constraints on the Hubble constant H_0 and on the equation of state w, a bit stronger than before for the top-hat case. Also, $\sim 5\sigma$ shifts rise on the neutrino mass $\sum m_\nu$ and the bias parameter b_0. Again, uncorrelated to the model used, the σ_8 parameter is shifted to
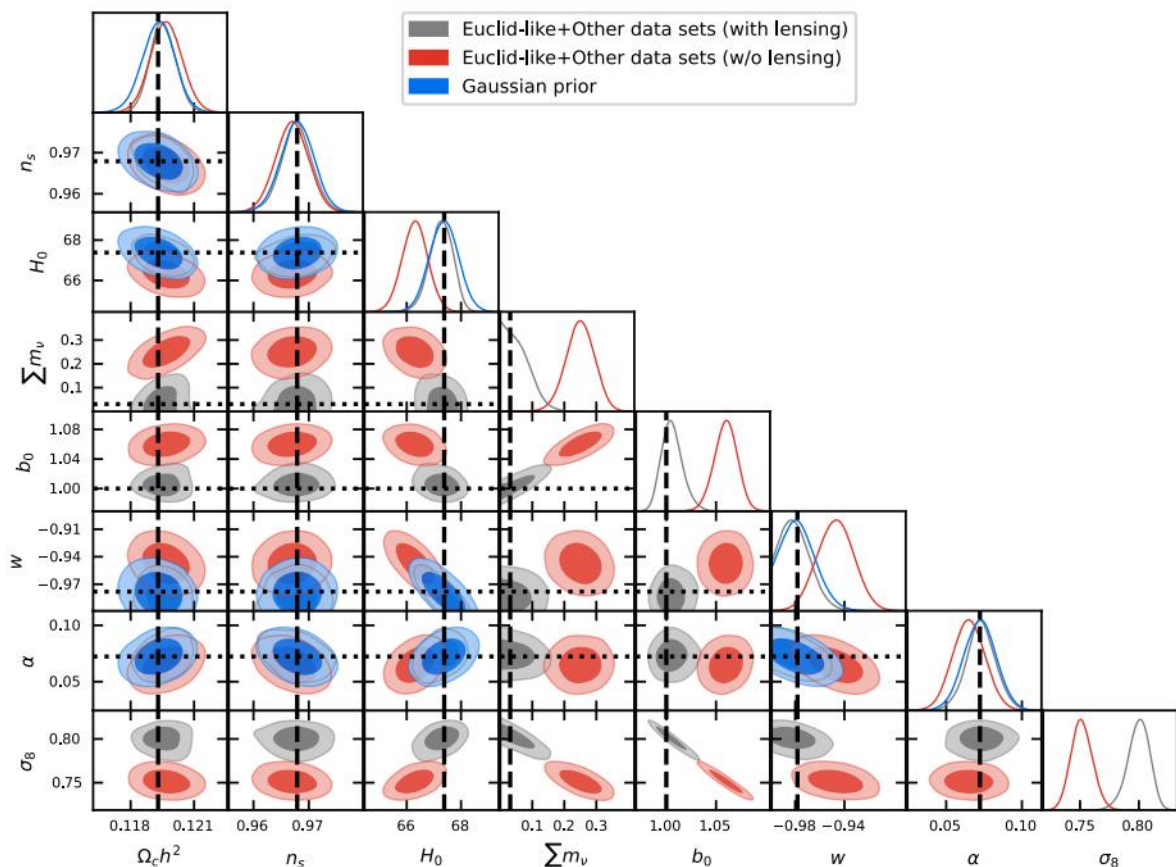
Figure 5.10: The 1-D and 2-D posteriors or the cosmological, survey and model parameters. Here the analysis uses a 5 redshift bins Gaussian galaxy density distribution. Gray (red) contours indicate results when lensing convergence is included (neglected), whereas in blue we show the Gaussian prior distribution. Black, dashed, vertical and black, dotted, horizontal lines indicate the values of the fiducial model.

lower values, that is, less structure.

The results from the gaussian case are in good agreement with the top-hat scenario used before, then the warning is the same: future surveys must carefully consider lensing convergence in their analyses. Also, it seems to not depend on the shape of the distribution used, although we will now confirm it with the 10 redshift bins analyses.

Top-hat: 10 redshift bins

Now we go back to the first analysis, but splitting the redshift range into ten bins, with the top-hat distribution in each one. We also summarise all the results in Table 5.11 and Figure 5.11. As before, when all contributions are considered we recover the fiducial cosmology, as all shifts are well inside the 1σ region. Also as before, when lensing convergence is neglected we find again shifts in the same parameters as in

i) Consistently including lensing: $\Delta\chi^2 = 0$					
Parameter	Mean	Best fit	σ	shift: Mean	shift: Best fit
$\Omega_{\mathrm{b}}h^2$	0.02245	0.02248	0.00011	0.2σ	0.2σ
$\Omega_{\mathrm{dm}}h^2$	0.1195	0.1193	0.0006	0.3σ	0.1σ
n_{s}	0.9682	0.9690	0.0028	0.1σ	0.4σ
$\ln 10^{10}A_{\mathrm{s}}$	3.045	3.048	0.013	$< 0.1\sigma$	0.4σ
τ_{reio}	0.0544	0.0556	0.0058	$< 0.1\sigma$	0.3σ
$H_0\left(\frac{\mathrm{km}}{\mathrm{s\cdot Mpc}}\right)$	67.32	67.40	0.39	0.2σ	$< 0.1\sigma$
w	-0.9788	-0.9792	0.011	$< 0.1\sigma$	$< 0.1\sigma$
b_0	1.006	1.004	0.010	0.6σ	0.4σ
$\sum m_\nu$ (eV)	0.0705	0.0612	0.048	0.8σ	0.6σ
α	0.0718	0.0685	0.010	$< 0.1\sigma$	0.4σ
ii) Neglecting lensing: $\Delta\chi^2 = 1988$					
Parameter	Mean	Best fit	σ	shift: Mean	shift: Best fit
$\Omega_{\mathrm{b}}h^2$	0.02240	0.02237	0.00012	0.5σ	0.8σ
$\Omega_{\mathrm{dm}}h^2$	0.1197	0.1198	0.0007	0.5σ	0.7σ
n_{s}	0.9678	0.9670	0.0029	$< 0.1\sigma$	0.3σ
$\ln 10^{10}A_{\mathrm{s}}$	3.0378	3.036	0.014	0.3σ	0.2σ
τ_{reio}	0.0516	0.0511	0.0061	0.4σ	0.5σ
$H_0\left(\frac{\mathrm{km}}{\mathrm{s\cdot Mpc}}\right)$	66.90	67.01	0.42	1.1σ	0.9σ
w	-0.9691	-0.9728	0.013	0.7σ	0.4σ
b_0	1.0384	1.0376	0.012	3.3σ	3.2σ
$\sum m_\nu$ (eV)	0.214	0.206	0.052	3.5σ	3.4σ
α	0.0708	0.0730	0.010	0.1σ	$< 0.1\sigma$

Table 5.11: The statistical results and the respective shifts with respect to the fiducial cosmology when we consider all the contributions to the angular power spectrum of number counts fluctuation (up) and when we neglect lensing convergence (down) for a 10 redshift bins top-hat galaxy density distribution.

the other two cases. Even though the shifts are slightly smaller, they are still important for parameters like the neutrino mass or the Hubble parameter, thus future surveys must care about modelling lensing. One may understand the smaller shifts as the effect of enlarging the precision due to more bins used to cover the same redshift range.

Gaussian: 10 redshift bins

As done before, we now consider a gaussian distribution for the ten redshift bins configuration. Results are shown in Figure 5.12 and Table 5.12. Similar conclusion are found, when lensing convergence is not neglected we do recover the fiducial cosmology, with almost perfect compatibility with the gaussian prior used. Once we neglect that contribution, shifts, both in the mean and best-fit value, start to appear
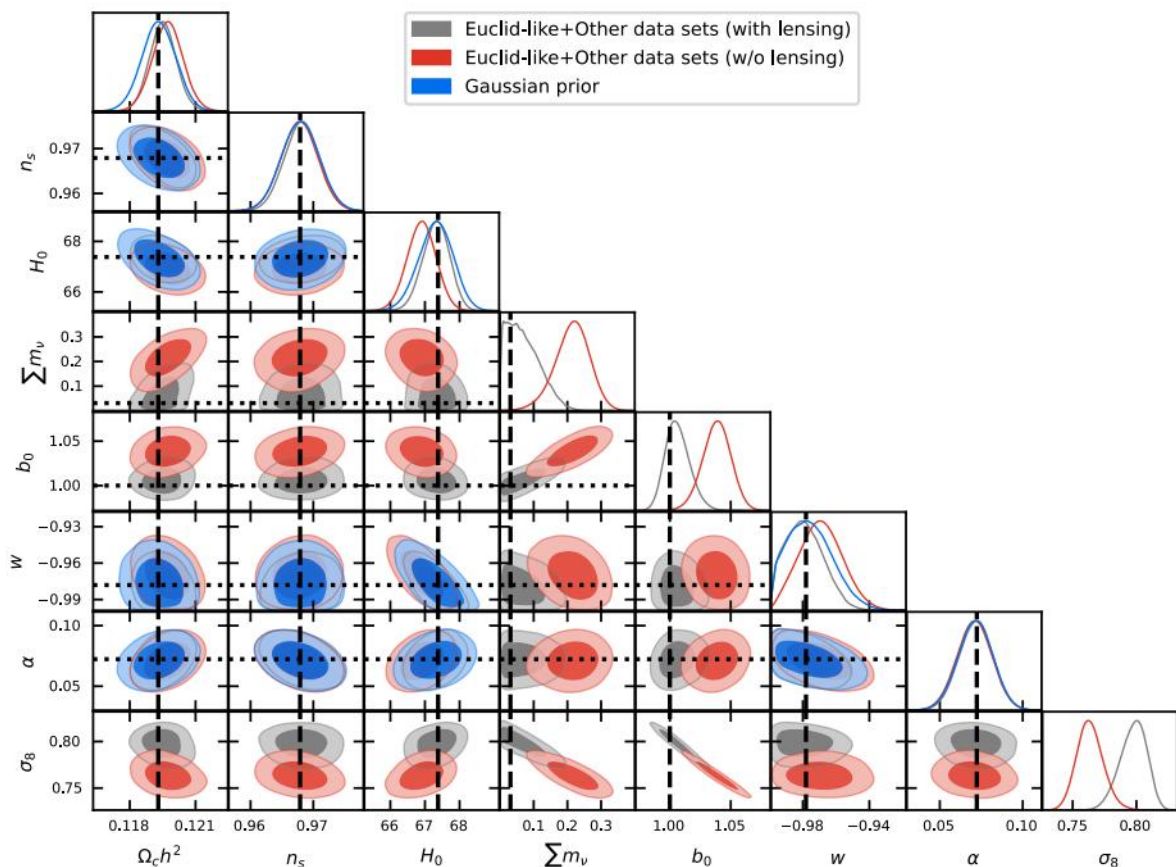
Figure 5.11: The 1-D and 2-D posteriors for the cosmological, survey and model parameters. Here the analysis uses a 10 redshift bins top-hat galaxy density distribution. Gray (red) contours indicate results when lensing convergence is included (neglected), whereas in blue we show the Gaussian prior distribution. Black, dashed, vertical and black, dotted, horizontal lines indicate the values of the fiducial model.

in certain parameters. The Hubble constant H_0 and the Dark Energy equation of state w have $\sim 1-2\sigma$ shifts while the neutrino mass and the bias parameter have $\sim 4\sigma$ shifts. The parameter σ_8 emerges with a lower value that is uncorrelated to the coupling parameter, which remains unaltered when lensing is neglected.

Consequently, we can infer that whatever configuration a EUCLID-like survey uses, lensing convergence inclusion is of crucial importance to avoid strong errors in the determination of cosmological parameters.

5.3.4 Final discussion

In this section, we have assessed the relevance of including or not lensing convergence when modelling the galaxy cluster counts in a future EUCLID-like survey. There has been an ongoing discussion on how relevant some contributions were, like the lensing one, in order to have unbiased results. Previous works (see for ex-

i) Consistently including lensing: $\Delta\chi^2 = 0$					
Parameter	Mean	Best fit	σ	shift: Mean	shift: Best fit
$\Omega_{\rm b}h^2$	0.02245	0.02242	0.00011	0.2σ	0.5σ
$\Omega_{\rm dm}h^2$	0.1195	0.1195	0.0006	0.3σ	0.4σ
$n_{\rm s}$	0.9682	0.9687	0.0029	0.1σ	0.3σ
$\ln 10^{10}A_{\rm s}$	3.044	3.046	0.013	$< 0.1\sigma$	0.1σ
$H_0 \left(\frac{\rm km}{\rm s\cdot Mpc}\right)$	67.29	67.26	0.4	0.2σ	0.3σ
$\sum m_\nu$ (eV)	0.06	0.06	0.04	0.7σ	0.8σ
b_0	1.006	1.005	0.010	0.6σ	0.5σ
w	-0.980	-0.983	0.011	$< 0.1\sigma$	0.2σ
$\tau_{\rm reio}$	0.0540	0.0549	0.0057	$< 0.1\sigma$	0.1σ
α	0.0717	0.0715	0.0102	0.1σ	0.1σ
ii) Neglecting lensing: $\Delta\chi^2 = 2435$					
Parameter	Mean	Best fit	σ	shift: Mean	shift: Best fit
$\Omega_{\rm b}h^2$	0.02239	0.02245	0.00012	0.6σ	0.1σ
$\Omega_{\rm dm}h^2$	0.1197	0.1196	0.0007	0.6σ	0.4σ
$n_{\rm s}$	0.9672	0.9681	0.0029	0.2σ	0.1σ
$\ln 10^{10}A_{\rm s}$	3.037	3.035	0.014	0.5σ	0.7σ
$H_0 \left(\frac{\rm km}{\rm s\cdot Mpc}\right)$	66.49	66.66	0.42	2.1σ	1.7σ
$\sum m_\nu$ (eV)	0.19	0.20	0.04	4.0σ	4.1σ
b_0	1.045	1.048	0.011	4.1σ	4.4σ
w	-0.955	-0.961	0.014	1.8σ	1.4σ
$\tau_{\rm reio}$	0.0511	0.0513	0.0060	0.5σ	0.5σ
α	0.0675	0.0695	0.0104	0.5σ	0.3σ

Table 5.12: The statistical results and the respective shifts to the fiducial cosmology when we consider all the contributions to the angular power spectrum of number counts fluctuation (up) and when we neglect lensing convergence (down) for a 10 bins Gaussian galaxy density distribution.

ample [156, 157, 158, 159]) demonstrated how not taking into account lensing convergence will lead to biased results for future surveys. In particular, mild or strong shifts can be induced in parameters like the Dark Energy equation of state w, non-Gaussianity $f_{\rm NL}$, neutrino mass $\sum m_\nu$ or spoil certain hints inside Modified Gravity scenarios. We want to highlight the case of the neutrino mass, that as we know by neutrino oscillations they are massive. Future surveys will certainly measure it as currents one are only able to set an upper limit. Therefore, having a wrong modelling of the galaxy cluster counts will spoil such results.

In our case, we used as a proxy the Dark Matter-Dark Energy Covariantised dark Thomson-like scattering for our fiducial cosmology and a EUCLID-like survey configuration. Results are not expected to be strongly dependant on the model due to its similarity to ΛCDM and its simplicity.
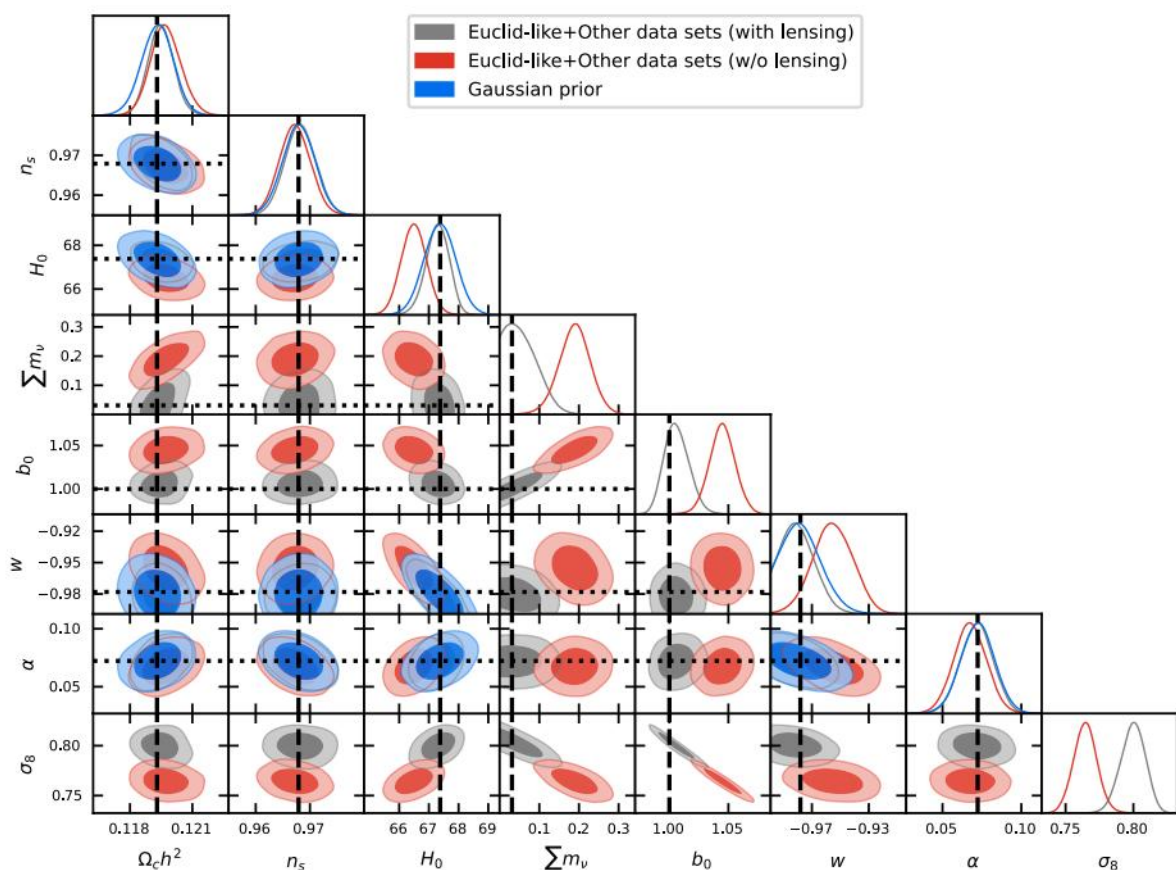
Figure 5.12: The 1-D and 2-D posteriors for the cosmological survey and model parameters. Here the analysis uses a 10 redshift bins Gaussian galaxy density distribution. Gray (red) contours indicate results when lensing convergence is included (neglected), whereas in blue we show the Gaussian prior distribution. Black, dashed, vertical and black, dotted, horizontal lines indicate the values of the fiducial model.

For the possible four configurations, that is five or ten bins and gaussian or top-hat galaxy distribution, we have seen continuously partially biased results on the Hubble parameter H_0 and in the Dark Energy equation of state w. Considering the fiducial cosmology used, when lensing is neglected in the analyses, some $\sim 1 - 2\sigma$ shifts with respect to such fiducial values have been found in all the four configurations. Provided such parameters were affected by a gaussian prior, these shifts should draw attention on how important is a good modelling of galaxy cluster counts in order to avoid wrong constraints. Considering the disruptive Hubble tension, here we have seen how neglecting the lensing convergence contribution may exacerbate the discrepancies between low and high redshift probes. Even more worrying is what happens with the bias parameter b_0 and the neutrino mass $\sum m_\nu$, as the shift with respect to the fiducial cosmology can be as larger as a 5σ shift. In the case of the neutrinos, there is even a full, wrong, detection of the combined mass when lensing is

162

neglected. Finally, also a shift to lower values appears in the σ_8 parameter, again exacerbating the tension between low and high redshift experiments. It is worth saying the coupling parameter is insensitive to the use or not of lensing convergence, therefore one can conclude the results are insensitive to the fiducial cosmology used here.

Since we have a very similar cosmology to the standard scenario without a large dependence on its coupling parameter shown, and that results are not strongly sensitive to the galaxy survey configuration used, we conclude the following: future surveys must consider lensing convergence in their analyses or biased result will appear.

5.4 Discussion and final comments on forecasts

In this chapter, we have performed three different forecast analyses considering as the fiducial cosmology the Covariantised dark Thomson-like scattering between Dark Energy and Dark Matter studied in the previous Chapter 4. Each analysis had a different aspiration and, for that goal, each one had different reference surveys. In particular, the three cases were:

- Galaxy survey and J-PAS forecast: we studied how the future surveys J-PAS, DESI and EUCLID measuring the clustering and the lensing signals will be able to constrain the coupling parameter α of the model.

- Dipole of the power spectrum and SKA forecast: we analysed how the measurement of the dipole of the Matter Power Spectrum can be used as a smoking gun for the pure momentum transfer interactions. We used the future SKA radiotelescope survey for that purpose.

- Cluster Counts and EUCLID forecast: we investigated the importance of a correct modelling of the lensing signal in future surveys like EUCLID to avoid having spoiled results.

With the two first analyses, we found that all of the future surveys considered will be able to strongly improve our constraints on the model studied. In particular, in the first case we demonstrated how future surveys studying the clustering signal would provide a 10σ detection if the interaction is there according to our fiducial cosmology. If we consider other scenarios where the cosmology might be different, the constraints with future surveys will be four times better than the one presented in Chapter 4 for the coupling parameter. However, lensing data will not have competitive results due to the specificities of the interaction. In the case of the analyses with the dipole of the Matter Power Spectrum, we have shown how the fact that this interaction can mimic the break of the equivalence principle led to having the dipole with SKA-like surveys as a smoking gun for the presence pure momentum transfer interactions, according to the competitive results obtained.

The third analysis, Cluster Counts and EUCLID forecast, had a completely different purpose. We tried to show how a bad modelling of the cluster counts observable may lead to wrong results on the constraints of the cosmological or model parameter. Specifically, we revealed how not including the lensing contribution resulted in having biased constraints on several cosmological parameters like the Hubble H_0 or the σ_8 parameters, which are affected by the respective tensions explained in Chapter 3. Therefore, a careful modelling of cluster counts is essential for future experiments.

Although all the previous analyses were done using a particular model, it has to be stressed that they are completely general to all the momentum transfer models, since the model considered here was just a convenient description with appealing properties as explained before. To conclude, future surveys will be able to strongly

constrain, if not detect or rule out, momentum exchanges involving a Dark Sector component.

NON-LINEAR SCALES

ntil now, we were only concerned about the large scale cosmological behaviour of the different models considered, meaning we were in the regime where linear perturbation theory works. However, there are vast regions in the Cosmos where perturbations have grown enough to overcome the linear regime. In fact, those regions are where the formation of high density structures, like galaxies, Dark Matter halos or clusters, takes places. This is nothing but the consequence of the Jeans instability, since matter has little pressure to counteract the gravitational collapse where the linear regime breaks apart. Although the large scale results give us the general dynamics of the Cosmos, we really need to understand how such galaxies or halos are formed. The very first reason for that is quite evident and human: we live in a galaxy, that is, in one of those structures that formed non-linearly. In some sense, non-linear analyses try to address the question of why we are here in our galaxy and not in one of the vast amount of extremely low density regions of the Cosmos. In a less philosophical sense, we try to understand how objects like our galaxy are formed, how they are distributed in the Cosmos and how they evolve. Thus, they are of crucial importance to fully characterise and test our cosmological models and, then, we should carefully study how the dynamics work here to accurately define how the Large Scale Structure is distributed. However, as the linear perturbation theory is no longer valid and provided there are no global analytical solutions for this regime in the literature, we have to resort to a new technique called N-body simulations, which usually are expensive in terms of computation resources and time.

The idea behind N-body simulations is very simple: consider a cubic box simulating a patch of the Universe and containing several point-like particles representing the matter content. Those particles can be later labelled as Dark Matter, Baryons

or anything we desire. Then, we should treat this system as a self-gravitating system made up of a large number of particles in a large volume whose evolution is dictated by the cosmological expansion, apart from gravity. This has three main consequences. The first one is that gravity is the leading force in this systems while the second one is the necessity of having a cosmological model to characterise the cosmological evolution encoded in the scale factor $a(t)$. The third one is that due to the large amount of particles required, we are treating a statistical mechanical system. This means that we are not really simulating the Universe in the sense we will obtain the Milky Way or Andromeda galaxy there. But what it is required is to compare the statistical properties extracted from the outcome of the N-body simulations with the statistical properties of the distribution of matter observed in our Universe. In that sense, observables like the profile of the halos, the amount of halos per cubic volume or the relative abundance of structures are a subject of study.

We are dealing with very large systems where each particle we commented before represents not a defined celestial body but a large amount of matter. We can do it provided the scales we are studying are extremely large compared to the mass we associate to each particle. We also consider that the matter in our simulations, that we now call particles of the simulation, are under weak gravitational potentials and the velocities of each particle are non-relativistic, which is something reasonable in our Universe for the times where structures formed. Since we are studying the dynamics of the structures of the Cosmos where Newton's laws are still valid, we can neglect in principle the relativistic effects. Moreover, as we have the expansion of the Universe according to a certain cosmological model, we will work with comoving coordinates to account for it so it is not swarming uncomfortably through our equations. Given the above, the master equation here is just the second law of motion according to Newton but, however, we have to rewrite it in comoving coordinates so we have

$$\frac{\mathrm{d}^2 \vec{x}_i}{\mathrm{d}t^2} + 2H(t)\frac{\mathrm{d}\vec{x}_i}{\mathrm{d}t} = -\frac{1}{a^2}\vec{\nabla}\phi_i(t,\vec{x}) \ , \tag{6.1}$$

where $\vec{x}_i$ and ϕ_i are the comoving coordinates and the perturbed gravitational potential of i-th particle of our system, while $H(t)$ is the Hubble function which encodes the cosmological model. The first term is just the acceleration of the i-th particle, while the second and third terms are the Hubble expansion and the gravitational force created in the i-th particle by all the other particles in the simulation. Of course, to close the system we need to define the form of the Hubble function $H(t)$ and the gravitational potential ϕ. The former is given by the cosmological model in each case while the latter is obtained from the well-known Poisson equation

$$\nabla^2 \phi(t,\vec{x}) = 4\pi G\rho(t)a^2\delta(t,\vec{x}) \ . \tag{6.2}$$

Here, we should not forget we are in the non-relativistic limit and the scales studied are small in cosmological terms. The first condition now translates in our previous equations to having particles of our system fulfilling the velocity condition $v \ll 1$[1],

---

[1]In our units $c = 1$.

which is nothing but cold particles as we expect Dark Matter and Baryons are, and feeling a gravitational potential such that $\phi \ll 1$, as expected for the times structure formation happens. The second one is just considering scales λ ensuring $\lambda \ll 1/H(t)$ for our system, that means well inside the horizon.

With the previous set of equations and once we choose the cosmological model, we just need to compute the force between each pair of particles for each time given certain initial conditions and evolve the system in time. Here is where it gets computationally expensive. It is absolutely required to compute the force between each pair of particle as we are dealing with gravity, a long range force. Accordingly, we typically resort to codes like RAMSES [162] or Gadget [163, 164] to perform this task. There are two main approaches when dealing with N-body simulations: Particle and Grid based methods. In the case of Particle methods, the two main algorithms are the Particle-Particle method and the Tree method. The first one basically consists in computing the total force applied to the i-th particle as the direct sum of all the forces each other particle exerts on the i-th particle. As for a very large amount of particles the previous summation will increase enormously in length and then in computational time, Tree methods appeared as an evolution of Particle-Particle method. In Tree algorithms, bunches of particles that are close enough among them and far away from the i-th particle are considered to form a group and the force summed is the one of the group not each individual one, then saving computation time. In the case of Grid methods, we have in the literature the Particle Mesh method and its evolution the Adaptive Particle Mesh method (AMR). The first one uses a grid over the simulation volume where each particle is assigned to the grid to have a density and velocity field, which allows us to solve the corresponding Fourier space Poisson equation with the help of Fast Fourier Transforms algorithms. In its evolution, the AMR method, the grid is redefined with shorter spacing in high density regions to obtain higher resolution there, without increasing the refining of the grid in other low density regions where it is not required. Of course, new codes make use of hybrid methods that basically profit the best parts of both techniques.

In this chapter, we will study how the non-linear dynamics behave with the help of the N-body numerical code called RAMSES [162]. We will use the Covariantised dark Thomson-like scattering in the case of Dark Energy and Dark Matter coupling, explained in Section 4.1. We choose only that case due to four reasons. Firstly, it is a simple model having similar background dynamics as the standard ΛCDM model and only one modification in Euler equations. Secondly, the modifications required are little and well located. As seen, we have three main equations, namely the comoving second law of motion, the Poisson equation and the Hubble equation, being the first equation the only one that should be modified. Thirdly, Dark Matter created the seeds for the formation of halos and galaxies and it is around five times more abundant than Baryons. Therefore, any interaction affecting Dark Matter will change

more the cosmological evolution than if it would affect Baryons. Finally, regarding the data analyses performed in previous chapters, this case was the most favoured by data. To end with, we want to highlight here that the analysis of non-linear scales is the most natural next step regarding what has been done in Chapters 4 and 5, since there all the linear investigation was completed including for future surveys. The organisation of the chapter is the following. Firstly, we will present how the general equations are modified in the context of N-body simulations while we explain how to adapt the previous derivations to the RAMSES language, in order to show how the code was modified to account for the model considered. After that, we will present the main effects and consequences on the creation and evolution of structures in the Cosmos due to the interaction. We finish with the conclusions and future work.

6.1 N-body implementation

Since we now want to analyse how the pure momentum transfer models change the non-linear scales, we have to adapt the available numerical codes to our model. In our case, we will work with the RAMSES code [162], although the following derivation should be identical in other codes apart from the specificities of each code. We choose to implement the Covariantised dark Thomson-like scattering studied in Chapter 4. Thus, we need to implement the changes due to our interaction which mainly consist in adding the new term to the Euler equation. We had two different scenarios, the first one was when Dark Energy is coupled to Dark Matter, having a modified Euler equation for Dark Matter (up to linear order in perturbations) given by

$$\theta'_{\rm dm} = -\mathcal{H}\theta_{\rm dm} + k^2\Phi + \Gamma(\theta_{\rm de} - \theta_{\rm dm}) \,, \tag{6.3}$$

where $\Gamma \equiv \bar{\alpha}\frac{a}{\rho_{\rm dm}}$ with the normalisation $\alpha = \frac{8\pi G}{3H_0^3}\bar{\alpha}$ as explained in Section 4.1. The second scenario was when the coupling acts between Dark Energy and Baryons, giving the following modified Euler equation

$$\theta'_{\rm b} = -\mathcal{H}\theta_{\rm b} + k^2\Phi + \Gamma_{\rm T}(\theta_\gamma - \theta_{\rm b}) + \Gamma(\theta_{\rm de} - \theta_{\rm b}) \,, \tag{6.4}$$

where $\Gamma \equiv \bar{\beta}\frac{a}{\rho_{\rm b}}$ with the normalisation $\beta = \frac{8\pi G}{3H_0^3}\bar{\beta}$ as explained in Section 4.2. Provided Thomson scattering is negligible for the scales of interest where formation of structures happened under the interaction being efficient, both cases are formally identical. Moreover, as we are not going to make use of hydrodynamics simulations[2], we will have that all the particles in our codes are treated equally in the original algorithm. Then, there is in principle no distinction between Baryons and Dark Matter. However, we do not want to apply the interaction to both at the same time as otherwise the interaction with the most abundance one, Dark Matter, would hide the

---

[2]Although that will be an interesting line of research in the future as it allows to perform simulations where baryons are treated like a fluid rather than a particle, allowing to study certain processes of formation of structures.

other coupling. Consequently, the second modification required in the codes consists in adding a categorisation or family, labelling if a particle is Dark Matter or Baryons according to their relative abundance, so we can apply the interaction to each one separately.

Since now we know both cases are formally equal and without hydrodynamics simulation options, we will perform here the derivation for the case of Dark Matter as the example. Consider the previous equation (6.3) that we want to rewrite as

$$\dot{\vec{v}}_i = -H\vec{v}_i + \sum_{j \neq i} \frac{Gm_j \vec{r}_{ij}}{|r_{ij}^3|} + F(\Gamma, \theta_{\mathrm{de}}, \theta_{\mathrm{dm}}) \;, \tag{6.5}$$

where $F(\Gamma, \theta_{\mathrm{de}}, \theta_{\mathrm{dm}})$ is the new term due to the momentum transfer. This equation corresponds to the second law of motion depicted in equation (6.1). Conversely, the other relevant equations in N-body simulations, the Poisson and Hubble equations, are not formally modified by the momentum transfer, rather than just adding the very standard wCDM model. Thus, we focus our efforts in the velocity equation (6.1) for this model. In equation (6.5), the first two terms correspond to the standard expansion term and the gravity which will remain unaltered and correspond to the first two terms of equation (6.3). Then we can forget about them in our derivation. We have the relation between the Fourier space velocity divergence and the velocity and between conformal time and cosmic time, both given by $\theta = i\vec{k}\cdot\vec{v}$ and by $a\mathrm{d}\tau = \mathrm{d}t$. The final subtlety is the presence of the Dark Energy velocity divergence θ_{de}. As N-body simulations deal with self-gravitating systems made up of a large amount of particles, there is no implementation of the Dark Energy fluid in principle. However, we should bear in mind our purpose here: very small scales. In such non-linear scales and for the standard scenario, Dark Energy velocity is negligible as the dynamics are controlled by gravity. But now, due to the coupling this might no longer be true. However, coming back to Chapter 4, we demonstrated there how for small scales and late times, when precisely the interaction was efficient and the formation of structures happened, Dark Energy velocity contribution to the new term in the Euler equation was negligible, while we consider sensible[3] values of the coupling parameter. This can be seen for example in Figure 4.7 or Figure 4.20. Consequently, we can rewrite the Euler equation as

$$\dot{\vec{v}}_i = -H\vec{v}_i + \sum_{j \neq i} \frac{Gm_j \vec{r}_{ij}}{|r_{ij}^3|} - \alpha \frac{H_0}{\Omega_{\mathrm{dm}}(t)} \vec{v}_i \;. \tag{6.6}$$

We can apply the same logic to the Dark Energy-Baryon coupling having then

$$\dot{\vec{v}}_i = -H\vec{v}_i + \sum_{j \neq i} \frac{Gm_j \vec{r}_{ij}}{|r_{ij}^3|} - \beta \frac{H_0}{\Omega_{\mathrm{b}}(t)} \vec{v}_i \;. \tag{6.7}$$

---

[3]By sensible we mean the values suggested by data in our MCMC analyses, that is $\alpha \sim \beta \sim \mathcal{O}(1)$.

Our previous approximation $v_{\rm dm} \gg v_{\rm de}$ or $v_{\rm b} \gg v_{\rm de}$ will, however, produce wrong results when looking at larger scales where the previous consideration no longer holds. The previous equation represents the master equation governing the behaviour of a self-gravitating system where the action of Hubble expansion and a pure momentum transfer takes place. To create the modified version of `RAMSES` code, the final step is to adapt the previous equation to the supercomoving coordinates defined by

$$\tilde{x} \equiv \frac{x}{L} \ , \tag{6.8}$$

$$d\tilde{t} \equiv \frac{H_0}{a^2} dt \ , \tag{6.9}$$

where L is the comoving size of the simulation box in Mpc/h and now $\tilde{x}$ and $\tilde{t}$ are dimensionless. The previous modified master equation was included in `RAMSES` code at the same time we add a label to the particles in the simulation, so that they are split according to the relative abundance into Baryons or Dark Matter. This allows us to switch on the interaction only to one of them or to both at the same time. For this PhD dissertation, we will only apply the interaction to the Dark Energy-Dark Matter case, since Dark Matter is more abundant and the possible consequences will be easier to spot. Finally, the wCDM Hubble function was included in the code. Before delving into the effects of the interaction, we may notice that we lack of a starting point, that is initial conditions. Profiting that the interaction does not act until very late times, we can use the standard generators of initial conditions as the high redshift results are indistinguishable whether the interaction is there or not. In our case, we use the `MUSIC2-monofonIC` code [165, 166].

6.2 Non-linear effects

Once the previous modifications were implemented, we tested the results from our modified version of `RAMSES` with the results obtained from our modified version of `CLASS`, giving different values for the coupling parameter. Although when seeing the effects we will notice the following, in Figure 6.1 we display the Matter Power Spectrum calculated from `CLASS` with and without the `HALOFIT` option and from `RAMSES`. We use this plot to check that our implementation works correctly. We did find a small difference in amplitude for very large scales $k \simeq 10^{-3} - 10^{-2}$ h/Mpc when the interaction was switched on. The amplitude of the Matter Power Spectrum was smaller calculated from `RAMSES` than when calculated from `CLASS`. The reason was already explained before. In our implementation, we did take the approximation $v_{\rm dm} \gg v_{\rm de}$, which was true only in smaller scales. For large scales like $k \simeq 10^{-3} - 10^{-2}$ h/Mpc, both velocities should be similar as all components in the Universe share the same rest-frame by the virtue of the Cosmological Principle. That unavoidably provokes the interacting term vanishes as it is proportional to $(v_{\rm dm} - v_{\rm de})$. With the approximation done to obtain the equations 6.6 or 6.7 the interacting term does not vanish, thus acting like a friction term even for large scales and, then, suppressing the Matter Power Spectrum. This effect is corroborated by the larger wrong suppression for
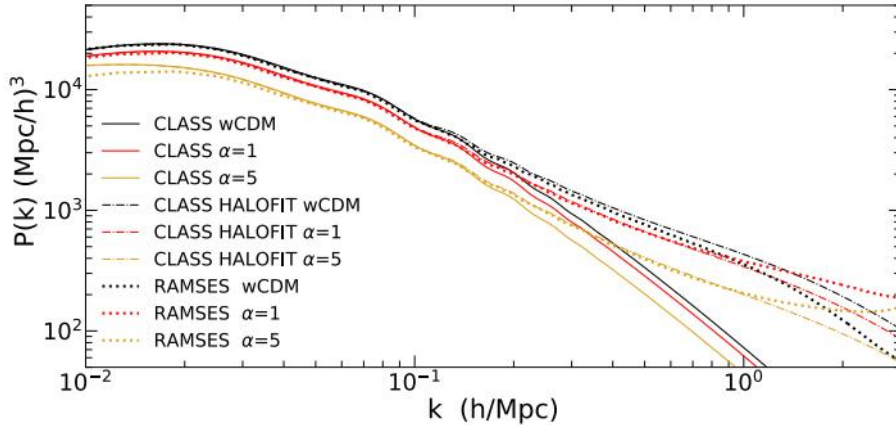
Figure 6.1: Matter Power Spectrum for different values of the coupling parameter α computed from the modified version of `CLASS` without and with `HALOFIT` and from `RAMSES`.

larger values of the coupling parameter. For very small scales $k > 10^{-1}$ h/Mpc we again found a difference. Of course, these are smaller scales where non-linear effects emerge and then the linear solver `CLASS` is no longer reliable. However, using the non-linear prescription of `CLASS` called `HALOFIT`, we can see how the results from our `RAMSES` implementation closely follow them up. This result is significant as `HALOFIT` was designed for ΛCDM, but due to the similarities between our model and the ΛCDM one, it can be also applied in our case. In very small scales, where of course `HALOFIT` is not reliable either, again differences appear. In the case of intermediate scales, both codes `RAMSES` and `CLASS` perfectly match. It was therefore concluded that the implementation was done correctly and we can proceed to study the different effects of the interaction in the non-linear small scales where we know our modified version of `RAMSES` is reliable.

In the following analyses, we will consider the case of Dark Energy-Dark Matter pure momentum transfer, analysed in Section 4.1. As explained, the larger the abundance of the interacting matter partner, the more evident and clear the effects are due to the interaction. We consider a wCDM background cosmology with cosmological parameters defined by $H_0 = 67.7$ Km/s/Mpc, $\Omega_{\rm b} = 0.045$, $\Omega_{\rm dm} = 0.269$, $A_{\rm s} = 2.1 \ 10^{-9}$, $n_{\rm s} = 0.968$ and $w = -0.98$. Finally, the initial conditions were obtained from `MUSIC2-monofonIC` code with the previous chosen cosmology. The following results are obtained using a simulation box with $L = 10^3$ Mpc/h populated with 512^3 particles.

Continuing with the previous study of the Matter Power Spectrum, we display it in Figure 6.2 for several redshifts. Taking out the very large scales where we already know our implementation fails, we can see how the interaction becomes efficient for very late times since in the first plot for $z = 1$ there is no distinction between the standard and the interacting case. Once it becomes efficient, it first affects the smaller scales as we can see in the second plot for $z = 0.42$. Eventually, more scales fall un-
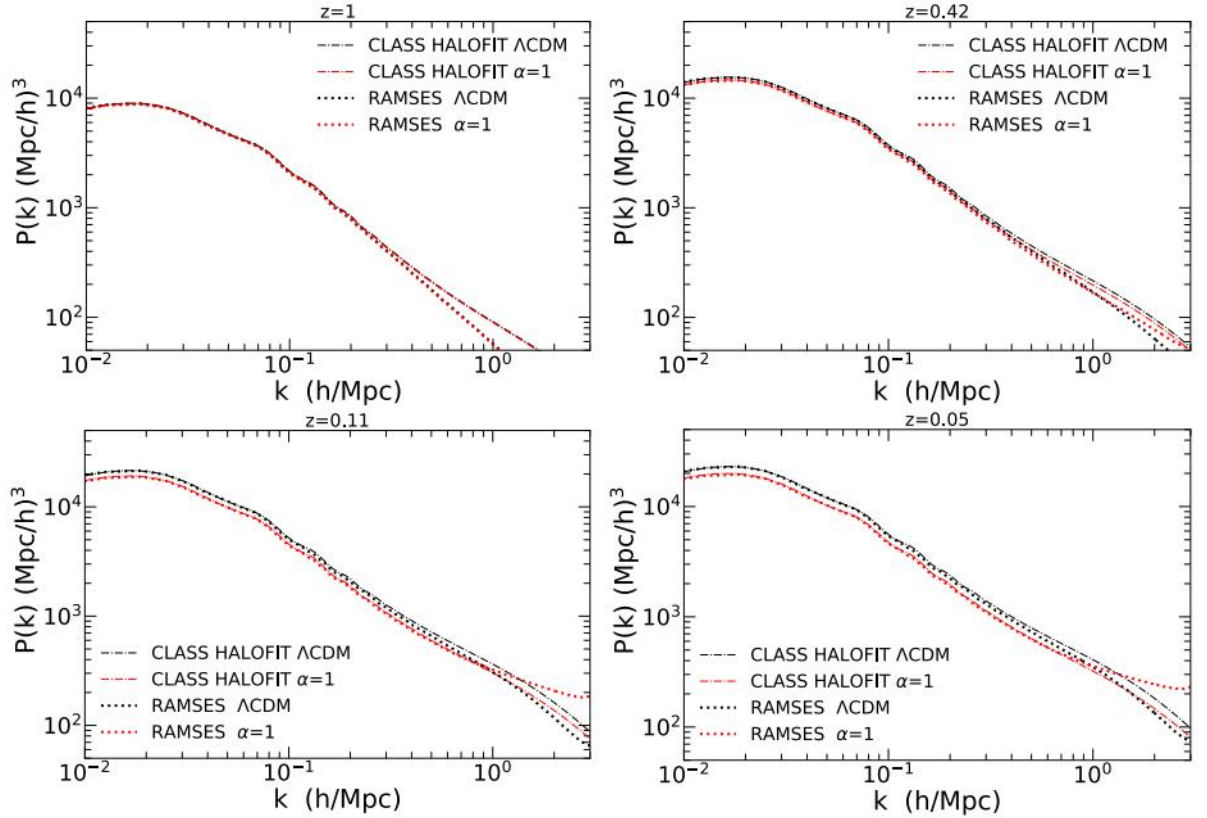
Figure 6.2: Matter Power Spectrum for different redshifts computed from the modified version of `CLASS` with `HALOFIT` and from `RAMSES`.

der the influence of the drag, having less structures formed and, hence, reducing the clustering. We can infer the previous consequence from the reduced amplitude of the spectrum comparing the standard scenario and the case with $\alpha = 1$, in Figure 6.2. For very small scales $k > 1\,h/\mathrm{Mpc}$, however, a different situation appears. We get an enhancement of the spectrum when the interaction is efficient. This change on the behaviour still represents an open question to be answered by future analyses.

Of course we did not perform N-body simulations in order to obtain a Matter Power Spectrum reliable for very small scales. Here, we are actually interested in how structures formed. To study that, we need to analyse how the basic components of Large Scale Structure are created and evolve. Those elements are the Dark Matter halos and the galaxies. We distinguish two basic types of analyses. On one hand, what we can call the large picture where we study how the different halos distribute and form. On the other hand, we can study each individual halo properties and how particles distribute to form each halo. We will focus here in the large picture while we keep the other case as a future work to enlarge our knowledge of pure momentum transfer interactions. Regarding that, we use the `MatchMaker`

174
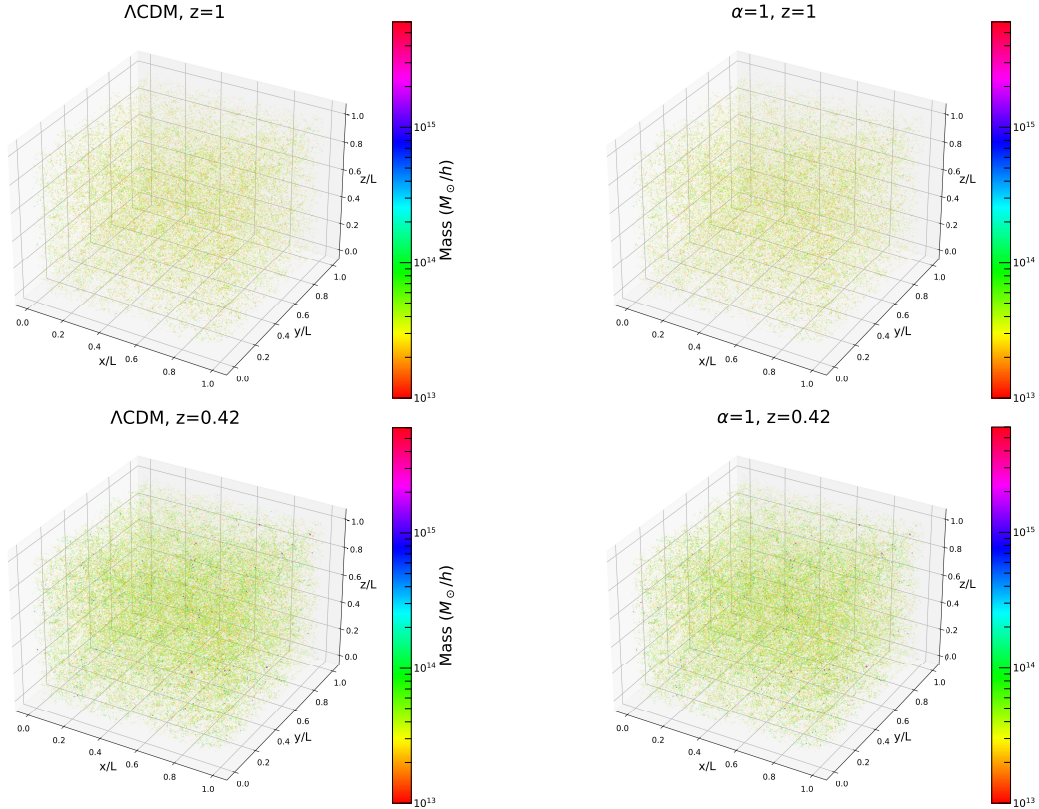
Figure 6.3: Spatial distribution in the simulation box of the halos found by `MatchMaker` algorithm. Each dot is an halo whose colour and dot-size are correlated to its mass.

algorithm[4], a friend-of-friend halo finder, with standard options given by the linking length in units of the mean inter-particle distance $b_{\mathrm{fof}} = 0.2$ and the minimum number of particles per halo $n_{\mathrm{min}} = 20$. As we are interested in the large picture behaviour, we are not going to distinguish between Dark Matter and Baryon particles to form the halo, although we should not forget the interaction does distinguish as it is only applied to Dark Matter. This a priori loss of information can be motivated as follows: galaxies form deep inside the potential wells created by Dark Matter, thus the future halos found have Baryons also as constituent elements. Under the previous considerations, we show in Figures 6.3 and 6.4 the spatial distribution of halos found by `MatchMaker` algorithm. Each dot there represents one single halo and the colour and dot-size are correlated to the amount of mass the halo has in units of $M_\odot/h$. Although we will later analyse in more detail, in Figures 6.3 and 6.4 we can see how the interaction reduces the creation of very massive halos. As larger halos are formed later than smaller halos, the hierarchical formation of structures inside Cold Dark Matter models, those larger ones feel the interaction when they are forming since this interaction becomes efficient at late times. As it was analysed in

---

[4]MatchMaker can be found at https://github.com/damonge/MatchMaker.

175
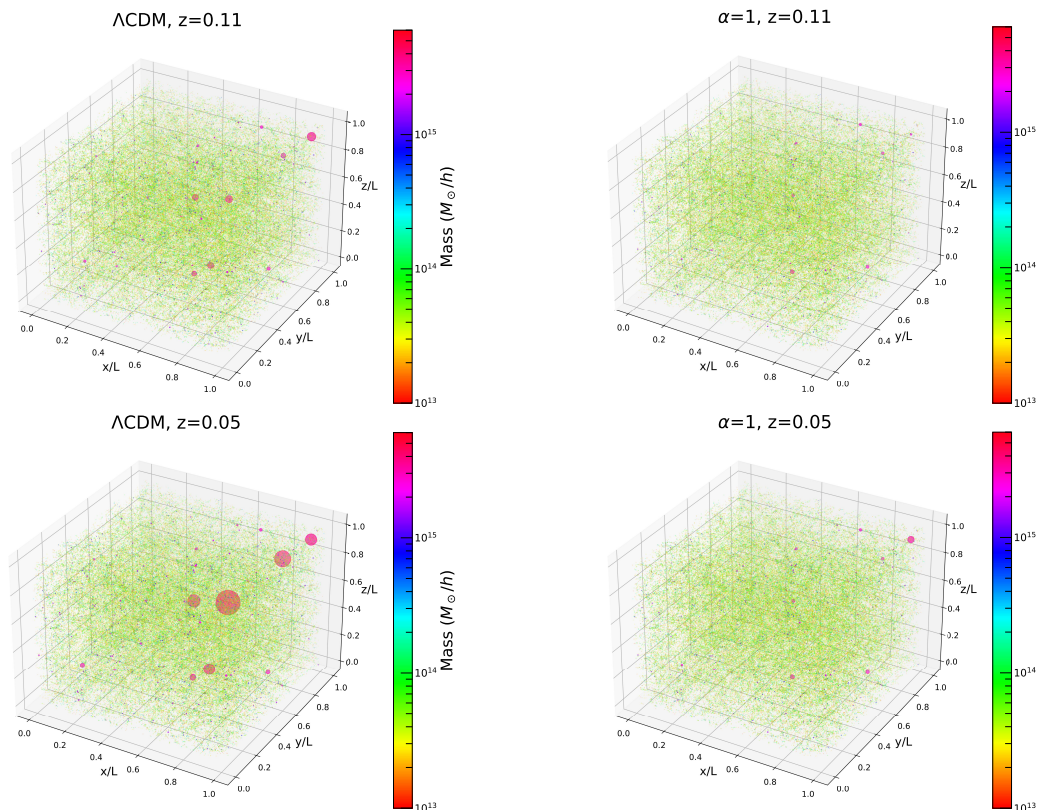
Figure 6.4: Spatial distribution in the simulation box of the halos found by `MatchMaker` algorithm. Each dot is an halo whose colour and dot-size are correlated to its mass.

Chapter 4, the momentum transfer does not destroy structures already formed but it freezes the accretion process, stopping density perturbations to grow, as we saw in Figure 4.5 for example.

Investigating deeper on how halos are formed, we can perform a number counts analysis to delve into the knowledge of such a process. In Figures 6.5 and 6.6, we display how many halos are created as a function of the number of particles each one has and how many halos are created as a function of the mass in $M_\odot/h$ units each one has, respectively. While the differences between the ΛCDM and the interaction on the amount of clusters with lower masses and less particles are statistically not significant, when we look into the more massive halos with more particles a departure appears. For early times $z = 1$, when the interaction is not efficient, no significant differences emerge. This means that as both cases had the same initial conditions and no different evolution yet, both simulated Universes create structures in the same way, as expected. When the interaction becomes efficient, less very massive halos appear in the case of the pure momentum transfer simulation. Also halos with a large amount of particles forming them are reduced in number. This closely follows what we saw with the spatial distribution.
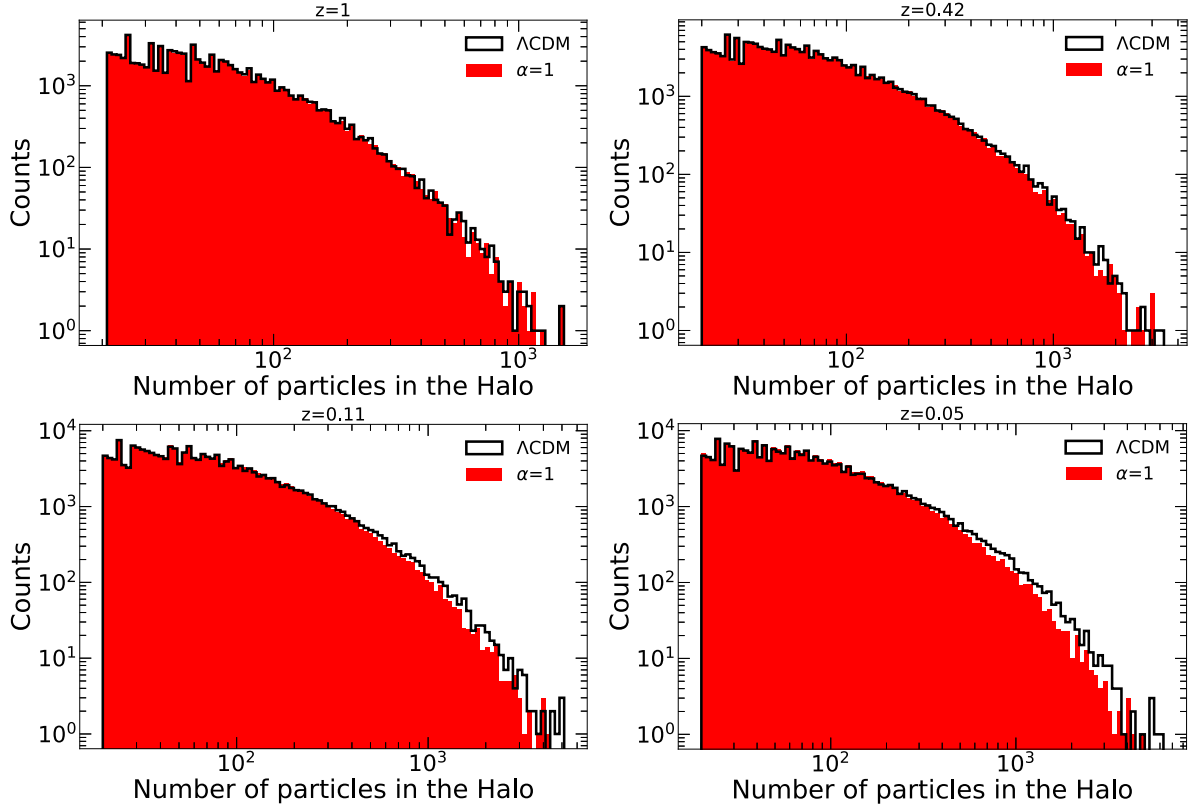
Figure 6.5: Distribution of halos according to the number of particles contained for the standard model and for the Covariantised dark Thomson-like scattering.

The first learnt conclusion is that the dynamics of smaller halos are not perturbed considerably by the interaction. This is explained by the fact the interaction is efficient at late times and, in a hierarchical structure formation model, smaller halos are formed the first, thus not being affected in their formation by the, at that moment, inefficient momentum transfer. But for larger halos this is not true. As they are formed later they do feel the interaction while they are under construction. Dark pure momentum transfer models induce the freezing of clustering of Dark Matter and, precisely, Dark Matter is the governing component of structure formation. Consequently, those larger halos cannot accrete more matter due to the interaction and, then, larger halos are strongly suppressed.

6.3 Discussion and final comments on non-linear analysis

In this chapter, we conducted a first approach into the non-linear regime of the pure momentum transfer models studied in Chapter 4. In particular, and due to its simplicity and similarity with the concordance model alongside with the appealing properties shown, we studied the non-linear dynamics of the Covariantised dark Thomson-like scattering in the case of Dark Energy and Dark Matter having the
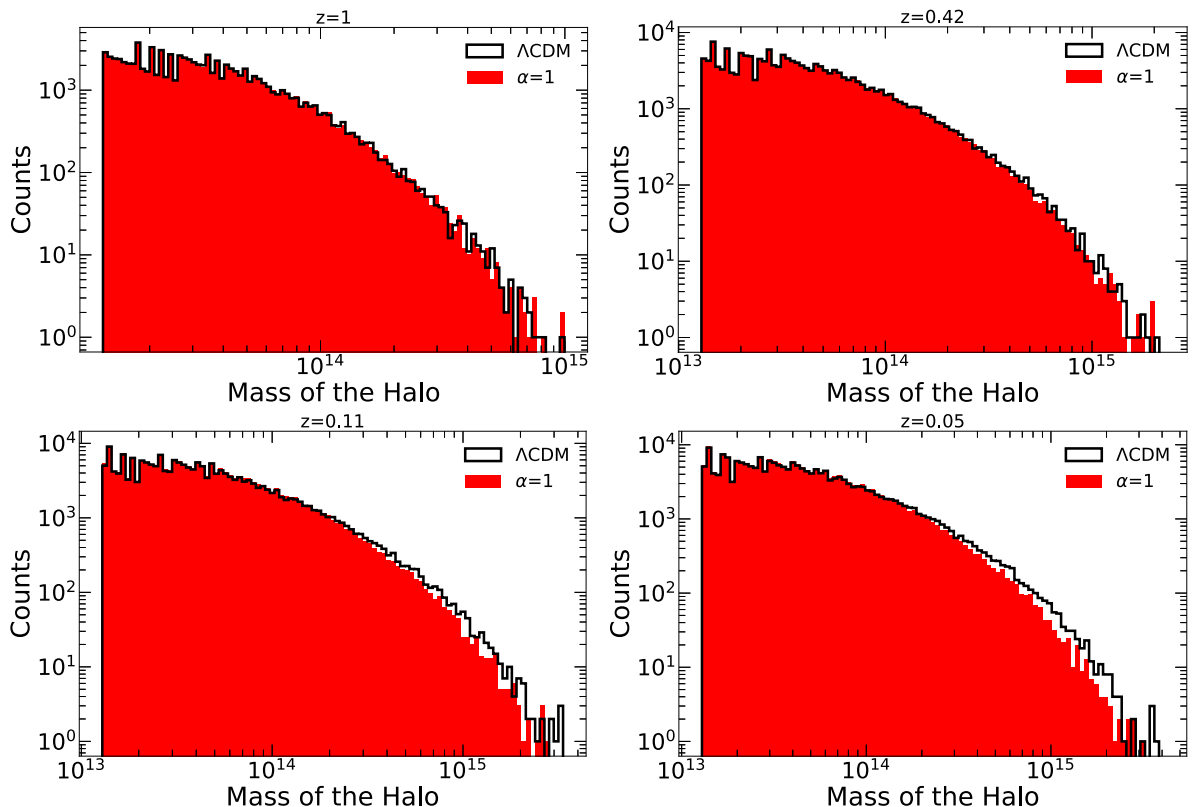
Figure 6.6: Distribution of halos according to their mass in $M_\odot/h$ units for the standard model and for the Covariantised dark Thomson-like scattering.

momentum exchange.

In our analyses, we first showed how, at the level of the Matter Power Spectrum, the momentum transfer induces a suppression of structures up to very small scales $k \sim 1\ h/\text{Mpc}$, as reflected by the amplitude of the Matter Power Spectrum. This continues with what we had already obtained for linear scales: once the interaction becomes efficient for late times it couples the velocity of both interacting fluids via a momentum exchange from Dark Energy to Dark Matter, leading to less matter falling into the potential wells and, finally, having less clustering. On smaller scales $k > 1\ h/\text{Mpc}$, the situation seemed to change and more clustering, represented by a larger amplitude of the spectrum, appeared. In principle, the refinement done should ensure this was not a numerical issues due to the mesh used. Thus, a carefully future study is required, using simulations with the focus on those very small scales, although also analytical investigation can shed light to that regime. This represents one of the main future targets in the wake of this PhD dissertation.

We have also studied the distribution of halos according to certain properties, namely: spatial position, number of particles per halo and mass of each halo. The results showed that the interaction provoked less abundance of larger halos, both in mass and number of particles, while the smaller halos remained similar to the stan-

dard scenario. The previous result is the consequence of the hierarchical process of formation of halos, since larger halos formed latter when precisely this interaction was efficient.

With the previous results we have mainly characterised the large picture of this interaction, but it is evident there is still a large way to go. We still miss a study on the individual properties of the halos, like for example the profiles or the distribution of particles in each halo. In that respect, one of the main future investigations that should emerge after this PhD dissertation would be seeing how the interaction affects the cusp-vs-core problem or if the erasing of very massive structures worsens the missing-satellite or the too-big-to-fail problems. Another interesting investigation would be to see what happens when the interaction is applied to Baryons instead of Dark Matter. In that context, the inclusion of hydrodynamics simulations could lead to an important step forward in the knowledge of these models. We can conclude that this part of the PhD dissertation should have a continuation in the future to fully understand all the intricate implications of the presence of a pure momentum transfer involving the Dark Sector.

7

CONCLUSIONS AND PROSPECTS

The concordance model has faced in recent years certain observations that have put pressure on it, then, taking into account most of our datasets agree with it, possible minimal extensions may be needed. Because of that, this PhD dissertation has been devoted to the examination of pure momentum transfer models involving the Dark Sector, since those scenarios preserve the background cosmology while only adding a minimal modification to the Euler equations. We have first derived their main equations controlling the background and linear perturbation dynamics and, after that, we have investigated the distinctive effects of each model in order to search for specific footprints of the interactions. Subsequently, we confronted our models to the latest data available to explore if they were preferred by observations or not. We have also analysed how future experiments will be able to detect or rule out the interactions presented. Finally, we have performed a first approach to the non-linear dynamics of the previous models.

In this PhD dissertation, we analysed the Covariantised dark Thomson-like scattering, first between Dark Energy and Dark Matter and, after, between Dark Energy and Baryons, and the Velocity-entrainment coupling. The mechanism of action was similar in all the cases. A late-time interaction between a pressurefull fluid and a pressureless fluid, such that the later gains momentum from the former. This provokes that the pressureless fluid, a non-relativistic matter component, stops falling into the gravitational potential wells due to that extra momentum acquired. Hence, as it does not fall into the potential wells, density perturbations of the matter fluid get frozen and, thus, the clustering is reduced and less structures are observed. This mechanism was further seen up to smaller scales when we performed the non-linear analyses thanks to the N-body simulations done with the first model studied.

With the previous analyses, we have demonstrated that those extensions tend

181

to erase structures when efficient, mainly in the late Universe and in the small scales regime. Moreover, thanks to the N-body simulations and the analyses of the linear perturbations, we can conclude that a pure momentum transfer does not destroy already virialised structures but it just freezes the growth of them. Particularly, we discovered that the pure momentum exchange only prevents the formations of very massive halos, keeping the small and middle size halos as in the concordance model. Although the reduction of structures is a general effect of pure momentum transfer models, the previous statement about the halo formation is arguably model dependent. In particular, dependent on when the interaction becomes efficient. In the cases studied, the suppression of only very massive halos was related to the hierarchical process of formation of structures.

We have also performed Monte Carlo Markov Chain analyses with the previous three models in order to see if current data prefer or not them to the concordance model. We have found that a detection of the interaction is possible when the local Universe data of the Sunyaev–Zeldovich effect on cluster count were used. With the Cosmic Microwave Background, the Baryonic Acoustic Oscillations and the Supernovae Ia data, we were only able to establish an upper limit for the coupling parameter that, in any case, was compatible with the results when adding the Sunyaev–Zeldovich data. According to the recent literature, the relation between that particular dataset and the pure momentum transfer models seems to be general, calling for more investigation to clarify whether the momentum interactions are really seen by those datasets or not and, if so, why.

Regarding the other cosmological parameters, we should highlight the H_0 and σ_8 parameters, which are affected by the two most prominent dataset tensions nowadays. In relation with the Hubble constant H_0, a pure momentum transfer cannot modify its value as H_0 belongs to the background cosmology, which remains unaltered in these scenarios. As expected, we did not see any significant alleviation of this tension when only a pure momentum transfer was applied. Because of that, we add the possibility of having extra radiation since that might alleviate both tensions simultaneously by two independent mechanisms. Before commenting those results, it is better to first explain what we have obtained for the σ_8 tension. We have found how the pure momentum transfer induces a lower value of the σ_8 or S_8 parameter by its intrinsic mechanism of action, which reduces the clustering and the structures for late times. When the Sunyaev–Zeldovich data were used, and then the interactions were detected, we had the σ_8/S_8 tension solved. But also without the Sunyaev–Zeldovich likelihood we did have a substantial alleviation of the tension. Coming back to the case when we had extra radiation, we have found how the alleviation of one of the previous tensions does not imply the worsening of the other, something common as seen in the literature. However, the possibilities of alleviating both tensions at the same time are limited as far as we have seen with the models studied. Anyhow, the easing of each tension was due to uncorrelated mechanisms in these scenarios, thus future models might better address both simultaneously.

Finally, we have used the Covariantised dark Thomson-like scattering between Dark Energy and Dark Matter to perform three different forecast analyses in this PhD dissertation. In the first case, we have demonstrated how the clustering data in the future J-PAS, DESI and EUCLID surveys will be able to heavily improve our previous constraints from the MCMC analyses. In particular, a $\sim 10\sigma$ detection of the model parameter will be found when the surveys will come their end, if the cosmology is compatible with $\alpha = 1$. If not, current constraints will improve by a factor ~ 4. Furthermore, we have also investigated if the relativistic corrections that appear in the dipole of the Matter Power Spectrum can be used as a smoking gun for these interactions in future experiments. Using a SKA-like configuration, we have found that these interactions will be spotted by the dipole with competitive constraints in the probable scenario galaxies are still faithful tracers of the underlaying matter density field. However, in the opposite case, a SKA-like survey will not be efficacious enough. Lastly, we have analysed if a bad modelling of the cluster counts in a future EUCLID-like survey could bias the cosmological constraints and/or provided a wrong detection of the interaction. We found that neglecting the lensing contribution to the cluster counts modelling induces biased results in several parameters. In particular, we showed that the H_0, σ_8 or bias parameter can get up to a 5σ shift in their value when lensing contribution was neglected. This can be connected with the well-known tensions as, with this analysis, we have shown how any miss-calibration, neglection of terms or anything similar can dramatically induce an apparent tension among datasets.

From the forecasts analyses, we can affirm that future surveys will be crucial to detect or rule out the pure momentum transfer interactions and that a correct modelling of the different observables is absolutely required.

Looking ahead, the investigations this PhD dissertation have condensed leave certain open questions. On one hand, the analysis of the non-linear dynamics still needs a more comprehensive examination. Even though the large picture of the non-linear scales has been studied, we should analyse the small picture. In particular, a thorough inspection on the properties of the individual halos should be performed, like for instance their density profiles or the formation of voids. Also, profiting the already developed numerical codes, the current core-vs-cusp, the missing-satellites or the too-big-to-fail problems will need to be examined under the pure momentum transfer models. Another interesting investigation to perform in the future would be to understand if when the interaction is applied to only one matter component, the movement of virialised galaxies and halos is coherent. In other words, if galaxies are still faithful tracers of the Dark Matter field when a momentum exchange appears as it has been considered in certain parts of this PhD dissertation.

On the other hand, we have not questioned the possible microphysics behind a pure momentum transfer. It is true that without any proper detection a Dark Matter

particle or a Dark Energy field in our laboratory experiments, the task seems arduous. But Physics has predicted particles from macro-effects even before we were technologically capable of inspecting the related microphysics. The future surveys will be able to set extremely precise constraints not only on cosmological parameters but also in any model parameter invoking a hidden interaction. Consequently, the space of parameters where a Dark Matter particle or a Dark Energy theory would live will get smaller and smaller and, with it, the range of possible interactions in the Dark Sector. Regarding this line of research and inspired by the similarity of some of these interactions with the Thomson scattering, it will be interesting to see if a recent dark (re)combination or dark (re)ionization would explain this coupling or, maybe, a more general mechanism might be behind a pure momentum transfer.

Now the journey is nearing its end, we conclude this PhD dissertation has thoroughly investigated the pure momentum transfer interactions, showing how they can be an appealing alternative to the current scenario and, at the same time, not changing dramatically the current concordance paradigm.

CONCLUSIONES Y EL PORVENIR

El modelo de concordancia de la cosmología actual, si bien extremadamente preciso según la mayoría de los observables disponibles, se enfrenta recientemente a ciertas observaciones que lo han puesto en duda o que han sugerido la presencia de algo más allá. Es por ello que esta tesis doctoral tiene por objetivo el estudio de los modelos de intercambio puro de momento que involucran al Sector Oscuro del Universo. Dichos modelos tienen por atributos la no modificación de la cosmología de fondo y solamente cambiar la descripción actual añadiendo una cierta modificación en las ecuaciones de Euler. En esta tesis, hemos obtenido las ecuaciones que gobiernan la cosmología de fondo y sus perturbaciones lineales para poder posteriormente investigar aquellos efectos de los modelos que nos permiten detectar su presencia o no. Después, hemos usado aquellos datos cosmológicos más recientes para constreñir la presencia o no de las interacciones que describen esos modelos. Además, hemos investigado cómo los experimentos futuros van a mejorar o no los anteriores resultados. Por último, hemos realizado un primer estudio de las escalas no lineales del Universo bajo estos modelos.

En la presente tesis doctoral, hemos estudiado un modelo de dispersión de tipo Thomson covariantizado entre Energía Oscura y Materia Oscura primero, y luego entre Energía Oscura y Bariones, y otro modelo de acoplamiento por arrastre en las velocidades perteneciente enteramente al Sector Oscuro. En los anteriores casos, la forma de actuación de las interacciones era similar, tratándose de una interacción eficiente en estadios tardíos del Universo entre un fluido con presión y otro sin ella, de tal manera que este último ganaba momento del anterior. Esta transferencia provocaba que el fluido sin presión, generalmente una componente fría de materia, dejara de ser acretado por los pozos de potencial y, por tanto, sus perturbaciones de densidad dejen de crecer reduciendo las acumulaciones de materia y las estructuras en diferentes escalas de Universo. Con los anteriores análisis hemos demostrado que dichas interacciones son capaces de eliminar estructuras en fases tardías y escalas pequeñas del Universo pero sin destruir las estructuras ya virializadas, sino que la transferencia pura de momento resultaría en la congelación de proceso de acumulación de materia. De hecho, sólo aquellos halos más masivos se verían afectados por estas interacciones, siempre y cuando sean eficientes tardíamente, pues los menos masivos se forman primero cuando la interacción no es eficiente.

Por otro lado, hemos realizado diferentes análisis por medio de métodos de ca-

denas de Markov Monte Carlo con los diferentes modelos estudiados con el fin de saber si los datos cosmológicos más actuales prefieren o no dichos modelos frente a la descripción de concordancia. Gracias a dichos análisis, hemos descubierto el rol que tiene los datos del efecto de Sunyaev–Zeldovich en los cúmulos, siendo este conjunto de datos el único que es capaz de dar una detección de las interacciones estudiadas. Sin embargo, con los datos del Fondo Cósmico de Microondas, de las Oscilaciones Acústicas de Bariones o de las Supernovas de tipo Ia solamente se pudo establecer un límite superior al parámetro de la interacción en cada caso. Esta relación entre los datos del efecto de Sunyaev–Zeldovich y los modelos con presencia de un intercambio puro de momento se ha encontrado recientemente en numerosos estudios con muy diferentes modelos en cada caso. Por tanto, más investigación es necesaria para aclarar dicha particular relación.

En los anteriores análisis, se halló que el valor del parámetro de Hubble H_0, el cual está afectado por la explicada tensión, no se veía modificado por las interacciones de trasferencia de momento. Dicho resultado era esperado pues en dichos escenarios la cosmología de fondo permanece impertérrita, siendo H_0 un parámetro que vive precisamente en la cosmología de fondo. En el caso del parámetro σ_8, que también está afectado por otra tensión, sí se vio como estas interacciones permiten reducir su valor y por tanto aliviar, sino resolver cuando se usan los datos del efecto de Sunyaev–Zeldovich, la anterior tensión. La explicación a ello se conecta con lo visto anteriormente, pues σ_8 mide la cantidad de estructuras en el Universo y por tanto, como estas interacciones las reducen, su valor se ve naturalmente menguado. De cara a poder aliviar ambas tensiones simultáneamente, se estudió la posibilidad de añadir radiación extra en cada caso. Se vio que no era posible resolver ambas tensiones simultáneamente, si bien aliviar una no implicaba empeorar la otra tensión como suele ser común vista la literatura. Cabe decir aquí que dado que el alivio de cada tensión se hace por mecanismos independientes, otros modelos podrían quizá sí resolver ambas tensiones.

Para terminar, hemos realizado diferentes análisis de tipo prospectivo usando el primero de los modelos estudiados, aquel dado entre la Energía Oscura y la Materia Oscura de dispersión de tipo Thomson covariantizado. En el primero de estos análisis, hemos demostrado como los experimentos futuros J-PAS, DESI y EUCLID van a ser capaces de darnos una detección de hasta 10σ del parámetro que controla la interacción si la cosmología es compatible con el resultado obtenido en los análisis anteriores $\alpha = 1$. Si no fuera este el caso, los resultados de los futuros experimentos se esperan mejoren hasta un factor cuatro aquellos resultados que ya disponemos. Además de lo anterior, en otro análisis hemos investigado si las correcciones relativistas que aparecen en el dipolo del Espectro de Materia pueden ser usadas como pruebas distintivas de la presencia de este tipo de interacciones. Gracias a una configuración similar al futuro experimento SKA, hemos encontrado que las interacciones que impliquen una transferencia pura de momento en el Sector Oscuro van

a poder ser detectadas con el dipolo en los futuros experimentos, siempre que las galaxias sigan actuando, a pesar de la interacción, como balizas de la distribución de la materia. En el caso que no fuera así, el dipolo no daría resultados competitivos. Finalmente, hemos analizado si una modelización incompleta, como se hace en ocasiones, del observable que condensa la distribución de los cúmulos puede resultar en parámetros mal medidos tanto de las interacciones como los cosmológicos. Si bien el parámetro de la interacción permaneció inmutable, parámetros como H_0, σ_8 o el parámetro de bias tuvieron errores de hasta 5σ, lo cual puede conectar con las tensiones anteriormente comentadas siendo una alerta para futuros experimentos. Podemos concluir por tanto que los experimentos futuros van a recavar grandes cantidades de información que nos va a permitir confirmar o descartar la presencia de interacciones de tipo intercambio puro de momento, por supuesto siempre y cuando su modelización sea la adecuada.

De cara al porvenir, sabemos que lo aquí investigado deja ciertos asuntos todavía por resolver y clarificar. Por una parte, el análisis de las escalas no lineales realizado es sólo un pequeño paso dentro de todo lo que se puede realizar a ese respecto. Por ejemplo, queda pendiente un estudio sobre las propiedades individuales de cada halo de materia, como podría ser sus perfiles de densidad, o, por otro lado, el estudio de cómo se forman y evolucionan los vacíos. Cabría también analizar cómo se encuadran en estos modelos los problemas sobre formación de estructuras anteriormente comentados o si el movimiento de las distribuciones de materia visible, galaxias, y oscura, halos, son coherentes cuando se da el intercambio de momento. Por otro lado, es cierto que durante esta tesis doctoral no se ha cuestionado el posible origen de dicha interacción ni su posible descripción microscópica. Si bien sin una detección en nuestros laboratorios de una partícula o de un campo de Energía Oscura o Materia Oscura sería una tarea difícil, no es la primera vez en la historia de la Física que se ha descrito a partir de los efectos macroscópicos un fenómeno microscópico tecnológicamente invisible en esas fechas. En esta línea, un proceso parecido a la recombinación o a la reionización pero en el Sector Oscuro podría explicar los intercambios de momento macroscópicos. Todo lo anterior quedará supeditado a los futuros experimentos que se han planeado para los siguientes años.

Ahora que se acerca el final del apasionante viaje que es una tesis doctoral, se puede cerrar concluyendo que esta tesis doctoral ha servido para llevar a cabo una profunda y detallada investigación sobre modelos donde un intercambio de momento puro se da, siendo estos una prometedora alternativa a la descripción actual por las propiedades descritas aquí.

A

STATISTICAL TOOLS

nalysing nature relies on two key concepts, the laws of nature and the observations we are able to perform. However, both concepts live in two different worlds. Laws of nature establish unambiguous equations that dictate how the world works while observations usually give raw data fully equipped with noise, uncertainties, statistical fluctuations, etc. As we need both concepts to be consistent between them to do science, we must be able to translate the laws of nature into what we should observe and, vice-versa, we should be able to process raw data into well defined distributions that will allow us to fit our laws of nature. Consequently, we need to connect them and here is where statistics are needed.

Statistics are the mathematical tools that, first, allow us to convert raw data into workable data and, then, use it to test and rule out or not a theory provided the observations we have. Therefore, lying as a central pillar in the scientific method. For the purpose of this thesis we are interested in Statistical Inference, which provides the tools to obtain the underlying distributions present in raw data observed in the different experiments we perform in Cosmology and, then, infer the value of the parameters of a certain theory. Once we know how current experiments behave, the next question would be how future experiments can help us. To that end, we will use the Fisher matrix formalism, a statistical tool that allows us to infer the goodness of a fit in a future experiment by only setting a fiducial model and the planned experiment specifications.

Through this Appendix, we first explore the basic concepts and notation of statistics and the notions of Bayesian inference. After that, we will explain how Markov Chain Monte Carlo techniques are used and, finally, what kind of criteria we use in the thesis when comparing different models. In the last part, we will explain the basic concepts of Fisher matrix formalism.

Basic concepts and notation

There are two main approaches to understand what probability of an event $P(A)$ really means, frequentist probability and Bayesian probability. From the frequentist point of view, the repeatability is the core idea as probability is defined upon the relative frequency of an event after many trials as

$$P(A) = \lim_{N_m \to \infty} \frac{N_A}{N_m} \, , \tag{A.1}$$

where N_A is the number of times the event A occurred and N_m is the total number of times we measured. From the previous equation (A.1), it is clear that only when we are able to repeat the experiment an infinite number of times the frequentist probability will converge to the "true" probability of the event. Hence, repeatability of an experiment becomes a must. In a few words, one should understand probability as frequency of an event.

On the other hand, Bayesian probability relies on the previous information we have regardless the number of times we can measure an experiment. In a more accurate way, Bayesian probability gives the degree of belief in a proposition based on the previous knowledge and the data we have. Before defining mathematically what Bayesian probability is, we need to understand what is joint probability, conditional probability and prior probability:

- Joint probability $P(A \bigcap B)$: the probability of event A and B happening together.

- Conditional probability $P(A|B)$: the probability of an event A given event B happened. It can be related to the joint probability as $P(A|B) = \frac{P(A \bigcap B)}{P(B)}$.

- Prior probability: probability distribution that captures our initial beliefs.

The cornerstone of Bayesian approach is the Bayes Theorem, which can be condensated into

$$P(A|B) = \frac{P(B|A) \, P(A)}{P(B)} \, , \tag{A.2}$$

where $P(A|B)$ is called the posterior probability, $P(B|A)$ is the conditional probability of B given A, $P(A)$ is called the prior probability of A.

The final key concept is the likelihood function which can be defined as follows. Given a probability distribution function $p(X|\theta)$, described by a parameter θ and a random variable X, and given data x, the likelihood function $\mathcal{L}$ is

$$\mathcal{L}(\theta) = p(X = x|\theta) \, . \tag{A.3}$$

Then, in order to infer the best fit for the parameter we should obtain the value of the parameter θ that makes the observed data x most probable, what is just maximising the likelihood or, equivalently, minimising the χ^2 value since $\mathcal{L}(\theta) \propto e^{-\chi^2/2}$.

Finally, the Table A.1 summarises the main differences between the frequentist and Bayesian approaches when dealing with probability distribution. Henceforth, we will only focus on the Bayesian approach as it is the one used.
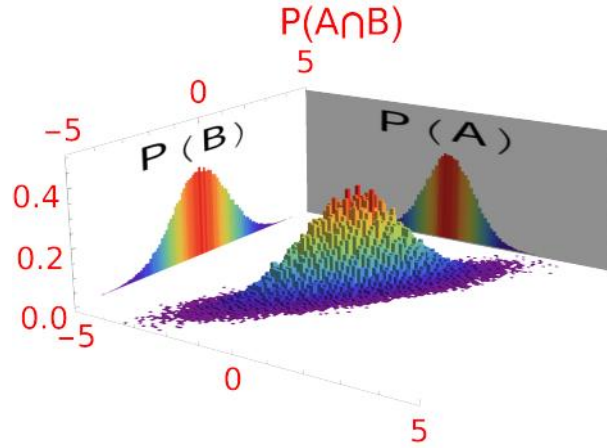
Figure A.1: Joint probability $P(A \bigcap B)$ given the probability of an event A, $P(A)$, and an event B, $P(B)$. The 2-dimensional constraints are just the top view of this image when A and B are parameters, as they should be understood as random variable in the Bayesian approach.

	Frequentist	**Bayesian**
Core idea	relative frequency	degree of belief
Parameters	fixed	random variable
Limiting factor	repeatability	previous information

Table A.1: Main differences when dealing with the frequentist and Bayesian approaches.

Bayesian inference

We can use the Bayes theorem to infer the value of the parameters by promoting the event A to be the parameters $\theta = \{\theta_1, \theta_2, ..., \theta_p\}$ and the event B to be the data $x = \{x_1, x_2, ..., x_n\}$. Here, one can realise how we are promoting the parameters of the model to be random variables instead of fixed constants we want to test, as in a frequentist approach one would do. The first consequence of treating our parameters as random variables is that they can be sampled from a probability distribution to search for the best fit given our data x, that is maximizing the likelihood. Thus, we can write the Bayes theorem as

$$P(\theta|x) = \frac{P(x|\theta)\,P(\theta)}{P(x)}\ ,\tag{A.4}$$

where $P(\theta|x)$ is the posterior distribution (usually called just posterior), $P(x|\theta)$ is the likelihood function, $P(\theta)$ is the prior distribution (usually called just prior) and $P(x)$ is called the marginal likelihood or the evidence, which guarantees the normalisation of the posterior. Consequently, the posterior now reflects the degree of belief about the value of the parameter θ after seen the data, given the previous information encoded in the prior.
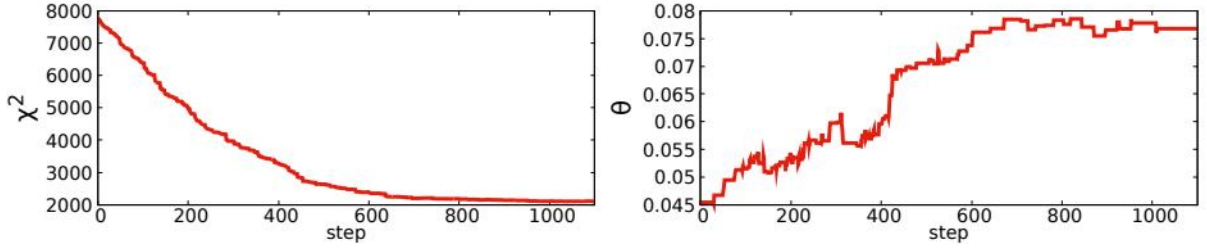
Figure A.2: Example of a MCMC process with $N_s = 1100$ fitting a parameter θ. We see the minimization of χ^2 (left plot) while the parameter value converges to the "true" value (right plot).

In view of the foregoing, how we select the prior becomes a central problem in Bayesian inference. In the literature, we have several types of priors which we can classify into the following categories:

- Informative priors: they reflect a known specific information about the parameter.

- Uninformative priors: they reflect unspecific or very general information about the parameter.

- Improper priors: they are not a valid probability density in the sense they do not converge as $\int P(\theta)\, d\theta = \infty$. Although they do not converge, we can use them while we are not interested in computing the evidence.

- Flat or uniform priors: a type of improper priors which reflect the completely lack of information about the parameter θ, as the probability distribution is constant for all possibles values of the parameter θ, then $P(\theta) = constant$.

Now that we have all the ingredients, we should explain the Bayesian inference algorithm which works as follows.

Let us have a vector of observations called $x = \{x_1, x_2, ...x_n\}$ sampled from a probability distribution $P(X|\theta)$, where $\theta = \{\theta_1, \theta_2, ..., \theta_p\}$ are the parameters and X is a random variable, then:

1. Before using the data, we set a prior for the parameters based on our previous beliefs.

2. We set a likelihood for the experiment that gives us the data.

3. We use the Bayes theorem to obtain the posteriors based on our data and our previous knowledge and, then, update our initial beliefs.

Markov Chain Monte Carlo techniques

For most of the cosmological datasets, the multi-dimensionality makes difficult and computationally expensive to sample the parameter space in order to obtain the final distribution for the parameters values. Here is where Monte Carlo methods appear

and, in the cosmology and astrophysics community, the Markov Chain Monte Carlo techniques (MCMC).

A Markov Chain is a sequence of events such that the i-th event only depends on the $(i-1)$-th event, that is, given an event the immediately previous event and the immediately next event are independent events. For our Bayesian statistical purposes, the most relevant property of the Markov Chains is the possible convergence to a stationary stage, that is a step-independent stage, such that the elements in the chain are samples from the posterior distribution we are interested in. Finally, Monte Carlo techniques are the algorithms which are able to calculate the specific value of a quantity by using a random number generator.

We are interested in obtaining the posterior distribution for a parameter θ, something which of course we can not do directly, but what we can do is to simulate a Markov Chain whose equilibrium distribution is $P(\theta|x)$. When the Markov Chains enters the stationary stage, the samples in the chain are proportional to the posterior we are trying to obtain. Consequently, the posterior mean for the parameter θ reads as

$$\hat{\theta} = \int P(\theta|x)\,\theta\,d\theta \simeq \frac{1}{N_{\mathrm{s}}} \sum_{i=1}^{N_{\mathrm{s}}} \theta^{(i)} \quad , \quad N_{\mathrm{s}} \to \infty \, , \tag{A.5}$$

with N_{s} the number of steps.

Although we have in the literature plenty of different implementations of the MCMC algorithm, here we will explain the Metropolis-Hasting (MH) algorithm [167, 168] as it is the one used in this thesis. It works as follows

1. Start from a random value θ with posterior probability $P(\theta|x)$.

2. Set a transition probability function $q(\theta, \theta')$ that generates a possible new point of the chain θ'.

3. Obtain the posterior probability for the new point $P(\theta'|x)$.

4. Generate a random number $u \in [0, 1]$.

5. Calculate the acceptance ratio as $\alpha(\theta, \theta') = \min\left\{\frac{P(\theta'|x)q(\theta',\theta)}{P(\theta|x)q(\theta,\theta')}, 1\right\}$ and accept the new θ' as the next step in the chain after θ if $u < \alpha$, otherwise reject θ' and the new point in the chain is again θ.

6. Repeat from 2. until convergence.

The natural question that emerges now is: when have we reached the convergence? In this thesis, to answer such question we use the Gelman-Rubin convergence criteria [169]. Let us have M different chains with N points per chain such that we call θ_i^j the value of the parameter θ corresponding to the i-th step of the j-th chain, with $i = 1, .., N$ and $j = 1, ..., M$. Following the equation (A.5), the mean value of the parameter θ for the j-th chain $\hat{\theta}^j$ and the mean value considering all the

chains $\hat{\theta}$ are

$$\hat{\theta}^j = \frac{1}{N} \sum_{i=1}^{N} \theta_i^j \,, \tag{A.6}$$

$$\hat{\theta} = \frac{1}{NM} \sum_{j=1}^{M} \sum_{i=1}^{N} \theta_i^j \,. \tag{A.7}$$

The between chain variance B/N and the averaged within chain variance W are defined as

$$\frac{B}{N} = \frac{1}{M-1} \sum_{j=1}^{M} (\hat{\theta}^j - \hat{\theta})^2 \,, \tag{A.8}$$

$$W = \frac{1}{M} \sum_{j=1}^{M} s_j^2 = \frac{1}{M(N-1)} \sum_{j=1}^{M} \sum_{i=1}^{N} (\theta_i^j - \hat{\theta}^j)^2 \,, \tag{A.9}$$

where s_j^2 is the variance of the j-th chain. Then, the Gelman-Rubin statistic is

$$R = \frac{\frac{N-1}{N}W + \frac{B}{N}(1 + \frac{1}{M})}{W} \,. \tag{A.10}$$

In this thesis, we consider a MCMC analysis has converged when $R - 1 < 0.01$.

Lastly and regarding the parameters, we will see when doing the analyses with the numerical codes that we have three different types of parameters, namely cosmological, nuisance and derived parameters. Of course in addition to the fixed parameters whose name self describe their role. The cosmological parameters are the ones we are really interested in constraining by the data we use. While the nuisance parameters, although they are also constrained by data, we are not interested in their constraints. We cannot neglect or fix them to a certain value as then they will spoil the constraints on the cosmological parameters since they have an impact on data. For example, a nuisance parameter can describe some uncertainty on data or it can be one of the parameters needed in the model describing the measurement of certain observable. Finally, derived parameters are not fixed directly by data but calculated from the cosmological parameters once data is applied to them.

Model selection and information criteria

Once we know how MCMC analysis works, one can apply it for several models and, as a consequence, one may ask the following question: how can we compare the goodness of the fit between different models? Our next step is, then, finding a tool which allows us to choose the best model according to the data we have.
A first and naive approach would be compare the maximum likelihood, or equivalently the minimum χ^2, as the Bayesian inference process tries to maximise the

likelihood. However, one can easily understand that adding new parameters to a fitting will always improve it, even if the new ones are completely irrelevant for the problem under study.

As a consequence, the information criteria were born to study the goodness of a fit weighing the number of parameters a certain model needs to explain the data. Among all the criteria in the literature we want to focus on the Akaike Information Criteria [170] and the Bayesian Information Criteria [171]:

- Akaike Information Criteria: $\text{AIC} = -2\ln\mathcal{L}_{\max} + 2k$, where $\mathcal{L}_{\max}$ is the maximum likelihood and k the number of parameters of the model.

- Bayesian Information Criteria: $\text{BIC} = -2\ln\mathcal{L}_{\max} + k\ln N$, where N is the number of data points used in the fit.

The exact value that each model gives is not important but its difference, therefore the model which has the lower AIC or BIC value will be the one preferred by data taking into account how many parameters each models needs.

Fisher Matrix

When designing a new, cosmological or not, experiment one of the main aims is finding improved constraints for the parameters under consideration. Of course, estimating the future constraints, usually called a forecast, is not an easy task as one must consider the ability of the experiment combined with, for example, all the possible uncertainties or the statistical fluctuations. Here is where Fisher Matrix formalism [172] becomes a powerful tool. It allows us to estimate analytically and quickly the precision with which a future experiment would measure the parameters of a certain model, given the fiducial cosmology and the survey specifications.

Consider we have a likelihood $\mathcal{L}$ based on a set of data x and a vector of parameters θ. We know from the Appendix A that in order to obtain the best fit for the parameters we have to find the maximum of the likelihood. Then, let us make a Taylor expansion of $\ln\mathcal{L}$ about its maximum $\hat{\theta}$[1]. The 0-th order term of the expansion has no dependence with the parameters θ as it is just a constant, and the 1-st order term has to vanish as we are in a maximum of the function. The 2-nd order term, usually called the Hessian Matrix, condenses the information about the parameters errors and their covariance, and when we average over the data defines the Fisher Matrix as

$$F_{\alpha\beta} = -\left\langle \frac{\partial^2 \ln\mathcal{L}}{\partial\theta_\alpha\partial\theta_\beta} \right\rangle , \qquad (A.11)$$

allowing us to rewrite the likelihood Taylor expansion as

$$\Delta\ln\mathcal{L} \propto (\theta_\alpha - \hat{\theta}_\alpha)F_{\alpha\beta}(\theta_\beta - \hat{\theta}_\beta) , \qquad (A.12)$$

---

[1]which will be the same maximum for $\ln\mathcal{L}$ and for $\mathcal{L}$ because of the properties of the logarithm function.
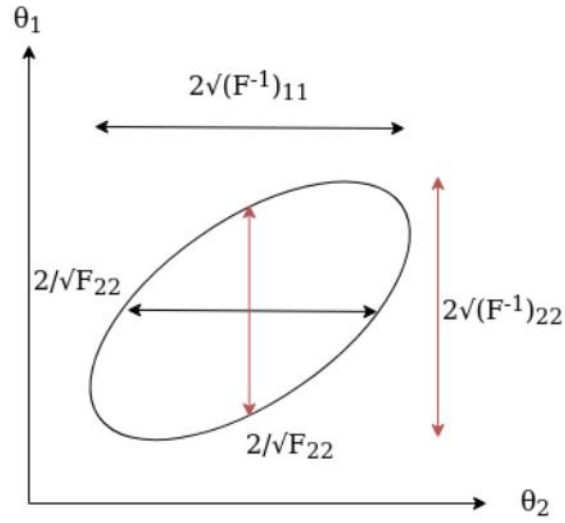
Figure A.3: Meaning of the entries of Fisher Matrix and its inverse matrix.

which of course collapses to computing $\Delta\chi^2 \propto \Delta \ln \mathcal{L} \propto F_{xx}(\theta_x - \hat{\theta}_x)^2$, when we have only one parameter θ_x. From equation (A.12) it is clearly seen the analogy between the Fisher Matrix and the inverse of the covariance matrix $C_{\alpha\beta}$. Finally, the Fisher matrix formalism relates to the 1σ uncertainty of a parameter once marginalised over the rest σ_i as

$$F_{\alpha\beta}^{-1} = C_{\alpha\beta} = \begin{pmatrix} \sigma_\alpha^2 & \sigma_{\alpha\beta} \\ \sigma_{\alpha\beta} & \sigma_\beta^2 \end{pmatrix} \, , \tag{A.13}$$

where $\sigma_{\alpha\beta} = \rho_{\alpha\beta}\sigma_\alpha\sigma_\beta$ with $\rho_{\alpha\beta}$ quantifying the correlation between the parameters. Schematically, the meaning of the Fisher Matrix for two parameters is shown in Figure A.3. The representation of the 1σ contour simply corresponds to the limits $(\hat{\theta}_\alpha - k\sigma_\alpha, \hat{\theta}_\alpha + k\sigma_\alpha)$ and $(\hat{\theta}_\beta - k\sigma_\beta, \hat{\theta}_\beta + k\sigma_\beta)$, where $k \simeq 1.52$. Usually one denotes the full length of the 1σ region by

$$\Delta_{1\sigma}\theta_\alpha \equiv 2\sqrt{F_{\alpha\alpha}^{-1}} \, . \tag{A.14}$$

DISTANCES IN COSMOLOGY

n Cosmology, the fact that the Universe is expanding forces us to think about what is the meaning of a distance. In principle, the most natural definition may emerge from the metric giving the well known proper distance. However, in an expanding Universe, it suffers from it and we may want to avoid having two object separating with time even though they do not move but expansion does. This is the concept of comoving distance. Others distances like angular distance or luminosity distance emerge from observations and, then, it will be useful to relate them to our previous more theoretical distances.

In this appendix, we summarise the previous distances with the main relations among them.

Proper distance

The distance between two events that occur at the same time. For simplicity and as we work along this thesis with it, we consider a flat Friedman-Lemaître-Robertson-Walker metric (FLRW) as

$$\mathrm{d}s^2 = -\mathrm{d}t^2 + a^2(t)\left(\mathrm{d}r^2 + r^2\,\mathrm{d}\theta^2 + r^2\sin^2\theta\,\mathrm{d}\phi^2\right) \ . \tag{B.1}$$

Then, if we consider two simultaneous events the radial distance is

$$\Delta s = \int_{s_A}^{s_B} \mathrm{d}s' = a(t)\int_{r_A}^{r_B} \mathrm{d}r' \ . \tag{B.2}$$

Considering null geodesics, that is $\mathrm{d}s = 0$ we can simply relate $\mathrm{d}t^2 = a(t)^2\mathrm{d}r^2$ and then the proper distance from us to an object reads as

$$s = a(t)\int_0^t \frac{\mathrm{d}t'}{a(t')} = \frac{a(t)}{H_0}\int_0^z \frac{\mathrm{d}z'}{E(z')} \ . \tag{B.3}$$

Comoving distance χ

The distance that remains constant for two points that move with the expansion of the Universe with no peculiar movements. It simply derives from the proper distance as

$$\chi = \frac{s}{a} = \frac{1}{H_0} \int_0^z \frac{\mathrm{d}z'}{E(z')} \; . \tag{B.4}$$

Angular diameter distance

Consider an object of size R with extremes in (t, χ, θ, ϕ) and $(t, \chi, \theta + \Delta\theta, \phi)$, then as the size of that object is very small compared to its distance we have

$$\Delta\theta \simeq \frac{R}{a(t)\chi} \; , \tag{B.5}$$

thus the angular diameter distance is defined as

$$D_A \equiv \frac{R}{\Delta\theta} = a\chi(a) = \frac{\chi(z)}{1+z} \; . \tag{B.6}$$

Luminosity distance

The luminosity distance is defined as

$$D_L^2 \equiv \frac{L}{4\pi F} \; , \tag{B.7}$$

where L is the absolute luminosity and F is the flux observed. The idea behind this distance is to still have the flux of a source following an inverse-square law in an expanding Universe, so now we the replace physical distance by this luminosity distance to preserve it. It can be related to previous distances as

$$D_L = (1+z)\chi = (1+z)^2 D_A \; . \tag{B.8}$$

207

[1]   A. Einstein, "The Foundation of the General Theory of Relativity," Annalen Phys. **49** no. 7, (1916) 769–822.

[2]   **BOSS** Collaboration, S. Alam et al., "The clustering of galaxies in the completed SDSS-III Baryon Oscillation Spectroscopic Survey: cosmological analysis of the DR12 galaxy sample," Mon. Not. Roy. Astron. Soc. **470** no. 3, (2017) 2617–2652, arXiv:1607.03155 [astro-ph.CO].

[3]   **ACTPol** Collaboration, T. Louis et al., "The Atacama Cosmology Telescope: Two-Season ACTPol Spectra and Parameters," JCAP **06** (2017) 031, arXiv:1610.02360 [astro-ph.CO].

[4]   **SPT** Collaboration, J. W. Henning et al., "Measurements of the Temperature and E-Mode Polarization of the CMB from 500 Square Degrees of SPTpol Data," Astrophys. J. **852** no. 2, (2018) 97, arXiv:1707.09353 [astro-ph.CO].

[5]   **Planck** Collaboration, N. Aghanim et al., "Planck 2018 results. VI. Cosmological parameters," Astron. Astrophys. **641** (2020) A6, arXiv:1807.06209 [astro-ph.CO]. [Erratum: Astron.Astrophys. 652, C4 (2021)].

[6]   D. M. Scolnic et al., "The Complete Light-curve Sample of Spectroscopically Confirmed SNe Ia from Pan-STARRS1 and Cosmological Constraints from the Combined Pantheon Sample," Astrophys. J. **859** no. 2, (2018) 101, arXiv:1710.00845 [astro-ph.CO].

[7]   **SDSS** Collaboration, M. Tegmark et al., "Cosmological parameters from SDSS and WMAP," Phys. Rev. D **69** (2004) 103501, arXiv:astro-ph/0310723.

[8]   **LIGO Scientific, VIRGO, KAGRA** Collaboration, R. Abbott et al., "Constraints on the cosmic expansion history from GWTC-3," arXiv:2111.03604 [astro-ph.CO].

[9]   M. Blomqvist et al., "Baryon acoustic oscillations from the cross-correlation of Lyα absorption and quasars in eBOSS DR14," Astron. Astrophys. **629** (2019) A86, arXiv:1904.03430 [astro-ph.CO].

[10] R. Jimenez and A. Loeb, "Constraining cosmological parameters based on relative galaxy ages," Astrophys. J. **573** (2002) 37–42, arXiv:astro-ph/0106145.

[11] J. Beltrán Jiménez, L. Heisenberg, and T. S. Koivisto, "The Geometrical Trinity of Gravity," Universe **5** no. 7, (2019) 173, arXiv:1903.06830 [hep-th].

[12] G. Gamow, My World Line : An Informal Autobiography. Viking Press,, New York, 1970.

[13] **Supernova Search Team** Collaboration, A. G. Riess et al., "Observational evidence from supernovae for an accelerating universe and a cosmological constant," Astron. J. **116** (1998) 1009–1038, arXiv:astro-ph/9805201.

[14] **Supernova Cosmology Project** Collaboration, S. Perlmutter et al., "Measurements of Ω and Λ from 42 high redshift supernovae," Astrophys. J. **517** (1999) 565–586, arXiv:astro-ph/9812133.

[15] E. Hubble, "A relation between distance and radial velocity among extra-galactic nebulae," Proc. Nat. Acad. Sci. **15** (1929) 168–173.

[16] G. Lemaitre, "Republication of: The beginning of the world from the point of view of quantum theory," Nature **127** (1931) 706.

[17] L. Roszkowski, E. M. Sessolo, and S. Trojanowski, "WIMP dark matter candidates and searches—current status and future prospects," Reports on Progress in Physics **81** no. 6, (May, 2018) 066201. https://doi.org/10.1088/1361-6633/aab913.

[18] D. J. Fixsen, "The Temperature of the Cosmic Microwave Background," Astrophys. Journal **707** no. 2, (Dec., 2009) 916–920, arXiv:0911.1955 [astro-ph.CO].

[19] **K2K** Collaboration, M. H. Ahn et al., "Indications of neutrino oscillation in a 250 km long baseline experiment," Phys. Rev. Lett. **90** (2003) 041801, arXiv:hep-ex/0212007.

[20] **Super-Kamiokande** Collaboration, Y. Fukuda et al., "Evidence for oscillation of atmospheric neutrinos," Phys. Rev. Lett. **81** (1998) 1562–1567, arXiv:hep-ex/9807003.

[21] **SNO** Collaboration, Q. R. Ahmad et al., "Direct evidence for neutrino flavor transformation from neutral current interactions in the Sudbury Neutrino Observatory," Phys. Rev. Lett. **89** (2002) 011301, arXiv:nucl-ex/0204008.

214

[22] V. J. Martinez, M.-J. Pons-Borderia, R. A. Moyeed, and M. J. Graham, "Searching for the scale of homogeneity," Mon. Not. Roy. Astron. Soc. **298** (1998) 1212, `arXiv:astro-ph/9804073`.

[23] J. Einasto and M. Gramann, "Transition Scale to a Homogeneous Universe," Astrophys. Journal **407** (Apr., 1993) 443.

[24] W. a Heisenberg, "Uber den anschaulichen Inhalt der quantentheoretischen Kinematik und Mechanik," Z. Phys. **43** (1927) 172–198.

[25] S. Dodelson, Modern Cosmology. Academic Press, Amsterdam, 2003.

[26] R. Bean and O. Dore, "Probing dark energy perturbations: The Dark energy equation of state and speed of sound as measured by WMAP," Phys. Rev. D **69** (2004) 083503, `arXiv:astro-ph/0307100`.

[27] C.-P. Ma and E. Bertschinger, "Cosmological perturbation theory in the synchronous and conformal Newtonian gauges," Astrophys. J. **455** (1995) 7–25, `arXiv:astro-ph/9506072`.

[28] A. G. Riess et al., "A Comprehensive Measurement of the Local Value of the Hubble Constant with 1 km s^{-1} Mpc^{-1} Uncertainty from the Hubble Space Telescope and the SH0ES Team," Astrophys. J. Lett. **934** no. 1, (2022) L7, `arXiv:2112.04510 [astro-ph.CO]`.

[29] **Planck** Collaboration, N. Aghanim et al., "Planck 2018 results. V. CMB power spectra and likelihoods," Astron. Astrophys. **641** (2020) A5, `arXiv:1907.12875 [astro-ph.CO]`.

[30] **Planck** Collaboration, P. A. R. Ade et al., "Planck 2015 results. XXIV. Cosmology from Sunyaev-Zeldovich cluster counts," Astron. Astrophys. **594** (2016) A24.

[31] **Planck** Collaboration, P. A. R. Ade et al., "Planck 2013 results. XX. Cosmology from Sunyaev–Zeldovich cluster counts," Astron. Astrophys. **571** (2014) A20, `arXiv:1303.5080 [astro-ph.CO]`.

[32] B. Audren, J. Lesgourgues, K. Benabed, and S. Prunet, "Conservative Constraints on Early Cosmology: an illustration of the Monte Python cosmological parameter inference code," JCAP **1302** (2013) 001, `arXiv:1210.7183 [astro-ph.CO]`.

[33] T. Brinckmann and J. Lesgourgues, "MontePython 3: boosted MCMC sampler and other features," Phys. Dark Univ. **24** (2019) 100260, `arXiv:1804.07261 [astro-ph.CO]`.

[34] **Planck** Collaboration, N. Aghanim et al., "Planck 2018 results. I. Overview and the cosmological legacy of Planck," Astron. Astrophys. **641** (2020) A1, `arXiv:1807.06205 [astro-ph.CO]`.

[35] **DES** Collaboration, M. A. Troxel et al., "Dark Energy Survey Year 1 results: Cosmological constraints from cosmic shear," Phys. Rev. D **98** no. 4, (2018) 043528, `arXiv:1708.01538 [astro-ph.CO]`.

[36] B. A. Reid et al., "Cosmological constraints from the clustering of the Sloan Digital Sky Survey DR7 luminous red galaxies," Monthly Notices of the Royal Astronomical Society **404** no. 1, (04, 2010) 60–85. `https://doi.org/10.1111/j.1365-2966.2010.16276.x`.

[37] S. Chabanier, M. Millea, and N. Palanque-Delabrouille, "Matter power spectrum: from Lyα forest to CMB scales," Mon. Not. Roy. Astron. Soc. **489** no. 2, (2019) 2247–2253, `arXiv:1905.08103 [astro-ph.CO]`.

[38] **SDSS** Collaboration, D. J. Eisenstein et al., "Detection of the Baryon Acoustic Peak in the Large-Scale Correlation Function of SDSS Luminous Red Galaxies," Astrophys. J. **633** (2005) 560–574, `arXiv:astro-ph/0501171`.

[39] T. Namikawa, T. Okamura, and A. Taruya, "Magnification effect on the detection of primordial non-Gaussianity from photometric surveys," Phys. Rev. D **83** (Jun, 2011) 123514. `https://link.aps.org/doi/10.1103/PhysRevD.83.123514`.

[40] V. C. Rubin and W. K. Ford, Jr., "Rotation of the Andromeda Nebula from a Spectroscopic Survey of Emission Regions," Astrophys. J. **159** (1970) 379–403.

[41] C. Pitrou, A. Coc, J.-P. Uzan, and E. Vangioni, "Precision big bang nucleosynthesis with improved Helium-4 predictions," Phys. Rept. **754** (2018) 1–66, `arXiv:1801.08023 [astro-ph.CO]`.

[42] G. Angloher et al., "Latest observations on the low energy excess in CRESST-III," in 14th International Workshop on the Identification of Dark Matter 2022. 7, 2022. `arXiv:2207.09375 [astro-ph.CO]`.

[43] **XENON** Collaboration, E. Aprile et al., "The XENON1T Dark Matter Experiment," Eur. Phys. J. C **77** no. 12, (2017) 881, `arXiv:1708.07051 [astro-ph.IM]`.

[44] A. Rubbia, "ArDM: a ton-scale liquid Argon experiment for direct detection of Dark Matter in the Universe," Journal of Physics: Conference Series **39** no. 1, (May, 2006) 129. `https://dx.doi.org/10.1088/1742-6596/39/1/028`.

[45] J. S. Bullock and M. Boylan-Kolchin, "Small-Scale Challenges to the ΛCDM Paradigm," Ann. Rev. Astron. Astrophys. **55** (2017) 343–387, arXiv:1707.04256 [astro-ph.CO].

[46] A. Del Popolo and M. Le Delliou, "Small scale problems of the ΛCDM model: a short review," Galaxies **5** no. 1, (2017) 17, arXiv:1606.07790 [astro-ph.CO].

[47] J. F. Navarro, C. S. Frenk, and S. D. M. White, "The Structure of Cold Dark Matter Halos," Astrophys. Journal **462** (May, 1996) 563, arXiv:astro-ph/9508025 [astro-ph].

[48] R. A. Flores and J. R. Primack, "Observational and Theoretical Constraints on Singular Dark Matter Halos," Astrophys. Journal Lett. **427** (May, 1994) L1, arXiv:astro-ph/9402004 [astro-ph].

[49] B. Moore, T. R. Quinn, F. Governato, J. Stadel, and G. Lake, "Cold collapse and the core catastrophe," Mon. Not. Roy. Astron. Soc. **310** (1999) 1147–1152, arXiv:astro-ph/9903164.

[50] S. Garrison-Kimmel, M. Boylan-Kolchin, J. S. Bullock, and E. N. Kirby, "Too big to fail in the Local Group," Monthly Notices of the Royal Astron. Soc. **444** no. 1, (Oct., 2014) 222–236, arXiv:1404.5313 [astro-ph.GA].

[51] M. Boylan-Kolchin, J. S. Bullock, and M. Kaplinghat, "Too big to fail? The puzzling darkness of massive Milky Way subhaloes," Monthly Notices of the Royal Astron. Soc. **415** no. 1, (July, 2011) L40–L44, arXiv:1103.0007 [astro-ph.CO].

[52] E. J. Tollerud, M. Boylan-Kolchin, and J. S. Bullock, "M31 Satellite Masses Compared to LCDM Subhaloes," Mon. Not. Roy. Astron. Soc. **440** no. 4, (2014) 3511–3519, arXiv:1403.6469 [astro-ph.GA].

[53] F. C. van den Bosch, A. Burkert, and R. A. Swaters, "The angular momentum content of dwarf galaxies: new challenges for the theory of galaxy formation," Mon. Not. Roy. Astron. Soc. **326** (2001) 1205, arXiv:astro-ph/0105082.

[54] M. S. Pawlowski et al., "Co-orbiting satellite galaxy structures are still in conflict with the distribution of primordial dwarf galaxies," Mon. Not. Roy. Astron. Soc. **442** no. 3, (2014) 2362–2380, arXiv:1406.1799 [astro-ph.GA].

[55] F. Lelli, S. S. McGaugh, and J. M. Schombert, "The Small Scatter of the Baryonic Tully-Fisher Relation," Astrophys. Journal Lett. **816** no. 1, (Jan., 2016) L14, arXiv:1512.04543 [astro-ph.GA].

[56] S. Capozziello and M. De Laurentis, "Extended Theories of Gravity," Phys. Rept. **509** (2011) 167–321, arXiv:1108.6266 [gr-qc].

217

[57]   M. Moresco et al., "Unveiling the Universe with emerging cosmological probes," Living Rev. Rel. **25** no. 1, (2022) 6, `arXiv:2201.07241 [astro-ph.CO]`.

[58]   N. Schöneberg, J. Lesgourgues, and D. C. Hooper, "The BAO+BBN take on the Hubble tension," JCAP **10** (2019) 029, `arXiv:1907.11594 [astro-ph.CO]`.

[59]   L. Pogosian, G.-B. Zhao, and K. Jedamzik, "Recombination-independent determination of the sound horizon and the Hubble constant from BAO," Astrophys. J. Lett. **904** no. 2, (2020) L17, `arXiv:2009.08455 [astro-ph.CO]`.

[60]   W. L. Freedman, B. F. Madore, T. Hoyt, I. S. Jang, R. Beaton, M. G. Lee, A. Monson, J. Neeley, and J. Rich, "Calibration of the Tip of the Red Giant Branch (TRGB)," `arXiv:2002.01550 [astro-ph.GA]`.

[61]   **WMAP** Collaboration, G. Hinshaw et al., "Nine-Year Wilkinson Microwave Anisotropy Probe (WMAP) Observations: Cosmological Parameter Results," Astrophys. J. Suppl. **208** (2013) 19, `arXiv:1212.5226 [astro-ph.CO]`.

[62]   **HST** Collaboration, W. L. Freedman et al., "Final results from the Hubble Space Telescope key project to measure the Hubble constant," Astrophys. J. **553** (2001) 47–72, `arXiv:astro-ph/0012376`.

[63]   K. C. Wong et al., "H0LiCOW – XIII. A 2.4 per cent measurement of H0 from lensed quasars: 5.3σ tension between early- and late-Universe probes," Mon. Not. Roy. Astron. Soc. **498** no. 1, (2020) 1420–1439, `arXiv:1907.04869 [astro-ph.CO]`.

[64]   E. Mortsell, A. Goobar, J. Johansson, and S. Dhawan, "Sensitivity of the Hubble Constant Determination to Cepheid Calibration," Astrophys. J. **933** no. 2, (2022) 212, `arXiv:2105.11461 [astro-ph.CO]`.

[65]   H.-Y. Wu and D. Huterer, "Sample variance in the local measurements of the Hubble constant," Mon. Not. Roy. Astron. Soc. **471** no. 4, (2017) 4946–4955, `arXiv:1706.09723 [astro-ph.CO]`.

[66]   C. Krishnan, R. Mohayaee, E. O. Colgáin, M. M. Sheikh-Jabbari, and L. Yin, "Does Hubble tension signal a breakdown in FLRW cosmology?," Class. Quant. Grav. **38** no. 18, (2021) 184001, `arXiv:2105.09790 [astro-ph.CO]`.

[67]   L. Hart and J. Chluba, "New constraints on time-dependent variations of fundamental constants using Planck data," Mon. Not. Roy. Astron. Soc. **474** no. 2, (2018) 1850–1861, `arXiv:1705.03925 [astro-ph.CO]`.

[68] V. Poulin, T. L. Smith, T. Karwal, and M. Kamionkowski, "Early Dark Energy Can Resolve The Hubble Tension," Phys. Rev. Lett. **122** no. 22, (2019) **221301**, arXiv:1811.04083 [astro-ph.CO].

[69] M. Viel, J. Lesgourgues, M. G. Haehnelt, S. Matarrese, and A. Riotto, "Constraining warm dark matter candidates including sterile neutrinos and light gravitinos with WMAP and the Lyman-alpha forest," Phys. Rev. D **71** (2005) 063534, arXiv:astro-ph/0501562.

[70] K. Vattis, S. M. Koushiappas, and A. Loeb, "Dark matter decaying in the late Universe can relieve the H0 tension," Phys. Rev. D **99** no. 12, (2019) 121302, arXiv:1903.06220 [astro-ph.CO].

[71] K. V. Berghaus and T. Karwal, "Thermal Friction as a Solution to the Hubble Tension," Phys. Rev. D **101** no. 8, (2020) 083537, arXiv:1911.06281 [astro-ph.CO].

[72] B. Wang, E. Abdalla, F. Atrio-Barandela, and D. Pavon, "Dark Matter and Dark Energy Interactions: Theoretical Challenges, Cosmological Implications and Observational Signatures," Rept. Prog. Phys. **79** no. 9, (2016) 096901, arXiv:1603.08299 [astro-ph.CO].

[73] S. Vagnozzi, L. Visinelli, O. Mena, and D. F. Mota, "Do we have any hope of detecting scattering between dark energy and baryons through cosmology?," Mon. Not. Roy. Astron. Soc. **493** no. 1, (2020) 1139–1152, arXiv:1911.12374 [gr-qc].

[74] T. Tröster et al., "Cosmology from large-scale structure: Constraining ΛCDM with BOSS," Astron. Astrophys. **633** (2020) L10, arXiv:1909.11006 [astro-ph.CO].

[75] **KiDS** Collaboration, M. Asgari et al., "KiDS-1000 Cosmology: Cosmic shear constraints and comparison between two point statistics," Astron. Astrophys. **645** (2021) A104, arXiv:2007.15633 [astro-ph.CO].

[76] **DES** Collaboration, L. F. Secco et al., "Dark Energy Survey Year 3 results: Cosmology from cosmic shear and robustness to modeling uncertainty," Phys. Rev. D **105** no. 2, (2022) 023515, arXiv:2105.13544 [astro-ph.CO].

[77] **ACT** Collaboration, S. Aiola et al., "The Atacama Cosmology Telescope: DR4 Maps and Cosmological Parameters," JCAP **12** (2020) 047, arXiv:2007.07288 [astro-ph.CO].

[78] M. Douspis, L. Salvati, and N. Aghanim, "On the Tension between Large Scale Structures and Cosmic Microwave Background," PoS **EDSU2018** (2018) 037, arXiv:1901.05289 [astro-ph.CO].

[79] A. Blanchard and S. Ilić, "Closing up the cluster tension?," Astron. Astrophys. **656** (2021) A75, `arXiv:2104.00756 [astro-ph.CO]`.

[80] Z. Sakr, S. Ilić, A. Blanchard, J. Bittar, and W. Farah, "Cluster counts: Calibration issue or new physics?," Astron. Astrophys. **620** (2018) A78, `arXiv:1803.11170 [astro-ph.CO]`.

[81] S. Das, A. Maharana, V. Poulin, and R. K. Sharma, "Nonthermal neutrino-like hot dark matter in light of the S8 tension," Phys. Rev. D **105** no. 10, (2022) 103503, `arXiv:2104.03329 [astro-ph.CO]`.

[82] G. Franco Abellán, R. Murgia, V. Poulin, and J. Lavalle, "Implications of the S_8 tension for decaying dark matter with warm decay products," Phys. Rev. D **105** no. 6, (2022) 063525, `arXiv:2008.09615 [astro-ph.CO]`.

[83] C. Wetterich, "The Cosmon model for an asymptotically vanishing time dependent cosmological 'constant'," Astron. Astrophys. **301** (1995) 321–328, `arXiv:hep-th/9408025`.

[84] L. Amendola, "Coupled quintessence," Phys. Rev. D **62** (2000) 043511, `arXiv:astro-ph/9908023`.

[85] W. Zimdahl, D. J. Schwarz, A. B. Balakin, and D. Pavón, "Cosmic antifriction and accelerated expansion," Phys. Rev. D **64** (Aug, 2001) 063501.

[86] G. R. Farrar and P. J. E. Peebles, "Interacting dark matter and dark energy," Astrophys. J. **604** (2004) 1–11, `arXiv:astro-ph/0307316`.

[87] A. Pourtsidou, C. Skordis, and E. Copeland, "Models of dark matter coupled to dark energy," Phys. Rev. D **88** no. 8, (2013) 083505, `arXiv:1307.0458 [astro-ph.CO]`.

[88] C. G. Boehmer, N. Tamanini, and M. Wright, "Interacting quintessence from a variational approach Part II: derivative couplings," Phys. Rev. D **91** no. 12, (2015) 123003, `arXiv:1502.04030 [gr-qc]`.

[89] T. S. Koivisto, E. N. Saridakis, and N. Tamanini, "Scalar-Fluid theories: cosmological perturbations and large-scale structure," JCAP **09** (2015) 047, `arXiv:1505.07556 [astro-ph.CO]`.

[90] M. Benetti, W. Miranda, H. A. Borges, C. Pigozzo, S. Carneiro, and J. S. Alcaniz, "Looking for interactions in the cosmological dark sector," JCAP **12** (2019) 023, `arXiv:1908.07213 [astro-ph.CO]`.

[91] V. Salzano et al., "J-PAS: forecasts on interacting vacuum energy models," JCAP **09** (2021) 033, `arXiv:2102.06417 [astro-ph.CO]`.

[92] F. Simpson, "Scattering of dark matter and dark energy," Phys. Rev. D **82** (2010) 083505, `arXiv:1007.1034 [astro-ph.CO]`.

[93] M. Baldi and F. Simpson, "Simulating Momentum Exchange in the Dark Sector," Mon. Not. Roy. Astron. Soc. **449** no. 3, (2015) 2239–2249, `arXiv:1412.1080 [astro-ph.CO]`.

[94] C. Skordis, A. Pourtsidou, and E. Copeland, "Parametrized post-Friedmannian framework for interacting dark energy theories," Phys. Rev. D **91** no. 8, (2015) 083537, `arXiv:1502.07297 [astro-ph.CO]`.

[95] A. Pourtsidou and T. Tram, "Reconciling CMB and structure growth measurements with dark energy interactions," Phys. Rev. D **94** no. 4, (2016) 043518, `arXiv:1604.04222 [astro-ph.CO]`.

[96] M. Baldi and F. Simpson, "Structure formation simulations with momentum exchange: alleviating tensions between high-redshift and low-redshift cosmological probes," Mon. Not. Roy. Astron. Soc. **465** no. 1, (2017) 653–666, `arXiv:1605.05623 [astro-ph.CO]`.

[97] S. Kumar and R. C. Nunes, "Observational constraints on dark matter–dark energy scattering cross section," Eur. Phys. J. C **77** no. 11, (2017) 734, `arXiv:1709.02384 [astro-ph.CO]`.

[98] R. Kase and S. Tsujikawa, "Scalar-Field Dark Energy Nonminimally and Kinetically Coupled to Dark Matter," Phys. Rev. D **101** no. 6, (2020) 063511, `arXiv:1910.02699 [gr-qc]`.

[99] R. Kase and S. Tsujikawa, "Weak cosmic growth in coupled dark energy with a Lagrangian formulation," Phys. Lett. B **804** (2020) 135400, `arXiv:1911.02179 [gr-qc]`.

[100] F. N. Chamings, A. Avgoustidis, E. J. Copeland, A. M. Green, and A. Pourtsidou, "Understanding the suppression of structure formation from dark matter-dark energy momentum coupling," Phys. Rev. D **101** no. 4, (2020) 043531, `arXiv:1912.09858 [astro-ph.CO]`.

[101] M. Asghari, J. Beltrán Jiménez, S. Khosravi, and D. F. Mota, "On structure formation from a small-scales-interacting dark sector," JCAP **04** (2019) 042, `arXiv:1902.05532 [astro-ph.CO]`.

[102] L. Amendola and S. Tsujikawa, "Scaling solutions and weak gravity in dark energy with energy and momentum couplings," JCAP **06** (2020) 020, `arXiv:2003.02686 [gr-qc]`.

[103] M. S. Linton, R. Crittenden, and A. Pourtsidou, "Momentum transfer models of interacting dark energy," `arXiv:2107.03235 [astro-ph.CO]`.

[104] F. Ferlito, S. Vagnozzi, D. F. Mota, and M. Baldi, "Cosmological direct detection of dark energy: Non-linear structure formation signatures of dark energy scattering with visible matter," Mon. Not. Roy. Astron. Soc. **512** no. 2, (2022) 1885–1905, arXiv:2201.04528 [astro-ph.CO].

[105] E. Di Valentino, A. Melchiorri, and J. Silk, "Planck evidence for a closed Universe and a possible crisis for cosmology," Nature Astron. **4** no. 2, (2019) 196–203, arXiv:1911.02087 [astro-ph.CO].

[106] W. Giarè, F. Renzi, O. Mena, E. Di Valentino, and A. Melchiorri, "Harrison-Zel'dovich spectrum gets back?," arXiv:2210.09018 [astro-ph.CO].

[107] M. G. Dainotti, B. De Simone, T. Schiavone, G. Montani, E. Rinaldi, G. Lambiase, M. Bogdan, and S. Ugale, "On the Evolution of the Hubble Constant with the SNe Ia Pantheon Sample and Baryon Acoustic Oscillations: A Feasibility Study for GRB-Cosmology in 2030," Galaxies **10** no. 1, (2022) 24, arXiv:2201.09848 [astro-ph.CO].

[108] J. B. Jiménez, D. Bettoni, D. Figueruelo, and F. A. Teppa Pannia, "On cosmological signatures of baryons-dark energy elastic couplings," JCAP **08** (2020) 020, arXiv:2004.14661 [astro-ph.CO].

[109] D. Figueruelo et al., "J-PAS: Forecasts for dark matter - dark energy elastic couplings," JCAP **07** (2021) 022, arXiv:2103.01571 [astro-ph.CO].

[110] J. Beltrán Jiménez, D. Bettoni, D. Figueruelo, F. A. Teppa Pannia, and S. Tsujikawa, "Velocity-dependent interacting dark energy and dark matter with a Lagrangian description of perfect fluids," JCAP **03** (2021) 085, arXiv:2012.12204 [astro-ph.CO].

[111] J. Beltrán Jiménez, D. Bettoni, D. Figueruelo, F. A. Teppa Pannia, and S. Tsujikawa, "Probing elastic interactions in the dark sector and the role of S8," Phys. Rev. D **104** no. 10, (2021) 103503, arXiv:2106.11222 [astro-ph.CO].

[112] A. Joyce, B. Jain, J. Khoury, and M. Trodden, "Beyond the Cosmological Standard Model," Phys. Rept. **568** (2015) 1–98, arXiv:1407.0059 [astro-ph.CO].

[113] J. Lesgourgues, "The Cosmic Linear Anisotropy Solving System (CLASS) I: Overview," arXiv e-prints (Apr., 2011) , arXiv:1104.2932 [astro-ph.IM].

[114] D. Blas, J. Lesgourgues, and T. Tram, "The Cosmic Linear Anisotropy Solving System (CLASS). Part II: Approximation schemes," JCAP **2011** no. 7, (July, 2011) 034, arXiv:1104.2933 [astro-ph.CO].

[115] D. Baumann, Cosmology. Cambridge University Press, 7, 2022.

[116] A. Lewis, A. Challinor, and A. Lasenby, "Efficient computation of CMB anisotropies in closed FRW models," Astrophys. J. **538** (2000) 473–476, arXiv:astro-ph/9911177.

[117] **SDSS** Collaboration, M. Betoule et al., "Improved cosmological constraints from a joint analysis of the SDSS-II and SNLS supernova samples," Astron. Astrophys. **568** (2014) A22, arXiv:1401.4064 [astro-ph.CO].

[118] L. Anderson et al., "The clustering of galaxies in the SDSS-III Baryon Oscillation Spectroscopic Survey: Baryon Acoustic Oscillations in the Data Release 9 Spectroscopic Galaxy Sample," Mon. Not. Roy. Astron. Soc. **427** no. 4, (2013) 3435–3467, arXiv:1203.6594 [astro-ph.CO].

[119] A. J. Ross, L. Samushia, C. Howlett, W. J. Percival, A. Burden, and M. Manera, "The clustering of the SDSS DR7 main Galaxy sample – I. A 4 per cent distance measure at $z = 0.15$" Mon. Not. Roy. Astron. Soc. **449** no. 1, (2015) 835–847, arXiv:1409.3242 [astro-ph.CO].

[120] F. Beutler, C. Blake, M. Colless, D. H. Jones, L. Staveley-Smith, L. Campbell, Q. Parker, W. Saunders, and F. Watson, "The 6dF Galaxy Survey: Baryon Acoustic Oscillations and the Local Hubble Constant," Mon. Not. Roy. Astron. Soc. **416** (2011) 3017–3032, arXiv:1106.3366 [astro-ph.CO].

[121] C. Heymans et al., "CFHTLenS tomographic weak lensing cosmological parameter constraints: Mitigating the impact of intrinsic galaxy alignments," Mon. Not. Roy. Astron. Soc. **432** (2013) 2433, arXiv:1303.1808 [astro-ph.CO].

[122] P. J. E. Peebles and J. T. Yu, "Primeval adiabatic perturbation in an expanding universe," Astrophys. J. **162** (1970) 815–836.

[123] B. F. Schutz and R. Sorkin, "Variational aspects of relativistic field theories, with application to perfect fluids," Annals Phys. **107** (1977) 1–43.

[124] J. Brown, "Action functionals for relativistic perfect fluids," Class. Quant. Grav. **10** (1993) 1579–1606, arXiv:gr-qc/9304026.

[125] Maplesoft, a division of Waterloo Maple Inc.., "Maple." https://hadoop.apache.org.

[126] J. M. Bardeen, "Gauge Invariant Cosmological Perturbations," Phys. Rev. D **22** (1980) 1882–1905.

[127] A. Lewis, "GetDist: a Python package for analysing Monte Carlo samples," arXiv:1910.13970 [astro-ph.IM]. https://getdist.readthedocs.io.

[128] A. Lewis and S. Bridle, "Cosmological parameters from CMB and other data: A Monte Carlo approach," Phys. Rev. D **66** (2002) 103511, `arXiv:astro-ph/0205436 [astro-ph]`.

[129] A. Lewis, "Efficient sampling of fast and slow cosmological parameters," Phys. Rev. D **87** (2013) 103529, `arXiv:1304.4473 [astro-ph.CO]`.

[130] J. Lesgourgues, G. Marques-Tavares, and M. Schmaltz, "Evidence for dark matter interactions in cosmological precision data?," JCAP **02** (2016) 037, `arXiv:1507.04351 [astro-ph.CO]`.

[131] K. Dawson et al., "The Baryon Oscillation Spectroscopic Survey of SDSS-III," The Astronomical Journal **145** no. 1, (Jan, 2013) 10, `arXiv:1208.0022 [astro-ph.CO]`.

[132] **DESI** Collaboration, A. Aghamousa et al., "The DESI Experiment Part I: Science,Targeting, and Survey Design," `arXiv:1611.00036 [astro-ph.IM]`.

[133] **DES** Collaboration, T. Abbott et al., "The dark energy survey," `arXiv:astro-ph/0510346`.

[134] **LSST Dark Energy Science** Collaboration, D. Alonso et al., "The LSST Dark Energy Science Collaboration (DESC) Science Requirements Document," `arXiv:1809.01669 [astro-ph.CO]`.

[135] P. Martí, R. Miquel, F. J. Castander, E. Gaztañaga, M. Eriksen, and C. Sánchez, "Precise photometric redshifts with a narrow-band filter set: The PAU Survey at the William Herschel Telescope," Mon. Not. Roy. Astron. Soc. **442** no. 1, (2014) 92–109, `arXiv:1402.3220`.

[136] A. Cenarro et al., "J-PLUS: The Javalambre Photometric Local Universe Survey," Astron. Astrophys. **622** (2019) A176, `arXiv:1804.02667 [astro-ph.GA]`.

[137] **J-PAS** Collaboration, N. Benitez et al., "J-PAS: The Javalambre-Physics of the Accelerated Universe Astrophysical Survey," `arXiv:1403.5237 [astro-ph.CO]`.

[138] R. Braun, T. Bourke, J. A. Green, E. Keane, and J. Wagg, "Advancing Astrophysics with the Square Kilometre Array," PoS **AASKA14** (2015) 174.

[139] W. Cardona and D. Figueruelo, "Momentum transfer in the dark sector and lensing convergence in upcoming galaxy surveys," JCAP **12** (2022) 010, `arXiv:2209.12583 [astro-ph.CO]`.

[140] J. B. Jiménez, E. Di Dio, and D. Figueruelo, "A smoking gun from the power spectrum dipole for elastic interactions in the dark sector," `arXiv:2212.08617 [astro-ph.CO]`.

[141] **EUCLID** Collaboration, R. Laureijs et al., "Euclid Definition Study Report,"
`arXiv:1110.3193 [astro-ph.CO]`.

[142] M. Aparicio Resco, A. L. Maroto, J. S. Alcaniz, L. R. Abramo,
C. Hernández-Monteagudo, N. Benítez, S. Carneiro, A. J. Cenarro,
D. Cristóbal-Hornillos, R. A. Dupke, and et al., "J-PAS: forecasts on dark
energy and modified gravity theories," Monthly Notices of the Royal
Astronomical Society **493** no. 3, (Feb, 2020) 3616–3631.

[143] M. Aparicio Resco and A. L. Maroto, "The Fisher gAlaxy suRvey cOde (FARO),"
JCAP **2021** no. 1, (Jan., 2021) 021, `arXiv:2007.05360 [astro-ph.CO]`.

[144] H.-J. Seo and D. J. Eisenstein, "Probing dark energy with baryonic acoustic
oscillations from future large galaxy redshift surveys," Astrophys. J. **598**
(2003) 720–740, `arXiv:astro-ph/0307460`.

[145] W. Hu, "Power spectrum tomography with weak lensing," Astrophys. J. Lett.
522 (1999) L21–L24, `arXiv:astro-ph/9904153`.

[146] C. Bonvin and P. Fleury, "Testing the equivalence principle on cosmological
scales," JCAP **05** (2018) 061, `arXiv:1803.02771 [astro-ph.CO]`.

[147] C. Bonvin, F. O. Franco, and P. Fleury, "A null test of the equivalence
principle using relativistic effects in galaxy surveys," JCAP **08** (2020) 004,
`arXiv:2004.06457 [astro-ph.CO]`.

[148] O. Umeh, K. Koyama, and R. Crittenden, "Testing the equivalence principle
on cosmological scales using the odd multipoles of galaxy cross-power
spectrum and bispectrum," JCAP **08** (2021) 049, `arXiv:2011.05876`
`[astro-ph.CO]`.

[149] S. Castello, N. Grimm, and C. Bonvin, "Rescuing constraints on modified
gravity using gravitational redshift in large-scale structure," Phys. Rev. D **106**
no. 8, (2022) 083511, `arXiv:2204.11507 [astro-ph.CO]`.

[150] K. Koyama, R. Maartens, and Y.-S. Song, "Velocities as a probe of dark sector
interactions," JCAP **10** (2009) 017, `arXiv:0907.2126 [astro-ph.CO]`.

[151] P. Bull, "Extending cosmological tests of General Relativity with the Square
Kilometre Array," Astrophys. J. **817** no. 1, (2016) 26, `arXiv:1509.07562`
`[astro-ph.CO]`.

[152] **SKA** Collaboration, D. J. Bacon et al., "Cosmology with Phase 1 of the Square
Kilometre Array: Red Book 2018: Technical specifications and performance
forecasts," Publ. Astron. Soc. Austral. **37** (2020) e007, `arXiv:1811.02743`
`[astro-ph.CO]`.

[153] D. Jeong, F. Schmidt, and C. M. Hirata, "Large-scale clustering of galaxies in general relativity," Phys. Rev. D **85** (2012) 023504, arXiv:1107.5427 [astro-ph.CO].

[154] J. Francfort, B. Ghosh, and R. Durrer, "Cosmological Number Counts in Einstein and Jordan frames," JCAP **09** (2019) 071, arXiv:1907.03606 [gr-qc].

[155] E. Di Dio, F. Montanari, J. Lesgourgues, and R. Durrer, "The CLASSgal code for Relativistic Cosmological Large Scale Structure," JCAP **11** (2013) 044, arXiv:1307.1459 [astro-ph.CO].

[156] **Euclid** Collaboration, F. Lepori et al., "Euclid preparation: XIX. Impact of magnification on photometric galaxy clustering," arXiv:2110.05435 [astro-ph.CO].

[157] C. S. Lorenz, D. Alonso, and P. G. Ferreira, "Impact of relativistic effects on cosmological parameter estimation," Phys. Rev. D **97** (Jan, 2018) 023537. https://link.aps.org/doi/10.1103/PhysRevD.97.023537.

[158] W. Cardona, R. Durrer, M. Kunz, and F. Montanari, "Lensing convergence and the neutrino mass scale in galaxy redshift surveys," Phys. Rev. D **94** no. 4, (2016) 043007, arXiv:1603.06481 [astro-ph.CO].

[159] C. Duncan, B. Joachimi, A. Heavens, C. Heymans, and H. Hildebrandt, "On the complementarity of galaxy clustering with cosmic shear and flux magnification," Mon. Not. Roy. Astron. Soc. **437** no. 3, (2014) 2471–2487, arXiv:1306.6870 [astro-ph.CO].

[160] L. Amendola et al., "Cosmology and fundamental physics with the Euclid satellite," Living Rev. Rel. **21** no. 1, (2018) 2, arXiv:1606.00180 [astro-ph.CO].

[161] F. Montanari and R. Durrer, "Measuring the lensing potential with tomographic galaxy number counts," JCAP **10** (2015) 070, arXiv:1506.01369 [astro-ph.CO].

[162] R. Teyssier, "Cosmological hydrodynamics with adaptive mesh refinement: a new high resolution code called ramses," Astron. Astrophys. **385** (2002) 337–364, arXiv:astro-ph/0111367.

[163] T. Sprenger, M. Archidiacono, T. Brinckmann, S. Clesse, and J. Lesgourgues, "Cosmology in the era of Euclid and the Square Kilometre Array," JCAP **02** (2019) 047, arXiv:1801.08331 [astro-ph.CO].

[164] V. Springel, "The cosmological simulation code gadget-2," Monthly Notices of the Royal Astronomical Society **364** no. 4, (12, 2005) 1105–1134. https://doi.org/10.1111/j.1365-2966.2005.09655.x.

[165] M. Michaux, O. Hahn, C. Rampf, and R. E. Angulo, "Accurate initial conditions for cosmological N-body simulations: Minimizing truncation and discreteness errors," Mon. Not. Roy. Astron. Soc. **500** no. 1, (2020) 663–683, arXiv:2008.09588 [astro-ph.CO].

[166] O. Hahn, C. Rampf, and C. Uhlemann, "Higher order initial conditions for mixed baryon–CDM simulations," Mon. Not. Roy. Astron. Soc. **503** no. 1, (2021) 426–445, arXiv:2008.09124 [astro-ph.CO].

[167] N. Metropolis, A. W. Rosenbluth, M. N. Rosenbluth, A. H. Teller, and E. Teller, "Equation of State Calculations by Fast Computing Machines," The Journal of Chemical Physics **21** no. 6, (1953) 1087–1092. https://doi.org/10.1063/1.1699114.

[168] W. K. Hastings, "Monte Carlo sampling methods using Markov chains and their applications," Biometrika **57** no. 1, (04, 1970) 97–109. https://doi.org/10.1093/biomet/57.1.97.

[169] A. Gelman and D. B. Rubin, "Inference from Iterative Simulation Using Multiple Sequences," Statistical Science **7** no. 4, (1992) 457 – 472. https://doi.org/10.1214/ss/1177011136.

[170] H. Akaike, "A New Look at the Statistical Model Identification," IEEE Transactions on Automatic Control **AC-19** no. 6, (December, 1974) 716–723.

[171] G. Schwarz, "Estimating the Dimension of a Model," The Annals of Statistics **6** no. 2, (1978) 461 – 464. https://doi.org/10.1214/aos/1176344136.

[172] R. A. Fisher, "The Logic of Inductive Inference," Journal of the Royal Statistical Society **98** no. 1, (1935) 39–82. http://www.jstor.org/stable/2342435.